Identification and Characterization of Potential Novel Targets in Thyroid Carcinoma: Evidence of Non-Oncogene Addiction Unveiling Tumor Cell Vulnerabilities

Thesis

Elena Cetti

Degree in Biological Sciences

OU personal identifier: C8575227

IDENTIFICATION AND CHARACTERIZATION OF POTENTIAL NOVEL TARGETS IN THYROID CARCINOMA: EVIDENCE OF NON-ONCOGENE ADDICTION UNVEILING TUMOR CELL VULNERABILITIES

Thesis presented for the Degree of Doctor of Philosophy

The Open University, Milton Keynes (UK)

Faculty of Science Technology Engineering and Mathematics (STEM)

School of Life, Health and Chemical Sciences

Date of submission: September 2017

Affiliated Research Centre:

Fondazione IRCCS Istituto Nazionale dei Tumori, Milan (Italy)

Director of studies: Dr. Angela Greco

External supervisor: Prof. Mahvash Tavassoli

Table of contents

Abstract

Thyroid cancer is the most frequent endocrine malignancy, with an incidence constantly increasing. Despite well-differentiated thyroid tumors are generally cured by conventional therapy, a fraction of them relapses and progresses towards undifferentiated forms, characterized by a poor prognosis. Target therapies introduced in clinical testing are often unsuccessful; therefore, novel therapeutic strategies are needed. To identify critical nodal points for therapeutic intervention, our laboratory faced the "non-oncogene addiction" (NOA) paradigm, which asserts that the tumorigenic state relies on the activity of genes that are essential to support the phenotype of cancer cells but not required to the same degree for normal cell viability. By screening a siRNA library on normal and tumor thyroid cell lines, we identified 15 genes whose silencing interfered with the growth of tumor but not normal thyroid cells.

The overall aim of this project was to validate NOA genes to identify thyroid tumor cell vulnerabilities and to explore their role in the regulation of thyroid tumor cell biology. Among the 15 hit genes, we selected MASTL, Cyclin D1 and COPZ1 for validation studies. We confirmed the growth inhibitory effect of their silencing in tumor but not normal thyroid cells and observed that these effects were common to a panel of thyroid tumor cell lines, irrespective of the histotype or genetic lesion. Functional studies on MASTL demonstrated that its depletion in thyroid tumor cells inhibited cell growth, led to mitotic catastrophe and induced DNA damage and cell death. COPZ1 depletion induced abortive autophagy, endoplasmic reticulum stress and apoptotic cell death in thyroid tumor cells, as well as tumor growth inhibition *in vivo*. Together, our studies identified *MASTL* and

COPZ1 as vulnerability genes for thyroid tumor cells and provided the rationale for future studies aimed to explore their targeting for potential therapeutic intervention.

1. Introduction

1.1. Thyroid cancer

Thyroid cancer (TC) is the most frequent malignancy of the endocrine system, and notably it is characterized by a global incidence increasing during the last decades. In the United States of America, TC is the fifth most common cancer in women, and accounts for more than 62000 cases occurred in men and women in 2015 (1). Thyroid is a butterfly-shaped organ located on the anterior surface of trachea, at the base of the neck, and it is formed by aggregates of lobules of spherical follicles filled with colloid (2). Epithelial follicular cells mark follicles and are responsible for the production and secretion of thyroid hormones thyroxine (T4) and triiodothyronine (T3), while parafollicular "C" cells, located within follicles, are the neuroendocrine cells responsible for calcitonin secretion (Figure 1.1). Thyroid tumors can originate from both follicular epithelial cells and parafollicular "C" cells. Tumors originating from the follicular cells are distinguished into different subtypes: papillary thyroid carcinoma (PTC, accounting for 80-85% of cases), follicular thyroid carcinoma (FTC, 10-15% of cases), poorly differentiated thyroid carcinoma (PDTC, about 5% of cases) and anaplastic thyroid carcinoma (ATC, 2-3% of cases) (3). Tumors originating from parafollicular C cells are known as medullary thyroid carcinoma (MTC) and account for a small proportion of thyroid malignancies (2-3% of cases).

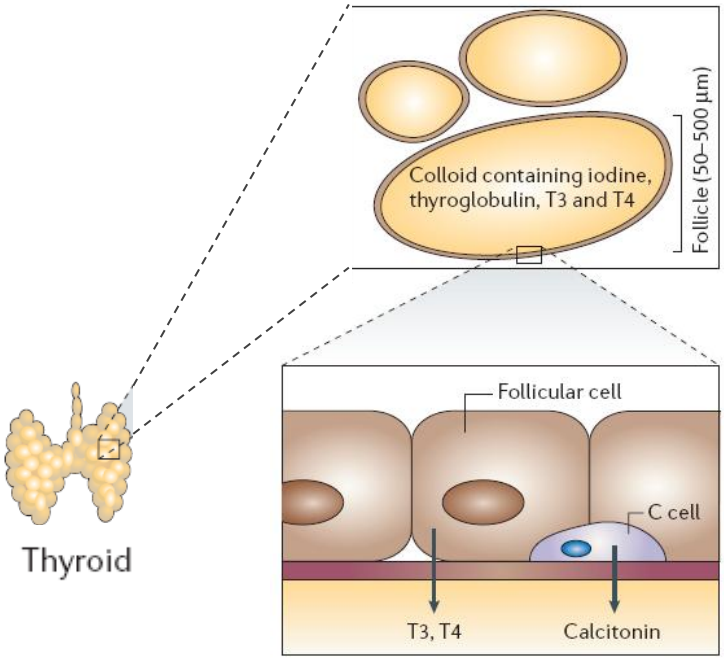

Figure 1.1 Structure of thyroid gland
Schematic representation of the thyroid; the structure of follicles, together with follicular and parafollicular thyroid cells, are indicated. Image adapted from (2).

Explanations for the worldwide increase of thyroid tumor incidence are controversial. Fine-needle aspiration biopsy (FNAB) and histopathological assessment are the cornerstone of diagnostic management of thyroid nodules; however, in the last years a progressive increase in the use of more sensitive techniques, that are high-resolution ultrasonography, computerized tomography, magnetic resonance or positron emission tomography, as diagnostic tools, was observed (4). According to some experts, the increased diagnosis of thyroid tumors is related to the increase in diagnostic sensitivity. Conversely, others attribute the increase of incidence rate to a major exposure to risk factors, like radiation exposure during medical procedures (5), obesity (6), chronic autoimmune thyroiditis (7), or environmental factors (8).

However, in contrast to incidence rates, mortality rates are stable or decreasing both in the United States (9) and in Europe (10), supporting the evidence that probably the increased incidence is mainly related to improvement of surveillance (11). On the other

hand, the problem of probable overdiagnosis of thyroid tumors has emerged as a growing public health concern (12).

1.1.1. Follicular cell-derived thyroid tumors

The majority of thyroid malignancies originates from follicular cells and is distinguished in different subgroups, according to their differentiation status, as well as to some histological and clinical features (Figure 1.2 and Table 1.1). PTC and FTC are classified together as well-differentiated thyroid carcinomas (WDTC) and are generally characterized by a good prognosis, with over 98% five-year survival rate in Europe and North America (13). By contrast, patients with ATC have a poor prognosis, with median survival of 5 months, and less than 20% are alive 1 year after diagnosis (14).

1.1.1.1. Papillary thyroid carcinoma (PTC)

PTC is the most common tumor histotype, occurring more frequently in women than in men, and is also the most common pediatric malignancy. PTC presents as an enlarged solid nodule in more than half of patients and often forms multifocal tumors that can be either unilateral or extended to both thyroid lobes (15). Lymphatic vessels are the main system for PTC diffusion; indeed, cervical lymph node metastases are clinically detectable on initial presentation.

"Classical" PTC is microscopically characterized by a papillary architecture and epithelial cells with "ground glass" nuclei, which include irregularities as grooves and nuclear pseudoinclusions (16). Psammoma bodies, which represent a typical PTC feature, are found in at least 50% of cases, are formed by focal areas of infarction of the tips of papillae and can be found also in tumor stroma and lymphatic spaces. Even if regional

lymph node metastases are common at initial presentation of usual PTC, this feature apparently does not affect long-term prognosis that is generally good for PTC patients.

In addition to classical PTC, which is the most frequent, several histological variants differing in morphological pattern as well as in prognosis, have been described. The most common are papillary thyroid microcarcinoma, follicular, oncocytic, clear cells, diffuse sclerosing, tall cell, columnar cell, solid and cribriform variants (17). These variants have good prognosis, similar to that of classical PTC, with the exception of tall cell, columnar cell, and solid variants, characterized by aggressive behavior, vascular invasion and worse outcome.

1.1.1.2. Follicular thyroid carcinoma (FTC)

FTC is characterized by evidence of follicular cell differentiation lacking the diagnostic nuclear features of PTC. It is more frequent in women over 50 years of age (18) and in iodine-deficient areas (19). FTC is an encapsulated tumor and generally presents as unifocal. Unlike PTC, it spreads hematogenously rather than by lymphatic vessels, and distant metastases, primarily to the lung and bone, can be found at the diagnosis (20). FTC can originate from follicular thyroid adenoma (FTA), which is a benign tumor of thyroid gland surrounded by a thin fibrous capsule (21). Indeed, FTAs can acquire oncogenic mutations and progress towards the malignant FTC form.

Hürtle cell carcinoma (HCC), or “oncocytic or oxyphilic”, is considered a rare variant of FTC (and less frequently of PTC) (22). The tumor is composed of at least 75% Hürtle cells, that are large polygonal cells characterized by an abundant eosinophilic granular cytoplasm, due to a high content of mitochondria. As FTCs, HCCs can spread hematogenously to metastasize to bone and lungs, but can also present regional lymph node involvement.

FTC is generally considered a more aggressive disease than PTC, with a prognosis depending on several factors, among which the degree of invasiveness of the tumor: patients with minimally invasive FTC have a survival expectance similar to that of normal population matched for age and sex, while 50% of patients with widely invasive carcinoma die of the disease (18).

1.1.1.3. Poorly Differentiated Thyroid Carcinoma (PDTC)

PDTCs comprise thyroid tumors showing histological and prognostic features that are intermediate between those of differentiated (PTC and FTC) on one hand and anaplastic (ATC) carcinomas on the other. A consensus meeting held in Turin established the diagnostic criteria for PDTC assessment, which include solid/trabecular/insular microscopic growth pattern, lack of well-developed nuclear features of PTCs, convoluted nuclei, tumor necrosis and high mitotic index (23). PDTC can either be the terminal stage of dedifferentiation process of PTC and FTC (Figure 1.2) or grow *ex novo* (19). It often presents as a unique thyroid mass rapidly growing, and has high rate of metastatic spread to lymph nodes and distant organs, such as lung and bone. Prognosis of PDTC patients is worse than that of PTC, with a 5 year survival rate from 20 to 60% (24).

1.1.1.4. Anaplastic Thyroid Carcinoma (ATC)

ATC is one of the most aggressive and deadly cancers among humans (25). Like PDTCs, it can develop from a pre-existing DTC or can arise *ex novo* (Figure 1.2). ATC is composed of undifferentiated cells (spindle, epithelioid and pleomorphic giant cells) retaining markers of an epithelial lineage. Histological features include invasiveness, extensive tumor necrosis, pleomorphic nuclei with irregular contours and high mitotic activity with atypical mitotic figures. ATC presents as a large rapidly growing thyroid mass infiltrating surrounding tissues that causes compressive symptoms in patients including dysphagia,

dysphonia, and dyspnea. The peak incidence is in the sixth and seventh decades of life, and the median survival is 6 months from the diagnosis (26). About 50% of patients present distant metastatic disease at the diagnosis, primarily in the lungs but also in bones and brain, and approximately 25% of patients will develop metastases during the clinical course of the disease: it can be so rapid that surgery procedures are often useless.

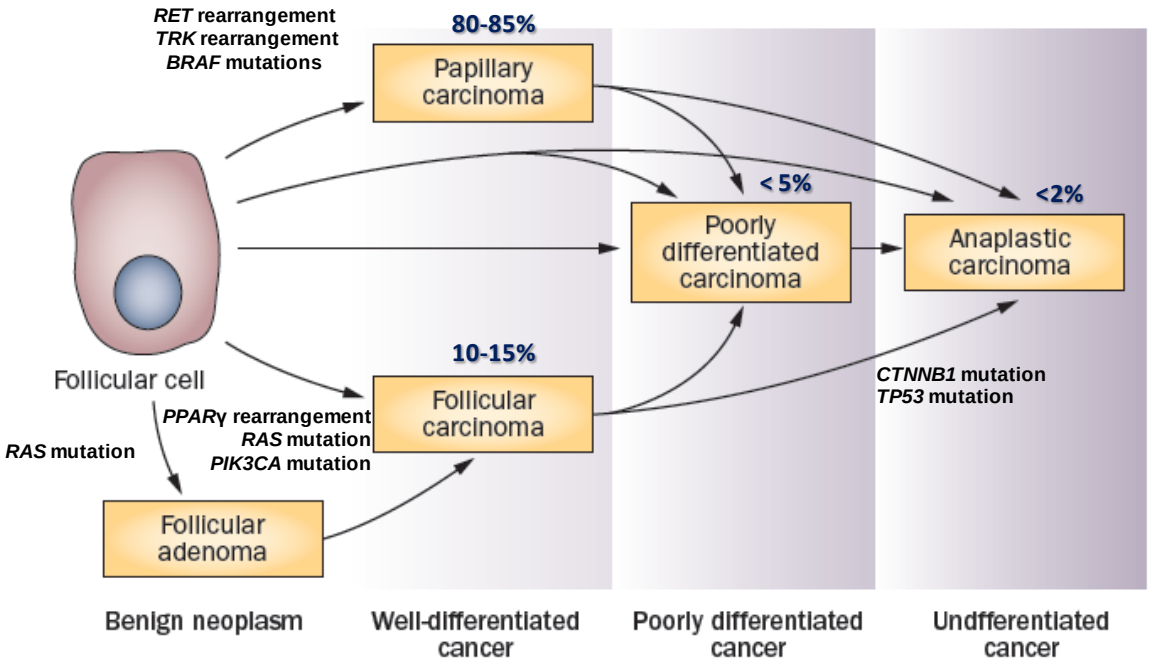

Figure 1.2 Multistep process of thyroid carcinogenesis
Scheme of the development and dedifferentiation of follicular-cell derived thyroid tumors. Tumor frequencies and molecular alterations that drive the multistep process are indicated. Image adapted from (27).

Tumour type	Cell of origin	Prevalence (% of thyroid cancers)	Standard care and prognosis	Characteristics
FTA	Follicular thyroid cells (which produce thyroid hormone and thyroglobulin)	This is a benign lesion	Conservative monitoring; thyroidectomy if symptomatic	Common benign thyroid tumour; similar architecture to FTC, but typically encapsulated; lacking capsular or vascular invasion; lacking metastasis; lacking nuclear features of PTC
PTC*	Follicular thyroid cells	80–85	Thyroidectomy and, in selected cases, radioiodine ablation (novel drugs for resistant disease); good overall prognosis	Well differentiated, with papillary architecture and characteristic nuclear features that include enlargement, oval shape, elongation, overlapping and clearing, inclusions and grooves; propensity for lymphatic metastasis; PTC subtypes include conventional PTC (CPTC), follicular-variant PTC (FVPTC), tall-cell PTC (TCPTC) and a few rare variants
FTC*	Follicular thyroid cells	10–15	Thyroidectomy and radioiodine ablation (novel drugs for resistant cases); good overall prognosis	Well differentiated, hypercellular, microfollicular patterns, lacking nuclear features of PTC; vascular or capsular invasion; propensity for metastasis via the blood stream; Hürthle cell thyroid cancer is a unique subtype of FTC that accounts for 2–3% of thyroid cancers and is characterized by large, mitochondria-rich oncocytic cells and dense nuclei and nucleoli, as well as a high propensity for metastasis and a poor prognosis
PDTC	Follicular thyroid cells	5–10	Surgery, radioiodine (in selected cases), chemotherapy, radiotherapy, novel drugs; poor prognosis	Poorly differentiated, often overlapping with PTC and FTC; intermediate aggressiveness between differentiated and undifferentiated thyroid cancers
ATC	Follicular thyroid cells	2–3	Surgery, chemotherapy, radiotherapy, novel drugs, palliative care; highly and rapidly lethal	Undifferentiated; admixture of spindle, pleomorphic giant and epithelioid cells; extremely invasive and metastatic; highly lethal; may occur *de novo* or derive from PTC, FTC or PDTC

Table 1.1 Characteristics of thyroid tumors
FTA, follicular thyroid adenoma; PTC, papillary thyroid carcinoma; FTC, follicular thyroid carcinoma; PDTC, poorly differentiated thyroid carcinoma; ATC, anaplastic thyroid carcinoma; *PTC and FTC are usually referred together as well-differentiated carcinomas (WDTC). Table adapted from (3).

1.1.2. Genetic alterations in thyroid cancer

In the last decades much effort has been made in studies aimed to identify molecular alterations at the basis of thyroid tumorigenesis (3). Nowadays, it is well known that thyroid cancer originates from various genetic and epigenetic alterations that include: activating/inactivating somatic mutations, alterations in gene expression patterns, microRNA deregulation, aberrant gene methylation; these lesions gradually accumulate to promote tumor progression. The main genetic lesions found in TC consist of point mutation, which is the result of a single nucleotide change within DNA chain, and chromosomal rearrangement, that is a genetic abnormality with breakage and fusion of parts of the same or different chromosomes. Among the different TC histotypes, PTCs have one of the lowest mutation densities of cancers that have been studied by means of whole-exome sequencing (28), while undifferentiated ATCs are characterized by a high

mutation burden (29). To date, it is well known that the main genetic alterations in TC are found in members of the mitogen-activated protein kinase (MAPK) and phosphatidylinositol 3-kinase/protein kinase B (PI3K/AKT) pathways (Figure 1.3).

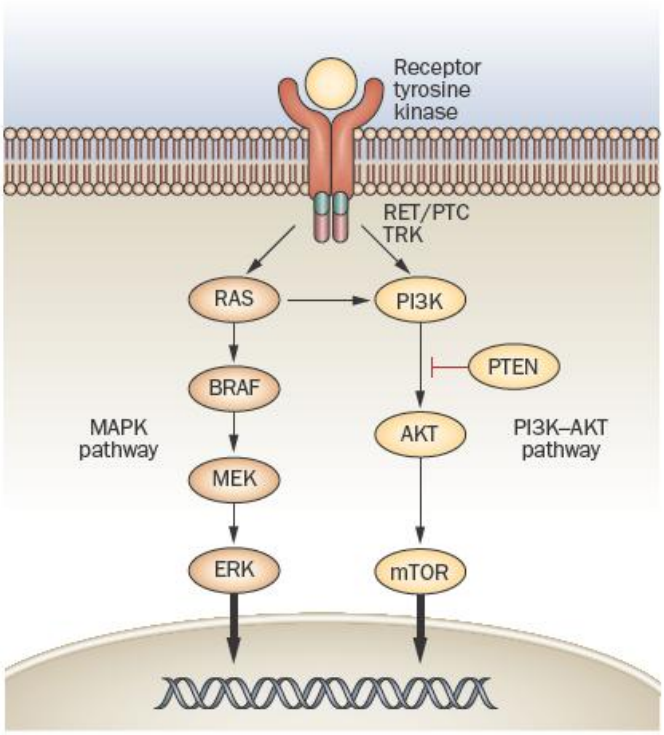

Figure 1.3 Main signaling pathways involved in thyroid carcinogenesis
The main genetic alterations that drive thyroid tumor formation and progression are found in members of the MAPK and PI3K/AKT signaling pathways. These signaling cascades have the important role of propagating signals from external stimuli, via cell membrane receptor tyrosine kinases, into the nucleus, to regulate cell proliferation, differentiation and survival processes. Image adapted from (27).

1.1.2.1. Next-generation sequencing (NGS) revolution

The introduction of next-generation sequencing (NGS) technologies improved, in the recent years, the understanding of alterations of genes and pathways involved in human carcinogenesis and tumor maintenance (30). NGS is a high-throughput method that allows a massive parallel sequencing of multiple targeted genomic regions, thus being more advantageous than the earlier genome-sequencing methods. It has been recently

applied also on thyroid cancer, with the aim of shedding light on the molecular alterations that drive thyroid tumorigenesis (31,32). In 2014, a study by the TCGA consortium had revolutionized the understanding of PTC genomic landscape (33). A comprehensive multiplatform analysis on a cohort of 496 PTC specimens, which was the largest cohort ever analyzed to date, was performed through next-generation DNA and RNA sequencing, copy-number analysis, DNA methylation and proteomic assays; as result, driving oncogenic lesions already known were confirmed, and novel driver mutations and gene fusions were detected, thus reducing from 25% to 3.5% the so-called "dark matter", that is the fraction of PTC cases with unknown genetic drivers. The study also proposed a reclassification of PTC into molecular subtypes, as tool for better management of the disease.

These findings paved the way for following NGS studies performed on FTC (34), PDTC (29) and ATC (29,35), with the aim of improving the knowledge of the genetic landscape thyroid tumors.

1.1.2.2. MAPK signaling pathway

The MAPK signaling pathway plays an important role in the regulation of cell growth and survival and also in human tumorigenic processes. In TC, the importance of this pathway has been well established, as many mutations in members belonging to this signaling cascade were identified (3).

- *BRAF*

BRAF (*v-Raf murine sarcoma viral oncogene homolog B1*) is a proto-oncogene, located on human chromosome 7p24, that encodes a cytosolic serine/threonine protein kinase expressed in most human cells, including thyroid follicular cells (2). BRAF plays a role in the MAPK pathway signal transduction, that is a crucial axis in the regulation of gene expression, cell proliferation and differentiation. Upon RAS activation, wild-type (wt)

BRAF is recruited to the plasma membrane and activated. Activated BRAF triggers sequential phosphorylation of its downstream target, that is mitogen-activated protein kinase kinase (MEK), which, in turn, activates the extracellular signal-regulated kinase (ERK), thus stimulating consequent effectors of the MAPK cascade.

In TC, *BRAF* can be activated by point mutations, small in-frame deletions or insertions, or chromosomal rearrangements, eventually leading to chronic stimulation of MAPK pathway. The most common mechanism of *BRAF* activation is a thymidine to adenine substitution at nucleotide position 1799 in exon 15. This nucleotide transversion results in a valine-to-glutamate replacement (V600E), producing the constitutively active BRAFV600E mutant protein by the disruption of hydrophobic interactions between residues in the ATP binding site (36). Other *BRAF* mutations include adenine to guanine substitution at nucleotide position 1801, which results in a lysine-to-glutamate replacement (K601E), and small in-frame insertions or deletions surrounding codon 600 (37). *BRAF* rearrangement *AKAP9/BRAF* was also described and it is the result of paracentric inversion of chromosome 7q that leads to the fusion of *BRAF*-kinase domain with a portion of *AKAP9* gene (38).

Activating *BRAF* mutations are not specific for TC. On the contrary, *BRAF* mutations were found in many types of cancer (39), with the highest prevalence (50%) in melanoma (40). *BRAF* mutations in TC are commonly found in nearly 60% of PTC (33), and are also present in nearly 30% of PDTC and 45% of ATC (29). It was demonstrated that transgenic mice with thyroid-specific expression of *BRAFV600E* developed PTC closely recapitulating those seen in human tumors (41), thus supporting the role of mutant *BRAF* in tumor initiation and differentiation. A multicentre study showed that *BRAFV600E* mutation was associated with aggressive behavior of PTC, including aggressive clinicopathological features, tumor recurrence and treatment failure (42).

- *RAS*

RAS (*rat sarcoma*) gene family encodes small-GTPases involved in signal transduction from the membrane to the nucleus (43), leading to protein synthesis and regulation of cell survival, proliferation and differentiation. In humans, *RAS* family consists of three genes: *NRAS*, *KRAS* and *HRAS*.

RAS is a monomeric guanosine-nucleotide binding protein which resides in the inner surface of cell membrane and cycles between an inactive form, when bound to guanosine diphosphate (GDP), and an active form, when bound to guanosine triphosphate (GTP). After binding of the ligand to tyrosine kinase and G-protein coupled receptors, RAS switches to the GTP-bound active conformation and transmits signals on downstream pathways, including MAPK and PI3K/AKT cascades. *RAS* mutations were found in many tumor types and are usually limited to a small number of amino acids (12, 13, 59 and 61) (44). These single point mutations cause the loss of the GTPase activity of RAS, which is blocked in the constitutively active GTP-bound form and continuously stimulates signal transduction.

NRAS and *HRAS* mutations at codon 61 are the most common in TC. In PTC, *RAS* mutation is the second most frequent genetic alteration identified (13-20%) and is commonly observed in the follicular variant (27,33). Mutations of *RAS* are found in benign FTAs (3), are common in FTC (49%) (45), and also present in PDTC (45%) and ATC (23%) (46). It is worth to note that, in TC, *BRAF* and *RAS* mutations are mutually exclusive (33,46). Even though activated mutant RAS is not sufficient to induce tumor formation *per se*, it may predispose normal cells to acquire further genetic or epigenetic alterations leading to a fully transformed phenotype (47).

- *RET*

RET (*rearranged during transfection*) encodes a transmembrane receptor tyrosine kinase (RTK) that binds, together with its co-receptors of the GDNF family receptor-α (GFRα1-4) family, members of the glial cell line-derived neurotrophic factor (GDNF) family of extracellular signaling molecules (48). Upon ligand binding to the co-receptor, RET dimerizes and autophosphorylates its intracellular tyrosine residues, which serve as docking sites for adaptor proteins that stimulate multiple downstream pathways such as MAPK and PI3K/AKT (49). *RET* is located in the pericentromeric region of chromosome 10q11.2, and is required for the normal development, maturation and maintenance of several tissues and cell types, such as nervous system, kidney and male germ cells (50). Germline loss-of-function mutations of *RET* cause impaired formation of the enteric nervous system and congenital aganglionosis of the colon (Hirschsprung's disease), while germline activating point mutations are causally related to the hereditary forms of MTC: multiple endocrine neoplasia type 2A and 2B (MEN2A, MEN2B) and familial MTC.

In follicular cell-derived TC, several fusions of *RET* with partner genes, as result of chromosomal rearrangements, were identified (48). *RET* rearrangements, which generate the so-called RET/PTC oncoprotein, occur in 7-20% of PTCs (27,33) and generally result in a juxtaposition of the *RET* 3' sequences, encoding the intracellular tyrosine kinase (TK) domain, with 5' sequences of other partner genes (51). To date, up to 20 different *RET* rearrangements were identified in TC, and all partner genes share the peculiarity of constitutive expression in thyroid follicular cells. The resulting chimeric fusion protein RET/PTC is located in the cytosol, instead of membrane, and is able to form dimers in a ligand-independent manner, leading to chronic stimulation of downstream signaling pathway and tumorigenesis in thyroid cells. The two most common *RET/PTC* rearrangements thus far identified in PTC are *RET/PTC1* and *RET/PTC3*, in which *RET* is

fused to *CCDC6* (also known as *H4*) and *NCOA4* (also known as *ELE1* or *RFG*), respectively. Both rearrangements are intrachromosomal inversions of the long arm of chromosome 10.

Several studies reported an increase in the prevalence of *RET/PTC* rearrangements in PTC patients with a radiation history (52,53). Indeed, ionizing radiations produce double-stranded breaks that can cause the misjoining of chromosome 10 loci, predisposing to intrachromosomal inversion and RET/PTC formation (51).

Apart from PTC, even if rare, *RET/PTC* rearrangements were also found in PDTC and ATC, mainly in tumors associated with a differentiated component (54).

The association of *RET/PTC* rearrangement with clinicopathological features of increased mortality in PTC is still controversial; however, a positive correlation with a more aggressive phenotype and tumor advanced stage was demonstrated in sporadic PTCs with *RET/PTC3* rearrangements, which had both large tumor size and an advanced disease stage at the time of diagnosis; other studies highlighted a role of *RET/PTC3* in metastatic spread (51).

Interestingly, RET rearrangements are not limited to TC, but were identified also other solid tumors such as lung, breast and colon carcinomas (55).

- *TRK*

TRK oncogenes are the product of rearrangements of *NTRK1* (*neurotrophic receptor tyrosin kinase A*, or *TRKA*) gene on chromosome 1q21-22 (56). *NTRK1* encodes the transmembrane high affinity receptor for the nerve growth factor (NGF), which exerts a critical role in the regulation of development and differentiation of peripheral and central nervous system. Following NGF binding, NTRK1 undergoes dimerization and autophosphorylation on intracellular tyrosine residues; these phosphorylated residues recruit adaptor proteins that activate multiple downstream pathways, such as MAPK and

PI3K/AKT (57). These signals, similar to those triggered by RET, culminate in the induction of genes that regulate cell proliferation and survival.

Deregulation of NTRK1 signaling was found associated with different human diseases: *NTRK1* mutations were found in CIPA (Congenital Insensitivity to Pain with Anhidrosis (58), acute myeloid leukemia (59), and deregulated NGF/NTRK1 activity was found associated with prostate (60) and breast (61) cancer development.

Several *TRK* oncogenes originating from *NTRK1* rearrangements were found in TC, particularly in the PTC histotype (56). The most frequent is *TRK*, that results from the fusion of the *NTRK1* sequence, encoding the TK domain, to sequences from of the *non-muscle tropomyosin* (*TMP3*) gene on chromosome 1q22-23. Other rearrangements include *TRK-T1* and *TRK-T2*, which derive both from the rearrangement of *NTRK1* with *translocated promoter region* (*TPR*) gene located on chromosome 1q25, but each displaying a different structure. *TRK-T3* oncogene derives from the fusion of portions of *NTRK1* and the ubiquitously expressed *TRK-fused gene* (*TFG*), located on chromosome 3q11-12 and first identified in this rearranged version (62).

Somatic rearrangements of *NTRK1* account for about 1-2% of genetic alterations in PTC. Although occurring less frequently than *RET* rearrangements, experimental evidence indicate that *TRK* oncogenes represent an early event in the thyroid carcinogenesis, as transgenic mice carrying *TRK-T1* under control of thyroglobulin promoter (Tg-TRK-T1 mice) develop hyperplasia and PTC (63).

As for *RET*, also *NTRK1* rearrangements were identified in solid tumors besides PTC: these consist in colorectal cancer, lung cancer, pediatric brain tumors and glioblastoma, cholangiocarcinoma and sarcoma (55).

1.1.2.3. PI3K/AKT signaling pathway

PI3K/AKT signaling pathways plays an important role in the regulation of several cellular functions such as growth, motility and survival (64). The relevance of this pathway in human tumorigenesis and its targeting as therapeutic approach have been widely investigated in the last decade (65,66), also in thyroid tumors (67).

- *PIK3CA*

Phosphatidylinositol-4,5-Bisphosphate 3-Kinase Catalytic Subunit α (*PIK3CA*) encodes the 110 kDa catalytic subunit of the class I PI3 kinase complex that is activated by RTKs and, when active, phosphorylates phosphatidylinositol-4,5-bisphosphate to produce phosphatidylinositol-3,4,5-trisphosphate (PIP3), the activator of AKT.

PIK3CA involvement in human cancer development is well documented, as somatic activating mutations of this gene were identified in a variety of tumors, such as colorectal, breast and ovarian carcinomas (68). In the context of thyroid, mutations of *PIK3CA* were identified in FTC and ATC histotypes, with a frequency of 10-15%, and in PDTC and ATC either recurrent or with metastatic disease (64). Also *PIK3CA* copy-number gain is reported in TC, mainly in FTC and ATC and uncommonly in PTC. This alteration results in *PIK3CA* amplification and is associated with overexpression of the protein and hyper-phosphorylation of AKT.

- *PTEN*

Phosphatase and tensin homolog (*PTEN*) encodes the protein phosphatase responsible for the degradation of PIP3, thus antagonizing and terminating the PI3K/AKT signaling. *PTEN* has a crucial role as tumor suppressor gene and different mechanisms inhibiting its activity were described for human cancers, including TC (64). These mechanisms include somatic mutations (although with low frequency), loss of heterozygosity or deletion, and promoter hypermethylation. Germline inactivating mutations of *PTEN* cause Cowden's

syndrome and predispose patients to develop tumors, including FTC. *PTEN* alterations are found in FTC and, more commonly, in ATC (15%) where, together with other genetic alterations of members of the PI3K/AKT pathway, can ideally cooperate and contribute to the aggressiveness of this thyroid tumor (29).

1.1.2.4. Other mutations

- *PAX8/PPARγ*

The *paired box 8/peroxisome proliferator-activated receptor-γ* fusion gene (*PAX8/PPARγ*) is another recombinant oncogene in TC, originating from translocation between chromosomal regions 2q13 (*PAX8*) and 3p25 (*PPARγ*) (69). PAX8 is a member of the paired box family of transcription factors required for normal thyroid development; it also induces the expression of thyroid-specific genes in the mature thyroid. PPARγ is a member of the nuclear receptor family of transcription factors and is the master regulator of adipogenesis; it is expressed at very low levels and has no known function in the normal thyroid. The fusion product *PAX8/PPARγ* encodes a nearly full length PPARγ, whose expression is under transcriptional control of PAX8 promoter which is highly active in thyroid follicular cells. Several *in vitro* experiments provided evidence that *PAX8/PPARG* acts as oncogene in TC (70-72), although the specific mechanism is yet to be defined. *PAX8/PPARγ* rearrangements are prevalent in FTC (30-35%), follicular variant of PTC (13%), and follicular adenomas, while they are absent in undifferentiated PDTC and ATC (73).

- *TP53*

TP53 encodes a transcription factor that acts as tumor suppressor, playing a pivotal role in regulation of cell proliferation, DNA damage response and apoptosis (74). In physiological conditions, p53 forms a complex with MDM2, an E3 ubiquitin protein ligase that promotes its degradation by the proteasome. Upon DNA damage or other cellular

stresses, various pathways activate and culminate in p53 activation by promoting its dissociation from MDM2. Once activated, p53 binds to DNA and drives the expression of several genes that lead to cell cycle arrest, apoptosis and/or senescence, contributing to the maintenance of genome stability. *TP53* mutations are found in up to 50% of human cancers and are generally loss-of-function missense mutations (75). *TP53* mutations are rare in well-differentiated PTC and FTC (76) and also in PDTC (about 8% of frequency), while they are a common genetic event in the undifferentiated ATCs (up to 73% of cases) (29). It was demonstrated that *TP53* mutations have a role in the progression from well-differentiated TC to the most aggressive ATC (77), thus supporting the notion that TC initiation and progression occurs through gradual accumulation of multiple genetic lesions.

1.1.3. Treatment of thyroid cancer

1.1.3.1. Conventional therapy

The treatment of choice for well-differentiated primary thyroid tumors is surgery, that consists of partial lobectomy or total thyroidectomy, based on the dimensions and the clinicopathological features of the thyroid nodule detected (78). Controversy still exists on the extent of the surgery: partial lobectomy was shown to have the same effects on patient overall free survival as total thyroidectomy did, but with less frequent adverse events (such as hypocalcemia and laryngeal nerve paralysis) (79). Nevertheless, with the exception of unifocal low-risk PTCs smaller than 1 cm, the American Thyroid Association (ATA) guidelines recommend the complete removal of the thyroid to minimize the risks of malignancy relapse (80). Together with the thyroid, patients diagnosed with primary PTC undergo lymph node removal even in the absence of clear nodal metastases, since from

22% to 90% of PTCs spread locally to lymphoid glands. Following surgery, patients are usually treated with radioactive iodine (RAI, ^{131}I), in order to remove potential occult WDTC foci and decrease the long-term risk of tumor recurrence. In addition to surgery and RAI, thyroid-stimulating hormone (TSH) suppressive treatment is practiced to prevent major adverse clinical events, since WDTCs are usually responsive to TSH stimulation in terms of cell growth. WDTC are generally cured by standard therapy; nevertheless, tumor recurrence can happen, as in up to 20% of patients the tumor relapses and in 10% of patients distant metastases occur (81).

Management of the undifferentiated ATCs is more challenging: surgical removal of the thyroid remains the first choice of therapeutic intervention, but many patients often present at diagnosis with extended local disease invading the surrounding structures (such as trachea and larynx) that makes the tumor mass unresectable (25). Moreover, ATCs are usually refractory to RAI therapy. When surgery is feasible, thyroidectomy is combined with locoregional radiation therapy and chemotherapy with agents such as taxanes or platinum-based antineoplastic drugs, like carboplatin. For patients with unresectable disease, palliative therapy to preserve the airway is mandatory, and a combination of radiations and chemotherapy is applied with the aim of achieving local tumor regression and/or durable local tumor control. However, even if multimodality therapy has shown to prolong patient survival, a successful standardized protocol has not been defined yet and the optimal sequence of multimodality therapy still remains to be determined.

1.1.3.2. Novel therapies

In the last decades, the increased knowledge on the molecular events that drive tumorigenesis allowed the development of the so-called precision medicine (82): in cancer, including TC, the improved understanding of the pathogenesis and genetics of

tumors prompted the development of new therapeutic opportunities for patient treatment (Figure 1.4) (83).

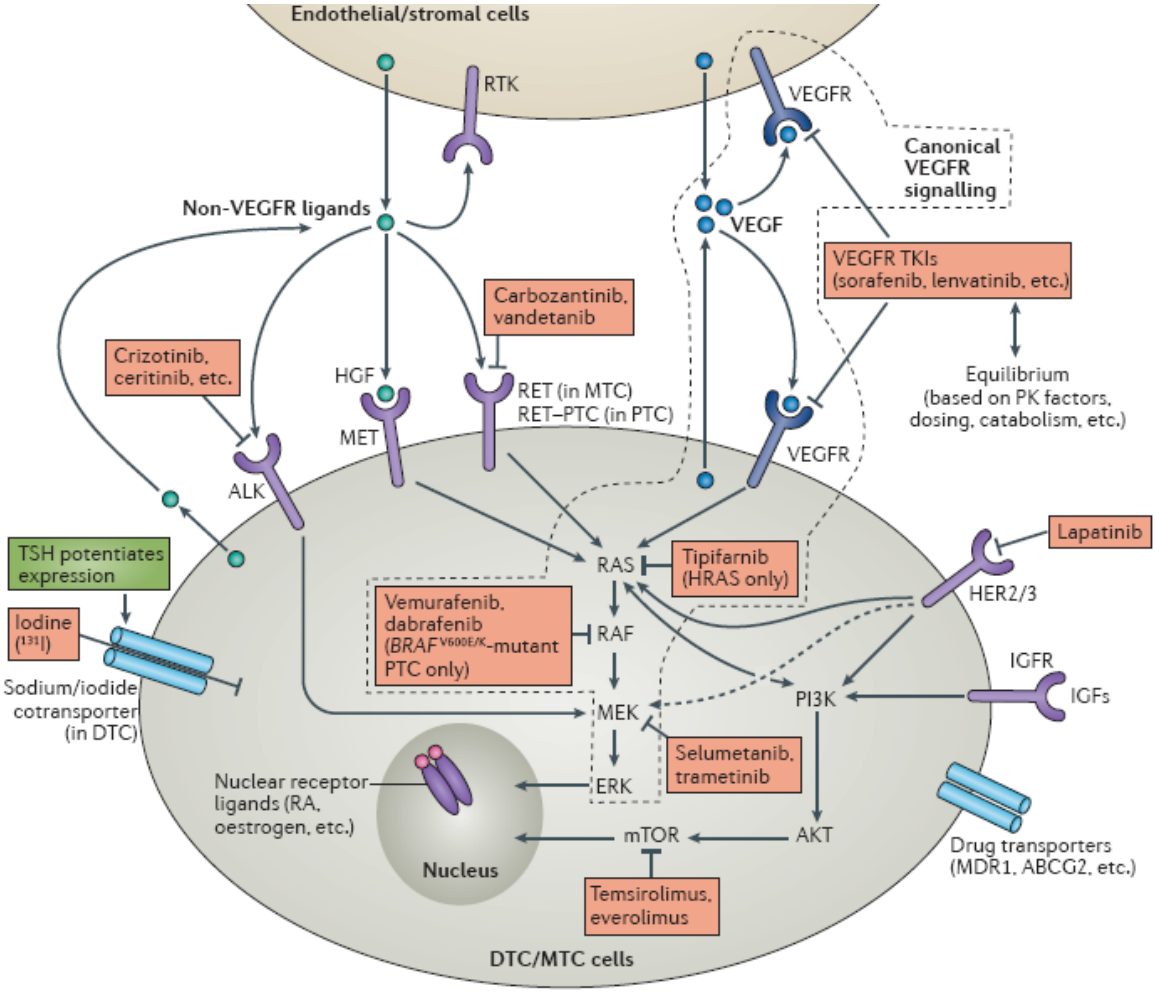

Figure 1.4 Signaling pathways involved in TC pathogenesis and their relevant inhibitors
Kinase receptors are shown with their corresponding ligands and downstream signaling pathways. Pharmacological inhibitors, which operate at different levels in signaling pathways, are indicated. Image from (83).

A variety of molecular-targeted agents able to inhibit RTKs or downstream effectors is nowadays available. These small molecules are competitive inhibitors of the ATP-binding domains of multiple kinases and acquired great interest as most of their targets belong to the main pathways involved in TC pathogenesis and progression. The potential of this relatively new class of drugs is that their activity may not be restricted to only one target, but that can act on multiple signaling pathways. WDTCs are characterized by increased

peritumoral angiogenesis and high secretion of the vascular endothelial growth factor (VEGF), and the blockade of its receptor (VEGFR) has shown promising results in attenuating tumor cell growth in vivo. Small-molecule tyrosine kinase inhibitors (TKI) often inhibit, in addition to the target kinase, VEGFR and other angiokinase receptors (such as PDGFR, FGFR), thus hindering multiple signaling pathways of potential therapeutic relevance (Table 1.2).

DRUG	VEGF-R	c-Kit	RET	PDGF-R	FGF-R	EGF-R	Other targets	Study phase	Approved for thyroid cancer treatment
Axitinib	Yes	Yes	No	Yes	No	No		II	No
Bevacizumab	No	No	No	No	No	No	dual PI3K/mTOR	II	No
Cabozantinib	Yes	Yes	Yes	No	No	No	MET, *RET- KIF5B rearrangement*	III*	Yes
Imatinib	No	Yes	No	Yes	No	No	Bcr-Abl	II	No
Lenvatinib	Yes	Yes	Yes	Yes	Yes	No	*RET-KIF5B, CCDC6-RET, NcoA4-RET rearrangement*	III*	Yes
Motesanib	Yes	Yes	Yes	Yes	No	No		II	No
Nintedanib	Yes	No	No	Yes	Yes	No		II	No
Pazopanib	Yes	Yes	No	Yes	No	No		II	No
Ponatinib	No	No	Yes	Yes	Yes	No	*Bcr-Abl*, FLT3, KIT	II	No
Selumetinib	No	No	No	No	No	No	MEK	III	No
Sorafenib	Yes	Yes	Yes	Yes	No	No	Raf, FLT3	III	Yes
Sunitinib	Yes	Yes	Yes	Yes	No	No	FLT3	II	No
Vandetanib	Yes	Yes	No	No	No	Yes	*RET-KIF5B rearrangement*	III*	Yes
Vemurafenib	No	No	No	No	No	No	$BRAF^{V600E}$, CRAF	II	No
Everolimus	No	No	No	No	No	No	mTOR	II	No
Temsirolimus	Yes	No	No	No	No	No	mTOR	II	No

Table 1.2 Small-molecule TKIs and their targets tested in clinical trials for TC
Adapted from (84)

Among the several TKIs tested in phase I, II and III trials for TC treatment, only 4 of them were approved for clinical treatment: sorafenib and lenvatinib for progressive DTC, vandetanib and cabozantinib for MTC (84). Despite the longer patient-free survival duration relative to placebo in randomized clinical trials, these drugs produced several side verse effects in patients (Table 1.3) and, to date, few data are available about the prolongation of patient overall survival. Of note, treatment of ATC with TKIs has still to be rigorously studied and defined: among the variety of molecules previously listed, only lenvatinib showed promising antitumor activity in ATC patients (85).

Drug	Vandetanib	Cabozantinib	Sorafenib	Lenvatinib
Name of the study	ZETA	EXAM	DECISION	SELECT
Tumour	MTC	MTC	DTC	DTC
Phase	III	III	III	III
Patients (*n*)	331	330	417	392
Partial response (%)	45	28	12.2	64.8
Stable disease ≥ 6 months (%)	87	NE	42	15.3
Median progression-free survival (months)	30.5*	11.2	10.8	18.3
Median overall survival (months)	NE	NE	NE	NE
Most frequent adverse events (%) Any grade	Diarrhoea (56) Skin rash (45) Nausea (33) Hypertension (32)	Diarrhoea (63) Hand-foot syndrome (50) Weight loss (47) Anorexia (45) Nausea (43) Fatigue (40)	Hand-foot syndrome (76) Diarrhoea (68) Alopecia (67) Skin rash (50) Fatigue (49) Weight loss (46) Hypertension (40) Anorexia (31)	Hypertension (67) Diarrhoea (59) Fatigue or asthenia (59) Anorexia (50) Weight loss (46) Nausea (41) Stomatitis (35)
Molecular targets	VEGF-R, c-Kit, RET, EGF-R, *RET-KIF5B rearrangement*	VEGF-R, c-Kit, RET, MET, *RET-KIF5B rearrangement*	VEGF-R, c-Kit, RET, PDGF-R, Raf, FLT3	VEGF-R, c-Kit, RET, PDGF-R, FGF-R, *RET-KIF5B, CCDC6-RET, NcoA4-RET rearrangement*

Table 1.3 TKIs approved for the treatment of TC and details of phase III trials
Adapted from (84)

As mortality is increased for patients with WDTCs that become refractory to RAI therapy, another strategy that has been developed in the last decades is the development of agents that promote tumor re-differentiation, which can make tumors radioiodine-avid again and therefore treatable with ^{131}I. Several agents, among which retinoic acid, were tested in RAI-refractory patients but gave no significant benefits (86). A promising candidate for RAI-resensitization is the MEK inhibitor selumetinib, which has been able to increase the uptake of RAI and gave a partial response and decrease in tumor size, especially in patients with *NRAS*-mutant tumors (87).

Another therapeutic approach for TC cell re-differentiation is the use of epigenetic drugs, specifically histone deacetylase (HDAC) inhibitors. Epigenetic alterations in tumor cells often result in the silencing of genes involved in cell differentiation, given by the hypermethylation of cytosines of the promoter and the subsequent recruitment of HDACs to repress expression of the genes (88). There are various classes of HDACs in cells, thus different compounds were developed to specifically target one class or another.

Suberoylanilide hydroxamic acid (SAHA, Vorinostat®) is a pan-HDAC inhibitor that was able to increase Na^+/I^- symporter (NIS) expression and reduce WDTC and ATC cell growth *in vitro*. Romidepsin (Istodax™) is a class I-HDAC inhibitor able to restore RAI avidity in some TC patients and therefore could potentially increase the response to RAI therapy. Panobinostat (Fraydak®) induced re-expression of NIS and increased response to RAI treatment *in vitro*, while valproic acid (Depakene®) was able to increase NIS mRNA expression. Nevertheless, none of these compounds produced significant responses in the clinics to date.

1.1.3.3. Conclusions

Despite the improvement of TC therapy, some areas of uncertainty persist (84). Limitations of targeted therapy are mainly made by the toxicity profiles that usually lead to the reduction of therapy doses, the onset of escape mechanisms of resistance to treatment, and notably no data about the long-term effects on patient quality of life is available. ATC still remains one of the deadliest diseases worldwide, as no effective therapy has been identified to date and targeted therapies are now tested in phase II clinical trials.

1.2. Non-Oncogene Addiction

1.2.1. Oncogene and non-oncogene addiction principles

Nowadays it is well known that cancer arises from a mutagenic multistep process during which transforming cells acquire several properties, such as uncontrolled proliferation, resistance to antiproliferative signals and resistance to apoptotic stimuli (89). These properties are shared by all tumor cells and are achieved through random mutations and epigenetic changes in oncogenes and tumor suppressor genes, which eventually lead to the modification of already existing cellular programs normally used during development. The concept of “oncogene addiction” indicates the dependency of tumor cells on the activity of oncogenes and oncogenic pathways that are essential for tumor cell survival (90). This concept put the rationale for therapeutic intervention by targeting the mutated components of key cellular pathways on which tumor cells became dependent. A variety of drugs targeting specific oncogenes in different tumors were developed and tested, such as HER2 in breast cancer (91), BRAF in melanoma (92), EGFR in non-small cell lung cancer (93) and BCR-ABL in chronic myeloid leukemia (94). However, even though remissions were observed in some cases, these were often followed by the recurrence of drug-resistant tumor cells. Moreover, the targeting of oncogenes like RAS or MYC is complex, as the identification of compounds specifically targeting them is difficult. Based on these observations, the “synthetic lethality” concept was exploited. It indicates a phenomenon of lethal combination of mutations/perturbations in two genes, where mutations in only one of those genes have no effect on cell viability (95). The targeting of a synthetic lethal partner of a mutated driver gene in tumor cells may provide two main advantages: the overcoming of the lack of inhibitors for certain oncogenes and the sparing of normal cells during therapeutic

intervention. An example of promising synthetic lethality application in the clinics is the use of poly ADP-ribose polymerase (PARP) inhibitors in advanced ovarian cancer patients with mutations in *BRCA1/2*, which exhibit specific DNA repair defect and result sensitive to this class of drugs (96).

Beyond the concept of oncogene addiction, it was observed that tumor cells often face increased levels of cellular stresses, caused by the sustained activation of oncogenic pathways, compared to normal cells (97). This phenomenon was referred to as "stress phenotype" of cancer cells (Figure 1.5).

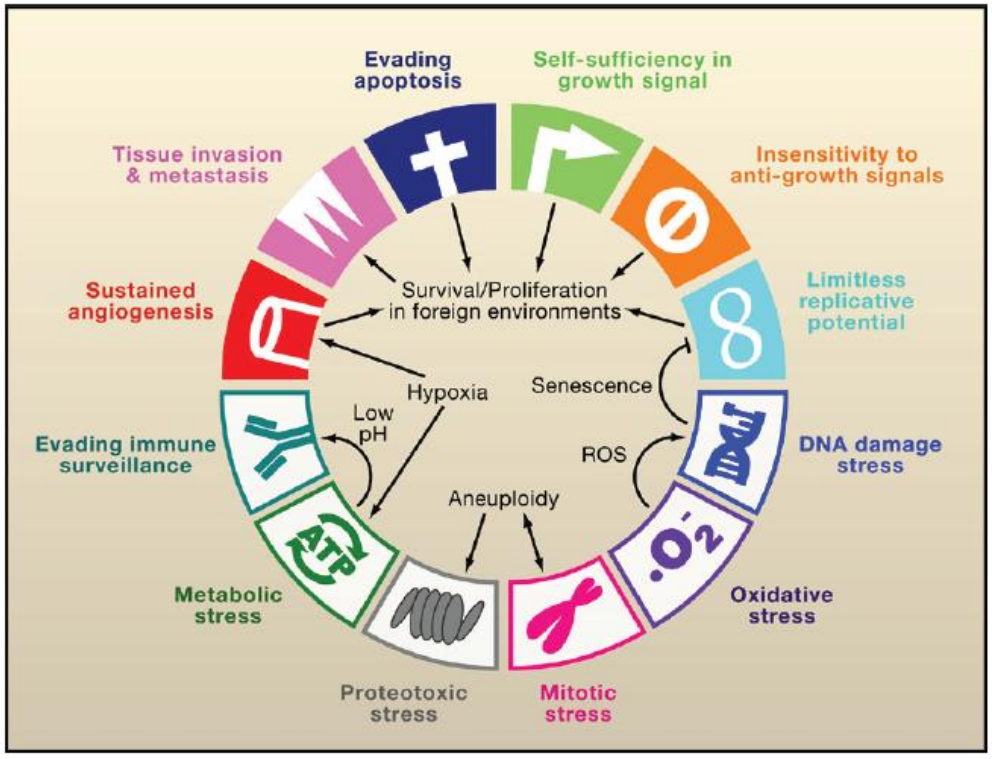

Figure 1.5 The hallmarks of cancer revisited
In addition to the six hallmarks of cancer initially proposed by Hanahan and Weinberg (89), additional hallmarks were proposed, in order to highlight the "stress phenotype" of cancer cells. These new hallmarks include DNA damage, metabolic, oxidative, mitotic and proteotoxic stresses and, together with the other cancer hallmarks, promote the tumorigenic state of cancer cells. Image from (98)

Increased cellular stresses associated with the oncogenic activity are tolerated by cancer cells through the activation of stress support pathways, on which they become therefore

addicted. These genes act in oncogenic pathways but are not classical oncogenes themselves, as they are not mutated, aberrantly expressed or responsible for tumorigenesis initiation (98). This phenomenon has been termed “non-oncogene addiction” (NOA) and highlights the potential of non-oncogenes as point of intervention for cancer therapy, since the impairment of their functions would ideally be lethal for tumor cells while sparing normal ones (Figure 1.6).

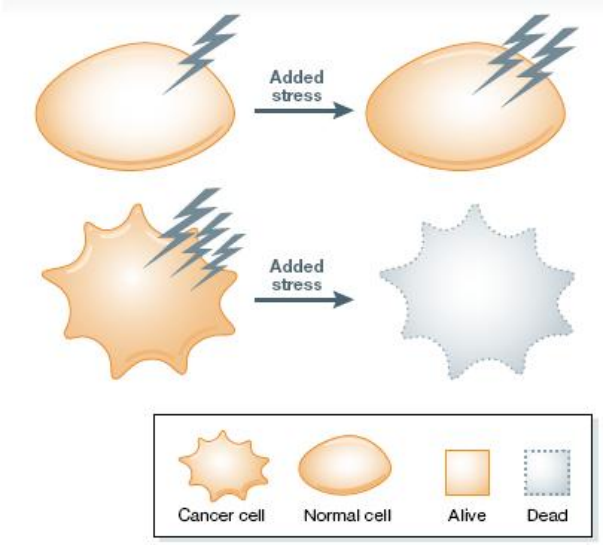

Figure 1.6 Schematic representation of cellular non-oncogene addiction effects
Cancer cells, according to NOA paradigm, face elevated cellular stresses produced by collateral events of the tumorigenic process. Interfering with the stress support pathways in tumor cells will lead to their killing, while normal cells are able to tolerate these perturbations. Image adapted from (99).

Tumor cell dependencies on NOA genes provide an attractive target for therapeutic intervention, which could be achieved through two different approaches: stress sensitization, that consists in diminishing the activity of stress support pathways in order to promote cell growth inhibition and cell death, and stress overload, that aims to intensify oncogenic stress to overload the stress support pathways in tumor cells and eventually lead to growth arrest or cell death. Stresses faced by tumor cells are DNA damage, mitotic, proteotoxic, metabolic and oxidative stress (Figure 1.7).

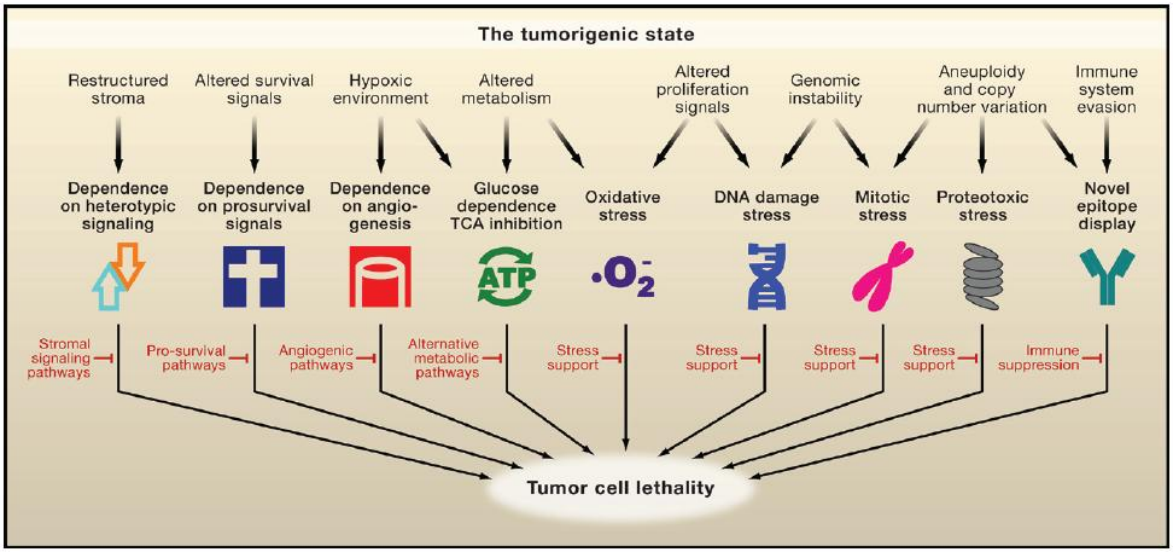

Figure 1.7 Non-oncogene addiction examples in tumor cells
The tumorigenic state of cancer cells results in several alterations of cellular homeostasis related to the hallmarks of cancer, described in Figure 1.5. These alterations represent potential tumor vulnerabilities, and interfering with regulators of these support pathways could display synthetic lethality with the tumor phenotype. Image from (98)

Because of the high degree of replication and the activity of oncogenes themselves, the rate of spontaneous DNA damage in tumor cells is increased, compared to the normal ones. Indeed, several studies demonstrated that inhibition of members of DNA damage response pathway, such as ATM and CHK1, exerted selective toxicity on tumor cells, as they increased DNA damage stress. Linked to the high degree of replication of tumor cells, there is also mitotic stress, which is the result of increased rates of chromosome segregation errors caused by mutations altering mitosis fidelity. The inhibition of proteins regulating mitosis was found effective in sensitizing tumor cells to stress overload, as it is commonly observed upon treatment with taxol or mitotic kinase inhibitors. Transcriptional alterations and copy-number variations normally happening in tumor cells also result in proteotoxic stress: these changes often produce alterations of protein dosage balance, thus resulting in steady activation of chaperone pathways to maintain normal proteome homeostasis and, in case of unfolded proteins, of the ubiquitin-

proteasome pathway. Indeed, inhibition of the proteasome with bortezomib has proven to be deleterious for tumor cells, and provides an example of proteotoxic stress overload. All these lines of evidence support the concept that NOA genes are attractive targets for therapeutic intervention, since they represent key functional nodes in the oncogenic network and their inhibition would result in system failure. According to the NOA paradigm, several groups already provided promising results in "targeting of non-oncogene addiction": PARP inhibition in glioblastoma (100), silencing of heat shock factor 1 (HSF1) in multiple cancer cells (101), and HDAC6 inhibition in breast cancer (102) resulted in inhibition of tumor cell growth.

1.2.2. Tools for the identification of cancer cell vulnerabilities

The traditional approach used to identify potential targets for cancer treatment, in the last decades, consisted in the identification of the specific genetic lesions at the basis of tumorigenic process, such as copy-number variations, gene mutations, transcriptional changes and epigenetic modifications (103). Despite being a powerful approach for identifying genetic changes in oncogenes or tumor suppressor genes, some limitations persist: sequencing techniques nowadays mostly limit to coding regions and therefore NOA genes and pathways are not detected, since they are not directly mutated albeit supportive in the tumorigenic process. However, the revolution of RNA interference (RNAi) technologies allowed the development of a functional approach to identify such critical nodal points for cancer therapeutic intervention (104). Functional RNAi screenings are indeed able to identify cancer vulnerabilities, as the investigation is not limited to mutated genes, such as oncogenes, but also includes genes and pathways important for tumor sustainment, that is NOA genes. This strategy is also powerful in terms of target

discovery, as either partial or complete loss of protein function strictly mimics the effects of a pharmacological inhibitor. The wide development of commercially available large-scale RNAi libraries, that can be constructed with different strategies (Figure 1.8), contributed to the improvement of the use of large-scale RNAi-based screenings with the aim of dissecting complex biological processes (105). Such large scale RNAi-based functional screenings performed both *in vitro* (106-108) and also *in vivo* (109,110) were successful in identifying genes essential for the regulation of different types of cancer.

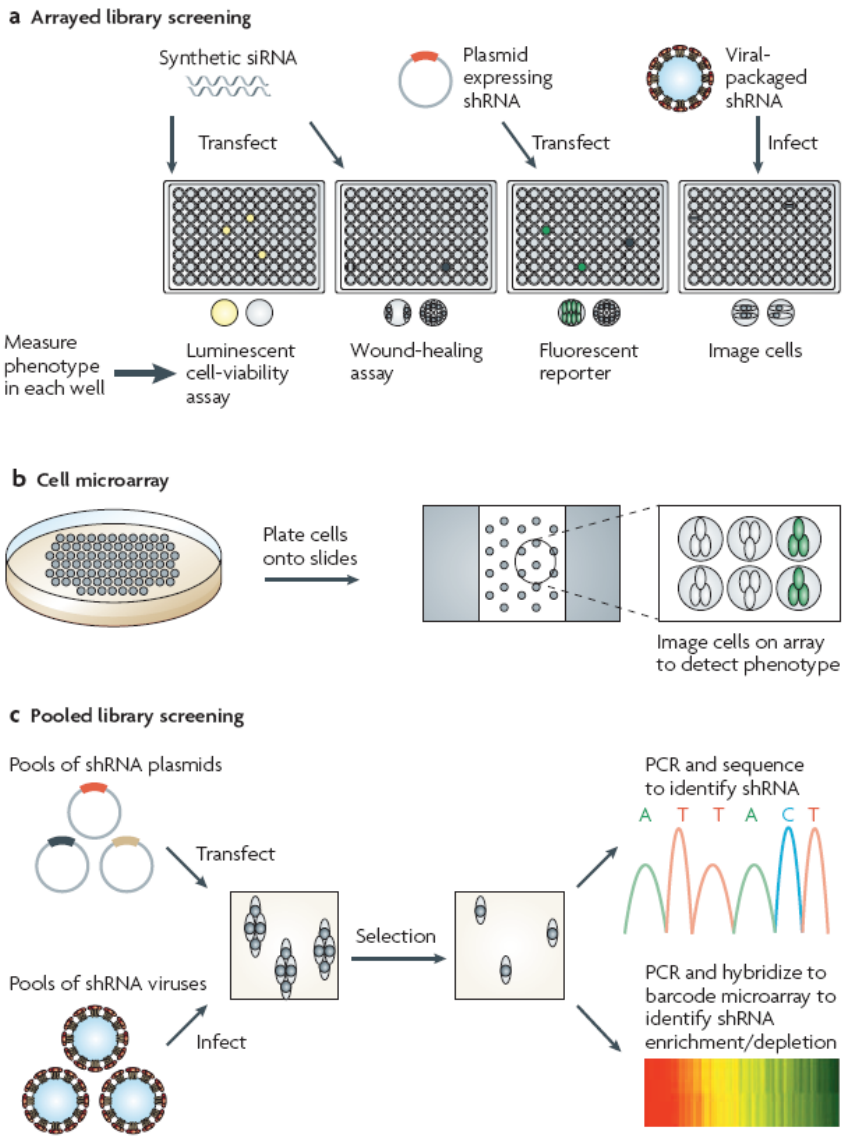

Figure 1.8 RNAi library screening approaches

RNAi screenings can be performed using different strategies. Arrayed library screening, using synthetic small interfering RNAs (siRNAs) or short hairpin RNAs (shRNAs), target each gene separately in a multiwell format and various readouts can be used to determine the silencing effect on the phenotype of interest *(a)*. Arrayed screening using cell microarrays allow to plate cells directly onto microarrays containing the siRNAs/shRNAs, and the target gene is identifiable by the position on the array *(b)*. Pooled library screens target many genes pools of shRNA expressing vectors are introduced into cells by transfection or infection for pooled library screening; cells are exposed to a selective agent and the shRNA-plasmids present in surviving cells are identified by DNA sequencing or barcode microarray analysis *(c)*. Image from (111).

Aim of the study

The non-oncogene addiction paradigm highlighted novel tumor cell vulnerabilities that could represent potential points for therapeutic intervention in cancer. Moreover, the improvement of RNAi technologies allowed the development of new tools, that are large-scale RNAi screening libraries, for the investigation of these critical nodal points in the complex cancer network. While NOA was approached for tumors such as myeloma and breast cancer, in the context of thyroid cancer the NOA paradigm is a completely novel concept. Given that current therapies for thyroid tumors are not always effective, particularly for the most aggressive and advanced cases, the identification of TC cell vulnerabilities would be useful for the development of new therapeutic approaches.

Using a siRNA library targeting the whole "druggable" genome, our laboratory has previously performed a loss-of-function based screening on a tumor and a normal thyroid cell lines, in order to identify genes whose silencing interfered with the growth of tumor but not normal cells. This screening allowed us to identify 15 differentially active hits in the tumor versus the normal cell lines.

The overall aim of the project was the identification of thyroid tumor cell vulnerability genes, according to the NOA paradigm, and the dissection of their role in thyroid tumor cell biology, in order to unveil potential novel targets for thyroid cancer treatment. Most of the work was devoted to hit gene validation studies and to studies on *MASTL*, a vulnerability gene we identified in TC cells. These two sections have been well developed and hereafter presented in two distinct chapters. The thesis includes a third chapter that summarized the studies regarding *COPZ1*, which is another vulnerability gene identified in TC cells, to which I collaborated.

2. Materials and methods

2.1. Cell Biology

2.1.1. Cell culture

Nthy-ori 3-1 cell line (SV-40 immortalized normal human thyroid follicular cells) was purchased from European Collection of Cell Cultures (ECACC) (Salisbury, UK); tumor BCPAP, TPC-1, WRO82-1, 8505C and KAT-18 cell lines were obtained from Prof. A. Fusco (University of Federico II, Naples, Italy); HTC/C3 cell line was purchased from Riken Cell Bank (Tsukuba, Japan). Information regarding the histotype derivation of cell lines and the mutational status are provided in Table 2.1. HEK 293T cell line was purchased from American Type Culture Collection (ATCC).

Nthy-ori 3-1 cells were cultured in RPMI 1640 medium (Gibco Life Technologies, Carlsbad, CA, USA) supplemented with 10% heat-inactivated fetal bovine serum (FBS) (EuroClone, Pero, Italy). The other cell lines were maintained in DMEM medium (Gibco Life Technologies, Carlsbad, CA, USA) containing 10% FBS and 2mM glutamine. All cell lines were cultured as monolayer at 37°C in a 5% CO_2 humidified atmosphere.

Cell lines were authenticated by short tandem repeat (STR) profiles using Stem Elite ID System (Promega Corporation, Madison, USA) by the Fragment Analysis Facility of Fondazione IRCCS Istituto Nazionale dei Tumori. The profiles obtained matched to their original profiles (112,113). WRO82-1 profile matched to that reported by Xu and colleagues (114) and HTC/C3 to that reported by JCRB Cell Bank (http://cellbank.nibio.go.jp/legacy/celldata/jcrb0164.htm).

Mycoplasma contamination was tested periodically and found negative in all cell lines (PCR Mycoplasma Detection Set, TAKARA Bio Inc).

Table 2.1 List of thyroid cell lines with histological derivation and mutational status

Cell lines	Hystological type	Mutational status
Nthy-ori 3-1	normal human thyrocytes	
BCPAP	PTC	BRAF V600E
TPC-1	PTC	RET/PTC1
WRO82-1	FTC	
8505C	ATC	BRAF V600E; TP53 R248L
HTC/C3	ATC	BRAF V600E; TP53 P152L
KAT-18	ATC	

2.1.2. Cell transfection and gene silencing

Transient gene silencing of the hit genes was obtained in thyroid cell lines by the transfection of specific siRNAs, detailed in Table 2.2, using Lipofectamine RNAiMAX reagent (Invitrogen Life Technologies, Carlsbad, CA, USA), according to manufacturer's protocol. Briefly, cells were seeded at the optimal density and transfected the following day by adding a mixture of Opti-MEM (Reduced Serum Media) (Gibco Life Technologies, Carlsbad, CA, USA) containing 20 nM siRNA and 3 µl/ml Lipofectamine RNAiMAX.

Table 2.2 List of siRNAs used for gene silencing

siRNA	Sequence/catalog number	Source
siNT	ON-TARGET plus Non-targeting Pool siRNA D-0018-10-05	ThermoScientific, Dharmacon Inc., Chicago, IL, USA
siPSMC3	MISSION esiRNA EHU107331	Sigma-Aldrich, St. Louis, MO, USA
siMASTL #1	ON-TARGET plus set of 4 siRNAs J-004020-12 5'-CCAUUGAGACGAAAGGUUU-3'	ThermoScientific, Dharmacon Inc., Chicago, IL, USA
siMASTL #2	ON-TARGET plus set of 4 siRNAs J-004020-11 5'-GCAAAUUGUAUGCAGUAAA -3'	ThermoScientific, Dharmacon Inc., Chicago, IL, USA
siMASTL #3	ON-TARGET plus set of 4 siRNAs J-004020-10 5'-ACUGGACGCUCUUGUGUAA-3'	ThermoScientific, Dharmacon Inc., Chicago, IL, USA
siMASTL #4	ON-TARGET plus set of 4 siRNAs J-004020-09 5'-GGACAAGUGUUAUCGCUUA-3'	ThermoScientific, Dharmacon Inc., Chicago, IL, USA
siMASTL#5	5'-UGUGGAUUCUGGUGGGAUAdTdT 3'	in house
siCCND1	MISSION esiRNA EHU153321	Sigma-Aldrich, St. Louis, MO, USA
siCOPZ1	MISSION esiRNA EHU1040461	Sigma-Aldrich, St. Louis, MO, USA
siMAP4K5	MISSION esiRNA EHU120861	Sigma-Aldrich, St. Louis, MO, USA
siCOPE	MISSION esiRNA EHU069701	Sigma-Aldrich, St. Louis, MO, USA
siPLA2G15 #1	ON-TARGET plus set of 4 siRNAs J-009622-08 5'-GAAGAUGGCUGGCUCAUGC-3'	ThermoScientific, Dharmacon Inc., Chicago, IL, USA
siPLA2G15 #2	ON-TARGET plus set of 4 siRNAs J-009622-07 5'-GCGAUGGUACUGUGAACUU -3'	ThermoScientific, Dharmacon Inc., Chicago, IL, USA
siPLA2G15 #3	ON-TARGET plus set of 4 siRNAs J-009622-06 5'-GGAGAUGUACCAGCUGUAU -3'	ThermoScientific, Dharmacon Inc., Chicago, IL, USA
siPLA2G15 #4	ON-TARGET plus set of 4 siRNAs J-009622-05 5'-CAGCGUGGGUUCCUAUUUC-3'	ThermoScientific, Dharmacon Inc., Chicago, IL, USA

2.1.3. Cell proliferation assays

2.1.3.1. CellTiter-Glo assay

For hit validation studies described in chapter 3, cells (500 cells/well) were reverse transfected in 96-well plate with 20 nM specific siRNAs using the Lipofectamine RNAiMAX reagent and, ten days later, cell viability was assessed by CellTiter-Glo® Luminescent Cell Viability Assay (Promega Corporation, Madison, USA), performed as recommended by the supplier. Luminescence signals were acquired using a microplate reader (TecanUltra, Tecan Trading AG, Switzerland).

For MASTL studies described in chapter 4, HTC/C3 and 8505C cells (1.9×10^5) were seeded in 60mm dishes transfected the day later with 20 nM of specific siRNAs using Lipofectamine RNAiMAX. 24 hours after transfection, cells were harvested and plated ($2x10^3$ cells/well) in 96-well plates; 8505C-TRIPZ-shMASTL #2 ($2x10^3$) cells were plated in 96-well plates in absence or presence of 2 μg/ml doxycycline. Growth rates were evaluated at the time points indicated in the growth curves after plating by CellTiter-Glo® Luminescent Cell Viability Assay as described above.

2.1.3.2. Trypan Blue exclusion test

BCPAP and 8505C ($1x10^5$), TPC-1 (6×10^4), WRO82-1, HTC-C3 and KAT-18 (8×10^4) cells were transfected the day after the seeding in 6-well plate with 20 nM of specific siRNAs using Lipofectamine RNAiMAX, following manufacturer's protocol. At different days after transfection (4 days for TPC-1, 8505C and HTC/C3 cells; 5 days for KAT-18 cells, 6 days for BCPAP cells, 7 days for WRO82-1 cells) the fraction of viable and dead cells was analyzed.

2.1.3.3. Growth inhibition Assay

For experiments with palbociclib, which is a CDK4 and CDK6 inhibitor (115), cells ($8x10^4$ cells/well) were seeded in black/clear bottom 96-well plates and, the following

day, treated with increasing doses of the palbociclib (PD 0332991) (Selleck Chemicals, Houston, TX, USA, cat. S2768). After 72 hours, cells were fixed with 3.7% paraformaldehyde solution for 30 minutes at room temperature, washed and stained with 1 mg/ml Hoechst 33342. The plates were analyzed with an ArrayScan VTI high-content screening reader (Thermo-Fisher Scientific, Pittsburgh, PA): at least 800 cells were acquired in each well with a 10X objective in one fluorescence channel (XF93 optical filter set). Cell nuclei were automatically recognized and counted in ten fields to estimate the cell number per well as proliferation readout. IC50 values were calculated by sigmoid curve fitting of experimental points.

For MASTL studies, HTC/C3 and 8505C (1.2 X 10^4) cells were plated in 24 well-plates and transfected the following day with 20 nM of siRNAs using the Lipofectamine RNAiMAX reagent (Invitrogen Life Technologies, Carlsbad, CA, USA). Seven days after transfection, cells were fixed with 3.7% formaldehyde solution (v/v) at room temperature for 15 minutes, washed with PBS and stained for 20 minutes with 0.1% crystal violet (w/v). Crystal violet was then dissolved in 10% acetic acid (v/v) for 30 minutes on a rocker and then diluted 1:4 in ddH_2O. Optical density at λ=590 nm was measured by using Ultrospec 2100 Pro spectrophotometer (GE Healthcare Bio-Sciences, Pittsburgh, PA).

2.1.4. Immunofluorescence analysis

For hit validation studies described in chapter 3, 8505C cells growing on glass coverslips were transfected with 20 nM control (NT) or MASTL siRNAs and fixed 48 hours later for 10 minutes with 4% paraformaldehyde (Sigma Aldrich, St Louis, Mo, USA). After permeabilization for 10 minutes with 1% BSA and 0.1% Triton X-100 in PBS, and incubation for 30 minutes with 1X blocking solution (2% BSA in PBS), cells were incubated with anti-β-tubulin (clone TUB 2.1: T4026, 1:400, Sigma Aldrich, St. Louis, MO, USA) or

anti-histone H3 (phospho S10) (E173: ab32107, 1:1000, Abcam, Cambridge, UK) primary antibodies for 1 hour. After washing with PBS, cells were incubated with Alexa Fluor® 546 rabbit (1:500, Invitrogen/Molecular Probes®) and Alexa Fluor 488® mouse (1:500, Invitrogen/Molecular Probes®) secondary antibodies for 1 hour. Slides were then prepared using ProLong Diamond Antifade mountant with DAPI (P36966, Molecular Probes®) and imaged with immunofluorescence microscopy (Eclipse E1000; Nikon Instruments, Inc. NY, USA).

For MASTL studies described in chapter 4, HTC/C3 and 8505C cells growing on glass coverslips were transfected with 20 nM NT or MASTL siRNAs and fixed 120 (for HTC/C3) and 76 (for 8505C) hours later for 10 minutes with 4% paraformaldehyde. After permeabilization performed as described above, slides were prepared using ProLong Diamond Antifade mountant with DAPI (P36966, Molecular Probes®) and imaged with immunofluorescence microscopy. A minimum of 1900-2000 (for HTC/C3) and 3000 (for 8505C) cells was counted for each siRNA treatment, and the number of cells with abnormal nuclei was expressed as percentage of the total count.

2.1.5. Annexin V assay

HTC/C3 (1.9×10^5) cells were seeded in 60mm dishes and transfected the following day with 20 nM NT and MASTL #5 siRNAs using Lipofectamine RNAiMAX. At 48, 72, 96 and 120 hours after transfection, both adherent and floating cells were harvested and processed for flow cytometry analysis using FITC Annexin V Apoptosis Detection Kit (Becton Dickinson, San Jose, CA, USA): after washing with PBS, cells were resuspended in Annexin V Binding Buffer and incubated with FITC-conjugated Annexin V for 15 minutes, at room temperature in the dark. TO-PRO-3 iodide (1:2000; Invitrogen/Molecular Probes®), instead of propidium iodide, was then added to each sample. Samples were

acquired using BD FACSCanto (Becton Dickinson, San Jose, CA, USA) instrument and analyzed with FlowJo v7.6 software (TreeStar).

2.1.6. Lentiviral-mediated stable *MASTL* silencing

2.1.6.1. Generation of lentiviral particles

For lentiviral particles generation, TRIPZ-shMASTL #1 (V2THS_177827, ThermoScientific, Dharmacon Inc., Chicago, IL, USA) or TRIPZ-shMASTL #2 (V2THS_261809, ThermoScientific, Dharmacon Inc., Chicago, IL, USA) plasmids were transfected in 293T cells by using the Trans-Lentiviral shRNA Packaging Kit (ThermoScientific, Dharmacon Inc., Chicago, IL, USA) according to manufacturer's instruction. In details, 293T ($5.5x10^6$) cells were plated in 100mm dishes and transfected the following day with a mixture of 42 µg of TRIPZ-shMASTL #1 or TRIPZ-shMASTL #2 plasmids, together with 30 µl of Trans-lentiviral packaging mix, by calcium phosphate protocol. After 16 hours, cells were washed and incubated with DMEM, supplemented with 5% FBS, for 48 hours. Supernatant containing lentiviral particles was then collected, centrifuged at 1600 *x g* at 4°C for 10 minutes, filtered through a sterile 0.45 µM filter (Millipore, Billerica, MA, USA), aliquoted and stored at -80°C. Lentiviral particles were titered according to manufacturer's instructions.

2.1.6.2. Lentiviral transduction

8505C ($6x10^4$) cells were seeded in 6-well plates and, the day after, growth medium was replaced with lentiviral particles-containing supernatant (multiplicity of infection, MOI=1), in presence of 6 µl/ml polybrene (Sigma-Aldrich, St. Louis, MO, USA), for 4 hours. After 4 hours incubation, supernatant was replaced with fresh lentiviral supernatant in presence of 6 µl/ml polybrene; 4 hours later supernatant was replaced with complete growth medium. After 48 hours of culture, 1 µg/ml puromycin (Sigma-Aldrich, St. Louis,

MO, USA) was added to medium, in order to select transduced cells. After one-week selection, cells were tested for shRNA production by 1 μg/ml and 2 μg/ml doxycycline (Sigma-Aldrich, St. Louis, MO, USA) administration.

2.2. Biochemical analysis

2.2.1. Protein extraction and sample preparation

Both adherent and floating cells were collected and centrifuged. Proteins were extracted in RIPA modified buffer (20mM Tris-HCl, pH 7.4, 150mM NaCl, 5mM EDTA, 1% NonidetP-40) supplemented with Complete Mini EDTA-free protease Inhibitor Cocktail (Roche, Manheim, Germany), 1mM Na_3VO_4 and 1mM PMSF. After incubation at 4°C for 20 minutes, samples were centrifuged at 13200 rpm for 30 minutes at 4°C and supernatant with proteins was then recovered. Total amount of protein for each sample was determined by Bradford protein assay (Bio-rad, Hercules, CA, USA) and a total amount of 30-40 μg protein extracts were boiled in NuPAGE LDS sample buffer (Invitrogen, Carlsbad, CA, USA) and then subjected to western blot analysis. Of note, for siCOPZ1-BCPAP and siCOPZ1-TPC-1 cells assayed for trypan blue exclusion test in chapter 3, the entire protein extract was subjected to western blot, as the amount of proteins recovered was less than 20 μg.

2.2.2. Western blot analysis

Protein samples were separated on 4-12% or 10% NuPAGE Novex Gel (Invitrogen, Carlsbad, CA, USA) in MOPS running buffer, under reducing conditions, and resolved proteins were then transferred onto nitrocellulose membranes (GE Healthcare Bio-Sciences, Pittsburgh, PA) using XCell II Blot Module (Invitrogen, Carlsbad, CA, USA). After blocking with 2% bovine serum albumin (BSA) (Sigma-Aldrich, St. Louis, MO, USA) in Tris-

Buffered Saline and Tween 20 (TBS-T [50mM Tris, 150mM NaCl, 0.1% Tween 20]), membranes were incubated overnight at 4°C with primary antibodies, listed in Table 2.3. Antibody binding was assessed by horseradish peroxidase (HRP)-conjugated secondary antibodies (1:5000, GE Healthcare Bio-Sciences, Pittsburgh, PA). Immunoreactive bands were visualized by enhanced chemiluminescence (GE Healthcare Bio-Sciences, Pittsburgh, PA). Densitometric analysis of the bands was performed by using Quantitative One software (Bio-rad, Hercules, CA, USA).

Table 2.3 List of antibodies used for western blot analysis

Actin	A2066	Sigma-Aldrich, St Louis, MO, USA
Cdc2	p34 17: sc-54	Santa Cruz, CA, USA
cleaved PARP (Asp214)	9541	Cell Signaling Technology, Danvers, MA, USA
cleaved-caspase 3 (Asp175)	9664	Cell Signaling Technology, Danvers, MA, USA
COPE	E-20: sc-12104	Santa Cruz, CA, USA
COPZ1	D-20: sc-13349	Santa Cruz, CA, USA
Cyclin D1	DCS-6: sc-20044	Santa Cruz, CA, USA
gamma-H2AX	A300-081A-M	Bethyl Laboratories, Montgomery, TX, USA
GAPDH	6C5: sc-3223	Santa Cruz, CA, USA
MAP4K5	N-19: sc-6429	Santa Cruz, CA, USA
MASTL	ab86387	Abcam, Cambridge, UK
NUDT9	V-22: sc-133857	Santa Cruz, CA, USA
phospho-cdc2 (Tyr15)	9111	Cell Signaling Technology, Danvers, MA, USA
PLA2G15	H-167: sc-135297	Santa Cruz, CA, USA
RASD1	4229	Cell Signaling Technology, Danvers, MA, USA
RGS3	C-20: sc-9304	Santa Cruz, CA, USA
Vinculin	V9131	Sigma-Aldrich, St Louis, MO, USA

2.3. Molecular biology

2.3.1. RNA extraction, RT-PCR and real time PCR

RNA extraction was performed using NucleoSpin® RNA II extraction kit (Macherey-Nagel GmbH, Düren, Germany). 1 µg of RNA was retro-transcribed using SuperscriptIII (Invitrogen, Carlsbad, CA, USA) with random examers. PCR products were separated on 2% agarose gels, stained with ethidium bromide and visualized under UV transillumination. Primers used for the detection of *RGS3*, *NUDT9*, *RASD1* and *OXTR* are listed in Table 2.4. *GAPDH* was used as housekeeping gene. For Real Time PCR analysis, 20 ng of retrotranscribed RNA were amplified in PCR reactions carried out in triplicate on an ABI PRISM 7900 using TaqMan gene expression assays (Applied Biosystem, Foster City, CA). Hs00212698_m1 was used for COPZ2 expression; human HPRT1 (HPRT-Hs99999909_A1) was used as housekeeping gene for the normalization among samples. Data analysis was performed using the SDS (Sequence Detection System) 2.4 software.

Table 2.4 List of primers used for *RGS3*, *NUDT9*, *RASD1*, *OXTR* and *GAPDH* detection by RT-PCR

Gene	Primers	Sequence
RGS3	forward	5'-ATGAGAGGCCTGTGGAGCACT-3'
	reverse	5'-TCATGTGTCGACTTGCAGGAG-3'
NUDT9	forward	5'-GCAGATCCTCAGATCAGTGAA-3'
	reverse	5'-TATAATGGGATCTGCAGCGTG-3'
RASD1	forward	5'-CGAGGTCTACCAGCTCGACAT-3'
	reverse	5'-CACGTCCACGTTCTCCTTGGT-3'
OXTR	forward	5'-ATGTGGAGCGTCTGGGATGC-3'
	reverse	5'-GCTCAGGACAAAGGAGGACG-3'
GAPDH	forward	5'-ACCATCTTCCCAGGAGCGAGAT-3'
	reverse	5'-GGCAGAGATGATGACCCTTT-3'

2.4. Gene expression analysis

The thyroid TCGA data set, which contains the molecular data of 496 PTC samples, is the largest data collection so far available (https://tcgadata.nci.nih.gov/tcga/tcgaCancerDetails.jsp?diseaseType=THCA&diseaseName=Thyroid). Illumina HiSeq Level 3 data were downloaded from TCGA Data Portal and RSEM (116) gene normalized expression values of selected genes were derived for 58 PTC patients, in tumor and adjacent normal samples, respectively. The statistical significance of gene expression difference between PTC and normal groups was assessed using Wilcoxon test.

3. Results: siRNA library screening hit validation

3.1. Introduction

The NOA paradigm (section 1.2.1) states that the uncontrolled growth of tumor cells relies on the activity of genes and pathways, not oncogenic themselves but whose activity is essential for tumor cell viability and not for normal ones (98). Genes presenting these features can be identified by loss-of-function RNAi-based genetic approaches that allow the generation of either "synthetic lethal signature", against specific oncogenes and tumor suppressors, or "cancer lethal signature", if using both normal and tumor cells for the screening. Several reports suggested that this approach was likely to shed new light on the mechanisms of tumor maintenance: myelomas were found to be addicted to an abnormal regulatory network controlled by *IRF4* regardless the oncogenic lesion (117), while genes synthetic lethal with mutant *KRAS* were identified in several tumors harboring this mutation (118). In order to identify a "cancer lethal signature" in thyroid tumors, our laboratory performed a loss of function siRNA library screening on tumor (BCPAP, PTC-derived, carrying the *BRAFV600E* oncogene) and normal immortalized (Nthy-ori 3-1) thyroid cell lines (119). Thyroid cell lines were transfected with a siRNA library containing oligos targeting about 9000 potentially druggable genes and colony forming assay (CFA) was performed after 7 (for Nthy-ori 3-1 cells) and 8 (for BCPAP cells) days (Figure 3.1A and 3.1B). Non-targeting siRNA (siNT) and a siRNA targeting the proteasomal subunit *PSMC3* (siPSMC3) were transfected as negative and positive controls, respectively. The screening identified genes whose silencing was capable of inhibiting the growth of both cell lines, referred to as "lethal hits", but also genes whose silencing

selectively inhibited the growth of tumor cells, referred to as “differential hits” (Figure 3.1C and 3.1D).

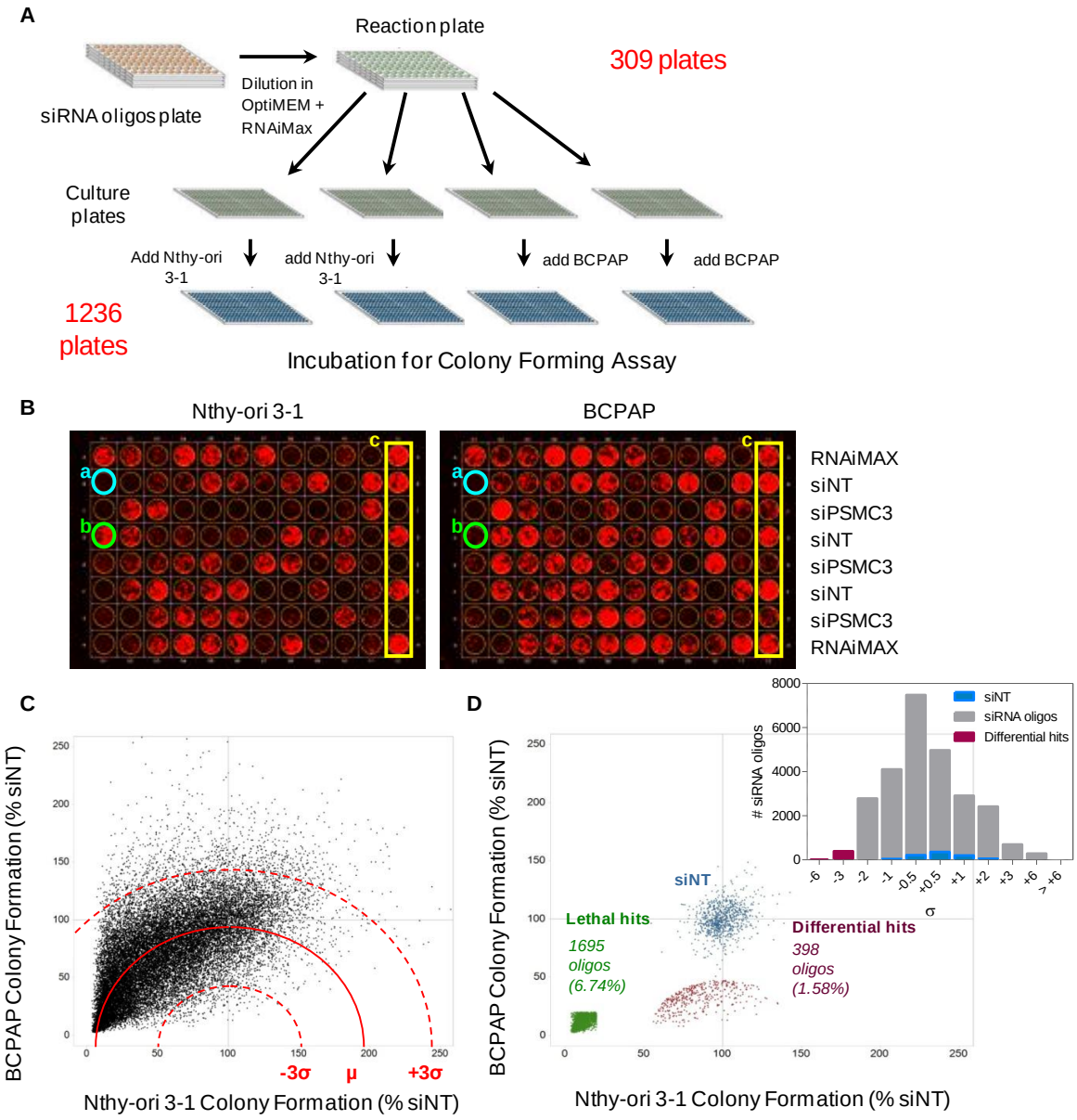

Figure 3.1 siRNA library screening on normal and tumor thyroid cell lines

A) Schematic representation of siRNA library screening automated procedure; 309 mother 96-well-plates, containing 25139 siRNA oligos targeting 9031 genes (three deconvoluted siRNAs for each gene), have been screened in duplicates in BCPAP and NThy-ori 3-1 cell lines. The effect of each siRNAs on the cell viability was analyzed at seven/eight days after transfection by a medium-high throughput CFA. **B)** Representative colony plates generated from transfection described in A); *a* indicates siRNA oligos lethal for both cell lines; *b* indicates siRNA oligos selectively lethal for BCPAP cells; siNT and siPSMC3 represent negative and positive controls, respectively. **C)** Scatter plot of Colony Formation (CF) values obtained from the screening, reported as % of growth respect to non targeting (siNT) for inter-plate data normalization (dots are the averages of two technical replicates performed in both cell lines). **D)** Scatter plot of normalized CF values showing the negative controls (siNT, blue), the lethal hits (green) and the differentially active hits (red); insert: distribution of normalized *d* values after sigma binning). Image adapted from (119).

Technical confirmation of differential hits was then performed by manual transfection of siRNAs on Nthy-ori 3-1 and BCPAP cells, with the same experimental conditions employed in the primary screening. A list of 15 confirmed hit genes, whose inhibition was able to inhibit the growth of tumor but not normal cell lines, was then generated (Table 3.1). Functional annotation analysis revealed that hit genes identified were involved in several biological processes, such as cell cycle and DNA damage checkpoint regulation, vesicular transport and intracellular signal transduction. The relevance and reliability of this screening in identifying TC cell vulnerabilities was given by two lines of evidence. First, among the confirmed hits we found *BRAF*; this was expected, as BCPAP cells are known to be addicted to *BRAFV600E* oncogene (120). Second, we identified genes whose silencing was lethal for both normal and tumor cell viability, and most of them were already identified to be essential survival genes by other RNAi screenings (121-123).

Gene Symbol	Full Gene Name	Accession	GO-BP Term
MASTL	microtubule associated serine/threonine kinase-like	NM_032844	**GO:0006468** protein amino acid phosphorylation **GO:0006793** phosphorus metabolic process
PLA2G15	phospholipase A2, group XV	NM_012320	**GO:0006575** cellular amino acid derivative metabolic process **GO:0006643** membrane lipid metabolic process
COPE	coatomer protein complex, subunit epsilon	NM_007263	**GO:0006890** retrograde vesicle-mediated transport, Golgi to ER transport **GO:0051640** organelle localization
RGS3	regulator of G-protein signaling 3	NM_017790	**GO:0000165** MAPKKK cascade **GO:0008277** regulation of G-protein coupled receptor protein signaling pathway
CCND1	Cyclin D1	NM_053056	**GO:0000075** cell cycle checkpoint **GO:0000077** DNA damage checkpoint
RASD1	RAS, dexamethasone-induced 1	NM_016084	**GO:0007264** small GTPase mediated signal transduction **GO:0016481** negative regulation of transcription
NUDT9	nudix (nucleoside diphosphate linked moiety X)-type motif 9	NM_024047	**GO:0006163** purine nucleotide metabolic process **GO:0006811** ion transport
OXTR	oxytocin receptor	NM_000916	**GO:0000165** MAPKKK cascade **GO:0003012** muscle system process
BRAF	v-raf murine sarcoma viral oncogene homolog B1	NM_004333	**GO:0000165**~MAPKKK cascade **GO:0010941** regulation of cell death
COPZ1	coatomer protein complex, subunit zeta 1	NM_016057	**GO:0006886** intracellular protein transport **GO:0006890** retrograde vesicle-mediated transport, Golgi to ER
MAP4K5	mitogen-activated protein kinase kinase kinase kinase 5	NM_006575	**GO:0000165** MAPKKK cascade **GO:0001932** regulation of protein amino acid phosphorylation
EPHB4	EPH receptor B4	NM_004444	**GO:0007169** transmembrane receptor protein tyrosine kinase signaling pathway **GO:0045765** regulation of angiogenesis
DNM3	dynamin 3	NM_015569	**GO:0006897** endocytosis **GO:0010324** membrane invagination
REM2	RAS (RAD and GEM)-like GTP binding 2	NM_173527	**GO:0006355** regulation of transcription, DNA-dependent **GO:0007264** small GTPase mediated signal transduction
SRPK1	SFRS protein kinase 1	NM_003137	**GO:0006396** RNA processing **GO:0007243** protein kinase cascade

Table 3.1 List of confirmed hits from the screening

The 15 hit genes, whose inhibition resulted to inhibit the growth of thyroid tumor cells, are listed. Representative Gene Ontology-Biological Process (GO-BP) terms are indicated for each of them, by means of DAVID6.7 functional annotation analysis.

3.2. Aims of the chapter

Functional siRNA library screening identified a number of genes whose silencing interfered selectively with tumor cell viability and, among those, 15 hit genes were confirmed by technical validation. The aims of this chapter are: to identify the molecular profile of selected hits in thyroid cancer; to validate the growth inhibitory effect of these genes by using different siRNA sequences in the two cell models used for the screening; to correlate the growth inhibitory effect with the extent of target gene knockdown; to extend the analysis of the growth inhibitory effect of their silencing on a large panel of thyroid tumor cell lines, representative of the different histotypes.

3.3. Results

3.3.1. Analysis of expression levels of hit genes in normal and PTC samples

In 2014, the TCGA consortium published an important study that improved our understanding of the genomic landscape of PTC (33) (section 1.1.2.1). The study reported analysis of the largest PTC cohort ever analyzed to date, with 58 out of 496 PTC specimens paired with the corresponding normal counterpart. We interrogated the thyroid TCGA dataset with the aim of assessing the expression level and the mutational status of the 15 genes identified by our functional screening. Expression analysis was investigated on both the whole dataset and on the 58 matched tumor and normal samples, and the results obtained were identical. By comparing normal and PTC samples, we classified hit genes in three groups, according to their expression levels (Figure 3.2): *i)* genes with significant high overexpression in PTC *vs* normal thyroid, which are *CCND1*, *RGS3*, *OXTR*, *RASD1*, *DNM3* (panel A); *ii)* genes with equal or slightly different expression in PTC compared to normal thyroid, that are *COPE*, *COPZ1*, *PLA2G15*, *SRPK1*, *REM2*, *EPHB4*, *BRAF* (panel B); *iii)* genes that are significantly downregulated in PTC compared to normal thyroid, which are *MASTL*, *MAP4K5*, *NUDT9* (panel C).

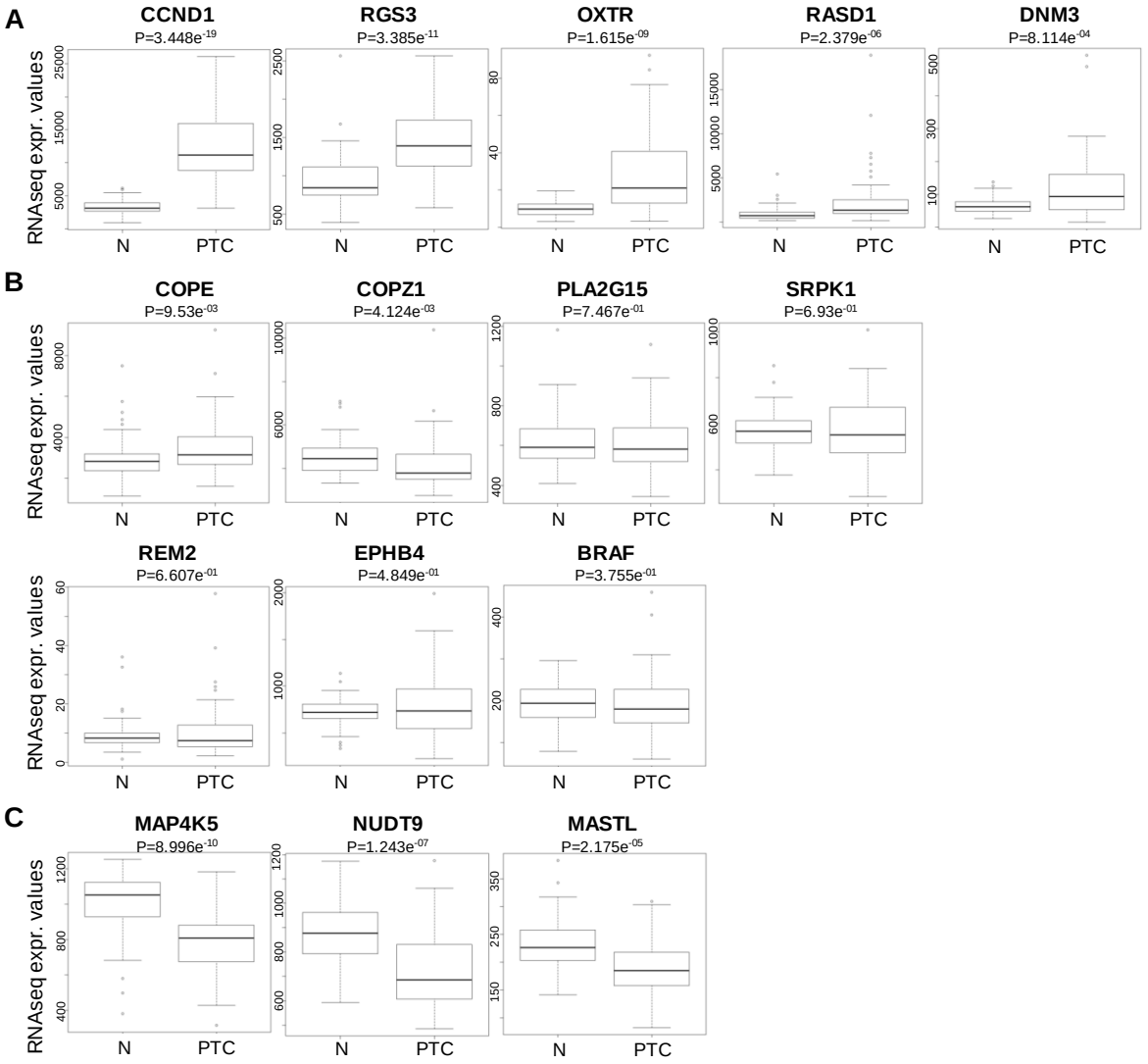

Figure 3.2 Hit gene expression levels in PTC *vs* normal thyroid specimens
Box plot distribution of RNAseq normalized expression values of the 15 hit genes from the thyroid TCGA dataset analysis in 58 matched normal (N) and PTC samples. **A)** Genes overexpressed in PTC *vs* N samples. **B)** Genes equally expressed in PTC and N samples. **C)** Genes downregulated in PTC *vs* N sample. Statistical significance of differences among the two groups of samples was assessed by Wilcoxon test.

For mutational status, we detected *BRAF* mutations with high frequency, as present in 248 out of 496 samples. With the exception of a silent mutation for *COPZ1* in one sample, no mutations affecting the other genes were detected in the whole dataset.

We also retrieved data from the Cancer Cell Line Encyclopedia (CCLE, *http://www.broadinstitute.org/ccle/home*), which provides public access to genomic data, analysis and visualization for about 1000 cell lines, among which the BCPAP cell line.

We found that all the hit genes are expressed by BCPAP cells, at variable level, ranging from “low expression” to “very high expression” (Table 3.2). *CCND1*, *MASTL*, *MAP4K5*, *SRPK1* and *EPHB4* were found to be at the wild type status, while no data for the mutational status of the other hit genes were available.

Table 3.2 Expression level of hit genes in BCPAP cells from CCLE

Gene	*Value*	*Expression level*
MASTL	5,2564	low
PLA2G15	6,7379	moderate
COPE	10,841	very high
RGS3	6,5896	moderate
CCND1	9,7431	high
RASD1	6,843	moderate
NUDT9	8,7534	high
OXTR	4,5271	low
BRAF	6,8071	moderate
COPZ1	10,779	very high
MAP4K5	8,6024	high
EPHB4	5,9189	low
DNM3	4,2194	low
REM2	6,0285	moderate
SRPK1	8,5579	high

3.3.2. Analysis of hit gene expression levels in TC cell lines

In order to assess whether these putative “non-oncogenes” are expressed by TC cell lines, we first searched for and purchased commercially available antibodies for western blot analysis for the first 11 hit genes except for *BRAF*. Of note, for some of these genes (*PLA2G15*, *RGS3*, *RASD1*, *NUDT9*, *OXTR*, *COPZ1*), no published working antibodies were available at the time of the analysis. We first tested the optimal working conditions for the antibodies purchased by western blot analysis of control cell lines indicated by the antibody datasheets. As reported in Figure 3.3A-F, we were successful in detecting the

expression of MASTL, PLA2G15, COPE, MAP4K5, Cyclin D1 and COPZ1. For RGS3, NUDT9 and RASD1 (Figure 3.3G-I), the antibodies tested did not allow the detection of the corresponding protein.

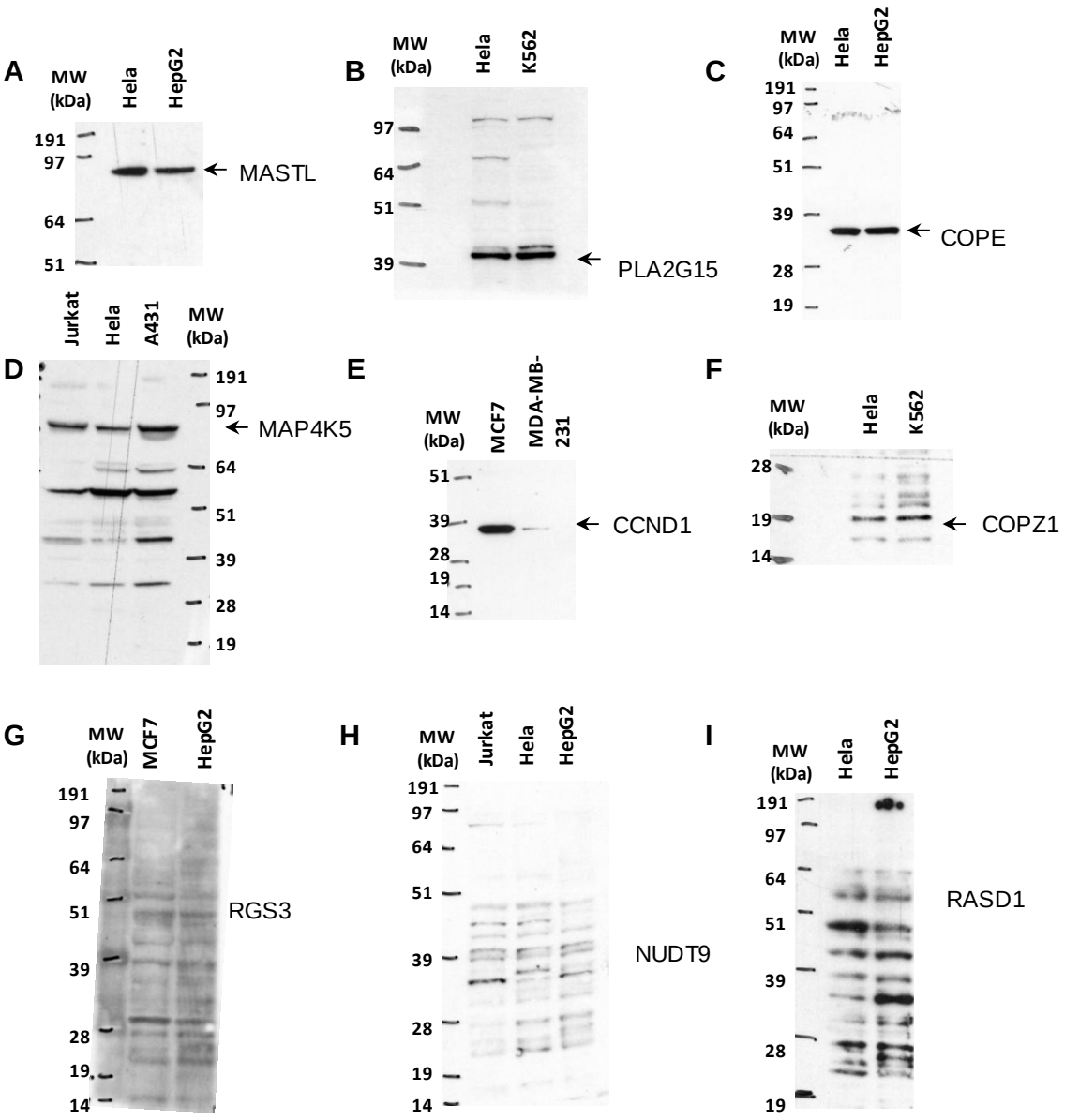

Figure 3.3 Analysis of working efficiency of antibodies for hit gene detection
Western blot analysis of control cell lines for the setup of working conditions of antibodies for: **A)** MASTL; **B)** PLA2G15; **C)** COPE; **D)** MAP4K5; **E)** Cyclin D1; **F)** COPZ1; **G)** RGS3; **H)** NUDT9; **I)** RASD1.

We investigated the expression of the hit genes in the normal (Nthy-ori 3-1) and tumor (BCPAP) cell lines used for the screening and in a panel of thyroid tumor cell lines, representative of the different histotypes and/or carrying different oncogenes: PTC-

derived (TPC-1, carrying the *RET/PTC1* oncogene), FTC-derived (WRO82-1), ATC-derived (8505C and HTC/C3, which carry *BRAFV600E* oncogene, KAT-18). MASTL, Cyclin D1, COPZ1, MAP4K5, PLA2G15 and COPE expression was investigated by western blot (Figure 3.4A). In comparison with Nthy-ori 3-1, MASTL was found to be less expressed in thyroid tumor cell lines; Cyclin D1 expression, except for KAT-18, was higher in the tumor cell lines compared to the normal one; also COPZ1 expression was higher in TC cell lines, compared to Nthy-ori 3-1; PLA2G15 expression was slightly reduced in all the tumor cell lines, except for BCPAP, and strongly reduced in KAT-18; MAP4K5 was found to be expressed at variable levels, with a slight increase in BCPAP, WRO82-1 and 8505C, and a decrease in the remaining; COPE expression in tumor cells was higher compared to normal Nthy-ori 3-1, with the exception of KAT-18. The expression of *RGS3*, *NUDT9*, *RASD1* and *OXTR* was investigated by RT-PCR. All the genes are expressed in the cell lines tested with no appreciable differences (Figure 3.4B).

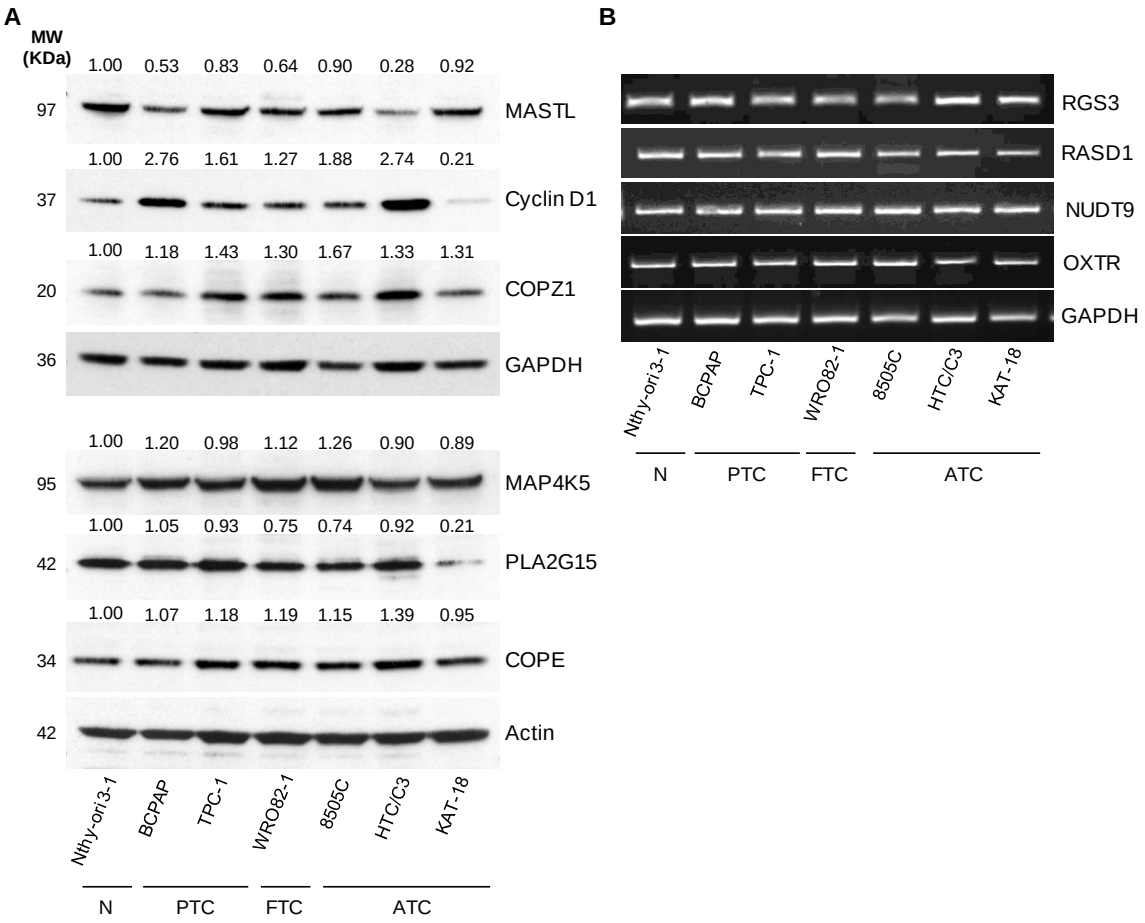

Figure 3.4 Hit gene expression levels in thyroid tumor cell lines
A) MASTL, Cyclin D1, COPZ1, MAP4K5, PLA2G15 and COPE expression level analyzed by western blot in a panel of normal (N) and tumor thyroid cell lines representative of the different histotypes (PTC, FTC, ATC); values represent band intensity assessed by densitometry analysis and reported as ratio to Nthy-ori 3-1; GAPDH and Actin were used as loading controls. **B)** RGS3, RASD1, NUDT9 and OXTR mRNA expression tested by RT-PCR on cell lines tested for A); GAPDH represents the housekeeping control.

3.3.3. Analysis of siRNA silencing efficiency for hit validation

Among the list of candidate "non-oncogenes" described above, we selected for validation studies only those genes for which western blot analysis was feasible. We purchased commercially available siRNAs, with oligonucleotide sequences different from those of the library, for *MASTL*, *PLA2G15*, *COPZ1*, *CCND1*, *COPE* and *MAP4K5*. Four different oligos for *MASTL* and *PLA2G15*, and a smart pool of oligos for *CCND1*, *COPZ1*, *MAP4K5* and *COPE*, were used. Nthy-ori 3-1 cells were transiently transfected with the

specific siRNAs and with non-targeting control (siNT) oligos and then subjected to western blot analysis, in order to evaluate silencing efficiency (Figure 3.5). For MASTL, we obtained the highest silencing efficiency with oligos #1 and #4 72 hours after transfection; oligos targeting Cyclin D1, COPZ1 and MAP4K5 completely abrogated protein expression at 72 hours. For PLA2G15 and COPE, siRNA oligos were inefficient or slightly efficient in abrogating protein expression, respectively. Notably, oligos with good silencing efficiency gave no macroscopic effects on the growth and survival of Nthy-ori 3-1 cells, in keeping with what obtained from siRNA library screening.

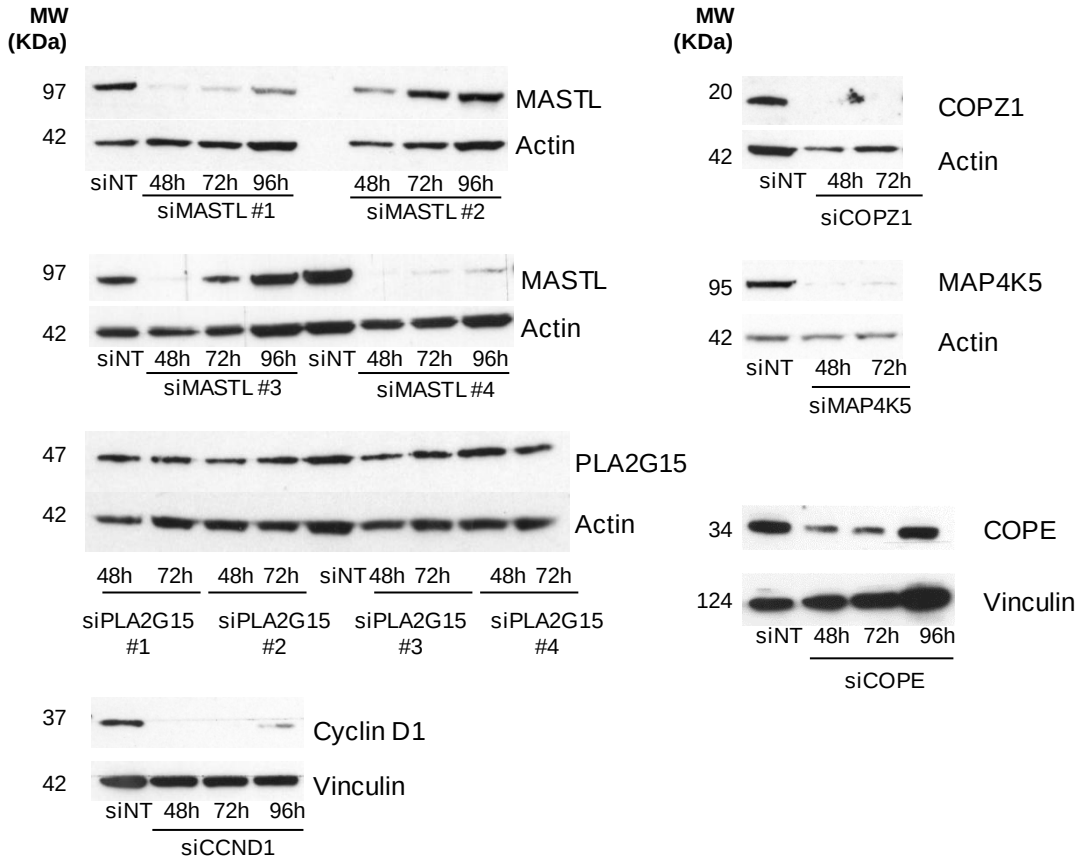

Figure 3.5 Evaluation of siRNA silencing efficiency for validation studies
Western blot analysis of MASTL, COPZ1, PLA2G15, MAP4K5, Cyclin D1 and COPE expression in Nthy-ori 3-1 cells, transiently transfected with the indicated siRNAs and collected at the indicated timepoints. Actin and vinculin represent loading controls.

3.3.4. Effects of MASTL, COPZ1 and Cyclin D1 depletion on BCPAP cell growth

Based on the silencing efficiency of siRNAs previously tested and on background literature data about the hit genes, we selected MASTL, COPZ1 and Cyclin D1 for the validation studies. We transfected siRNAs in the two cell lines used for the screening, Nthy-ori 3-1 and BCPAP. We used the same protocol as for the screening: cells were transfected in 96-well plates with the oligos described in section 3.3.3 and siNT and siPSMC3 controls, and cell growth was evaluated 10 days later by CellTiter-Glo® assay. The luminescence signal, indicative of viable cells, is reported in the scatter plot in Figure 3.6A, normalized with respect to siNT. We observed that siMASTL #1, siMASTL #4, siCOPZ1 and siCCND1 reduced BCPAP cell growth by 60%, 93%, 94% and 86%, respectively; this efficiency is comparable to that of positive control siPSMC3, that is 93% reduction. We did not observe any significant reduction of the growth of BCPAP cells transfected with siMASTL #2 and siMASTL #3; this result is in keeping with the low siRNA silencing efficiency we previously observed in Nthy-ori 3-1 (Figure 3.5). Of note, no significant reduction of Nthy-ori 3-1 cell growth was observed with *MASTL*-, *COPZ1*- and *CCND1*-targeting oligos, while the positive control siPSMC3 was able to reduce cell growth as for BCPAP. We further confirmed the effect of *MASTL*, *COPZ1* and *CCND1* silencing with a different experimental approach. BCPAP cells were transfected in 6-well plates with the oligos that previously resulted to be efficient in gene silencing: siMASTL #1 and #4, siCOPZ1 and siCCND1. We also used an additional in-house synthesized siRNA targeting MASTL, that was found to be efficient in MASTL silencing when transfected in Nthy-ori 3-1 (Figure 3.6B). At 6 days after transfection, we noticed an evident effect of *MASTL*, *COPZ1* and *CCND1* silencing by microscopy observation: BCPAP cells were less confluent compared to negative control (siNT), with a large number of floating cells (Figure 3.6C). By trypan blue exclusion test, we found a reduction of cell growth, in comparison with

control (siNT), of: 69.5%, 59.7% and 71% for siMASTL #1, #4 and #5, respectively; by 99.6% for siCOPZ1; by 91.5% for siCCND1 (Figure 3.6D). The same cells were tested by western blot at the end of the experiment and complete abrogation of MASTL and Cyclin D1 expression was observed; an insufficient amount of protein extract was recovered from siCOPZ1-transfected cells, due to the massive lethal effect on this cell line, so western blot analysis was not informative (Figure 3.6E).

On the whole, our results confirmed the growth inhibitory effect of MASTL, COPZ1 and Cyclin D1 knockdown on BCPAP cells, thus validating them as vulnerability genes of BCPAP.

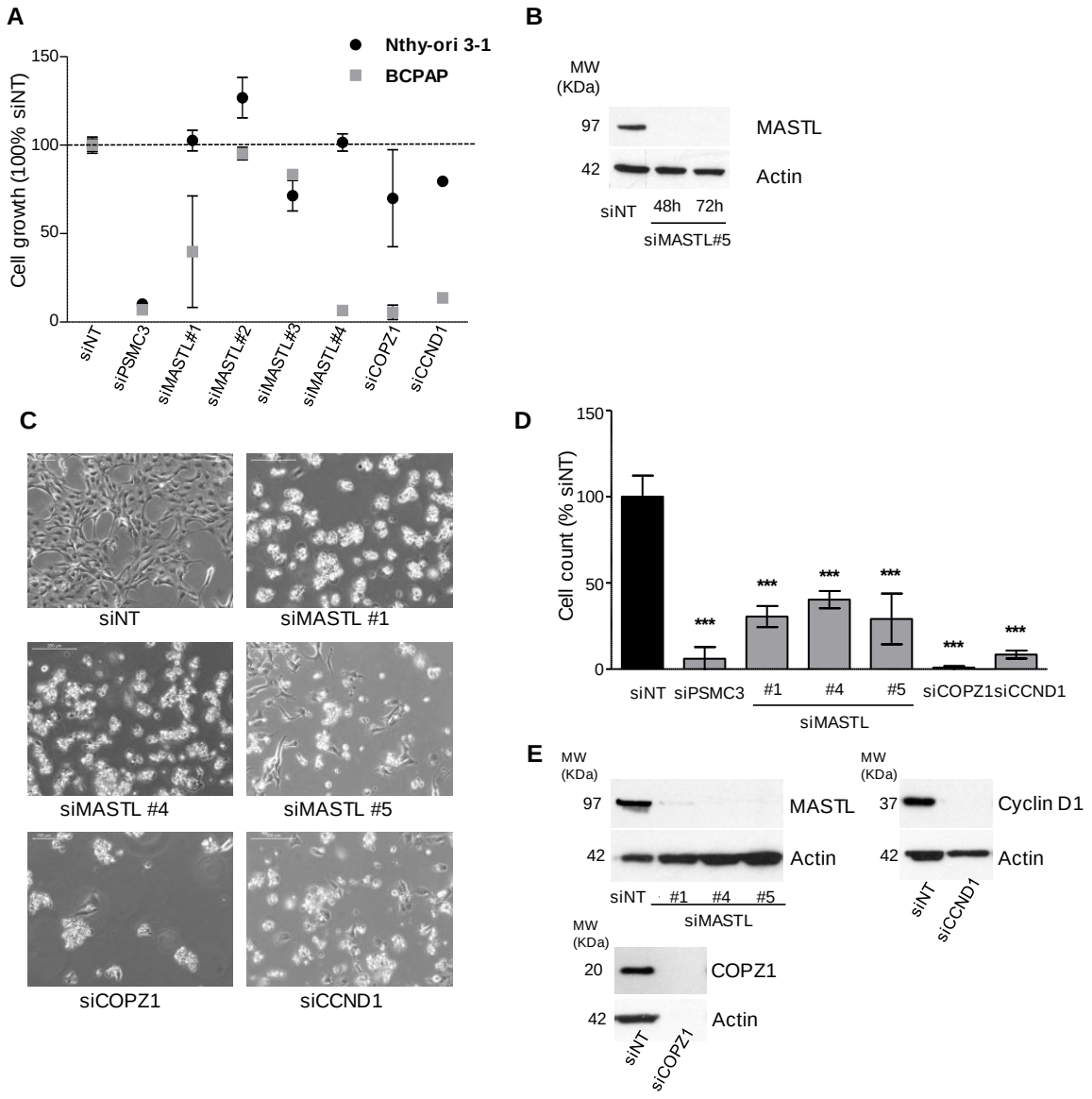

Figure 3.6 Effects of MASTL, COPZ1 and Cyclin D1 depletion on BCPAP cell line

A) Scatter plot representing the percentage of cell growth (luminescence values of CellTiter-Glo® assay), normalized to control (siNT), of Nthy-ori 3-1 and BCPAP cells, 10 days after transfection with the indicated siRNAs. One representative out of three experiments is shown. **B)** Western blot analysis of MASTL expression in Nthy-ori 3-1 cells, transiently transfected with the control (siNT) and the new MASTL (siMASTL #5) siRNAs, and collected at the indicated time points. Actin represents loading control. **C)** Representative pictures of BCPAP cells 6 days after transfection with the indicated siRNAs. **D)** BCPAP cell growth evaluated by trypan blue exclusion test 6 days after transfection; cell count of viable cells was normalized to that of control (100% of siNT); data represent the mean +/- sd of two independent experiments; asterisks indicate statistical significant differences by unpaired Student's t-test (***p<0.001); **E)** Western blot analysis of MASTL, Cyclin D1 and COPZ1 expression in BCPAP cells, assayed in panel D; actin was used as loading control.

3.3.5. Effects of MASTL, COPZ1 and Cyclin D1 depletion on the growth of several TC cell lines

According to NOA paradigm, tumor cells may share common vulnerabilities based on the stress support pathways needed for sustaining the tumorigenic phenotype, regardless the main oncogenic drivers. We decided to assess whether the survival genes previously confirmed in BCPAP may be involved in such common pathways and therefore represent common vulnerabilities for thyroid tumors. To this aim, we evaluated the functional effects of MASTL, COPZ1 and Cyclin D1 silencing on the panel of TC cell lines in which we have previously determined their expression levels (see Figure 3.4). TC cell lines were transfected in 96-well plates with control (siNT and siPSMC3) siRNAs and siRNAs targeting *MASTL*, *COPZ1* and *CCND1*, and cell viability was evaluated by CellTiter-Glo® assay 10 days later. We found that silencing of the three genes induced variable extents, ranging from 15% to 95%, of cell growth inhibition (Figure 3.7A) in the majority of cell lines tested, compared to control. Only for *CCND1* in 8505C and KAT-18, and for *MASTL* in KAT-18 cell lines, we did not observe any effect of gene silencing on cell viability. We additionally assessed the effects on cell growth by performing trypan blue exclusion test from 4 to 7 days after cell transfection in 6-well plates, as already performed on BCPAP (detailed previously in 3.3.4). A reduction in the growth of cells upon transfection of siRNAs targeting *MASTL*, *COPZ1* and *CCND1*, compared to control (siNT) transfected cells, was appreciable by microscopy observation (Figure 3.7B). Cell count revealed that, with the exception of KAT-18 cell lines, silencing of MASTL, COPZ1 and CCND1 significantly reduced the growth of all cell lines tested (Figure 3.7C). Compared to control, inhibition of cell viability was observed by: 30-63% for siMASTL #1, 35-75% for siMASTL #4, 40-75% for siMASTL #5, 75-99% for siCOPZ1 and 70-94% for siCCND1. In KAT-18, we found a decrease of cell growth by 31% for siMASTL #1, 53% for siCOPZ1 and 43% for CCND1; siMASTL #4

and #5 had no significant effect on cell viability; *PSMC3* silencing in KAT-18 had a growth inhibitory effect of 53%. We performed western blot analysis on the same samples at the end point of the experiment and observed a high efficiency of gene silencing in all of them (Figure 3.7D). As for BCPAP cells, also in TPC-1 cells we were not able to recover enough protein extract to assess COPZ1 knockdown in siCOPZ1-transfected samples, due to the massive lethal effect of gene silencing on this cell line. Of note, by this alternative approach we were able to notice a growth inhibitory effect of *CCND1* silencing in 8505C and KAT-18, and of *MASTL* silencing in KAT-18 cells, which was not previously observed; this could be related to the variability of silencing efficiency and/or experimental conditions.

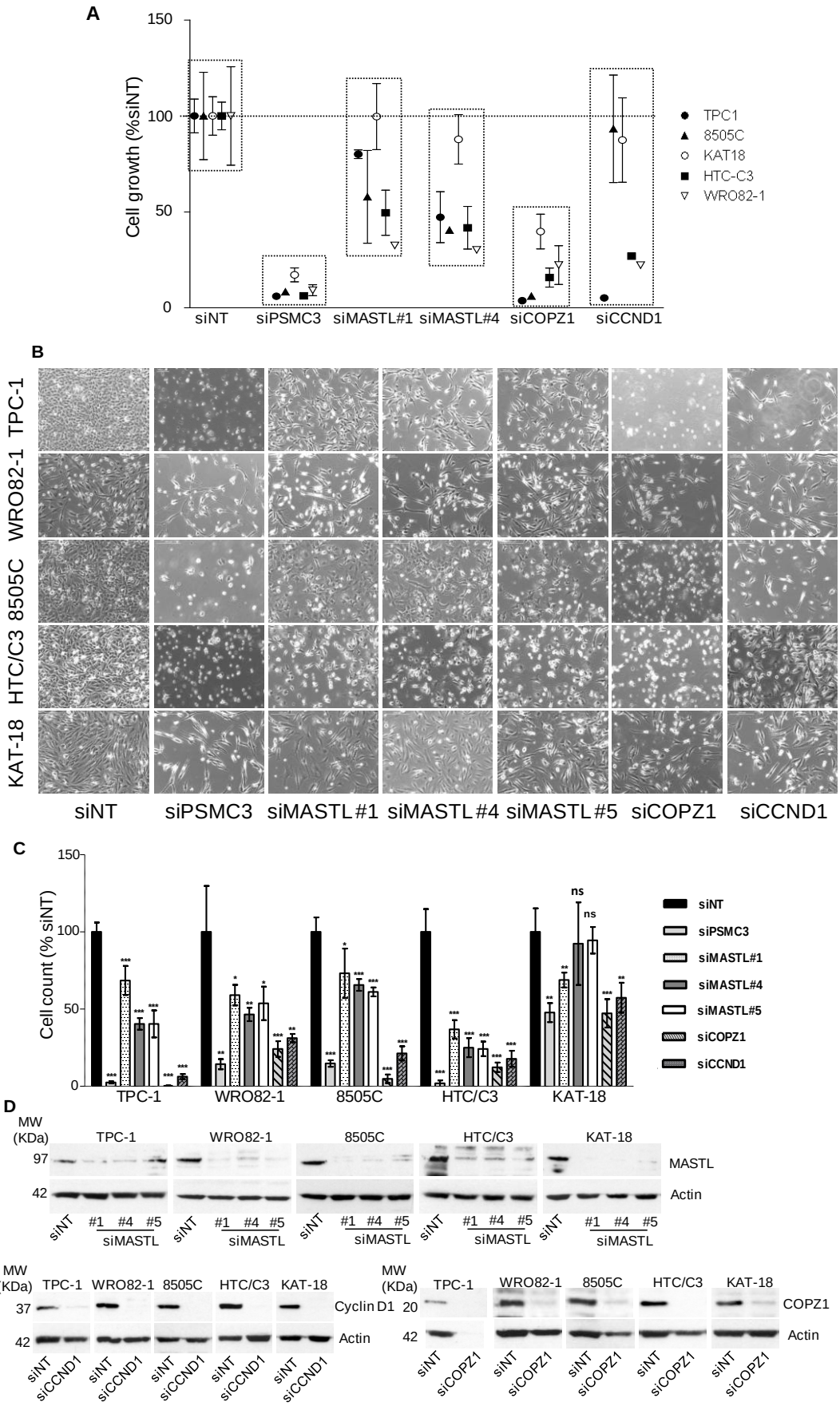
A
Cell growth (%siNT)
150
100
50
0
siNT
siPSMC3
siMASTL#1
siMASTL#4
siCOPZ1
siCCND1
TPC1
8505C
KAT18
HTC-C3
WRO82-1
B
TPC-1
WRO82-1
8505C
HTC/C3
KAT-18
siNT
siPSMC3
siMASTL#1
siMASTL#4
siMASTL#5
siCOPZ1
siCCND1
C
Cell count (% siNT)
150
100
50
0
TPC-1
WRO82-1
8505C
HTC/C3
KAT-18
ns
siNT
siPSMC3
siMASTL#1
siMASTL#4
siMASTL#5
siCOPZ1
siCCND1
D
MW (KDa)
97
42
MASTL
Actin
siNT
#1 #4 #5
siMASTL
37
Cyclin D1
20
COPZ1
siCCND1
siCOPZ1

Figure 3.7 Effects of MASTL, COPZ1 and Cyclin D1 depletion on a panel of TC cell lines
A) Scatter plot representing the percentage of cell growth (luminescence values of CellTiter-Glo® assay), normalized to control (siNT), of the indicated TC cell lines 10 days after transfection with the indicated siRNAs. One representative out of three experiments is shown. **B)** Representative images of TPC-1, WRO82-1, 8505C, HTC/C3 and KAT-18 cells, transfected with the indicated siRNAs, before the trypan blue exclusion test. **D)** Cell proliferation assayed by trypan blue exclusion test 4 days (for TPC-1, 8505C and HTC/C3 cells), 5 days (for KAT-18 cells), 6 days (for BCPAP cells) and 7 days (for WRO82-1 cells) after siRNA transfection; cell count was normalized to that of siNT (100% growth) and expressed as mean +/- sd of two independent experiments; statistically significant differences are indicated by asterisks (ns: not significant; *p<0.05; **p<0.01;, ***p<0.001; according to unpaired Student's t-test). **E)** Western blot analysis of MASTL, COPZ1 and Cyclin D1 expression in TC cells assayed in panel D; actin was used as loading control.

3.3.6. Characterization of TC cell dependency on CCND1, MASTL and COPZ1

In order to explore the potential of MASTL, Cyclin D1 and COPZ1 targeting in TC we performed additional experiments.

Given that Cyclin D1 acts as activator of its dependent kinases CDK4 and CDK6, we tested whether TC cell lines may be susceptible to palbociclib (PD-0332991), a specific inhibitor of CDK4 and 6 (115). The panel of TC cell lines previously tested was treated with palbociclib for 72 hours. The effects of palbociclib administration were appreciable by microscopy observation: after 72 hours, all TC cells treated with palbociclib were less confluent compared to the control (CTRL) (Figure 3.8A). The treatment with increasing doses of palbociclib showed a consistent growth inhibitory effect on all TC cell lines tested (Figure 3.8B). The IC50 values were variable, ranging from <0.003 μM for BCPAP cells to 0.20 μM for HTC/C3 cells (Figure 3.8C).

Since it was reported that MASTL depletion induced multiple mitotic defects (124), we tested whether MASTL-depleted 8505C cells could present the same defects. 48 hours after *MASTL* silencing in 8505C, immunofluorescence analysis for β-tubulin, phosphorylated histone H3 (Ser10) and DAPI revealed the presence of aberrant mitotic figures (Figure 3.8D): while no anomalies were observed in control siNT (*i*), MASTL

knockdown was associated with formation of multinuclear cells (*ii*), lagging chromosomes not aligned to metaphase plate (*iii*) and chromatin bridges connecting daughter cells (*iv*).

COPZ1 vulnerability of tumor cells was found to be associated with the downregulation of its paralogous *COPZ2* (125). We performed real time PCR in normal (Nthy-ori 3-1) and TC cell lines to assess *COPZ2* expression level (Figure 3.8E): we found that all tumor cells, except for WRO82-1, showed a downregulation of *COPZ2* mRNA, compared to normal thyrocytes.

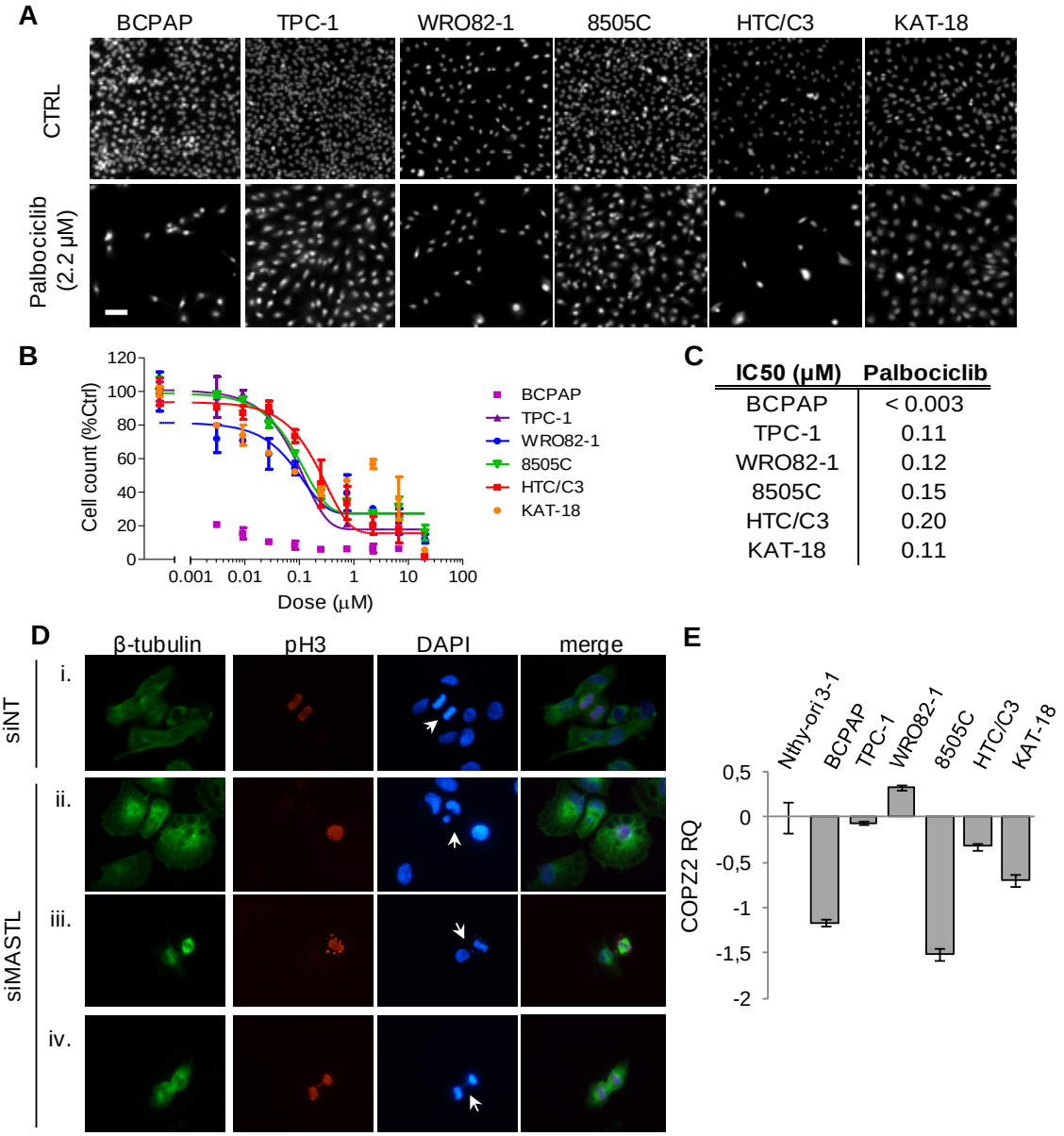

Figure 3.8 Characterization of Cyclin D1, MASTL and COPZ1 vulnerabilities of TC cells

A) Representative ArrayScan fields of TC cell lines untreated (CTRL) or treated with 2.2 µM palbociclib for 72 hours and stained with Hoechst (scalebar: 50µm). **B)** Dose-response curve of TC cell growth treated with palbociclib for 72 hours; nuclei were stained with Hoechst and counted in each well by an ArrayScan high-content screening reader; cell count values derived from nuclear staining (reported as growth parameter normalized with respect to untreated controls) are presented as mean +/- sd of two replicates. **C)** IC50 values (µM) obtained using a sigmoid function of nonlinear interpolation of experimental points; for KAT-18, IC50 value was derived from graphical analysis. **D)** Immunofluorescence analysis for β-tubulin (microtubules, green), phosphorylated histone H3 Ser10 (red) and DAPI (nuclei, blue) on 8505C cells 48 hours after transfection with control (siNT) and MASTL (siMASTL) siRNAs; arrows indicate normal mitosis (*i*), multinuclear cell (*ii*), lagging chromosomes (*iii*) and DNA bridge (*iv*). **E)** Real time PCR analysis of *COPZ2* expression; results are presented as log10-transformed relative quantity (RQ) of *COPZ2* mRNA normalized for *HPRT* housekeeping expression and presented as mean +/- sd of three independent experiments.

3.4. Discussion

Our laboratory performed a loss of function siRNA-based screening on normal and tumor thyroid cell lines, with the aim of identifying potential "non-oncogenes" in thyroid tumor cells. A list of 15 genes, whose silencing was detrimental for tumor but not normal cell viability, was generated. We analyzed their molecular profiles in normal and PTC samples by TCGA dataset interrogation and found, with the exception of *BRAF*, no mutations of hit genes in PTC samples, while their expression level was equal or differential (both upregulation and downregulation) between normal and tumor specimens. We documented their expression in a panel of thyroid tumor cell lines and selected *MASTL*, *COPZ1* and *CCND1* for validation studies. We confirmed their inhibitory effect on BCPAP cell growth, by using siRNA oligos different from those of the library, and verified the abrogation of their expression at protein level in BCPAP cells. Importantly, we observed that their depletion resulted to be detrimental for the growth and survival of several thyroid tumor cell lines, representative of the different histotypes and carrying different oncogenic lesions.

Molecular studies performed in the last years extensively characterized the genomic landscape of PTCs and ATCs. These findings were translated into the use of small-molecule inhibitors, specifically TKIs, in the clinics for the treatment of advanced TC patients who do not respond to conventional therapy (126); even though TKIs showed promising therapeutic strategies, their efficacy gave contrasting evidence in clinical trials, since mechanisms of resistance to TKIs often develop and severe side verse effects present (127). This evidence underlines the need for alternative approaches aimed to identify novel targets for TC treatment. Large scale RNAi-based functional screenings are a tool nowadays widely used to identify tumor cell vulnerabilities for potential

therapeutic goals (106,107,110). Indeed, these high-throughput screening approaches permit to discover potential target genes to which cancer cells are addicted and that are not necessarily oncogenic themselves. In this chapter, we presented the results of a high-throughput siRNA phenotypic screening on normal and tumor thyroid cells, aimed to identify thyroid tumor cell vulnerabilities (119). For the first time, we identified a panel of genes whose silencing preferentially inhibited the growth of the tumor cell line as compared to that of normal thyrocytes. TCGA dataset analysis revealed no mutations of hit genes (besides *BRAF*); this suggests that alterations of their function in thyroid tumor cell biology may be excluded, and that they represent "non-oncogenes" in TC. We verified that these genes were actually expressed in the cell models used for the screening and also extended the analysis to a panel of thyroid tumor cell lines; this first approach allowed us to select some of them for validation studies, according to the availability of reagents such as commercial antibodies efficiently working. For hit genes whose expression was not ascertainable by western blot analysis, due to antibodies not efficiently working, we assessed their mRNA expression in TC cell lines by RT-PCR; since western blot was not feasible for them, they were excluded from validation studies. To validate the remaining hits, we first tested siRNA oligos different from those of the library and found that some of them were actually not efficient, thus making further investigation not feasible. We selected *MASTL*, *COPZ1* and *CCND1* for the confirmation studies in BCPAP.

Cyclin D1 is a cell cycle regulator that forms a complex with cyclin-dependent kinases (CDK) 4 and 6 to activate them and promote the transition from G1 to S phase of the cell cycle (128). *CCND1* is frequently found deregulated in tumors: gene mutations and amplifications, as well as protein overexpression, are events frequently reported. For this reason, Cyclin D1 has been proposed as therapeutic target for cancer treatment. Its

targeting may result difficult since it lacks enzymatic activity; a more feasible approach would be the inhibition of its associated kinases CDK4 and CDK6. Indeed, several CDK4/6 inhibitors are currently under clinical evaluation in different tumors (129). Cyclin D1 was frequently found overexpressed at both protein (130) and mRNA (131,132) levels in TC, but no functional data about its role in thyroid tumorigenesis were reported. We demonstrated that Cyclin D1 inhibition impaired the growth of all TC cell lines tested. Interestingly, the expression level of Cyclin D1 was heterogeneous among them; this finding suggests that TC cell dependency on *CCND1* may not require the aberrant expression of the protein. Moreover, we observed that TC cell lines are sensitive to the CDK4/6 inhibitor palbociclib, that is already used for the treatment of ER+/HER2- breast cancer in combination with letrozole (133). Our results prompt the evidence that Cyclin D1 represents a TC cell vulnerability and provide a rationale for further preclinical and clinical studies aimed to develop a therapeutic strategy to inhibit it, directly or indirectly by using CDK4/6 inhibitors, for TC treatment.

MASTL (microtubule associated serine/threonine kinase-like) is a regulator of mitosis as its activity is required for the inhibition of PP2A/B55δ, the main protein phosphatase complex responsible for dephosphorylation of CDK1 substrates. MASTL activity was shown to be necessary to prevent defects in chromosome segregation and avoid prometaphase arrest and mitotic failure (134). Little was known about the role of MASTL in cancer. In lung cancer, it was reported that MASTL inhibition was able to sensitize tumor cells to radiations and to promote cytokinesis defects (135). Another study (136) reported that MASTL has a role in head and neck tumor recurrence and resistance to chemotherapy with cisplatin, thus proposing it as possible therapeutic target. They also found MASTL to be overexpressed in prostate, breast and recurrent head and neck tumors, compared to normal counterpart. In this chapter, we identified MASTL as a

vulnerability gene for thyroid tumors. We observed that its inhibition interfered with the growth of TC cell lines, with variable extents. We also found that MASTL-depleted 8505C exhibited errors in the mitotic process. Moreover, we found no mutations in PTC samples and observed that MASTL is not associated with overexpression in PTC compared to normal samples. Together, these findings highlighted that further investigations about the role of MASTL in TC cell biology were needed, in order to assess whether it could represent a therapeutic target for TC. These studies are presented in the next chapter of the thesis together with a more deepened discussion.

COPZ1 (coatomer protein complex ζ1) is the zeta-subunit of the secretory coatomer protein complex I (COPI), which is involved in vesicular trafficking from Golgi apparatus to endoplasmic reticulum, endosome maturation, autophagy (137,138) and lipid homeostasis (139). Shtutman and colleagues (125) proposed COPZ1 as therapeutic target as they observed that tumor cells become dependent on *COPZ1* because of downregulation of *COPZ2* and *COPZ1* silencing dramatically induced apoptotic cell death. In this chapter, we showed that *COPZ1* is a TC vulnerability gene as its silencing led to growth inhibition of all TC cell lines tested. We also found *COPZ2* downregulation in the majority of TC cell lines, apart from WRO82-1: even if *COPZ2* mRNA level was higher than control, this cell line resulted to be sensitive to *COPZ1* depletion; this finding suggests that other mechanisms may be involved in determining *COPZ1* sensitivity in TC cells. Further experiments were needed to better understand the mechanisms by which COPZ1 affects TC cell viability, and are presented in an independent chapter of the thesis.

In conclusion, in this chapter we described the identification of a “cancer lethal signature” for thyroid carcinoma, as result of a siRNA-based functional screening on normal and tumor thyroid cell lines. Among the novel potential therapeutic targets that emerged, we functionally characterized Cyclin D1, MASTL and COPZ1 and demonstrated

that their depletion was deleterious for TC cell growth irrespective of tumor histotype and/or genetic lesion. These findings indicate that they represent common examples of “non-oncogene addiction” in thyroid cancer, highlighting them as attractive targets for new therapeutic approaches for thyroid tumors which would spare normal cells, thus having limited side effects.

4. Results: MASTL studies

4.1. Introduction

Microtubule associated serine/threonine kinase-like (*MASTL*) is the human orthologue of *greatwall* (*GWL*), a gene first discovered in *Drosophila* in 2004, which encodes a kinase involved in the regulation of mitosis (140). The name "*greatwall*" came from the evidence that mutations in this gene caused defects in chromosome condensation and delay in mitotic progression, thus suggesting that it had a role in protecting chromosome structure. A following study in *Xenopus* egg extracts revealed that GWL was involved in the complex regulatory feedback loop that drives the phosphorylation of proteins in mitosis progression (141). Central to this complex regulatory loop is *cell division cycle protein 2 homolog* (*cdc2*), also known as *cyclin-dependent kinase 1* (*CDK1*): it encodes a serine/threonine kinase that has the essential role of promoting G2/M transition and mitosis entry, once bound to Cyclin B1, thus forming the maturation promoting factor (MPF) complex (142). CDK1 activation is tightly controlled during cell cycle, in order to ensure correct progression through mitosis: during G1, S and G2 phases, MYT1 and WEE1 kinases phosphorylate CDK1 on Thr14 and Tyr15 inhibitory residues, in order to maintain it in an inactive state; at the onset of mitosis, CDC25 phosphatase removes these inhibitory modifications, allowing the activation of CDK1 and, consecutively, of MPF complex (Figure 4.1). Active CDK1 is able to further activate CDC25, as well as to inactivate its inhibitor WEE1. Furthermore, it also phosphorylates polo-like kinase 1 (PLK1), which contributes to a further activation of CDC25. Yu and colleagues showed that, during mitosis, GWL was phosphorylated and activated by CDK1, and GWL depletion

led to accumulation of inhibitory phosphorylations on CDK1 that prevented mitosis progression. It was later demonstrated that GWL contributed to mitosis progression by inhibiting the protein phosphatase 2A (PP2A) associated with the B55δ regulatory subunit (PP2A/B55δ), which is the main phosphatase complex responsible for the dephosphorylation of mitotic substrates of the MPF complex (143). This inhibition was shown to be mediated by two proteins identified as GWL substrates, namely cyclic adenosine monophosphate–regulated phosphoprotein 19 (ARPP19) and α-Endosulfine (ENSA); once activated by GWL, they associated with PP2A/B55δ and inhibited it, thus promoting mitotic entry (144,145). Until recently, no specific regulators of GWL were identified; only the work from Ma and colleagues (146) suggested that protein phosphatase 1 (PP1) could be responsible for GWL inactivation.

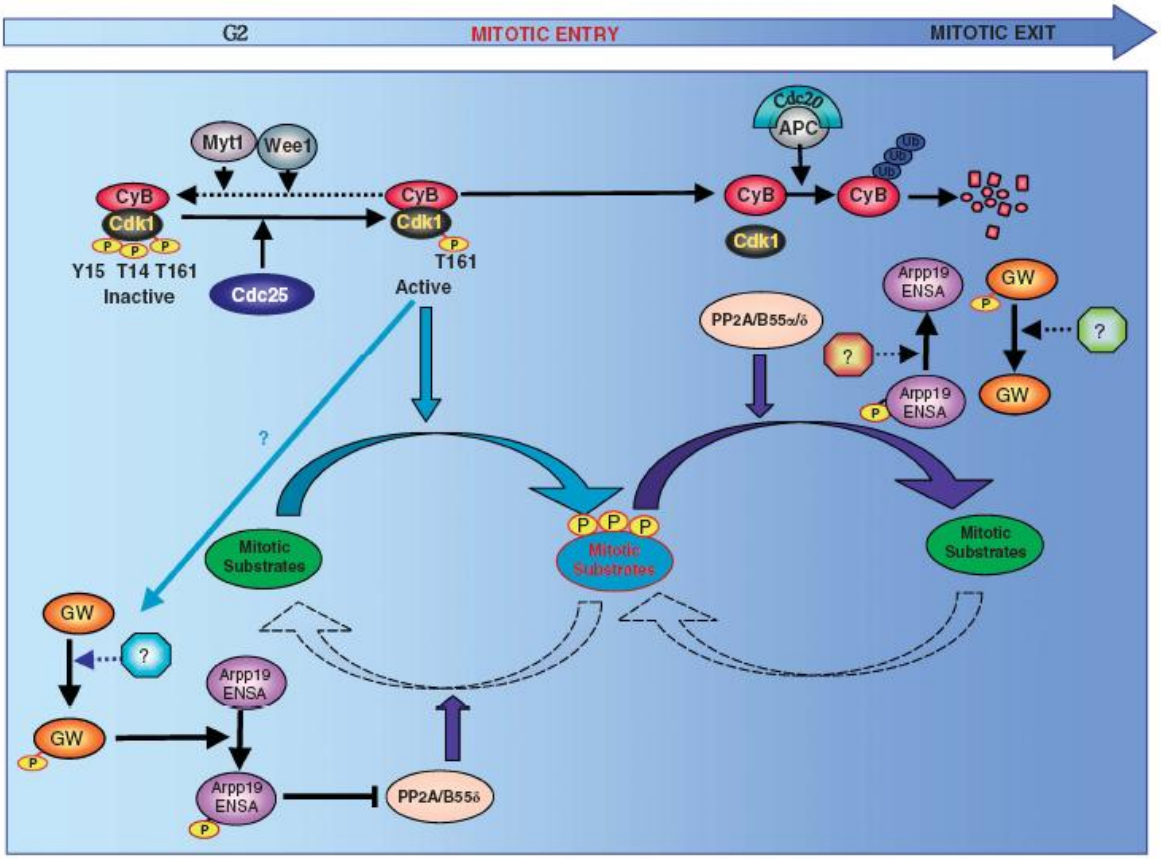

Figure 4.1 Regulatory network model of GWL during mitosis entry and exit
At G2/M transition, CDK1/Cyclin B1 complex and GWL are activated. CDK1/CycB1 phosphorylates mitotic substrates and GWL, which contributes to maintenance of mitotic substrate activation by inhibiting PP2A/B55δ complex through ARPP19/ENSA activation. PP2A/B55δ inhibition fully activates mitotic substrates and promotes entry in mitosis. At mitotic exit, Cyclin B1 is ubiquitinated by APC-CDC20 ubiquitin ligase and degraded; GWL is therefore inactivated and PP2A/B55δ consequent activation removes activating phosphorylations from mitotic substrates. Image from (147).

The functional orthologue of *GWL* in humans is *MASTL*, a gene that shares 50.2% and 65.7% of sequence homology to *Drosophila* and *Xenopus GWL*, respectively, and whose function is well-conserved (148). *MASTL* is located on chromosome 10 and encodes a protein kinase composed of 879 amino acids and with a molecular mass of about 97 kDa (Figure 4.2). To date, no crystal structures of full-length MASTL are available. Bioinformatic analysis revealed that MASTL has an unusual kinase structure: it contains the DFG and APE motifs, which are commonly shared by protein kinases and delimitate the activation segment (149) but, in between these two motifs, there is a large non-

conserved middle region (NCMR) of about 500 amino acids (150). The structure and the function of NCMR are still ambiguous, but it was demonstrated that this domain prevented MASTL to be expressed in a soluble form in *Escherichia coli*.

Figure 4.2 MASTL protein structure
Schematic representation of MASTL kinase structure: between the conserved DFG and APE motifs, it contains a ~500 amino acid region (non-conserved middle region, NCMR) whose function is still not clear; amino acid boundaries of the N- and C-terminals are indicated, as well as the Ser875 phosphorylation site known to be essential for MASTL function. Image from (150).

MASTL has a nuclear localization pattern throughout interphase but, during mitosis, it is exported to the cytoplasm before nuclear envelop breakdown (151). As for *Drosophila* and *Xenopus* GWL, MASTL has the crucial role of inhibiting the phosphatase activity of PP2A/B55δ complex during mitosis, in order to sustain the phosphorylation of CDK1 substrates (124); moreover, its inhibition caused multiple mitotic defects, such as lagging chromosomes, DNA bridges and cytokinesis failure. Also in human cells, MASTL was shown to be inactivated by PP1 phosphatase activity (152).

In addition to the regulation of mitotic progression, GWL was shown to function also as regulator of the DNA damage response (DDR); its depletion was associated with the delay of both checkpoint recovery and progression into cell cycle upon DNA damage induction (153). Human MASTL maintained this function and was also shown to be an essential player for the maintenance of genome integrity: its downregulation delayed the

entry in mitosis of damaged cells, caused a premature activation of the APC/C complex and induced genomic instability associated with genome endoreduplication (154).

In the recent years, evidence of both MASTL involvement in cancer progression and its targeting as promising approach for cancer therapy were provided. MASTL inhibition sensitized recurrent head and neck tumor cells to cisplatin treament (136) and lung cancer cells to radiation therapy (135). In breast cancer, MASTL upregulation was associated with a more advanced clinical stage (136) and also proposed as indicator of metastatic and disease relapse risk within the ER+ breast tumor subtype (155). Moreover, in both breast and colon cancer cell lines, it was demonstrated that upregulation of MASTL promoted tumor cell growth through the degradation of the phosphatase PHLPP, which usually inhibits AKT activity, thus leading to AKT hyperactivation (156). Based on these recent findings that characterized MASTL as a highly valuable drug target for cancer treatment, a preliminary small-molecule MASTL inhibitor was developed (150); of note, it was created starting from the structure of the GWL minimal kinase domain, since the crystallization of full-length human GWL was not feasible.

4.2. Aims of the chapter

We have previously demonstrated, as described in chapter 3, that *MASTL* is a vulnerability gene for thyroid tumor cells, since its inhibition interfered with the growth of tumor but not of normal thyroid cells. In this chapter we aimed to dissect the molecular mechanisms that are at the basis of TC cell dependency on MASTL function. In particular, we depleted MASTL in TC cells by using RNAi, and investigated the effects of its silencing on cell proliferation, cell division, cell viability and accumulation of DNA damage.

4.3. Results

4.3.1. Effects of MASTL depletion on TC cell growth

We have previously observed that MASTL depletion led to inhibition of the growth of a panel of TC cell lines (section 3.3.5). For the studies hereafter presented, we selected two ATC-derived cell lines, namely HTC/C3 and 8505C; the results obtained would ideally contribute to the design of alternative strategies to ATC treatment, as they currently lack effective therapies (already described in section 1.1.1.4). HTC/C3 and 8505C cells were transfected with control (siNT) and three MASTL (siMASTL #1, #4 and #5) siRNAs and plated 24 hours later for both silencing efficiency and proliferation analyses (Figure 4.3A). By western blot we confirmed the effective silencing of *MASTL* in both HTC/C3 (Figure 4.3B) and 8505C (Figure 4.3C) cells. Cell proliferation was investigated by CellTiter-Glo assay and we found that MASTL siRNAs reduced the growth of both HTC/C3 (Figure 4.3D) and 8505C cells (Figure 4.3E), although with different extents. The effect of MASTL depletion on cell growth was also tested by colony forming assay as alternative approach: HTC/C3 and 8505C cells were transfected with control and MASTL siRNAs and stained 7 days later with crystal violet (Figure 4.3F-G); even if with different extents, cell growth inhibition was observed for all three MASTL siRNAs used, compared to control. Overall, these results suggest that MASTL is required for the proliferation of TC cells.

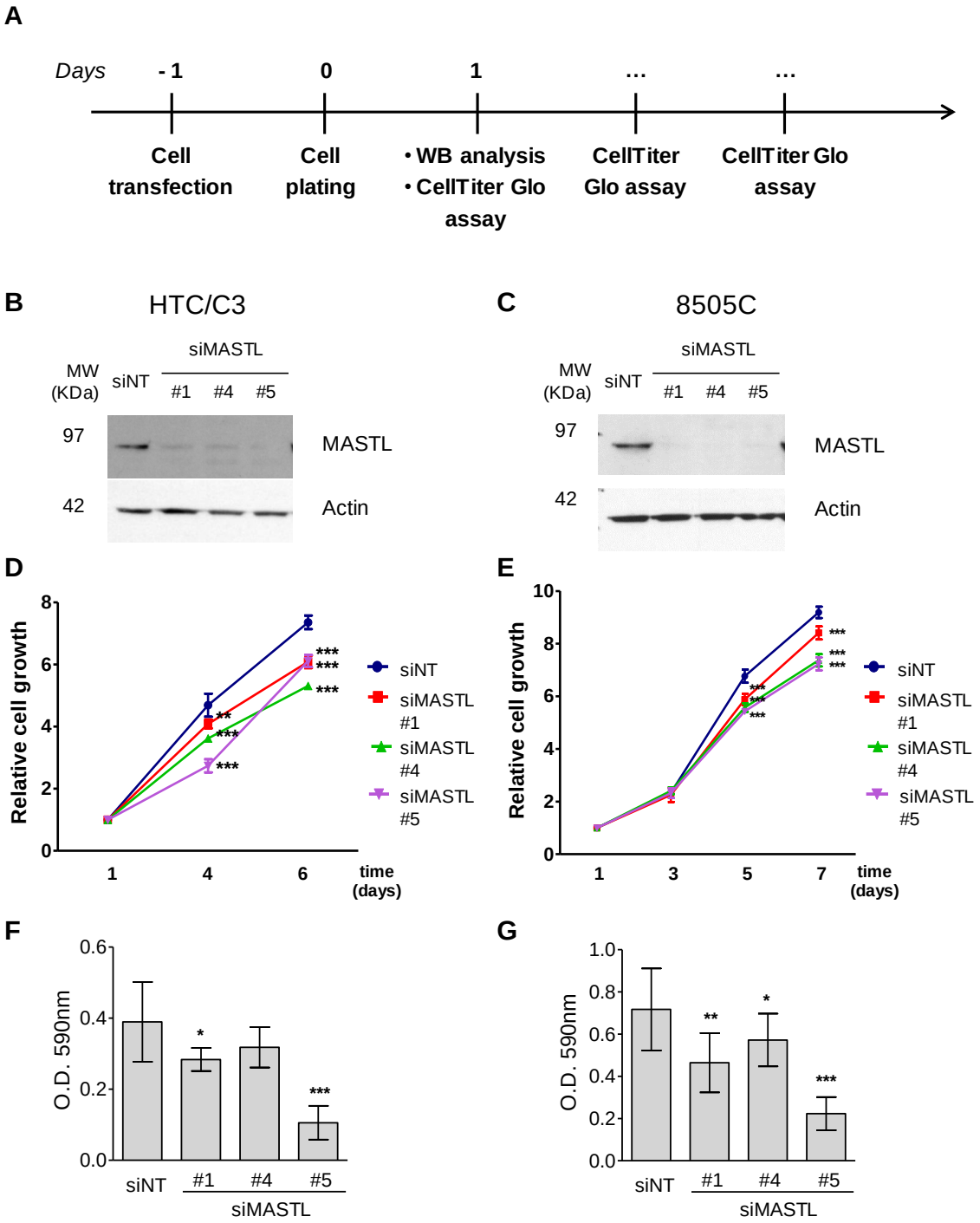

Figure 4.3 Effects of MASTL knockdown on TC cell proliferation

A-E) HTC/C3 and 8505C cells were transfected with control (siNT) and MASTL (siMASTL #1, #4 and #5) siRNAs and the following day were plated for silencing efficiency and proliferation ability testing as outlined in (A). Western blot analysis of MASTL expression in HTC/C3 (B) and 8505C (C); actin represents loading control. Growth curves of HTC/C3 (D) and 8505C (E) transfected and analyzed as indicated in A); cell growth was evaluated by CellTiter-Glo assay at the indicated time points after plating, plotted as mean +/- sd and normalized on day 1 values. **E-F)** Colony forming assay of HTC/C3 (E) and 8505C (F) cells 7 days after transfection with the indicated siRNAs; values represent optical density of Crystal Violet and are indicated as mean +/- sd of two (for HTC/C3) or three (for 8505C) independent experiments. Unpaired Student's t-test was used to compare control *vs* MASTL siRNAs (*p<0.05; **p<0.01; ***p<0.001).

4.3.2. Effects of MASTL knockdown on mitosis

MASTL plays a crucial role in the regulation of mitosis progression (124) and we have previously observed the presence of aberrant mitotic figures in TC cells upon its depletion (section 3.3.6). Since it is well established that aberrant mitoses can generate cells with abnormal nuclei (157), such as multiple/lobate nuclei, nuclear blebs and micronuclei, we investigated whether such nuclear aberrations could be produced by MASTL depletion. HTC/C3 cells transfected with control (siNT) and MASTL (siMASTL #1, #4 and #5) siRNAs were scored for the presence of aberrant nuclear structures 120 hours later by immunofluorescence (Figure 4.4A). The nuclear anomalies previously listed were observed in 16.9% of siMASTL #1-cells, 19.3% of siMASTL #4-cells and 21.1% of siMASTL #5-cells, but only 6.1% of control siNT-cells (Figure 4.4B). We performed the same analysis on 8505C cells 76 hours after siRNA transfection (Figure 4.4C). Also in this case, we observed a significant increase of cells displaying aberrant nuclei (Figure 4.4D): 28.1% for siMASTL #1, 36.8% for siMASTL #4 and 41.1% for siMASTL #5, in comparison with 14% for siNT. On the whole, these results suggest that MASTL depletion interferes with TC cell division process originating cells with abnormal nuclei.

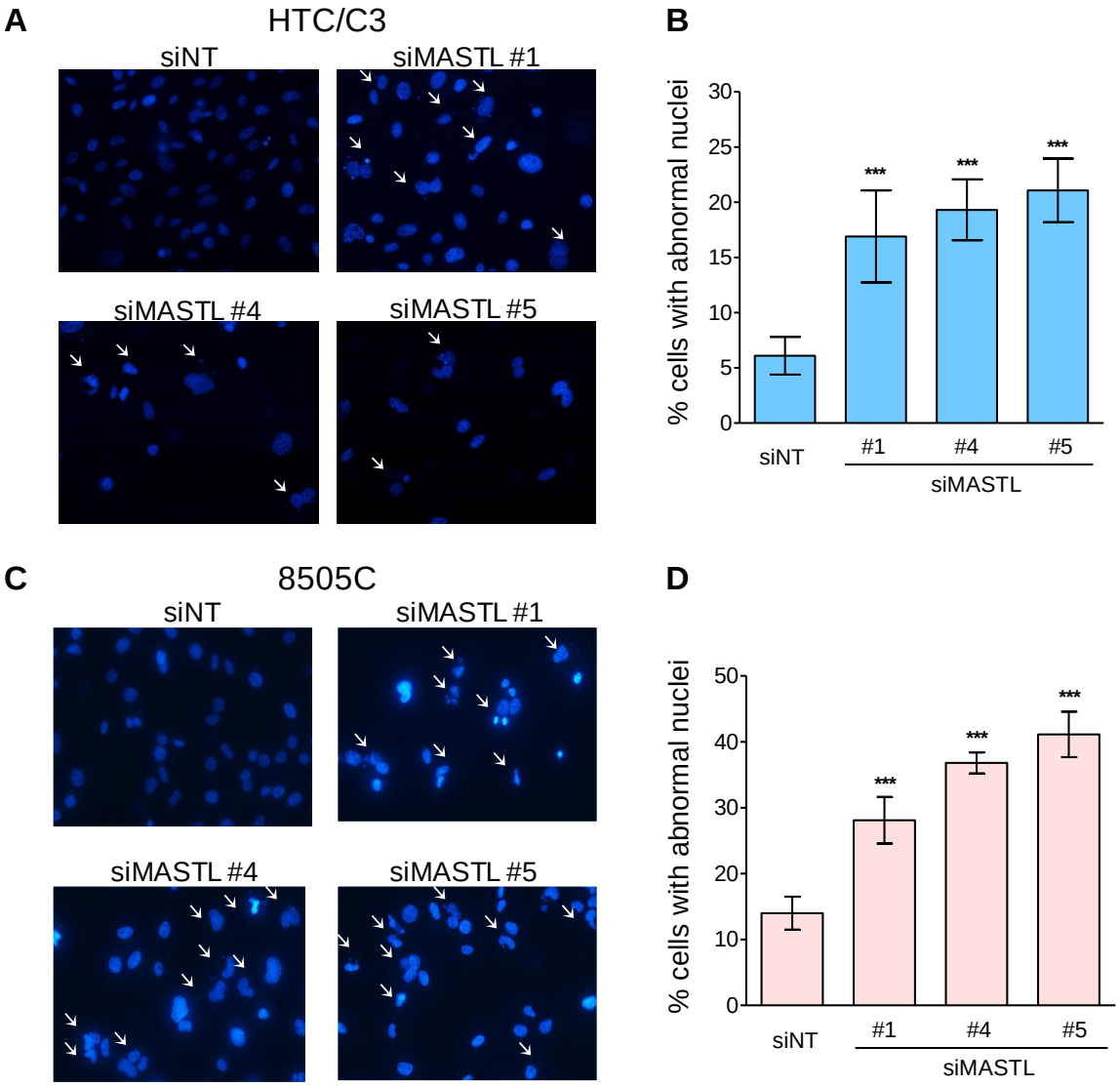

Figure 4.4 Analysis of the effects of MASTL knockdown on the structure of TC cell nuclei
A and C) Representative images of HTC/C3 and 8505C cells transfected with control (siNT) and three MASTL siRNAs and stained for nuclei (blue, DAPI) 120 (A) and 76 (C) hours later; cells with aberrant nuclei are indicated by arrows. **B and D)** Quantification of HTC/C3 and 8505C cells with abnormal nuclei analyzed in A and C); for each set, the percentage of abnormal nuclei (represented as mean +/- sd) was determined by counting a total number of 1900-2000 cells (B) and 3000 cells (D) from 8 and 6 independent experiments, respectively. Unpaired two-tailed Student's t-test was used to compare control (siNT) vs MASTL (siMASTL #1, #4, #5) depleted cells; asterisks indicate statistical significance (***p<0.001)

4.3.3. Effects of MASTL depletion on TC cell viability

Mitotic aberrations and formation of cells with abnormal nuclei (such as multiple nuclei and micronuclei) are generally described as "mitotic catastrophe", an event that eventually leads to cell death by apoptosis or necrosis (158). Since we observed both a

reduction of TC cell growth (section 4.3.1) and an increase of TC cells displaying nuclear aberrations upon MASTL depletion (section 4.3.2), we investigated whether *MASTL* silencing might be associated with occurrence of TC cell death. For the studies hereafter presented, we used siMASTL #5 oligo to deplete MASTL, as we previously observed that it gave the maximum effects on growth inhibition and aberrant nuclei formation. HTC/C3 and 8505C were transfected with siNT and siMASTL #5 and analyzed at different time points. Starting from 72 hours after transfection, we observed morphological changes in HTC/C3 depleted cells, as some appeared to be enlarged in size, together with the presence of floating cells (Figure 4.5A). Western blot analysis showed efficient MASTL silencing, as early as 48 hours after transfection, and an increase of apoptotic markers cleaved Caspase 3 and cleaved PARP, starting from 72 hours after transfection (Figure 4.5B). Moreover, we observed an increase of phosphorylated-CDK1 levels on Tyrosine 15 at the latest time points, thus supporting impairment in cell cycle progression. For 8505C cells, although morphological changes were not marked as for HTC/C3, we observed the presence of floating cells starting from 96 hours after transfection of MASTL siRNA (Figure 4.5C). Similarly to HTC/C3, western blot analysis showed efficient MASTL silencing and increased expression of cleaved Caspase 3, cleaved PARP and phosphorylated-CDK1 in MASTL-depleted cells, compared to control (Figure 4.5D). These findings suggest that MASTL depletion is associated with apoptotic cell death.

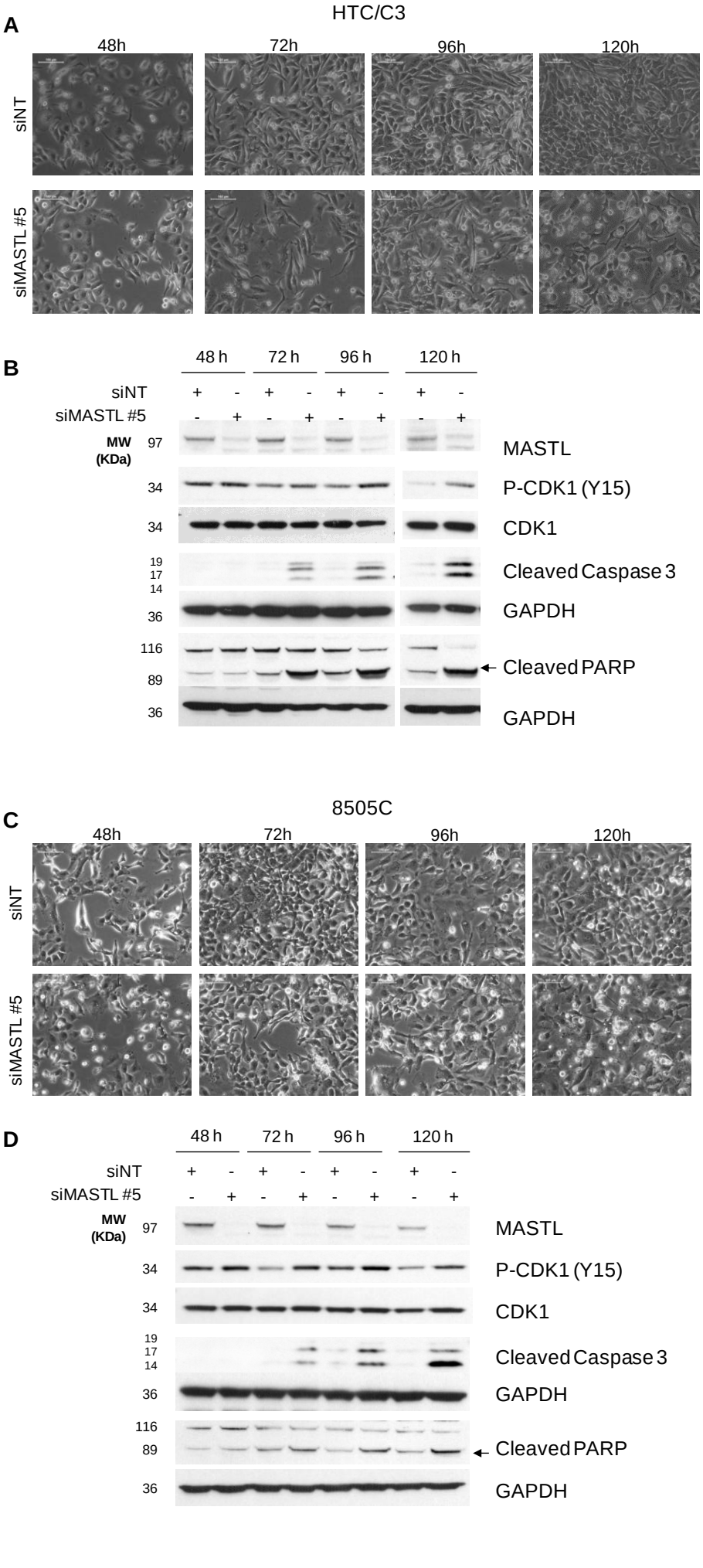
A
HTC/C3
48h
72h
96h
120h
siNT
siMASTL #5
B
48 h
72 h
96 h
120 h
siNT
siMASTL #5
MW (KDa)
97
34
34
19
17
14
36
116
89
36
MASTL
P-CDK1 (Y15)
CDK1
Cleaved Caspase 3
GAPDH
Cleaved PARP
GAPDH
C
8505C
48h
72h
96h
120h
siNT
siMASTL #5
D
48 h
72 h
96 h
120 h
siNT
siMASTL #5
MW (KDa)
97
34
34
19
17
14
36
116
89
36
MASTL
P-CDK1 (Y15)
CDK1
Cleaved Caspase 3
GAPDH
Cleaved PARP
GAPDH

Figure 4.5 Effects of MASTL knockdown on TC cell viability
A and C) Representative images of HTC/C3 (A) and 8505C (C) at the indicated time points after transfection with control (siNT) and MASTL (siMASTL #5) siRNAs. **B and D)** Western blot analysis of HTC/C3 (B) and 8505C (D) cells for MASTL, phosphorylated CDK1 (Tyr15), total CDK1, cleaved Caspase 3 and cleaved PARP expression; GAPDH was used as loading control. One representative out of two independent experiments is shown for each cell line.

To further corroborate the occurrence of TC cell death upon MASTL depletion, we performed Annexin V assay on MASTL-depleted and control HTC/C3 cells followed by flow cytometry analysis (Figure 4.6A). We observed that MASTL depletion reduced the number of viable cells in comparison with control (Figure 4.6B): siNT-HTC/C3 viable cells (TO-PRO-3^-/Annexin V^-) were 92.7% at 48 hours, 80.2% at 72 hours, 62.2% at 96 hours and 71.0% at 120 hours after transfection; siMASTL-HTC/C3 viable cells were 91.4% at 48 hours, 65.5% at 72 hours, 27.6% at 96 hours and 30.6% at 120 hours after transfection. The percentage of early apoptotic cells (TO-PRO-3^-/Annexin V^-) of siNT and siMASTL transfected cells respectively were: 0.9% and 0.6% at 48 hours, 1.9% and 4.5% at 72 hours, 3.4% and 4.0% at 96 hours, 3.6% and 1.3% at 120 hours. Dead cells in apoptosis (TO-PRO-3^+/Annexin V^+) for control and MASTL-depleted groups respectively were: 4.1% and 3.5% at 48 hours, 13.0% and 22.7% at 72 hours, 28.6% and 42.5% at 96 hours, 18.1% and 31.4% at 120 hours. Cells considered either necrotic or which already ended cell death through apoptosis (TO-PRO-3^+/Annexin V^-) were respectively for siNT and siMASTL: 2.3% and 4.5% at 48 hours, 5.0% and 7.3% at 72 hours, 5.8% and 26.0% at 96 hours, 7.1% and 36.6% at 120 hours after transfection. The same analysis is currently in progress on 8505C cells. Overall, our findings indicate that MASTL depletion is associated with decreased TC cell viability and increased cell death. This was associated with apoptosis but, given that we also observed an increase of MASTL-depleted cells that are considered either necrotic or apoptotic cells having already lost membrane integrity and Annexin V staining, we could not exclude that also necrotic cell death may occur.

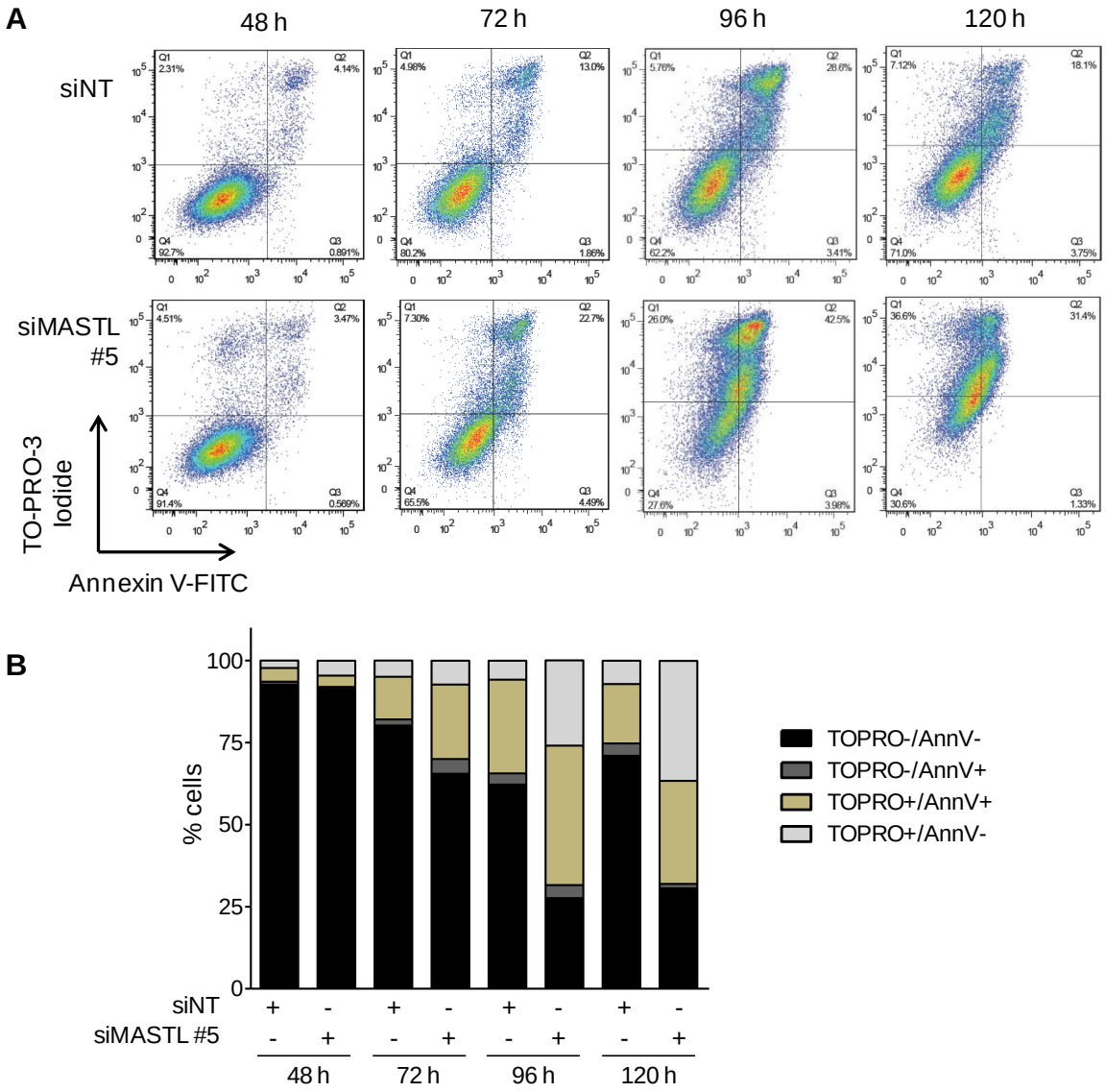

Figure 4.6 Characterization of MASTL knockdown effects on HTC/C3 viability
Representative dot plot **(A)** and relative histogram representation **(B)** of FACS analysis of HTC/C3 cells, transfected with control (siNT) and MASTL (siMASTL #5) siRNAs, at the indicated time points after transfection; cells were stained with FITC Annexin V Apoptosis Detection Kit (BD Pharmingen™), in which TO-PRO-3 iodide replaced propidium iodide; TO-PRO-3$^-$/Annexin V$^-$ staining represent viable cells, TO-PRO-3$^-$/Annexin V$^+$ represents early apoptotic cells, TO-PRO-3$^+$/Annexin V$^+$ indicates apoptotic cells; TO-PRO-3$^+$/Annexin V$^-$ indicates necrotic cells and dead cells that have already ended apoptosis and have lost membrane integrity and Annexin V staining. One representative out of two independent experiments is shown.

4.3.4. Effects of MASTL depletion on DNA damage

It is well established that chromosome segregation errors are often associated with occurrence of structural chromosomal aberrations and DNA double strand breaks (DSB) (159). Given the effects on mitosis observed upon MASTL depletion, together with

evidence of MASTL involvement in response to DNA damage (136), we investigated whether its depletion may induce DNA DSBs in TC cells. To this aim, we analyzed by western blot the expression of phosphorylated histone H2AX on Serine 139 (referred to as γH2AX), an established marker of DNA DSBs (160), in control (siNT) and MASTL depleted (siMASTL #5) cells. Together with efficient MASTL silencing as early as 48 hours after siRNA transfection, we observed a gradual increase of γH2AX expression levels in both HTC/C3 (Figure 4.7A) and 8505C (Figure 4.7B) MASTL-depleted cells starting from 72 hours after transfection. These results suggest that MASTL depletion may lead to accumulation of DNA damage in TC cells.

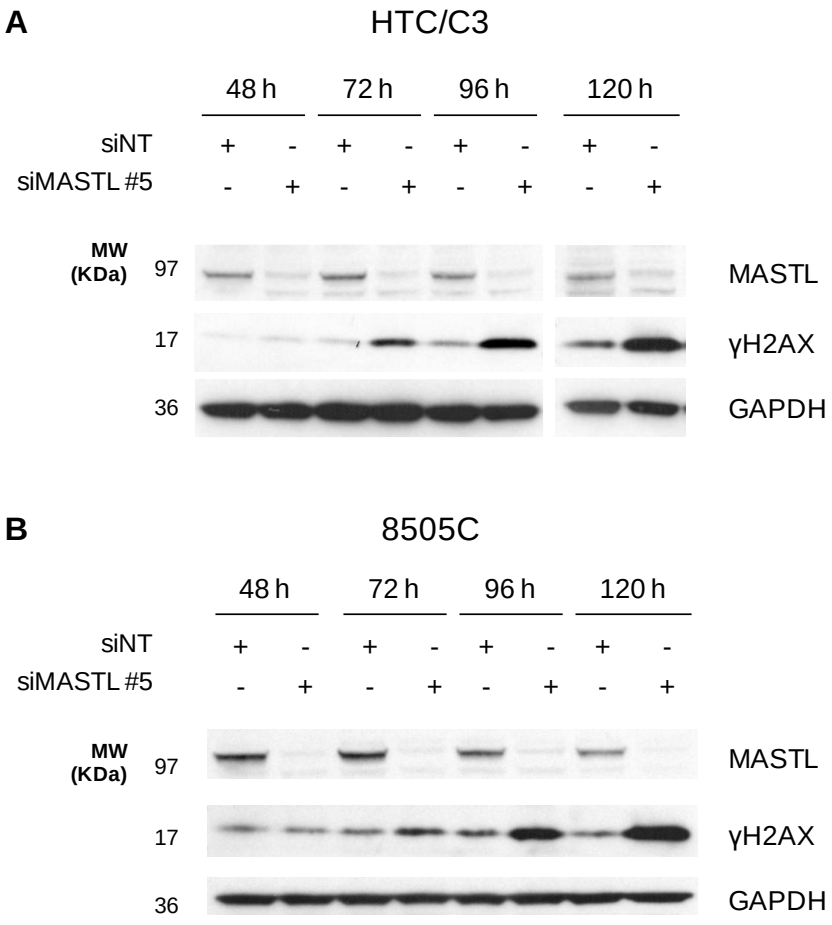

Figure 4.7 Effects of MASTL depletion on occurrence of DNA damage
Western blot analysis of MASTL and γH2AX expression in HTC/C3 **(A)** and 8505C **(B)** cells at the indicated time points after transfection with control (siNT) and MASTL (siMASTL #5) siRNAs. GAPDH was used as loading control. One representative out of two independent experiments is shown. Protein extracts used in panel A for HTC/C3 are the same used in figure 4.4.

4.3.5. Lentiviral-mediated stable *MASTL* silencing in TC cells

We searched for a system to stably inhibit MASTL expression for future studies, in order to obtain a more controlled MASTL knockdown and to explore the long-term effects of its depletion in TC cells. To this aim we purchased an inducible lentiviral shRNA system, namely TRIPZ (Figure 4.8A): the lentiviral vector carried a specific shRNA together with *red fluorescent protein* (*RFP*) under the control of a tetracycline-inducible promoter, thus allowing the expression of the shRNA only upon doxycycline administration. The plasmid also contained a puromycin-resistance cassette to allow the selection of stably transduced cells. TRIPZ system was already demonstrated to produced efficient gene silencing in other cell models (161,162). We purchased TRIPZ vectors containing two different shRNA sequences targeting MASTL, namely TRIPZ-shMASTL #1 and TRIPZ-shMASTL #2. We transduced 8505C cells with the two vectors and selected transduced cells with puromycin. Cells were then treated with 1 μg/ml and 2 μg/ml doxycycline and RFP expression was monitored: as early as 24 hours after treatment, both 8505C-TRIPZ-shMASTL #1 and 8505C-TRIPZ-shMASTL #2 cells were positive for RFP at fluorescent microscope observation (Figure 4.8B). Western blot analysis of 8505C-TRIPZ-shMASTL #1 and 8505C-TRIPZ-shMASTL #2 cells showed a gradual decrease of MASTL expression upon doxycycline administration, in comparison with untreated cells (Figure 4.8C), thus indicating that the shRNAs targeting MASTL are induced together with RFP after doxycycline administration. These observations support the effectiveness of the system to stably inhibit MASTL expression in 8505C cells.

A

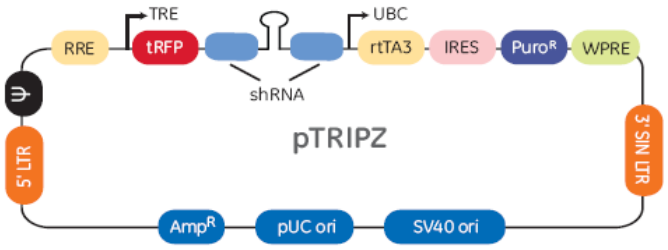
TRE
UBC
RRE
tRFP
rtTA3
IRES
Puro^R
WPRE
shRNA
pTRIPZ
5' LTR
3' SIN LTR
Amp^R
pUC ori
SV40 ori

B

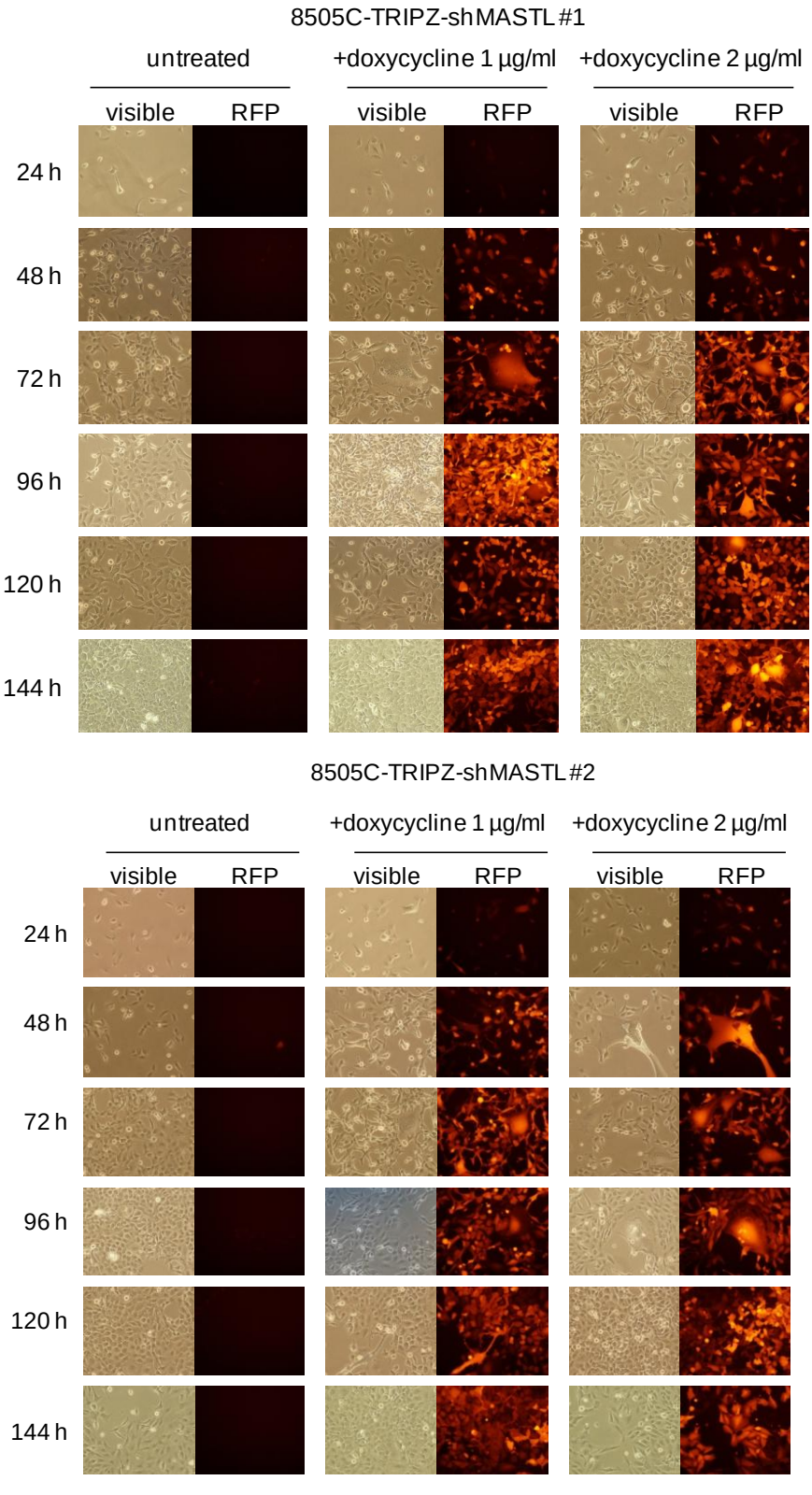
8505C-TRIPZ-shMASTL#1
untreated
+doxycycline 1 µg/ml
+doxycycline 2 µg/ml
visible
RFP
24 h
48 h
72 h
96 h
120 h
144 h
8505C-TRIPZ-shMASTL#2

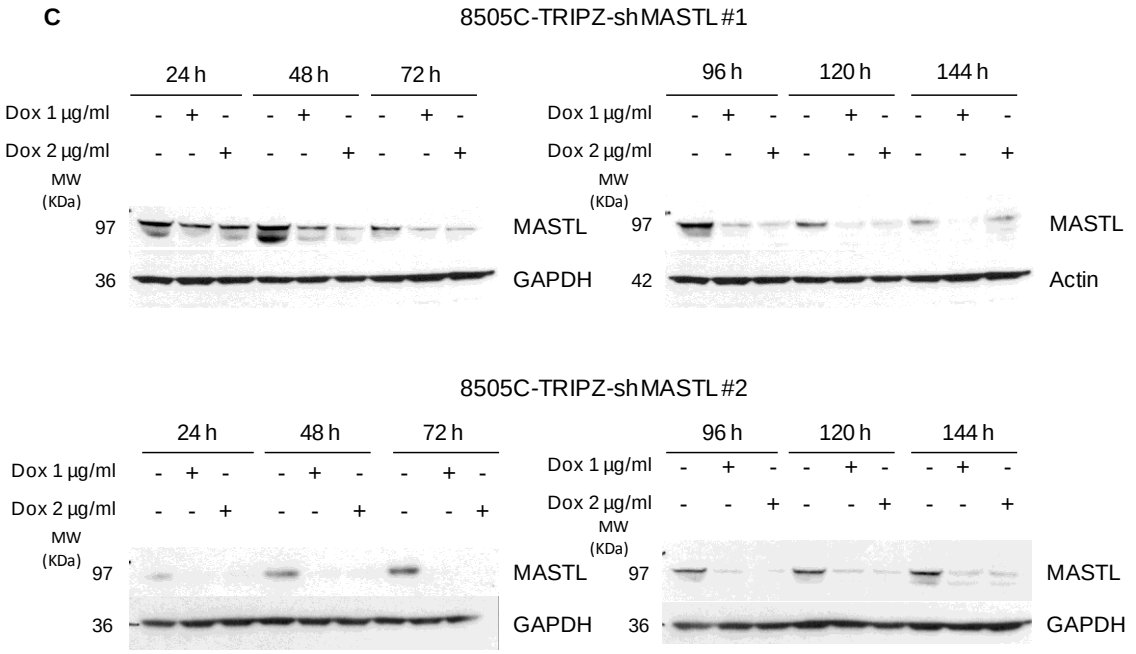

Figure 4.8 Stable MASTL silencing in TC cells
A) Schematic representation of the pTRIPZ Inducible Lentiviral shRNA and relevant features (TRE: tetracycline-inducible promoter, RFP: red fluorescent protein, UBC: human ubiquitin C promoter for constitutive expression of rtTA3 and puromycin resistance genes; rtTA3: reverse tetracycline-transactivator 3 for tetracycline-dependent induction of the TRE promoter, $Puro^R$: Puromycin resistance to selectively propagate stable integrants). **B)** Representative images of 8505C cells stably transduced with either TRIPZ-shMASTL #1 or TRIPZ-shMASTL #2 lentiviral vectors; cells were treated with 1 µg/ml doxycycline, 2 µg/ml doxycycline or left untreated, and pictures were taken at the indicated time points to monitor RFP expression in the different populations. **C)** Western blot analysis of MASTL expression levels in 8505C-TRIPZ-shMASTL #1 and 8505C-TRIPZ-shMASTL #2 cells represented in B); GAPDH and Actin represent loading controls.

We performed a preliminary experiment to test the growth of 8505C-TRIPZ-shMASTL #2 upon MASTL depletion. We induced the expression of RFP and shMASTL #2 by administration of 2 µg/ml doxycycline and monitored RFP expression, which was clearly detectable even 11 days later in treated cells, and absent in untreated ones (Figure 4.9A). We observed, by western blot analysis and CellTiter-Glo assay respectively, that doxycycline treatment decreased MASTL expression (Figure 4.9B) and inhibited 8505C cell growth (Figure 4.9C), in comparison with untreated cells. Together, these results further support the effectiveness of lentiviral system and suggest that long-term MASTL depletion impairs the growth of TC cells.

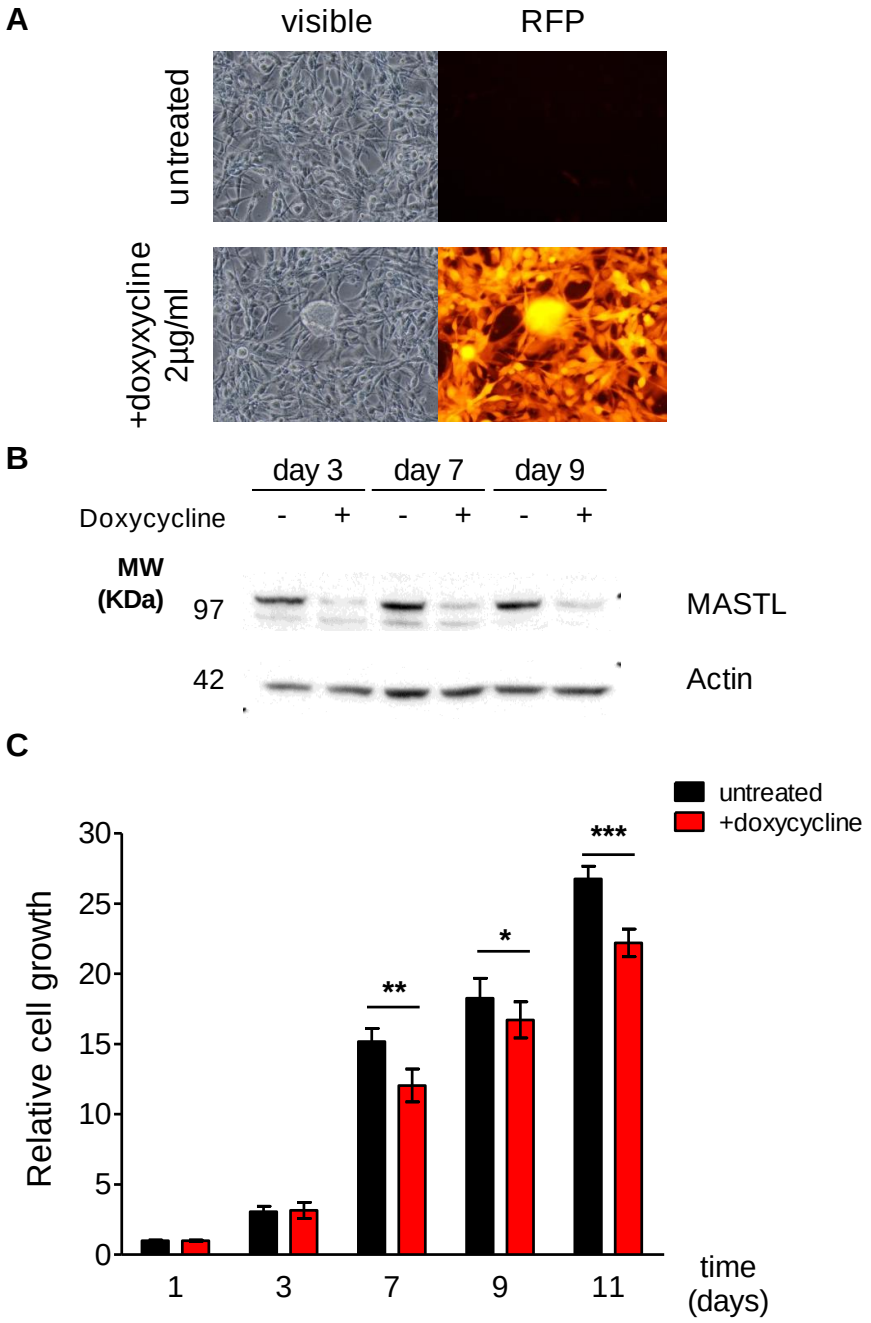

Figure 4.9 Effects of MASTL knockdown on long-term 8505C cell growth
8505C cells transduced with TRIPZ-shMASTL #2 lentiviral vector were tested for RFP expression, MASTL silencing and proliferation ability. **A)** Representative images of treated and untreated cells cells at 11 days after doxycycline administration; both visible and RFP fluorescence images are reported. **B)** Western blot analysis of MASTL expression at the indicated time points after doxycycline treatment in cells represented in A); actin was used as loading control. **C)** Growth rates of cells, represented in A) and B), at the indicated time points; cell growth was evaluated by CellTiter-Glo assay at the indicated time points after plating, plotted as mean +/- sd and normalized on day 1 values; unpaired two-tailed Student's t-test was used to compare untreated *vs* doxycycline-treated cells (*p<0.05; **p<0.01; ***p<0.001).

4.3.6. Set up of IHC analysis of MASTL expression

As preliminary for future studies aimed to assess MASTL expression in thyroid tissues, we purchased MASTL antibody (clone 4F9, Millipore) used for immunohistochemistry (IHC) analysis in the study presented by Wang and colleagues (136) and tested its working conditions on 8505C cells transfected with siNT and siMASTL as positive and negative controls, respectively. By western blot analysis, we first confirmed the reduction of MASTL expression in siMASTL-cells, in comparison with siNT (Figure 4.10A). Then, in collaboration with the immunohistochemistry facility of our institute, we embed 8505C siNT and siMASTL cells in paraffin, in order to mimic conditions of IHC tissue analysis, and performed IHC; nuclear MASTL staining was observed in the positive (siNT) but not negative (siMASTL) control (Figure 4.10B). These observations assert the effectiveness of the antibody for IHC applications and support the feasibility of future studies aimed to assess MASTL expression in thyroid tissues by IHC.

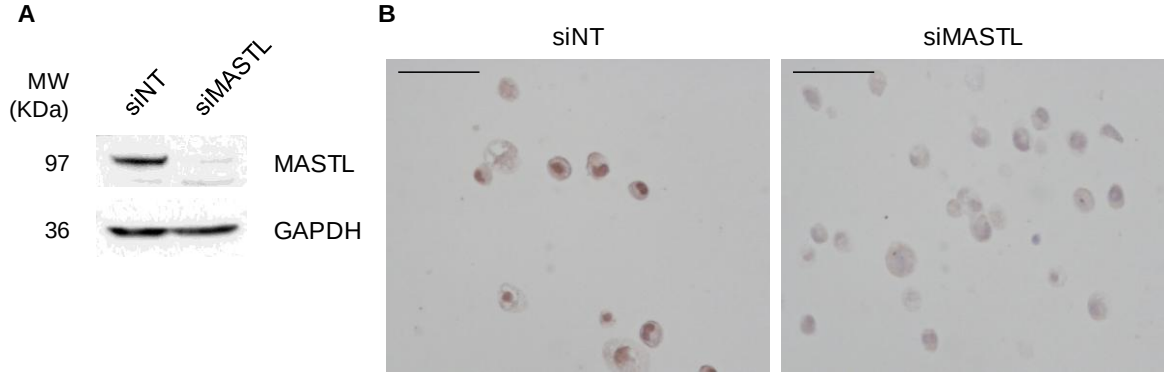

Figure 4.10 IHC analysis of MASTL expression in paraffin embedded 8505C cells
8505C cells were transfected with control and MASTL siRNAs and embedded in paraffin 48 hours later for IHC testing of MASTL antibody. **A)** Western blot analysis for MASTL expression in siNT and siMASTL 8505C cells; GAPDH represents loading control. **B)** Representative images of IHC analysis of MASTL expression in 8505C siNT and siMASTL cells; scale bar=50 µm.

4.4. Discussion

In this chapter, we dissected the effects of MASTL depletion on the regulation of thyroid tumor cell biology. We knocked down MASTL in two ATC-derived cell lines by using three different siRNAs and demonstrated a significant reduction of the growth of TC cells, compared to control. We found that MASTL-depleted TC cells displayed increased nuclear aberrations, such as multiple nuclei, micronuclei or lobular nuclei. MASTL depletion also led to increased expression of apoptotic markers, cell death and DNA damage, compared to control.

MASTL recently emerged as promising therapeutic target for cancer treatment: its inhibition was able to reduce the viability of head and neck tumor cells when combined with cisplatin treatment (136) and of non small cell lung cancer cells when combined to radiation therapy (135). Notably, these studies reported that MASTL inhibition alone had a partial (136) or null (135) growth inhibitory effect on tumor cells. To date, MASTL role in the regulation of thyroid tumor cell biology has been never explored. Our studies demonstrated that its inhibition hampered the growth of thyroid tumor cells, thus further pointing out its relevance as possible target for cancer treatment. Of note, we observed that the three different MASTL siRNAs produced different extents of growth inhibition on TC cells. We hypothesized that these differences may be related to the different sequences of siRNAs: as they target different MASTL exons, it may be possible that the secondary structure of the mRNA influences their stability and silencing efficacy during time. Moreover, we decided to set a lentiviral-mediated inducible system to stably silence MASTL expression, in order to obtain a more controlled inhibition of MASTL expression that would last during time; we already tested the system on 8505C cells and observed its

efficacy in depleting MASTL in cells together with inhibition of the growth. This system will be useful for future studies on the role exert by MASTL in thyroid tumor cell biology.

We described in the previous chapter the presence of aberrant mitotic figures in MASTL-depleted TC cells, which were in line with previous observations in other cell models (124,151). The outcome of such aberrant mitoses is indicated as “mitotic catastrophe”, that is an aberrant form of mitosis, whose ultimate step consists in the formation of cells with aberrant nuclear structures, as multiple nuclei, micronuclei and lobular nuclei (158). Mitotic catastrophe is considered as a process preceding cell death, which may occur through apoptotic or necrotic mechanisms either after or during deregulated mitosis. Here, we observed that MASTL silencing led to the increase of TC cells displaying such nuclear anomalies, thus suggesting that MASTL inhibition may cause mitotic catastrophe in TC cells. Moreover, we observed increased cell death upon MASTL depletion. Western blot analysis showed occurrence of apoptosis, but Annexin V assay suggested that also necrotic cell death may occur. Together, these findings agree with the current knowledge about the outcome of cells undergoing mitotic catastrophe (158). The stimulation of mitotic catastrophe emerged as a promising strategy for cancer treatment. As a matter of fact, tumor cells often displayed mitotic catastrophe features upon treatment with ionizing radiations (163) or with drugs that hinder proper cell division, such as agents targeting microtubules, mitotic checkpoint components (164), and mitotic regulators as Aurora kinases, PLK1 and MPS1 (164). The final result of these treatments was tumor cell death (165). With regards to thyroid tumors, the targeting of mitotic regulators has already been explored and promising results were provided: targeting of PLK1 (166) and Aurora kinases (167) through small-molecule inhibitors significantly reduced the growth and induced cell death in ATC-derived cell lines. Our study, by showing unequivocal reduction of cell viability and increase of cell death upon MASTL

depletion, identified a novel mitotic target and strengthened the evidence of mitotic regulators as promising targets for thyroid tumor treatment.

We also found that MASTL silencing led to the accumulation of DNA damage in TC cell; we hypothesized that this increase may be related to different mechanisms. Chromosome segregation errors during mitosis are known to generate structural damage to chromosomes (159) and it is known that mitotic catastrophe cells accumulate chromosomal breaks that eventually trigger DNA damage response and cell death (168). As we observed both aberrant mitotic figures and mitotic catastrophe features in TC cells upon MASTL depletion, we hypothesized that the inhibition of MASTL may lead to structural DNA damage in TC cells. On the other hand, it is known that tumor cells exhibit higher levels of endogenous DNA damage, compared to normal ones, as result of the activity of oncogenes that promote uncontrolled cell growth; therefore, tumor cells become dependent on the activity of pathways that promote damage repair in order to sustain tumorigenic processes (169). Since MASTL is involved in both the regulation of DNA damage response (153) and the maintenance of genome stability during DNA damage response (154), we hypothesized that its inhibition in TC cells may lead to further accumulation of damaged DNA. Whether MASTL-associated DNA damage accumulation is related to one or the other mechanisms, or even related to both, remains to be investigated.

On the whole, our studies supported the notion that MASTL represents a vulnerability for thyroid tumor cells: its inhibition hindered thyroid tumor cell growth and was associated with mitotic catastrophe, cell death and increased DNA damage. Our results, together with recent literature data, propose MASTL as valuable target for cancer therapy, putting the rationale for the development of small-molecule inhibitors to be tested for therapeutic purposes.

5. Results: COPZ1 studies

As previously reported, the aim of our studies was to identify thyroid tumor cell vulnerabilities; as described in chapter 3, among the putative non-oncogenes identified through the functional siRNA screening, we found *COPZ1*. Even though the majority of my studies were aimed to the dissection of MASTL role in TC cell biology, in our laboratory we also studied the role exerted by COPZ1 in the regulation of TC cell viability, to which I directly collaborated.

COPZ1 encodes the *ζ*-subunit of coatomer protein complex I (COPI), which is a heptameric vesicular-carrier protein complex (137). COPI most characterized function is the transport of proteins from the Golgi complex back to the endoplasmic reticulum and in between Golgi compartments. In addition to this function, COPI complex was also found to be involved in the maturation of endosomes and regulation of autophagy: depletion of COPI subunits impaired transport of autophagic vacuoles into early endosomes with the consequent accumulation of autophagic vacuoles and inhibition of the autophagic flux (138). Moreover, COPI was identified as regulator of lipid storage and subsequent maintenance lipid homeostasis (139).

COPZ1 recently emerged as target gene for tumor therapy (125). It was demonstrated that tumor cells become dependent on COPZ1 activity because of the downregulation of its isoform COPZ2. The suppression of COPZ1 activity was effective in inducing cell death in both proliferating and non-diving tumor cells, while leaving unaffected normal cells. Also other members of COPI complex were reported to be promising targets for cancer therapy. *COPA*, which encodes the α-subunit of the complex, emerged from a siRNA screening as vulnerability gene in mesothelioma cells, as its

silencing inhibited both *in vitro* and *in vivo* tumor cell growth (170). *KRAS* mutant tumors showed synthetic lethality with *COPB2*, that encodes the β'-subunit of COPI (171). The targeting of different members of the COPI complex was associated with abortive autophagy and induction of cell death in different types of tumor cell lines (172) and a recent work identified *ARCN1*, which encodes the δ-subunit of the complex, as valuable target to block cell growth in different tumors (173). Interestingly, COPZ1 crystal structure was produced, thus laying the foundation for future studies aimed to design specific COPZ1 inhibitors (174).

COPZ1 was among the top-ranked hit genes resulted from the functional screening described in chapter 3; the aim of the studies presented in this chapter was to dissect the mechanisms through which COPZ1 knockdown inhibited the growth of TC cells. The results of this study are hereafter summarized.

We demonstrated that COPZ1 depletion by transient siRNA transfection dramatically impaired the growth of TC cell lines, representative of the different histotypes and carrying different genetic lesions; we also found that its silencing did not affect the growth and viability of normal thyrocytes and human mammary epithelial HME-1 cells. We demonstrated in a PTC-derived (TPC-1) and an ATC-derived (8505C) cell lines that COPZ1 depletion impaired productive autophagy by causing the accumulation of autophagosomes and block of autophagic flux, thus producing an abortive autophagy process. We also observed endoplasmic reticulum stress and unfolded protein response activation upon COPZ1 depletion, that eventually caused apoptotic cell death. *In vivo* silencing of *COPZ1* in 8505C mouse xenografts significantly reduced tumor growth and immunohistochemical analysis on explanted tumors showed decrease of proliferation markers and increase of necrosis. We analyzed the expression levels of *COPZ2,* that is *COPZ1* isoform*,* in publicly available thyroid data sets, and found that is downregulated in

TC specimens, compared to normal thyroid, thus supporting the hypothesis that COPZ1 vulnerability of TC cells may be related to the absence of its paralogous COPZ2.

Together, our findings demonstrated that *COPZ1* represents a vulnerability for TC cells, thus providing a new potential target for the design of therapeutic strategies.

Details and results of the study are presented in the attached reprint of the paper (Appendix B):

- Anania MC, Cetti E, Lecis D, Todoerti K, Gulino A, Mauro G, Di Marco T, Cleris L, Pagliardini S, Manenti G, Belmonte B, Tripodo C, Neri A, and Greco A. Targeting COPZ1 non-oncogene addiction counteracts the viability of thyroid tumor cells. *Cancer Letters* (2017) in press doi: 10.1016/j.canlet.2017.09.024.

6. General discussion and future perspectives

6.1. Discussion and conclusions

The global aim of the thesis was to identify potential novel targets for thyroid cancer treatment. The entire project arose from the evidence that current therapies for thyroid tumors, which are the most common endocrine malignancy, are still not effective in treating the recurrent and advanced forms (84). Most of thyroid tumors are represented by well-differentiated forms, which generally have a good prognosis and standard therapy is generally effective (78). Nevertheless, some tumors relapse and progress to the undifferentiated forms, whose treatment is still a demanding challenge. Despite the recent improvement in both the diagnosis and the knowledge of molecular alterations that drive thyroid tumorigenesis, the lack of effective therapies, especially for the advanced forms, is still present (1). The use of novel therapies such as small-molecule kinase inhibitors improved the survival of patients not responding to conventional treatment, but also produced severe side verse effects that hampered quality of life of patients (84). To identify nodal points for therapeutic intervention, our laboratory faced the concept of non-oncogene addiction (NOA) in thyroid tumors. NOA concept states that, in response to activation of oncogenes, tumor cells undergo increased cellular stresses and therefore rely on the activity of genes involved in stress support pathways, in order to maintain their tumorigenic capacity (98). Normal cells are not dependent on these genes, as their stress levels are not increased. NOA genes, which are not oncogenes themselves, become therefore attractive targets for therapeutic intervention, as their targeting would ideally be detrimental for tumor cell growth while not affecting normal

cells. To identify potential NOA genes in thyroid tumors, our laboratory performed a loss-of-function screening on tumor and normal thyroid cell lines using a siRNA library targeting about 9000 genes considered “druggable”. RNAi-based loss of function screenings, at variance with the current approaches of NGS technologies that allow the identification of genetic lesions at the basis of tumorigenic processes, demonstrated to be a successful strategy for the identification of “non-onogenes” essential for tumor growth (106-108,110). Our functional screening identified a list of 15 genes whose inhibition inhibited the growth of tumor but not normal thyroid cells.

The first part of the thesis aimed to validate the 15 hit genes in the original cell models used for the screening and to extend the analysis of the effects of their silencing on the viability of various thyroid cell lines, representative of the different TC histotypes. Thyroid TCGA dataset interrogation showed that hit genes had variable expression levels among PTC samples and the normal counterpart and, notably, were not mutated, thus uncovering their reliability as putative “non-oncogenes”. After selection of efficiently working antibodies and siRNAs, we selected 3 out of the 15 hit genes for validation studies: *MASTL* (encoding a mitotic kinase), *CCND1* (encoding a regulator of CDK4/6 activity) and *COPZ1* (encoding a regulator of protein vesicular transport). Functional studies confirmed the growth inhibitory effect of *MASTL*, *CCND1* and *COPZ1* silencing in the tumor but not normal cell lines used for the screening and, interestingly, we demonstrated that the growth of other TC cell lines, derived from different tumor histotypes and carrying different genetic lesions, was sensitive to their inhibition. These results demonstrated that MASTL, Cyclin D1, and COPZ1 represent thyroid tumor cell vulnerabilities and are noteworthy for further studies, aimed to explore their targeting as possible strategy for therapeutic intervention. Moreover, this validation study highlighted the effectiveness of large-scale RNAi-based functional screening in identifying tumor cell

vulnerabilities, thus supporting the strength of RNAi-based approaches in the discovery of novel therapeutic targets (106-110).

The studies presented in the second and third part of the thesis aimed to identify the mechanisms through which the inhibition of MASTL and COPZ1, respectively, hindered TC cell growth. We observed that MASTL silencing in two ATC-derived cell lines reduced cell proliferation ability. In parallel, cells exhibited features of mitotic catastrophe, documented by the increase of aberrant nuclear morphologies as micronuclei or multiple nuclei. Moreover, MASTL depletion was associated with TC cell death that was possibly mediated by both apoptotic and necrotic mechanisms, as already discussed in section 4.4. We also found that MASTL silencing led to increased DNA damage levels in TC cells. With regards to COPZ1, we observed that its silencing inhibited the growth of various TC cell lines by inducing autophagosome accumulation and abortive autophagy, endoplasmic reticulum stress and unfolded protein response, which ultimately led to apoptotic cell death. Moreover, COPZ1 silencing inhibited *in vivo* tumor growth in mouse xenograft and was associated with decreased expression of proliferation markers and increase of necrosis; these findings further supported the reliability of COPZ1 targeting *in vivo* as potential therapeutic strategy.

Collectively, our studies suggest that MASTL and COPZ1 may effectively represent "non-oncogenes" in thyroid cancer. As previously discussed, thyroid TCGA dataset interrogation revealed that neither *MASTL* nor *COPZ1* were overexpressed in PTC compared to normal counterpart, and, except for one silent mutation of *COPZ1*, no mutations were reported for both of them in about 500 PTC samples. Thus, both MASTL and COPZ1 properly comply with the concept of NOA (98).

We hypothesized that MASTL may act on mitotic stress support pathway and its depletion may impair stress support and cause tumor cell death (98). Tumor cells often

face with elevated mitotic stress, due to the high number of mutations that alter mitosis fidelity and cause chromosome missegregation; thus, in order to avoid excessive genomic instability, they become dependent on stress support pathways (175). Both sensitization and overload of mitotic stress were exploited as strategies to interfere with tumor cell growth, and are widely exemplified by the targeting of mitotic machinery elements, such as PLK1 and Aurora kinases, as well as by the use of microtubule-targeting agents like chemotherapy drugs (already discussed in section 4.4). Other regulators of mitotic process, such as the spindle assembly checkpoint (SAC) components Mad2 and BubR1, triggered cell death when genetically eliminated in mice and were therefore proposed as targets for inducing further chromosomal instability and consequent cell death in tumor cells (176). Our results suggest that MASTL may effectively represent an example of non-oncogene acting on the mitotic stress support pathway, since we observed that its silencing interfered with TC cell mitosis and was associated with mitotic catastrophe and cell death. On the other hand, also DNA damage and replication stress is often present in tumor cells, as a result of the high degree of replication and the rate of spontaneous DNA damage formation. Targeting of elements that promote DNA repair, such as ATM, was successful in causing stress sensitization and tumor cell death (177). Also radiations and chemotherapy were effective in overloading DNA damage and replication stress and leading to tumor cell death. The increase of DNA damage and cell death observed upon MASTL depletion suggest that MASTL vulnerability of TC cells may be related also to impaired DNA damage stress support pathway.

Regarding COPZ1, our results suggest that its depletion may be associated with proteotoxic stress. COPZ1 depletion in thyroid tumor cells blocked autophagic flux and increased endoplasmic reticulum stress, ultimately leading to apoptosis. It was demonstrated that prolonged endoplasmic reticulum stress results in cell death (178) and

that tumor cells rely on autophagy as mechanism to clear damaged/unfolded proteins and to lower proteotoxic stress (179). We hypothesized that COPZ1 depletion may affect protein balance in cells, leading to an overload of proteotoxic stress that, together with block of productive autophagy, could ultimately drive tumor cell fate towards a programmed form of cell death.

Remarkably, we demonstrated that the growth inhibitory effect of MASTL and COPZ1 targeting was restricted to thyroid tumor cells and did not affect viability of normal cells, as previously reported for other tumor types (125,135,136); these observations support the hypothesis that their targeting *in vivo* may produce limited side verse effects.

In conclusion, we identified putative non-oncogenes in thyroid cancer and validated MASTL and COPZ1 as “Achille’s heel” of thyroid tumors, thus providing evidence that they represent valuable elements for future studies, aimed to test their inhibition as strategy for thyroid cancer treatment.

6.2. Future perspectives

The studies presented in the thesis highlighted MASTL and COPZ1 as valuable candidates for future studies aimed to validate their targeting as potential therapeutic approach in thyroid cancer management.

MASTL represents an interesting mitotic element that recently emerged as potential target for cancer therapy (135,136) and our studies demonstrated its significance as thyroid tumor cell vulnerability.

To assess its reliability as target for thyroid tumor treatment, the effects of its inhibition *in vivo* will be investigated using a thyroid tumor mouse xenograft model, already used for COPZ1 studies. MASTL silencing will be performed by *in vivo* siRNA injection. The set up of the optimal conditions for treatment is in progress.

Deregulated mitoses can cause mitotic cell death and this mechanism often occurs upon mitotic catastrophe (158). Live imaging on TC cells expressing the fluorescent nuclear marker H2B-GFP will allow us to the assess the fate of MASTL-depleted TC cells at single cell level, by monitoring cell division and observing nuclear structural changes.

Analysis of the activation status of regulators of DNA damage response pathway will allow us to clarify the effects of MASTL silencing on DNA damage accumulation.

MASTL overexpression was found in head and neck, prostate and advanced breast carcinomas (136), while for other tumors, including thyroid cancer, its expression level has been never explored. MASTL expression at protein level will be assessed by IHC analysis of normal and tumor thyroid tissues, and correlated with gene expression data derived from analysis of publicly available thyroid dataset. Together, these results will allow the characterization of MASTL expression status in thyroid cancer.

References

1. Cabanillas ME, McFadden DG, and Durante C Thyroid cancer. Lancet 2016;

2. Kondo T, Ezzat S, and Asa SL Pathogenetic mechanisms in thyroid follicular-cell neoplasia. Nat Rev Cancer 2006;6:292-306.

3. Xing M Molecular pathogenesis and mechanisms of thyroid cancer. Nat Rev Cancer 2013;13:184-99.

4. Pellegriti G, Frasca F, Regalbuto C, Squatrito S, and Vigneri R Worldwide increasing incidence of thyroid cancer: update on epidemiology and risk factors. J Cancer Epidemiol 2013;2013:965212.

5. Mettler FA, Jr., Bhargavan M, Faulkner K et al. Radiologic and nuclear medicine studies in the United States and worldwide: frequency, radiation dose, and comparison with other radiation sources--1950-2007. Radiology 2009;253:520-31.

6. Kitahara CM, Platz EA, Freeman LE et al. Obesity and thyroid cancer risk among U.S. men and women: a pooled analysis of five prospective studies. Cancer Epidemiol Biomarkers Prev 2011;20:464-72.

7. Repplinger D, Bargren A, Zhang YW, Adler JT, Haymart M, and Chen H Is Hashimoto's Thyroiditis a Risk Factor for Papillary Thyroid Cancer? J Surg Res 2007;.:

8. Pellegriti G, De VF, Scollo C et al. Papillary thyroid cancer incidence in the volcanic area of Sicily. J Natl Cancer Inst 2009;101:1575-83.

9. Davies L and Welch HG Increasing incidence of thyroid cancer in the United States, 1973-2002. JAMA 2006;295:2164-7.

10. Bosetti C, Bertuccio P, Malvezzi M et al. Cancer mortality in Europe, 2005-2009, and an overview of trends since 1980. Ann Oncol 2013;24:2657-71.

11. Rahib L, Smith BD, Aizenberg R, Rosenzweig AB, Fleshman JM, and Matrisian LM Projecting cancer incidence and deaths to 2030: the unexpected burden of thyroid, liver, and pancreas cancers in the United States. Cancer Res 2014;74:2913-21.

12. Morris LG, Sikora AG, Tosteson TD, and Davies L The increasing incidence of thyroid cancer: the influence of access to care. Thyroid 2013;23:885-91.

13. La Vecchia C, Malvezzi M, Bosetti C et al. Thyroid cancer mortality and incidence: a global overview. Int J Cancer 2015;136:2187-95.

14. Keutgen XM, Sadowski SM, and Kebebew E Management of anaplastic thyroid cancer. Gland Surg 2015;4:44-51.

15. Al Afif A, Williams BA, Rigby MH et al. Multifocal Papillary Thyroid Cancer Increases the Risk of Central Lymph Node Metastasis. Thyroid 2015;25:1008-12.

16. LiVolsi VA Papillary thyroid carcinoma: an update. Mod Pathol 2011;24 Suppl 2:S1-S9.

17. Lloyd RV, Buehler D, and Khanafshar E Papillary thyroid carcinoma variants. Head Neck Pathol 2011;5:51-6.

18. Sobrinho-Simoes M, Eloy C, Magalhaes J, Lobo C, and Amaro T Follicular thyroid carcinoma. Mod Pathol 2011;24 Suppl 2:S10-S18.

19. Delellis, R. A., Lloyd, R. V., Heitz, P. U., and Eng, C. Pathology and genetics of tumors of endocrine organs. *In* IARC Press (ed.), World Health Organization classification of tumours Lyon: IARC Press, 2004.

20. Baloch ZW and LiVolsi VA Our approach to follicular-patterned lesions of the thyroid. J Clin Pathol 2007;60:244-50.

21. McHenry CR and Phitayakorn R Follicular adenoma and carcinoma of the thyroid gland. Oncologist 2011;16:585-93.

22. Montone KT, Baloch ZW, and LiVolsi VA The thyroid Hurthle (oncocytic) cell and its associated pathologic conditions: a surgical pathology and cytopathology review. Arch Pathol Lab Med 2008;132:1241-50.

23. Volante M, Collini P, Nikiforov YE et al. Poorly differentiated thyroid carcinoma: the Turin proposal for the use of uniform diagnostic criteria and an algorithmic diagnostic approach. Am J Surg Pathol 2007;31:1256-64.

24. Sanders EM, Jr., LiVolsi VA, Brierley J, Shin J, and Randolph GW An evidence-based review of poorly differentiated thyroid cancer. World J Surg 2007;31:934-45.

25. Cabanillas ME, Zafereo M, Gunn GB, and Ferrarotto R Anaplastic Thyroid Carcinoma: Treatment in the Age of Molecular Targeted Therapy. J Oncol Pract 2016;12:511-8.

26. Molinaro E, Romei C, Biagini A et al. Anaplastic thyroid carcinoma: from clinicopathology to genetics and advanced therapies. Nat Rev Endocrinol 2017;

27. Nikiforov YE and Nikiforova MN Molecular genetics and diagnosis of thyroid cancer. Nat Rev Endocrinol 2011;7:569-80.

28. Alexandrov LB, Nik-Zainal S, Wedge DC et al. Signatures of mutational processes in human cancer. Nature 2013;500:415-21.

29. Landa I, Ibrahimpasic T, Boucai L et al. Genomic and transcriptomic hallmarks of poorly differentiated and anaplastic thyroid cancers. J Clin Invest 2016;126:1052-66.

30. Serrati S, De Summa S, Pilato B et al. Next-generation sequencing: advances and applications in cancer diagnosis. Onco Targets Ther 2016;9:7355-65.

31. Smallridge RC, Chindris AM, Asmann YW et al. RNA sequencing identifies multiple fusion transcripts, differentially expressed genes, and reduced expression of immune function genes in BRAF (V600E) mutant vs BRAF wild-type papillary thyroid carcinoma. J Clin Endocrinol Metab 2014;99:E338-E347.

32. Leeman-Neill RJ, Kelly LM, Liu P et al. ETV6-NTRK3 is a common chromosomal rearrangement in radiation-associated thyroid cancer. Cancer 2014;120:799-807.

33. The Cancer Gene Atlas Research Network Integrated genomic characterization of papillary thyroid carcinoma. Cell 2014;159:676-90.

34. Swierniak M, Pfeifer A, Stokowy T et al. Somatic mutation profiling of follicular thyroid cancer by next generation sequencing. Mol Cell Endocrinol 2016;433:130-7.

35. Tiedje V, Ting S, Herold T et al. NGS based identification of mutational hotspots for targeted therapy in anaplastic thyroid carcinoma. Oncotarget 2017;8:42613-20.

36. Wan PT, Garnett MJ, Roe SM et al. Mechanism of activation of the RAF-ERK signaling pathway by oncogenic mutations of B-RAF. Cell 2004;%19;116:855-67.

37. Hou P, Liu D, and Xing M Functional characterization of the T1799-1801del and A1799-1816ins BRAF mutations in papillary thyroid cancer. Cell Cycle 2007;6:377-9.

38. Ciampi R, Knauf JA, Kerler R et al. Oncogenic AKAP9-BRAF fusion is a novel mechanism of MAPK pathway activation in thyroid cancer. J Clin Invest 2005;115:94-101.

39. Davies H, Bignell GR, Cox C et al. Mutations of the BRAF gene in human cancer. Nature 2002;417:949-54.

40. Ascierto PA, Kirkwood JM, Grob JJ et al. The role of BRAF V600 mutation in melanoma. J Transl Med 2012;10:85.

41. Knauf JA, Ma X, Smith EP et al. Targeted expression of BRAFV600E in thyroid cells of transgenic mice results in papillary thyroid cancers that undergo dedifferentiation. Cancer Res 2005;65:4238-45.

42. Xing M BRAF mutation in thyroid cancer. Endocr Relat Cancer 2005;12:245-62.

43. Karnoub AE and Weinberg RA Ras oncogenes: split personalities. Nat Rev Mol Cell Biol 2008;9:517-31.

44. Pylayeva-Gupta Y, Grabocka E, and Bar-Sagi D RAS oncogenes: weaving a tumorigenic web. Nat Rev Cancer 2011;11:761-74.

45. Nikiforova MN, Lynch RA, Biddinger PW et al. RAS point mutations and PAX8-PPAR gamma rearrangement in thyroid tumors: evidence for distinct molecular pathways in thyroid follicular carcinoma. J Clin Endocrinol Metab 2003;88:2318-26.

46. Xu B and Ghossein R Genomic Landscape of poorly Differentiated and Anaplastic Thyroid Carcinoma. Endocr Pathol 2016;27:205-12.

47. Miller KA, Yeager N, Baker K, Liao XH, Refetoff S, and Di CA Oncogenic Kras requires simultaneous PI3K signaling to induce ERK activation and transform thyroid epithelial cells in vivo. Cancer Res 2009;69:3689-94.

48. Mulligan LM RET revisited: expanding the oncogenic portfolio. Nat Rev Cancer 2014;14:173-86.

49. Santoro M, Carlomagno F, Melillo RM, and Fusco A Dysfunction of the RET receptor in human cancer. Cell Mol Life Sci 2004;61:2954-64.

50. Arighi E, Borrello MG, and Sariola H RET tyrosine kinase signaling in development and cancer. Cytokine Growth Factor Rev 2005;16(4-5):441-67.

51. Romei C, Ciampi R, and Elisei R A comprehensive overview of the role of the RET proto-oncogene in thyroid carcinoma. Nat Rev Endocrinol 2016;12:192-202.

52. Nikiforova MN, Stringer JR, Blough R, Medvedovic M, Fagin JA, and Nikiforov YE Proximity of chromosomal loci that participate in radiation-induced rearrangements in human cells. Science 2000;290:138-41.

53. Fagin JA Challenging dogma in thyroid cancer molecular genetics--role of RET/PTC and BRAF in tumor initiation. J Clin Endocrinol Metab 2004;89:4264-6.

54. Mochizuki K, Kondo T, Nakazawa T et al. RET rearrangements and BRAF mutation in undifferentiated thyroid carcinomas having papillary carcinoma components. Histopathology 2010;57:444-50.

55. Schram AM, Chang MT, Jonsson P, and Drilon A Fusions in solid tumours: diagnostic strategies, targeted therapy, and acquired resistance. Nat Rev Clin Oncol 2017;

56. Greco A, Miranda C, and Pierotti MA Rearrangements of NTRK1 gene in papillary thyroid carcinoma. Mol Cell Endocrinol 2010;321:44-9.

57. Kaplan DR and Miller FD Neurotrophin signal transduction in the nervous system. Curr Opin Neurobiol 2000;10:381-91.

58. Pierotti MA and Greco A Oncogenic rearrangements of the NTRK1/NGF receptor. Cancer Lett 2006;232:90-8.

59. Reuther GW, Lambert QT, Caligiuri MA, and Der CJ Identification and characterization of an activating TrkA deletion mutation in acute myeloid leukemia. Mol Biol Cell 2000;20:8655-66.

60. Weeraratna AT, Dalrymple SL, Lamb JC et al. Pan-trk inhibition decreases metastasis and enhances host survival in experimental models as a result of its selective induction of apoptosis of prostate cancer cells. Clin Cancer Res 2001;7:2237-45.

61. Descamps S, Lebourhis X, Delehedde M, Boilly B, and Hondermarck H Nerve growth factor is mitogenic for cancerous but not normal human breast epithelial cells. J Biol Chem 1998;273:16659-62.

62. Greco A, Mariani C, Miranda C et al. The DNA rearrangement that generates the *TRK-T3* oncogene involves a novel gene on chromosome 3 whose product has a potential coiled-coil domain. Mol Cell Biol 1995;15:6118-27.

63. Russell JP, Powell DJ, Cunnane M et al. The *TRK-T1* fusion protein induces neoplastic transformation of thyroid epithelium. Oncogene 2000;19:5729-35.

64. Xing M Genetic alterations in the phosphatidylinositol-3 kinase/Akt pathway in thyroid cancer. Thyroid 2010;20:697-706.

65. Vivanco I and Sawyers CL The phosphatidylinositol 3-Kinase AKT pathway in human cancer. Nat Rev Cancer 2002;2:489-501.

66. Liu P, Cheng H, Roberts TM, and Zhao JJ Targeting the phosphoinositide 3-kinase pathway in cancer. Nat Rev Drug Discov 2009;8:627-44.

67. Saji M and Ringel MD The PI3K-Akt-mTOR pathway in initiation and progression of thyroid tumors. Mol Cell Endocrinol 2010;321:20-8.

68. Samuels Y, Wang Z, Bardelli A et al. High frequency of mutations of the PIK3CA gene in human cancers. Science 2004;304:554.

69. Kroll TG, Sarraf P, Chen CJ, Mueller E, Spiegelman BM, and Fletcher JA PAX8-PPARgamma1 fusion oncogene in human thyroid carcinoma. Science 2000;289:1357-60.

70. Gregory PJ, Wang X, Allard BL et al. The PAX8/PPARgamma fusion oncoprotein transforms immortalized human thyrocytes through a mechanism probably involving wild-type PPARgamma inhibition. Oncogene 2004;23:3634-41.

71. Au AY, McBride C, Wilhelm KG, Jr. et al. PAX8-peroxisome proliferator-activated receptor gamma (PPARgamma) disrupts normal PAX8 or PPARgamma transcriptional function and stimulates follicular thyroid cell growth. Endocrinology 2006;147:367-76.

72. Vu-Phan D, Grachtchouk V, Yu J, Colby LA, Wicha MS, and Koenig RJ The thyroid cancer PAX8-PPARG fusion protein activates Wnt/TCF-responsive cells that have a transformed phenotype. Endocr Relat Cancer 2013;20:725-39.

73. Eberhardt NL, Grebe SK, McIver B, and Reddi HV The role of the PAX8/PPARgamma fusion oncogene in the pathogenesis of follicular thyroid cancer. Mol Cell Endocrinol 2010;321:50-6.

74. Levine AJ and Oren M The first 30 years of p53: growing ever more complex. Nat Rev Cancer 2009;9:749-58.

75. Muller PA and Vousden KH p53 mutations in cancer. Nat Cell Biol 2013;15:2-8.

76. Fagin JA and Mitsiades N Molecular pathology of thyroid cancer: diagnostic and clinical implications. Best Pract Res Clin Endocrinol Metab 2008;22:955-69.

77. McFadden DG, Vernon A, Santiago PM et al. p53 constrains progression to anaplastic thyroid carcinoma in a Braf-mutant mouse model of papillary thyroid cancer. Proc Natl Acad Sci U S A 2014;111:E1600-E1609.

78. Regalbuto C, Frasca F, Pellegriti G et al. Update on thyroid cancer treatment. Future Oncol 2012;8:1331-48.

79. Kuba S, Yamanouchi K, Hayashida N et al. Total thyroidectomy versus thyroid lobectomy for papillary thyroid cancer: Comparative analysis after propensity score matching: A multicenter study. Int J Surg 2017;38:143-8.

80. Haugen BR, Alexander EK, Bible KC et al. 2015 American Thyroid Association Management Guidelines for Adult Patients with Thyroid Nodules and Differentiated Thyroid Cancer: The American Thyroid Association Guidelines Task Force on Thyroid Nodules and Differentiated Thyroid Cancer. Thyroid 2016;26(1):1-133.

81. Stokkel MP, Duchateau CS, and Dragoiescu C The value of FDG-PET in the follow-up of differentiated thyroid cancer: a review of the literature. Q J Nucl Med Mol Imaging 2006;50:78-87.

82. Jameson JL and Longo DL Precision medicine--personalized, problematic, and promising. N Engl J Med 2015;372:2229-34.

83. Bible, K. C. and Ryder, M. Evolving molecularly targeted therapies for advanced-stage thyroid cancers. 2016.

84. Valerio L, Pieruzzi L, Giani C et al. Targeted Therapy in Thyroid Cancer: State of the Art. Clin Oncol (R Coll Radiol) 2017;29:316-24.

85. Tahara M, Kiyota N, Yamazaki T et al. Lenvatinib for Anaplastic Thyroid Cancer. Front Oncol 2017;7:25.

86. Carneiro RM, Carneiro BA, Agulnik M, Kopp PA, and Giles FJ Targeted therapies in advanced differentiated thyroid cancer. Cancer Treat Rev 2015;41:690-8.

87. Ho AL, Grewal RK, Leboeuf R et al. Selumetinib-enhanced radioiodine uptake in advanced thyroid cancer. N Engl J Med 2013;368:623-32.

88. Frohlich E and Wahl R The current role of targeted therapies to induce radioiodine uptake in thyroid cancer. Cancer Treat Rev 2014;S0305-S7372.

89. Hanahan D and Weinberg RA The hallmarks of cancer. Cell 2000;100:57-70.

90. Weinstein IB Cancer. Addiction to oncogenes--the Achilles heal of cancer. Science 2002;297:63-4.

91. Slamon DJ, Leyland-Jones B, Shak S et al. Use of chemotherapy plus a monoclonal antibody against HER2 for metastatic breast cancer that overexpresses HER2. N Engl J Med 2001;344:783-92.

92. Flaherty KT, Puzanov I, Kim KB et al. Inhibition of mutated, activated BRAF in metastatic melanoma. N Engl J Med 2010;363:809-19.

93. Lynch TJ, Bell DW, Sordella R et al. Activating mutations in the epidermal growth factor receptor underlying responsiveness of non-small-cell lung cancer to gefitinib. N Engl J Med 2004;%20;350:2129-39.

94. Hughes TP, Kaeda J, Branford S et al. Frequency of major molecular responses to imatinib or interferon alfa plus cytarabine in newly diagnosed chronic myeloid leukemia. N Engl J Med 2003;349:1423-32.

95. McLornan DP, List A, and Mufti GJ Applying synthetic lethality for the selective targeting of cancer. N Engl J Med 2014;371:1725-35.

96. Brown JS, Kaye SB, and Yap TA PARP inhibitors: the race is on. Br J Cancer 2016;114:713-5.

97. Solimini NL, Luo J, and Elledge SJ Non-oncogene addiction and the stress phenotype of cancer cells. Cell 2007;130:986-8.

98. Luo J, Solimini NL, and Elledge SJ Principles of cancer therapy: oncogene and non-oncogene addiction. Cell 2009;136:823-37.

99. Nagel R, Semenova EA, and Berns A Drugging the addict: non-oncogene addiction as a target for cancer therapy. EMBO Rep 2016;17:1516-31.

100. Nitta M, Kozono D, Kennedy R et al. Targeting EGFR induced oxidative stress by PARP1 inhibition in glioblastoma therapy. PLoS One 2010;5:e10767.

101. Dai C, Whitesell L, Rogers AB, and Lindquist S Heat shock factor 1 is a powerful multifaceted modifier of carcinogenesis. Cell 2007;130:1005-18.

102. Putcha P, Yu J, Rodriguez-Barrueco R et al. HDAC6 activity is a non-oncogene addiction hub for inflammatory breast cancers. Breast Cancer Res 2015;17:149.

103. Koboldt DC, Steinberg KM, Larson DE, Wilson RK, and Mardis ER The next-generation sequencing revolution and its impact on genomics. Cell 2013;155:27-38.

104. Mohr SE, Smith JA, Shamu CE, Neumuller RA, and Perrimon N RNAi screening comes of age: improved techniques and complementary approaches. Nat Rev Mol Cell Biol 2014;15:591-600.

105. Cullen LM and Arndt GM Genome-wide screening for gene function using RNAi in mammalian cells. Immunol Cell Biol 2005;83:217-23.

106. McDonald ER, III, de Weck A, Schlabach MR et al. Project DRIVE: A Compendium of Cancer Dependencies and Synthetic Lethal Relationships Uncovered by Large-Scale, Deep RNAi Screening. Cell 2017;170:577-92.

107. Cowley GS, Weir BA, Vazquez F et al. Parallel genome-scale loss of function screens in 216 cancer cell lines for the identification of context-specific genetic dependencies. Sci Data 2014;1:140045.

108. Petrocca F, Altschuler G, Tan SM et al. A genome-wide siRNA screen identifies proteasome addiction as a vulnerability of basal-like triple-negative breast cancer cells. Cancer Cell 2013;24:182-96.

109. Rudalska R, Dauch D, Longerich T et al. In vivo RNAi screening identifies a mechanism of sorafenib resistance in liver cancer. Nat Med 2014;20:1138-46.

110. Bossi D, Cicalese A, Dellino GI et al. In Vivo Genetic Screens of Patient-Derived Tumors Revealed Unexpected Frailty of the Transformed Phenotype. Cancer Discov 2016;6:650-63.

111. Iorns E, Lord CJ, Turner N, and Ashworth A Utilizing RNA interference to enhance cancer drug discovery. Nat Rev Drug Discov 2007;6:556-68.

112. Schweppe RE, Klopper JP, Korch C et al. Deoxyribonucleic acid profiling analysis of 40 human thyroid cancer cell lines reveals cross-contamination resulting in cell line redundancy and misidentification. J Clin Endocrinol Metab 2008;93:4331-41.

113. Zhao M, Sano D, Pickering CR et al. Assembly and initial characterization of a panel of 85 genomically validated cell lines from diverse head and neck tumor sites. Clin Cancer Res 2011;17:7248-64.

114. Xu X, Ding H, Rao G et al. Activation of the Sonic Hedgehog pathway in thyroid neoplasms and its potential role in tumor cell proliferation. Endocr Relat Cancer 2012;19:167-79.

115. Fry DW, Harvey PJ, Keller PR et al. Specific inhibition of cyclin-dependent kinase 4/6 by PD 0332991 and associated antitumor activity in human tumor xenografts. Mol Cancer Ther 2004;3:1427-38.

116. Li B and Dewey CN RSEM: accurate transcript quantification from RNA-Seq data with or without a reference genome. BMC Bioinformatics 2011;12:323.

117. Shaffer AL, Emre NC, Lamy L et al. IRF4 addiction in multiple myeloma. Nature 2008;454:226-31.

118. Scholl C, Frohling S, Dunn IF et al. Synthetic lethal interaction between oncogenic KRAS dependency and STK33 suppression in human cancer cells. Cell 2009;137:821-34.

119. Anania MC, Gasparri F, Cetti E et al. Identification of thyroid tumor cell vulnerabilities through a siRNA-based functional screening. Oncotarget 2015;6:34629-48.

120. Sos ML, Levin RS, Gordan JD et al. Oncogene mimicry as a mechanism of primary resistance to BRAF inhibitors. Cell Rep 2014;8:1037-48.

121. Tiedemann RE, Zhu YX, Schmidt J et al. Identification of molecular vulnerabilities in human multiple myeloma cells by RNA interference lethality screening of the druggable genome. Cancer Res 2012;72:757-68.

122. Schlabach MR, Luo J, Solimini NL et al. Cancer proliferation gene discovery through functional genomics. Science 2008;319:620-4.

123. Murrow LM, Garimella SV, Jones TL, Caplen NJ, and Lipkowitz S Identification of WEE1 as a potential molecular target in cancer cells by RNAi screening of the human tyrosine kinome. Breast Cancer Res Treat 2010;122:347-57.

124. Burgess A, Vigneron S, Brioudes E, Labbe JC, Lorca T, and Castro A Loss of human Greatwall results in G2 arrest and multiple mitotic defects due to deregulation of the cyclin B-Cdc2/PP2A balance. Proc Natl Acad Sci U S A 2010;107:12564-9.

125. Shtutman M, Baig M, Levina E et al. Tumor-specific silencing of COPZ2 gene encoding coatomer protein complex subunit zeta 2 renders tumor cells dependent on its paralogous gene COPZ1. Proc Natl Acad Sci U S A 2011;108:12449-54.

126. Haraldsdottir S and Shah MH An update on clinical trials of targeted therapies in thyroid cancer. Curr Opin Oncol 2014;26:36-44.

127. Laursen R, Wehland M, Kopp S et al. Effects and Role of Multikinase Inhibitors in Thyroid Cancer. Curr Pharm Des 2016;22:5915-26.

128. Musgrove EA, Caldon CE, Barraclough J, Stone A, and Sutherland RL Cyclin D as a therapeutic target in cancer. Nat Rev Cancer 2011;11:558-72.

129. O'Leary B, Finn RS, and Turner NC Treating cancer with selective CDK4/6 inhibitors. Nat Rev Clin Oncol 2016;13:417-30.

130. Seybt TP, Ramalingam P, Huang J, Looney SW, and Reid MD Cyclin D1 expression in benign and differentiated malignant tumors of the thyroid gland: diagnostic and biologic implications. Appl Immunohistochem Mol Morphol 2012;20:124-30.

131. Lee JJ, Au AY, Foukakis T et al. Array-CGH identifies cyclin D1 and UBCH10 amplicons in anaplastic thyroid carcinoma. Endocr Relat Cancer 2008;15:801-15.

132. Khoo ML, Ezzat S, Freeman JL, and Asa SL Cyclin D1 protein expression predicts metastatic behavior in thyroid papillary microcarcinomas but is not associated with gene amplification. J Clin Endocrinol Metab 2002;87:1810-3.

133. Cadoo KA, Gucalp A, and Traina TA Palbociclib: an evidence-based review of its potential in the treatment of breast cancer. Breast Cancer (Dove Med Press) 2014;6:123-33.

134. Kishimoto T Entry into mitosis: a solution to the decades-long enigma of MPF. Chromosoma 2015;

135. Nagel R, Stigter-van WM, Buijze M et al. Genome-wide siRNA screen identifies the radiosensitizing effect of downregulation of MASTL and FOXM1 in NSCLC. Mol Cancer Ther 2015;

136. Wang L, Luong VQ, Giannini PJ, and Peng A Mastl kinase, a promising therapeutic target, promotes cancer recurrence. Oncotarget 2014;5:11479-89.

137. Beck R, Rawet M, Wieland FT, and Cassel D The COPI system: molecular mechanisms and function. FEBS Lett 2009;583:2701-9.

138. Razi M, Chan EY, and Tooze SA Early endosomes and endosomal coatomer are required for autophagy. J Cell Biol 2009;185:305-21.

139. Beller M, Sztalryd C, Southall N et al. COPI complex is a regulator of lipid homeostasis. PLoS Biol 2008;6:e292.

140. Yu J, Fleming SL, Williams B et al. Greatwall kinase: a nuclear protein required for proper chromosome condensation and mitotic progression in Drosophila. J Cell Biol 2004;164:487-92.

141. Yu J, Zhao Y, Li Z, Galas S, and Goldberg ML Greatwall kinase participates in the Cdc2 autoregulatory loop in Xenopus egg extracts. Mol Cell 2006;22:83-91.

142. Jackson PK Climbing the Greatwall to mitosis. Mol Cell 2006;22:156-7.

143. Castilho PV, Williams BC, Mochida S, Zhao Y, and Goldberg ML The M phase kinase Greatwall (Gwl) promotes inactivation of PP2A/B55delta, a phosphatase directed against CDK phosphosites. Mol Biol Cell 2009;20:4777-89.

144. Mochida S, Maslen SL, Skehel M, and Hunt T Greatwall phosphorylates an inhibitor of protein phosphatase 2A that is essential for mitosis. Science 2010;330:1670-3.

145. Gharbi-Ayachi A, Labbe JC, Burgess A et al. The substrate of Greatwall kinase, Arpp19, controls mitosis by inhibiting protein phosphatase 2A. Science 2010;330:1673-7.

146. Ma S, Vigneron S, Robert P et al. Greatwall dephosphorylation and inactivation upon mitotic exit is triggered by PP1. J Cell Sci 2016;129:1329-39.

147. Lorca T and Castro A The Greatwall kinase: a new pathway in the control of the cell cycle. Oncogene 2013;32:537-43.

148. Voets E and Wolthuis RM MASTL is the human orthologue of Greatwall kinase that facilitates mitotic entry, anaphase and cytokinesis. Cell Cycle 2010;9:3591-601.

149. Nolen B, Taylor S, and Ghosh G Regulation of protein kinases; controlling activity through activation segment conformation. Mol Cell 2004;15:661-75.

150. Ocasio CA, Rajasekaran MB, Walker S et al. A first generation inhibitor of human Greatwall kinase, enabled by structural and functional characterisation of a minimal kinase domain construct. Oncotarget 2016;7:71182-97.

151. Alvarez-Fernandez M, Sanchez-Martinez R, Sanz-Castillo B et al. Greatwall is essential to prevent mitotic collapse after nuclear envelope breakdown in mammals. Proc Natl Acad Sci U S A 2013;110:17374-9.

152. Rogers S, Fey D, McCloy RA et al. PP1 initiates the dephosphorylation of MASTL, triggering mitotic exit and bistability in human cells. J Cell Sci 2016;129:1340-54.

153. Peng A, Yamamoto TM, Goldberg ML, and Maller JL A novel role for greatwall kinase in recovery from DNA damage. Cell Cycle 2010;9:4364-9.

154. Wong PY, Ma HT, Lee HJ, and Poon RY MASTL(Greatwall) regulates DNA damage responses by coordinating mitotic entry after checkpoint recovery and APC/C activation. Sci Rep 2016;6:22230.

155. Zhuge BZ, Du BR, Meng XL, and Zhang YQ MASTL is a potential poor prognostic indicator in ER+ breast cancer. Eur Rev Med Pharmacol Sci 2017;21:2413-20.

156. Vera J, Lartigue L, Vigneron S et al. Greatwall promotes cell transformation by hyperactivating AKT in human malignancies. Elife 2015;4:

157. Fenech M, Kirsch-Volders M, Natarajan AT et al. Molecular mechanisms of micronucleus, nucleoplasmic bridge and nuclear bud formation in mammalian and human cells. Mutagenesis 2011;26:125-32.

158. Vakifahmetoglu H, Olsson M, and Zhivotovsky B Death through a tragedy: mitotic catastrophe. Cell Death Differ 2008;15:1153-62.

159. Janssen A, van der BM, Szuhai K, Kops GJ, and Medema RH Chromosome segregation errors as a cause of DNA damage and structural chromosome aberrations. Science 2011;333:1895-8.

160. Rogakou EP, Boon C, Redon C, and Bonner WM Megabase chromatin domains involved in DNA double-strand breaks in vivo. J Cell Biol 1999;146:905-16.

161. Malureanu LA, Jeganathan KB, Hamada M, Wasilewski L, Davenport J, and van Deursen JM BubR1 N terminus acts as a soluble inhibitor of cyclin B degradation by APC/C(Cdc20) in interphase. Dev Cell 2009;16:118-31.

162. Liu Y, Zhang X, Han C et al. TP53 loss creates therapeutic vulnerability in colorectal cancer. Nature 2015;520:697-701.

163. Maier P, Hartmann L, Wenz F, and Herskind C Cellular Pathways in Response to Ionizing Radiation and Their Targetability for Tumor Radiosensitization. Int J Mol Sci 2016;17:

164. Mc Gee MM Targeting the Mitotic Catastrophe Signaling Pathway in Cancer. Mediators Inflamm 2015;2015:146282.

165. Denisenko TV, Sorokina IV, Gogvadze V, and Zhivotovsky B Mitotic catastrophe and cancer drug resistance: A link that must to be broken. Drug Resist Updat 2016;24:1-12.

166. Russo MA, Kang KS, and Di CA The PLK1 inhibitor GSK461364A is effective in poorly differentiated and anaplastic thyroid carcinoma cells, independent of the nature of their driver mutations. Thyroid 2013;23:1284-93.

167. Baldini E, Tuccilli C, Prinzi N et al. Effects of selective inhibitors of Aurora kinases on anaplastic thyroid carcinoma cell lines. Endocr Relat Cancer 2014;21:797-811.

168. Imreh G, Norberg HV, Imreh S, and Zhivotovsky B Chromosomal breaks during mitotic catastrophe trigger gammaH2AX-ATM-p53-mediated apoptosis. J Cell Sci 2011;124:2951-63.

169. van Vugt MA and Reinhardt HC Editorial: Cancer-Associated Defects in the DNA Damage Response: Drivers for Malignant Transformation and Potential Therapeutic Targets. Front Genet 2015;6:355.

170. Sudo H, Tsuji AB, Sugyo A et al. Knockdown of COPA, identified by loss-of-function screen, induces apoptosis and suppresses tumor growth in mesothelioma mouse model. Genomics 2010;95:210-6.

171. Christodoulou EG, Yang H, Lademann F, Pilarsky C, Beyer A, and Schroeder M Detection of COPB2 as a KRAS synthetic lethal partner through integration of functional genomics screens. Oncotarget 2017;

172. Claerhout S, Dutta B, Bossuyt W et al. Abortive autophagy induces endoplasmic reticulum stress and cell death in cancer cells. PLoS One 2012;7:e39400.

173. Oliver D, Ji H, Liu P et al. Identification of novel cancer therapeutic targets using a designed and pooled shRNA library screen. Sci Rep 2017;7:43023.

174. Lunev S, Semmelink MF, Xian JL et al. Crystal structure of truncated human coatomer protein complex subunit zeta1 (Copzeta1). Acta Crystallogr F Struct Biol Commun 2017;73:1-8.

175. Weaver BA and Cleveland DW Decoding the links between mitosis, cancer, and chemotherapy: The mitotic checkpoint, adaptation, and cell death. Cancer Cell 2005;8:7-12.

176. Manchado E, Guillamot M, and Malumbres M Killing cells by targeting mitosis. Cell Death Differ 2012;19:369-77.

177. Helleday T, Petermann E, Lundin C, Hodgson B, and Sharma RA DNA repair pathways as targets for cancer therapy. Nat Rev Cancer 2008;8:193-204.

178. Breckenridge DG, Germain M, Mathai JP, Nguyen M, and Shore GC Regulation of apoptosis by endoplasmic reticulum pathways. Oncogene 2003;22:8608-18.

179. Ozpolat B and Benbrook DM Targeting autophagy in cancer management - strategies and developments. Cancer Manag Res 2015;7:291-9.

List of figures

List of tables

List of abbreviations

AKT	Protein kinase B
ATC	Anaplastic thyroid carcinoma
BRAF	v-Raf murine sarcoma viral oncogene homolog B1
CCND1	Cyclin D1
CDK1	Cyclin dependent kinase 1
CDK4	Cyclin dependent kinase 4
CDK6	Cyclin dependent kinase 6
COPE	coatomer protein complex , subunit epsilon
COPZ1	Coatomer protein complex, subunit zeta-1
DNM3	Dynamin 3
EPHB4	EPH receptor B4
FNAB	Fine-needle aspiration bioppsy
FTA	Follicular thyroid adenoma
FTC	Follicular thyroid carcinoma
HCC	Hürtle cell carcinoma
HDAC	Histone deacetylase
MAP4K5	Mitogen-activated protein kinase kinase kinase kinase 5
MAPK	Mitogen-activated protein kinase
MASTL	Microtubule associated serine/threonine kinase-like
MTC	Medullary thyroid carcinoma
NGS	Next-generation sequencing
NOA	Non-oncogene addiction
NTRK1	Neurotrophic receptor tyrosin kinase A
NUDT9	Nudix (nucleoside diphosphate linked mojety X)-type motif 9
OXTR	Oxytocin receptor
PAX8	Paired box 8
PDTC	Poorly differentiated thyroid carcinoma
PI3K	Phosphatidylinositol 3-kinase
PIK3CA	Phosphatidylinositol-4,5-biphosphate 3-kinase catalytitc subunit α
PLA2G15	Phospholipase A2, group XV
PP2A	Protein phosphatase 2A
PPARγ	Peroxisome proliferator-activated receptor γ
PTC	Papillary thyroid carcinoma

PTEN	Phosphatase and tensin homolog
RAI	Radioactive iodine
RAS	Rat sarcoma
RASD1	RAS, dexamethasone-induced 1
REM2	RAS (RAD and GEM)-like GTP binding 2
RET	Rearranged during transfection
RGS3	Regulator of G-protein signaling 3
RNAi	RNA interference
RTK	Receptor tyrosine kinase
SRPK1	SFRS protein kinase 1
TC	Thyroid cancer
TKI	Tyrosine kinase inhibitor
WDTC	Well-differentiated thyroid carcinoma

Publications

- Anania MC, Gasparri F, Cetti E, Fraietta I, Todoerti K, Miranda C, Mazzoni M, Re C, Colombo R, Ukmar G, Camisasca S, Pagliardini S, Pierotti M, Neri A, Galvani A and Greco A. Identification of thyroid tumor cell vulnerabilities through a siRNA-based functional screening. *Oncotarget* 6, 34629-34648 (2015). doi: 10.18632/oncotarget.5282.

- Anania MC, Cetti E, Lecis D, Todoerti K, Gulino A, Mauro G, Di Marco T, Cleris L, Pagliardini S, Manenti G, Belmonte B, Tripodo C, Neri A, and Greco A. Targeting COPZ1 non-oncogene addiction counteracts the viability of thyroid tumor cells. *Cancer Letters* (2017) 410:201-211 doi: 10.1016/j.canlet.2017.09.024.

Appendixes

Appendix A

Original publication: Identification of thyroid tumor cell vulnerabilities through a siRNA-based functional screening. Anania MC, Gasparri F, Cetti E, et al., Oncotarget 2015

Supplementary Table S1, Table S2 and Table S3 were not included in Appendix A due to their size; they can be downloaded at the following link:

http://www.impactjournals.com/oncotarget/index.php?journal=oncotarget&page=rt&op=suppFiles&path[]=5282&path[]=0

Appendix B

Original publication: Targeting COPZ1 non-oncogene addiction counteracts the viability of thyroid tumor cells. Anania MC, Cetti E, Lecis D, et al. Cancer Letters 2017

Appendix A

Identification of thyroid tumor cell vulnerabilities through a siRNA-based functional screening

Maria Chiara Anania[1,*], Fabio Gasparri[2,*], Elena Cetti[1], Ivan Fraietta[2], Katia Todoerti[3], Claudia Miranda[1], Mara Mazzoni[1], Claudia Re[2], Riccardo Colombo[2], Giorgio Ukmar[2], Stefano Camisasca[2], Sonia Pagliardini[1], Marco A. Pierotti[4], Antonino Neri[5,6], Arturo Galvani[2], Angela Greco[1]

[1]Molecular Mechanisms Unit, Fondazione IRCCS Istituto Nazionale dei Tumori, Milan, Italy

[2]Cell Biology Department, Nerviano Medical Sciences Srl, Nerviano (MI), Italy

[3]Laboratory of Pre-Clinical and Translational Research, IRCCS-CROB, Referral Cancer Center of Basilicata, Rionero in Vulture, Italy

[4]Scientific Directorate, Fondazione IRCCS Istituto Nazionale dei Tumori, Milan, Italy

[5]Department of Clinical Sciences and Community Health, University of Milan, Milan, Italy

[6]Hematology Unit, Fondazione IRCCS Ca' Granda, Ospedale Maggiore Policlinico, Milan, Italy

[*]These authors have contributed equally to this work

Correspondence to:
Angela Greco, **e-mail:** angela.greco@istitutotumori.mi.it
Fabio Gasparri, **e-mail:** fabio.gasparri@nervianoms.com

Keywords: *thyroid cancer, non-oncogene addiction, MASTL, Cyclin D1, COPZ1*

Received: *June 06, 2015* ***Accepted:*** *September 14, 2015* ***Published:*** *September 25, 2015*

ABSTRACT

The incidence of thyroid carcinoma is rapidly increasing. Although generally associated with good prognosis, a fraction of thyroid tumors are not cured by standard therapy and progress to aggressive forms for which no effective treatments are currently available. In order to identify novel therapeutic targets for thyroid carcinoma, we focused on the discovery of genes essential for sustaining the oncogenic phenotype of thyroid tumor cells, but not required to the same degree for the viability of normal cells (non-oncogene addiction paradigm). We screened a siRNA oligonucleotide library targeting the human druggable genome in thyroid cancer BCPAP cell line in comparison with immortalized normal human thyrocytes (Nthy-ori 3–1). We identified a panel of hit genes whose silencing interferes with the growth of tumor cells, while sparing that of normal ones. Further analysis of three selected hit genes, namely *Cyclin D1*, *MASTL* and *COPZ1*, showed that they represent common vulnerabilities for thyroid tumor cells, as their inhibition reduced the viability of several thyroid tumor cell lines, regardless the histotype or oncogenic lesion. This work identified non-oncogenes essential for sustaining the phenotype of thyroid tumor cells, but not of normal cells, thus suggesting that they might represent promising targets for new therapeutic strategies.

INTRODUCTION

The incidence of thyroid cancer (TC), the most common endocrine malignancy, has increased significantly over the last few decades [1]. All TCs, except medullary thyroid carcinoma, are derived from thyroid follicular cells. Differentiated tumors, namely papillary and follicular carcinoma (PTC and FTC, 80% and 10% of cases, respectively) are generally cured by current treatment involving surgery, thyroid hormone and radioactive iodine therapy; however, they occasionally progress into undifferentiated, more aggressive and lethal carcinomas. Poorly differentiated (PDTC) and anaplastic (ATC) carcinoma, although rare, are the most clinically aggressive TCs; for ATC patient the survival is reduced to few months [2].

Genetic studies performed in the last 25 years have dissected the molecular bases of TC. PTC is associated with a high frequency of deregulation of RTK/RAS/RAF/MAPK pathway [3]. This includes oncogenic

rearrangements of the *RET* and *NTRK1* receptors, and point mutations in the *BRAF* and *RAS* genes, with the *BRAFV600E* as the most frequent PTC alteration. The genetic landscape of PTC has been very recently expanded by integrated genomic characterization studies which identified several novel driver alterations [4]. FTC is associated with *RAS* mutations and *PAX8/PPARγ* rearrangements. *RAS* mutations are common in PDTC. ATC is associated with mutations of *BRAF*, *RAS*, *TP53*, *PTEN*, and *PIK3CA*. The identification and functional characterization of differentially expressed genes and miRNAs have also contributed to the understanding of thyroid tumor biology, and provided important diagnostic/prognostic tools [5–8].

Molecular findings have been translated into the clinical setting, leading to clinical experimentation of agents targeting thyroid oncoproteins or downstream pathways [9]. Several kinase inhibitors, primarily targeting BRAF and angiogenic kinases, are under evaluation in clinical trials [10]. Nevertheless, no effective targeted therapies are currently available for aggressive TC that are not curable by the standard therapeutic approaches.

The traditional approach for cancer target discovery is based on the identification of driver oncogenes through the characterization of the molecular alterations of primary tumors. However, according to the concept of "non-oncogene addiction" (NOA), the uncontrolled growth of cancer cells often relies on normal genes, that are not themselves oncogenes or otherwise mutated, whose activity is essential for tumor cells but not required to the same extent by normal cells [11]. NOA genes cannot be identified by genetic approaches aimed at identifying gene mutation/aberrancy, but rather by large-scale siRNA-based functional screening, a strategy which is nowadays widely used for the identification of tumor cell vulnerabilities to be explored for therapeutic purposes [12–15].

In order to identify novel, unforeseen molecular targets for thyroid carcinoma, in this study we have undertaken the screening of a siRNA oligonucleotide library in tumor (BCPAP) and normal (Nthy-ori 3–1) thyroid cell lines, and we have identified a set of genes whose silencing reduces the growth of tumor cells, while sparing growth of non-transformed cells of the same tissue origin. Among the top ranked genes, we selected *Cyclin D1 (CCND1)*, *MASTL* and *COPZ1*. All of them passed a secondary confirmation study, which unequivocally demonstrated the dependency of BCPAP cells upon their activity. Interestingly, we found that silencing of *Cyclin D1*, *MASTL* and *COPZ1* inhibits the growth of several further thyroid tumor cell lines.

RESULTS

Druggable genome siRNA screening

To identify genes affecting growth of thyroid tumor cells, we conducted an RNAi-based phenotypic screening, examining effects on cell growth. The papillary thyroid carcinoma BCPAP cell line, carrying the *BRAFV600E* mutation, and the immortalized normal human thyrocyte Nthy-ori 3–1 cell line were transfected with a siRNA library containing 25139 siRNA oligos targeting about 9000 potentially "druggable" genes (3 duplexes/gene, on average), and with a non-targeting siRNA (siNT) and a siRNA targeting the proteasomal subunit *PSMC3* as negative and positive controls, respectively. Cells were transfected at low density in 96-well plates and colony formation assay (CFA) was performed after 7 (Nthy-ori 3–1) or 8 (BCPAP) days. Images of a representative plate for each of these lines are shown in Figure 1A. We preferred CFA to short-term (48–72 hours) proliferation assay, since it allows the detection of long-term consequences of "weak" phenotypes (our unpublished results). The screening results are shown in Figure 1B: scatter plots represent the fluorescence signal, derived from CFA acquisition, normalized with respect to siNT (% siNT) of Nthy-ori 3–1 and BCPAP cells transfected in duplicate with the library siRNA oligos (the complete list is reported in Table S1). Of note, the uneven distribution of data across graph diagonal denotes slightly higher transfection efficiency for Nthy-ori 3–1 than for BCPAP. Genes essential for cell viability of BCPAP, but not Nthy-ori 3–1 cells, were identified through the "*d* parameter" (defined in Materials and Methods). *d* values close to 0 denote preferential inhibition of BCPAP cell proliferation with respect to Nthy-ori 3–1. Based on data distribution, a threshold of -3σ (corresponding to $d = 47.2$) was applied to define differentially active hits: 398 siRNA oligos (1.58%), targeting 386 genes, were found to be below this threshold and thus were defined as "differential hits" (Figure 1C; hit list is reported in Table S2). A significant preferential activity towards BCPAP cells was observed for 12 genes with 2 oligos out of 3, and for the remaining 374 genes with 1 oligo out of 3; the latter include *BRAF*, consistent with the notion that BCPAP cells are addicted to *BRAFV600E* oncogene [16]. No genes emerged with 3/3 oligos among hits. Functional annotation clustering analysis was performed on the 386 gene list (382 DAVID IDs), using Gene Ontology-Biological Process (GO-BP) and Gene Ontology–Molecular Function (GO-MF) annotation terms and medium classification stringency. A significant Enrichment score (>1.3) was found in 15 out of the 117 annotation clusters that were globally identified. The top ranked GO-terms, representative for the 15 significant clusters, have been reported in Figure S1A.

By setting an arbitrary threshold of 20% colony growth with respect to siNT controls, we identified 1695 siRNA oligonucleotides (6.74%) capable of inhibiting cell growth both in BCPAP and Nthy-ori 3–1, therefore defined as "lethal hits" (Figure 1C). Two hundred and seventeen genes emerged as indiscriminately lethal hits with 2/3 (163) or 3/3 (54) oligonucleotides (Table S3). Most of them encode proteins involved in fundamental processes,

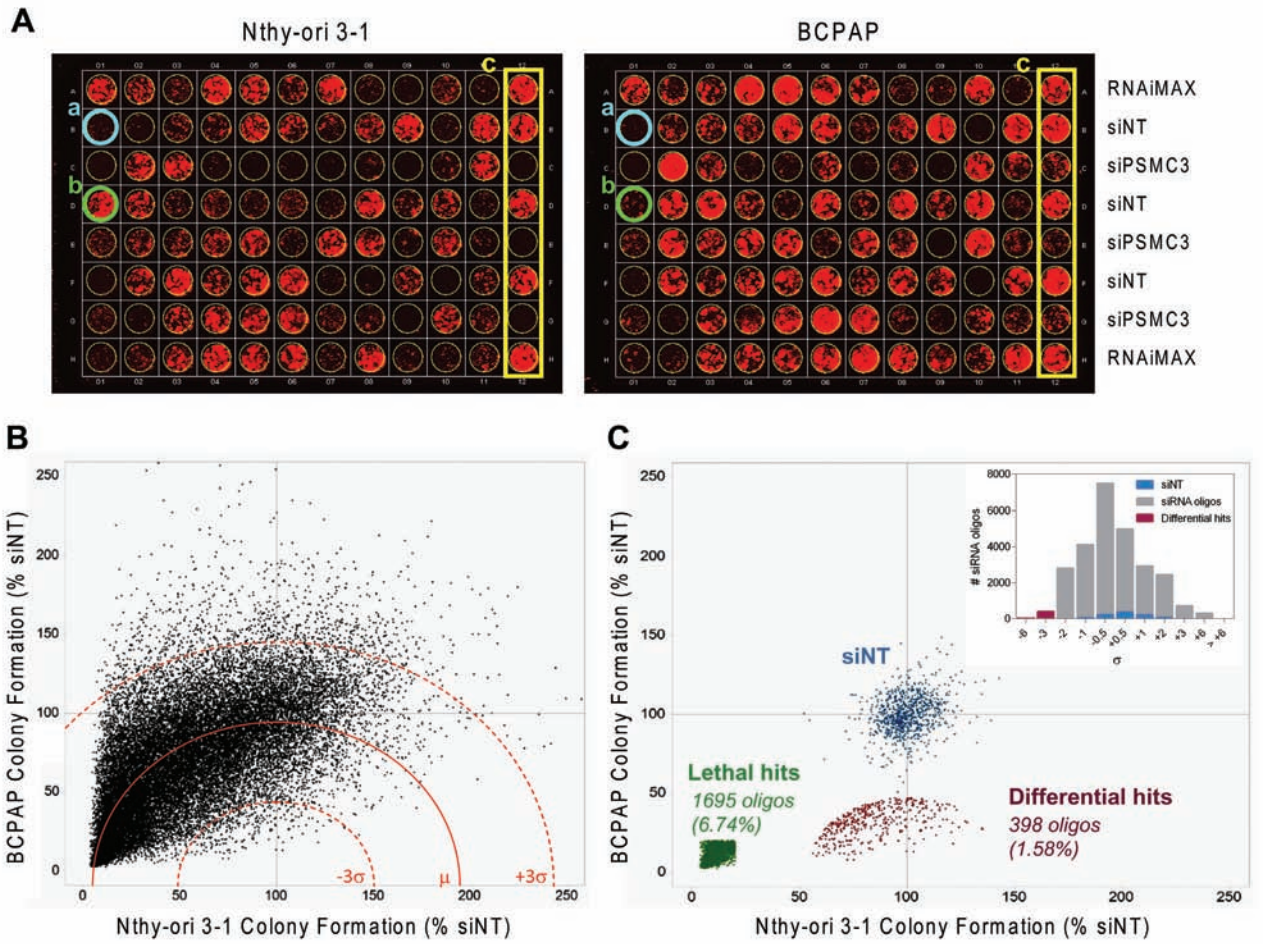

Figure 1: siRNA screening results. A. Representative colony plates generated by transfecting Nthy-ori 3–1 (left) and BCPAP (right) cell lines with the same siRNA oligo mother plate. a. siRNA oligo lethal for both cell lines (blue); b. siRNA oligo selectively lethal for BCPAP (green); c. controls (yellow). **B.** Scatter plot of Colony Formation (CF) values obtained from 25139 unique siRNA oligos transfected in Nthy-ori 3–1 and BCPAP, reported as % of growth respect to NT for inter-plate data normalization (dot are the averages of two technical replicates performed in both cell lines). The mean *d* value (μ) is represented by a red line (dashed red lines: +/− 3σ). **C.** Scatter plot of normalized CF values showing the negative controls (siNT, blue), the lethal hits (green) and the differential hits (red). Insert: distribution of normalized *d* values after sigma binning.

and some, such as the kinases PLK1, WEE1, AURKB and several proteasome subunits, have previously been shown to be essential for cell survival, emerging as top-ranking lethal hits in RNAi-mediated phenotypic proliferation screens in different tumor cell lines [14, 17, 18].

Confirmation of differentially active hits

Eightyfour siRNA oligonucleotides, targeting 28 genes, were selected for confirmatory studies. Hits were prioritized for technical confirmation based on *d* values of individual oligos and on specific interest of identifying candidate druggable target genes. siRNAs were picked from library plates and transfected manually in triplicate on Nthy-ori 3–1 and BCPAP cells using the same experimental conditions as employed in primary screening. In these experiments a threshold of -2σ (corresponding to $d = 49.8$) was applied to define oligos with significantly low *d* values, i.e. displaying differential activity. We considered equally confirmed any siRNA oligos that in confirmation experiments gave the same phenotype of the screening, including the ones inactive or lethal for both cell lines. Figure 2A shows the comparison between primary screening and confirmation results. Eighteen out of 35 siRNA oligos (targeting 15 genes), which had shown differential activity ($d < -3\sigma$) in the primary screening were confirmed by manual transfection ($d < -2\sigma$). All of 49 oligos which were not found to be differentially active in the screening run ($d > -3\sigma$) were confirmed as such by manual transfections ($d > -2\sigma$). Overall, the phenotype of 67 out of 84 oligos was confirmed. Representative images of outgrown colonies from the confirmatory study are shown in Figure 2B and the corresponding quantifications are reported in Figure 2C. The list of confirmed hits is shown in Table 1: 3 genes were confirmed with 2 oligos (*MASTL*,

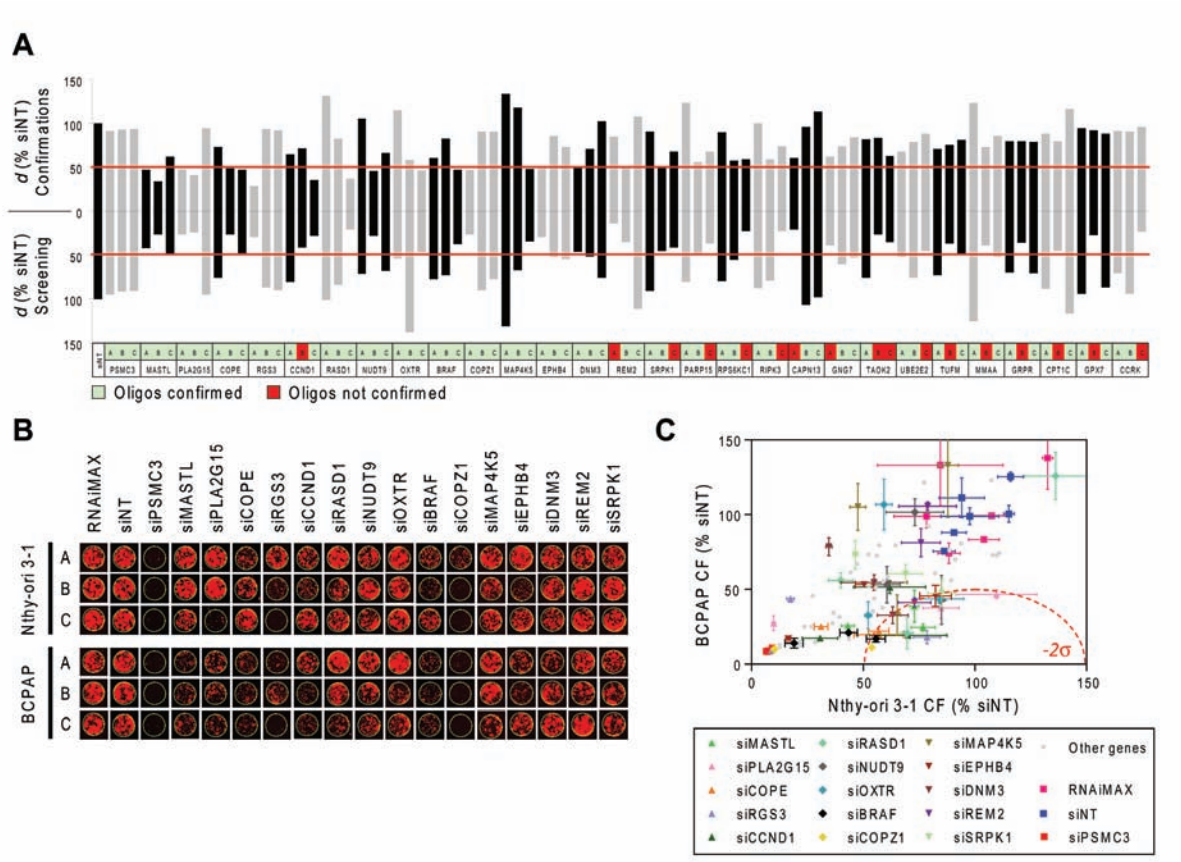

Figure 2: Confirmation of differentially active hits. A. Comparison between *d* values obtained from the screening (bottom) and from confirmation experiments (top) performed with 84 siRNA oligos targeting 28 genes selected among the top ranked hits (A, B and C: three oligos per gene). Non-targeting Oligo (siNT) and siRNA oligos against PSMC3 were respectively used as negative and positive controls of transfection. Values represent the means of two technical replicates. The thresholds used to define differentially active oligos are shown in red ($d = 47.2$ for screening and $d = 49.8$ for confirmations). **B.** Representative pictures of individual wells showing colony formation in confirmation experiments after transfection of Nthy-ori 3–1 and BCPAP cells with the indicated siRNA oligos. **C.** Colony Formation (% siNT) values from image acquisition in B. All 84 oligos used for confirmation are shown; among these, oligos corresponding to the 15 genes are reported in B and are highlighted in color with standard deviation bars.

PLA2G15 and *COPE*) and 12 genes were confirmed with 1 oligo (*RGS3*, *CCND1*, *RASD1*, *NUDT9*, *OXTR*, *BRAF*, *COPZ1*, *MAP4K5*, *EPHB4*, *DNM3*, *REM2, SRPK1*). Functional annotation analysis indicates that these genes are involved in several biological processes, such as cell cycle control, DNA damage and cell death, vesicular transport and endocytosis, cellular metabolic processes and intracellular signal transduction (Table 1). Network analysis performed by Ingenuity Pathway Analysis (IPA) identified two major connection networks as reported in Figure S1B.

Molecular profiling of confirmed hit genes

The thyroid TCGA data set [4], including 496 PTC samples, 58 of which matched with normal thyroid, was interrogated for assessing the mutational status and the expression level of hit genes in PTC. As expected, oncogenic *BRAF* mutations were detected with high frequency, being present in 248 samples. No mutations affecting the other genes were detected, with the exception of a silent mutation in *COPZ1* gene in one case (data not shown). Expression analysis of hit genes was investigated on the whole data set (data not shown), as well as on the 58 matched tumor and normal samples (Figure 3); in both cases identical results were obtained. According to their expression levels, hit genes can be classified in three groups: 1) genes with significantly high overexpression in PTC vs normal thyroid: *CCND1*, *RGS3*, *OXTR*, *RASD1*, *DNM3*; 2) genes with equal or slightly different expression in PTC and normal thyroid: *COPE*, *COPZ1*, *PLA2G15*, *SRPK1*, *REM2*, *EPHB4*, *BRAF*; 3) genes that are significantly downregulated in PTC vs normal thyroid: *MAP4K5*, *NUDT9*, *MASTL*. No differences among different PTC variants (classical, follicular, tall cell) or tumor stage were observed (data not shown).

Data retrieved from the Cancer Cell Line Encyclopedia (http://www.broadinstitute.org/ccle/home) showed that all the hit genes are expressed in BCPAP cells, with levels ranging from "low" to "very high" (data not

Table 1. List of the confirmed hits after the primary screening.

Gene Symbol	Full Gene Name	Accession	GO-BP Term	Confirmed active oligos	*d* (active oligos)
MASTL	microtubule associated serine/ threonine kinase-like	NM_032844	**GO:0006468** protein amino acid phosphorylation **GO:0006793** phosphorus metabolic process	2/2	33.75 (B) - 47.36 (A)
PLA2G15	phospholipase A2, group XV	NM_012320	**GO:0006575** cellular amino acid derivative metabolic process **GO:0006643** membrane lipid metabolic process	2/2	40.56 (B) - 47.71 (A)
COPE	coatomer protein complex, subunit epsilon	NM_007263	**GO:0006890** retrograde vesicle-mediated transport, Golgi to ER transport **GO:0051640** organelle localization	2/2	47.40 (C) - 48.45 (B)
RGS3	regulator of G-protein signaling 3	NM_017790	**GO:0000165** MAPKKK cascade **GO:0008277** regulation of G-protein coupled receptor proteinsignaling pathway	1/1	28.04 (A)
CCND1	Cyclin D1	NM_053056	**GO:0000075** cell cycle checkpoint **GO:0000077** DNA damage checkpoint	1/2	35.57 (C)
RASD1	RAS, dexamethasone-induced 1	NM_016084	**GO:0007264** small GTPase mediated signal transduction **GO:0016481** negative regulation of transcription	1/1	36.74 (C)
NUDT9	nudix (nucleoside diphosphate linked moiety X)-type motif 9	NM_024047	**GO:0006163** purine nucleotide metabolic process **GO:0006811** ion transport	1/1	45.6 (B)
OXTR	oxytocin receptor	NM_000916	**GO:0000165** MAPKKK cascade **GO:0003012** muscle system process	1/1	46.59 (C)
BRAF	v-raf murine sarcoma viral oncogene homolog B1	NM_004333	**GO:0000165** MAPKKK cascade **GO:0010941** regulation of cell death	1/1	47.45 (C)
COPZ1	coatomer protein complex, subunit zeta 1	NM_016057	**GO:0006886** intracellular protein transport **GO:0006890** retrograde vesicle-mediated transport, Golgi to ER	1/1	47.46 (A)

(*Continued*)

Gene Symbol	Full Gene Name	Accession	GO-BP Term	Confirmed active oligos	*d* (active oligos)
MAP4K5	mitogen-activated protein kinase kinase kinase kinase 5	NM_006575	**GO:0000165** MAPKKK cascade **GO:0001932** regulation of protein amino acid phosphorylation	1/1	47.88 (C)
EPHB4	EPH receptor B4	NM_004444	**GO:0007169** transmembrane receptor protein tyrosine kinase signaling pathway **GO:0045765** regulation of angiogenesis	1/1	48.98 (A)
DNM3	dynamin 3	NM_015569	**GO:0006897** endocytosis **GO:0010324** membrane invagination	1/1	49.29 (A)
REM2	RAS (RAD and GEM)-like GTP binding 2	NM_173527	**GO:0006355** regulation of transcription, DNA-dependent **GO:0007264** small GTPase mediated signal transduction	1/2	49.33 (B)
SRPK1	SFRS protein kinase 1	NM_003137	**GO:0006396** RNA processing **GO:0007243** protein kinase cascade	1/2	49.80 (B)
PARP15	poly (ADP-ribose) polymerase family, member 15	NM_152615		0/1	–
RPS6KC1	ribosomal protein S6 kinase, 52kDa, polypeptide 1	NM_012424		0/1	–
RIPK3	receptor-interacting serine-threonine kinase 3	NM_006871		0/1	–
CAPN13	calpain 13	NM_144575		0/1	–
GNG7	guanine nucleotide binding protein (G protein), gamma 7	NM_052847		0/1	–
TAOK2	TAO kinase 2	NM_004783		0/2	–
UBE2E2	ubiquitin-conjugating enzyme E2E 2 (UBC4/5 homolog, yeast)	NM_152653		0/1	–
TUFM	Tu translation elongation factor, mitochondrial	NM_003321		0/1	–
MMAA	methylmalonic aciduria (cobalamin deficiency) cblA type	NM_172250		0/1	–
GRPR	gastrin-releasing peptide receptor	NM_005314		0/1	–

(*Continued*)

Gene Symbol	Full Gene Name	Accession	GO-BP Term	Confirmed active oligos	*d* (active oligos)
CPT1C	carnitine palmitoyltransferase 1C	NM_152359		0/1	–
GPX7	glutathione peroxidase 7	NM_015696		0/1	–
CCRK	cell cycle related kinase	NM_012119		0/1	–

Genes are listed according to the number of active oligos; A, B and C represent three different oligos targeting the same gene. *d* values (<49.8) for each oligo, from the confirmation experiment, are also reported. NM: RefSeq Accession Number (http://www.ncbi.nlm.nih.gov/refseq/about/). Representative Gene Ontology-Biological Process (GO-BP) terms are selected for each of the 15 validated genes, by means of DAVID6.7 functional annotation analysis.

shown). Mutation analysis data indicated a low number (50/1651) of mutated genes in BCPAP cells. *Cyclin D1*, *MASTL*, *MAP4K5*, *SRPK1* and *EPHB4* genes were found to be of wild-type status, whereas no information was available for the remaining hit genes. These findings suggest that the addiction of BCPAP cells to the activity of the hit genes is unlikely related to alterations of the cognate proteins caused by mutations.

Hit gene expression in thyroid cell lines

We investigated the expression of 10 genes (the top 11 hits except *BRAF*, see Table 1), in the normal (Nthy-ori 3–1) and tumor (BCPAP) cell lines used for the siRNA library screening, as well as in a panel of thyroid tumor cell lines, representative of different tumor histotypes, and/or carrying different oncogenes: PTC-derived (TPC-1, carrying the *RET/PTC1* oncogene); FTC-derived (WRO82–1); ATC-derived (8505C and HTC/C3, carrying the *BRAFV600E* oncogene; KAT-18). The expression of MASTL, PLA2G15, COPE, Cyclin D1, COPZ1 and MAP4K5 was investigated by western blot analysis (Figure 4A). Cyclin D1 was found to be 1.3 to 2.7 fold overexpressed in 6 out of 7 tumor cell lines with respect to Nthy-ori 3–1, with the exception of KAT-18, in which it was found less expressed. For COPE a slight increase in the protein expression levels in tumor cells, except KAT-18, with respect to Nthy-ori 3–1 was observed. MASTL was found frequently less expressed in tumor cells, in keeping with what was observed by gene expression analysis in tumor samples (Figure 3). COPZ1 protein expression was slightly increased in all the tumor cell lines, and greater in 8505C. PLA2G15 expression was slightly reduced in all the tumor cell lines, except BCPAP, and strongly reduced in KAT-18. For MAP4K5, a slight increase in BCPAP, WRO82–1 and 8505C, and a decrease in the remaining cell lines were observed.

The expression of *RASD1*, *NUDT9*, *RGS3* and *OXTR* genes was investigated by RT-PCR, as we failed to unequivocally detect the specific protein by western blot analysis (data not shown). As shown in Figure 4B, the genes are expressed in all the cell lines analyzed, and no differences can be appreciated.

Hit validation in BCPAP cell line

Among the candidate BCPAP vulnerability genes identified by the screening we selected *CCND1*, *MASTL* and *COPZ1* for a validation study using commercially available siRNAs, different from those of the library screening. Four different oligos for *MASTL*, and a smart pool of oligos for *CCND1* and *COPZ1* were used (details are reported in Table S4). Firstly, the efficiency of gene knock-down was evaluated by investigating the expression of corresponding proteins in Nthy-ori 3–1 cells transiently transfected with specific siRNAs and with non-targeting oligos (siNT) as control (Figure 5A). For MASTL the highest silencing efficiency was obtained with oligos 1 and 4 (89 and 95% of inhibition at 72 hours, respectively). siRNA targeting *COPZ1* and *CCND1* completely abrogated protein expression. Of note, in keeping with the siRNA library screening results, no macroscopic effects on Nthy-ori 3–1 cell growth/survival were observed (data not shown).

To investigate the effect of *MASTL*, *CCND1* and *COPZ1* gene silencing on BCPAP and Nthy-ori 3–1 cell viability, cells were transfected in 96 well plates with the different oligos above described, or with NT and PSMC3 siRNAs as controls, and analyzed by CellTiter-Glo assay 10 days later. Scatter plots in Figure 5B represent the luminescence signal (average of two replicates, normalized with respect to siNT) of cells transfected with each siRNA oligo. siMASTL#1, siMASTL#4, siCCND1 and siCOPZ1 reduced cell viability by 60%, 93%, 94% and 86%, respectively, an efficiency comparable to that of the control siRNA PMSC3 (93%). No effects were observed for siMASTL#2 and siMASTL#3, in keeping with their low silencing efficiency (Figure 5A).

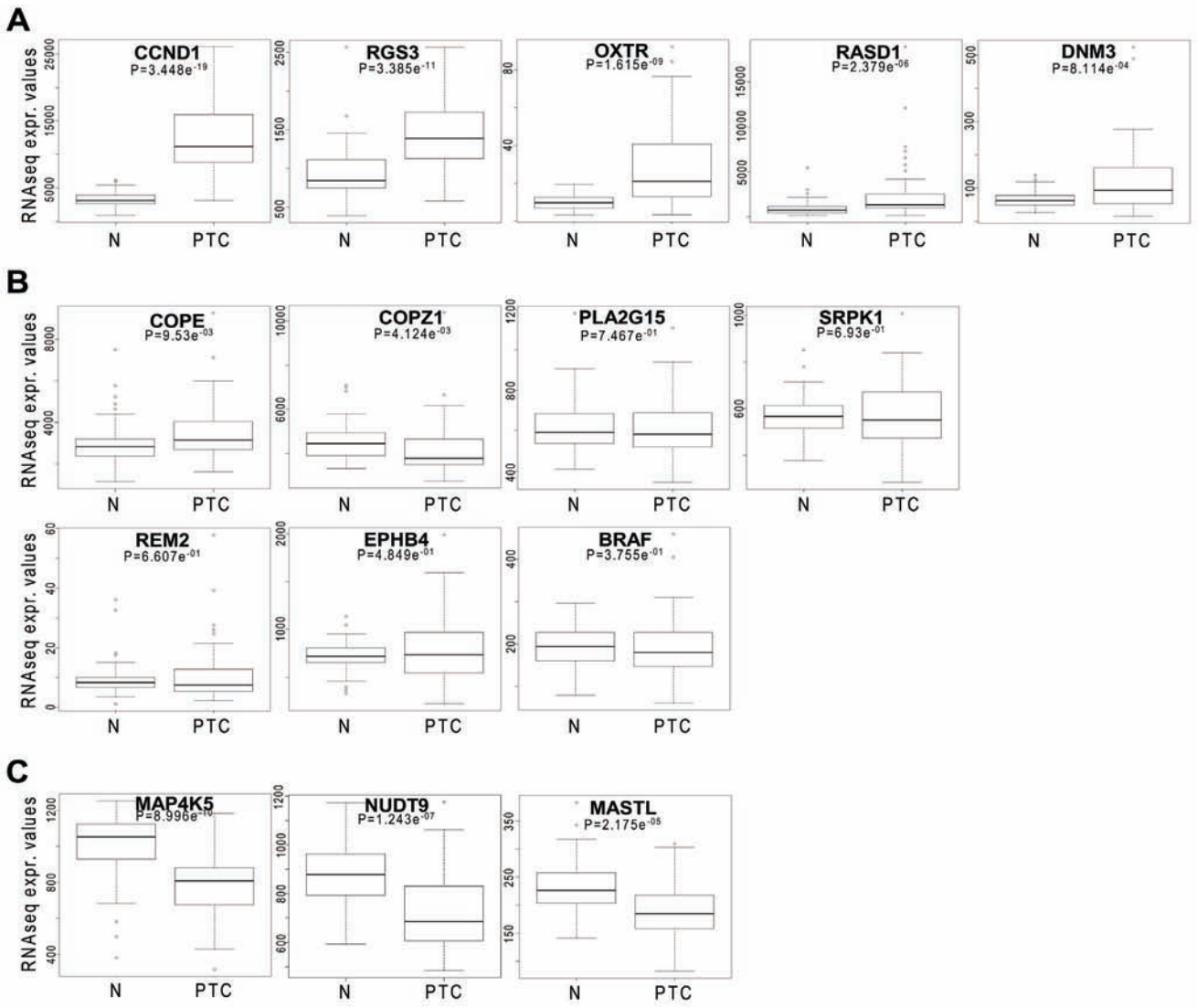

Figure 3: Hit gene expression levels in PTC. Box plot distribution of RNAseq normalized expression values from the thyroid TCGA dataset of 15 selected genes in 58 matched normal (N) and PTC samples; **A, B** and **C.** represent genes overexpressed, equally or downregulated in PTC vs normal samples, respectively. The statistical significance of differences among the groups was assessed using Wilcoxon test.

The effect of *MASTL*, *CCND1*, *COPZ1* gene silencing in BCPAP cells was further confirmed by a different experimental approach. Cells were transfected in 6-well plates with the oligos which showed efficient silencing in the previous experiment (siCCND1 and siCOPZ1 smart pools, siMASTL #1 and #4 oligos), and the newly in house synthesized MASTL oligo #5 (see Figure S2 for silencing efficiency). Six days later the effect of *MASTL*, *COPZ1* and *CCND1* silencing on both cell growth and cell viability was evident by microscope observation: silenced BCPAP cultures were less confluent than control (siNT); in addition, they presented numerous floating (most likely dead) cells (Figure 5C). Trypan blue exclusion assay showed a reduction of cell growth by 69.5%, 59.7% and 71% for siMASTL#1, #4 and #5, respectively; by 99.6% for siCOPZ1, by 91.5% for siCCND1 in comparison with the control (siNT). Western blot analysis performed at the end point of the experiment (Figure 5E) showed the complete abrogation of MASTL and Cyclin D1 protein expression. The same analysis was not feasible for COPZ1: due to the massive lethal effect of siCOPZ1, an insufficient amount of protein extract was recovered (data not shown).

Overall these results confirmed the growth inhibitory effect of *Cyclin D1*, *MASTL*, and *COPZ1* gene silencing, thus providing evidence that BCPAP cells are addicted to the activity of these genes.

Effect of *Cyclin D1*, *MASTL* and *COPZ1* gene silencing on different thyroid tumor cell lines

Irrespective of the specific oncogenic driving lesion and histotypes, thyroid tumors may share common effector

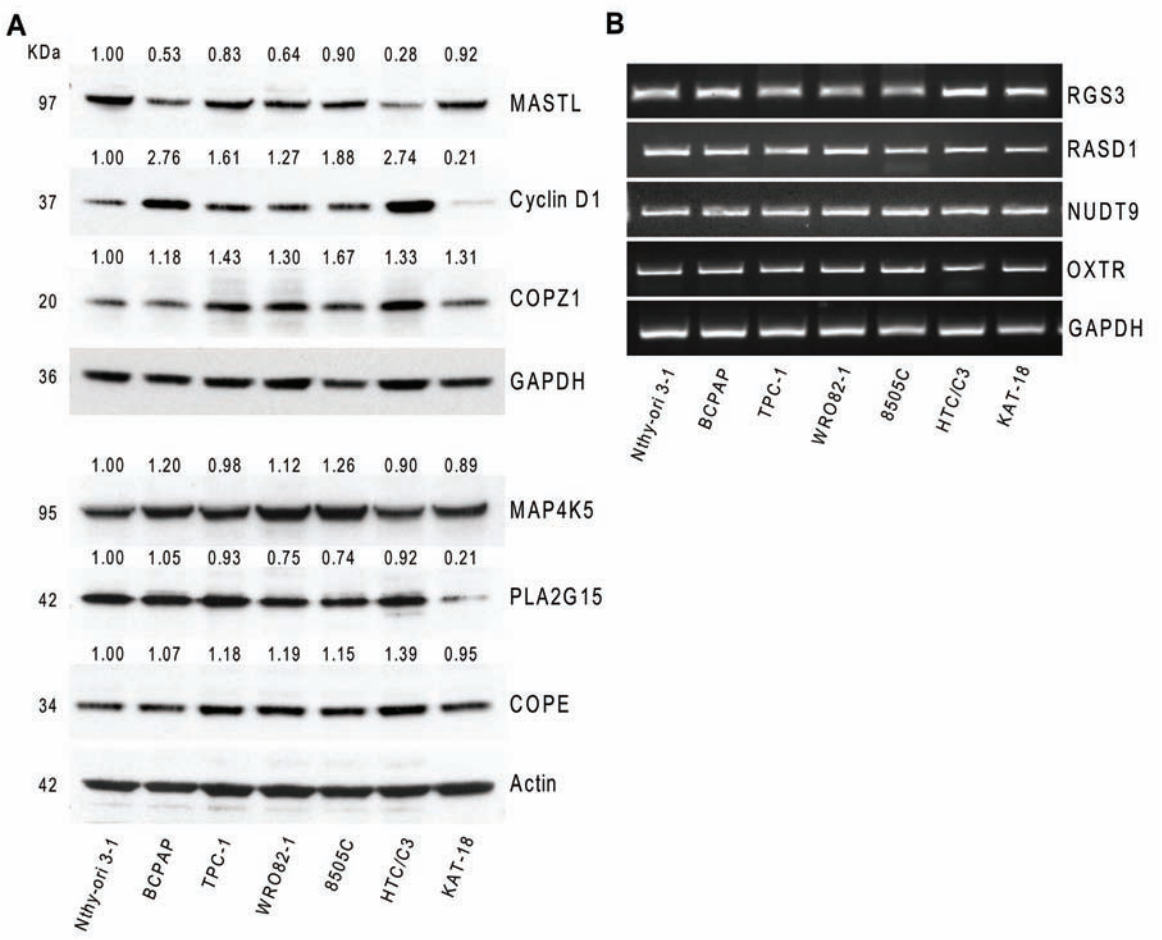

Figure 4: Hit gene expression in different thyroid tumor cells. A. Western blot analysis of MASTL, Cyclin D1, COPZ1, MAP4K5, PLA2G15 and COPE protein expression in a panel of thyroid cell lines; values represent band intensity, assessed by densitometry analysis, reported as the ratio to actin (loading control) and normalized for the Nthy-ori 3–1 value. **B.** *RGS3*, *RASD1*, NUDT9 and *OXTR* mRNA expression by RT-PCR in a panel of thyroid cell lines; *GAPDH* was used as housekeeping control. One out of three representative experiments is shown.

pathways for sustaining their transformed phenotype. To assess whether the survival genes confirmed in BCPAP cells are involved in such common pathways, we investigated the effect of *CCND1*, *MASTL* and *COPZ1* gene silencing in a panel of thyroid tumor-derived cell lines representative of different tumor histotypes.

Cell lines were transfected in 96 well plates with oligos targeting *MASTL*, *CCND1* and *COPZ1* genes and analyzed by CellTiter-Glo assay 10 days later. As reported in Figure 6A, gene silencing induced variable extents (15–95%) of cell growth inhibition in the majority of cell lines tested; no effect of *CCND1* silencing in 8505C and KAT-18 cells, and of *MASTL* silencing in KAT-18 was observed. We also assessed viability of cells transfected in 6-well plates by trypan blue exclusion assay performed four-seven days after siRNAs transfection. As reported in Figure 6B, in all the cell lines analyzed (except KAT-18), *MASTL*, *COPZ1* and *CCND1* gene silencing led to a significant decrease of cell viability: by 30–63% for siMASTL#1, by 35–75% for siMASTL#4, by 40–75% for siMASTL#5, by 75–99% for COPZ1 and by 70–94% for siCCND1. KAT-18 cells were found to be less sensitive to all the siRNA oligos: we found a decrease of cell growth by 31% for siMASTL#1, by 53% for si siCOPZ1 and by 43% for CCND1, and by 52.3% for the siPSMC3 control, and no effect for siMASTL#4 and #5. The reduction of cell growth in all the cell lines was also documented by images taken before cell count: silenced cells appeared less confluent in comparison with the control, and presented variable fractions of detached and floating cells (Figure S3). Concomitantly, western blot in Figure 6C shows the high efficiency of *MASTL*, *CCND1* and *COPZ1* silencing in the same samples. The same analysis was not feasible for TPC1 cells transfected with siCOPZ1, due to massive lethal effect (data not shown). Importantly, this experiment revealed a growth inhibitory effect of *CCND1* silencing in 8505C and KAT18, and of *MASTL* silencing in KAT18 cells, which was not previously observed. This could be ascribed to variability in the experimental conditions and/or silencing efficiency.

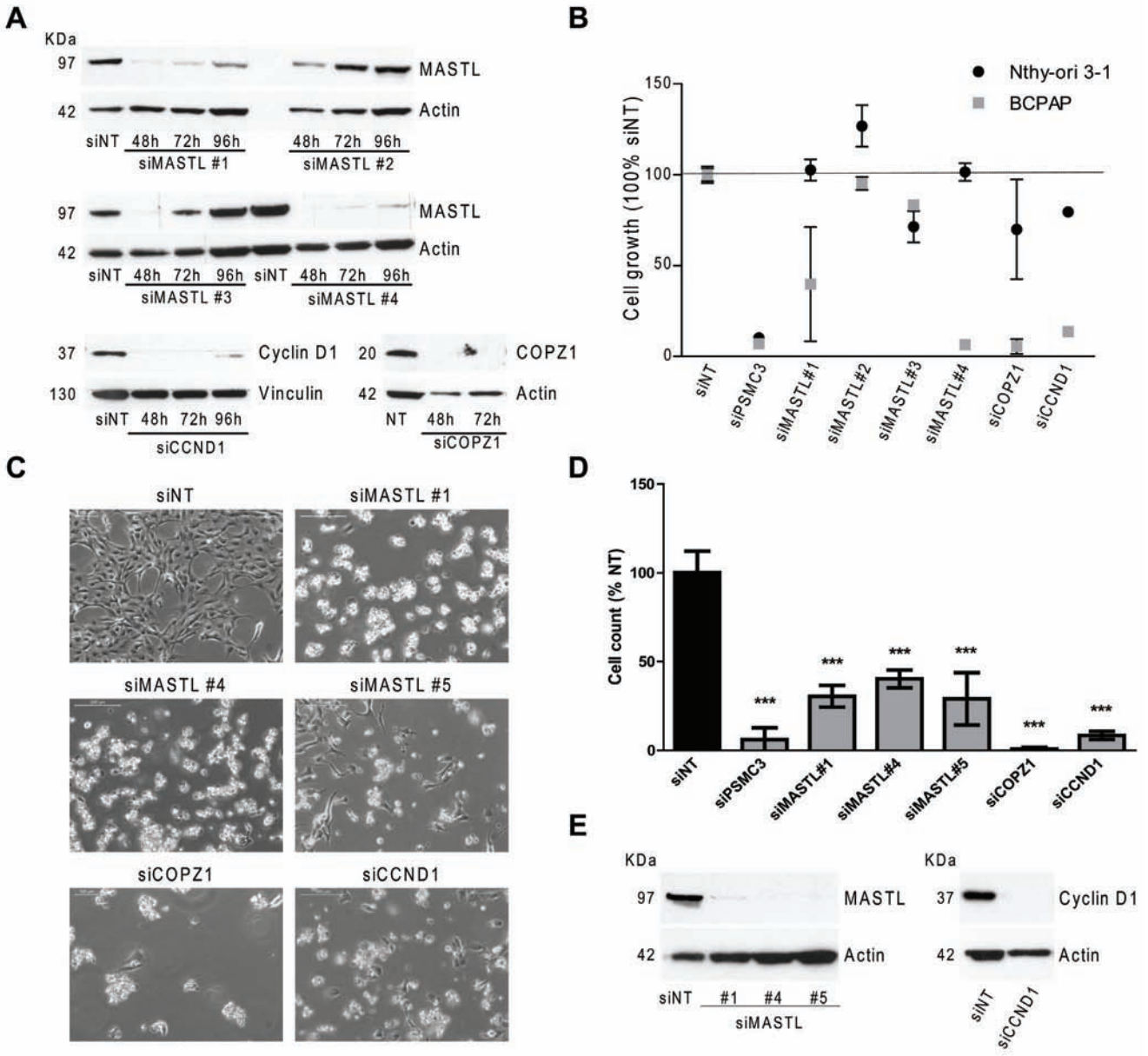

Figure 5: Effect of *MASTL*, *CCND1* and *COPZ1* silencing on BCPAP cells. A. Western blot analysis of MASTL, Cyclin D1 and COPZ1 protein expression in Nthy-ori 3–1 cells, transiently transfected with siRNAs; actin was used as loading control. **B.** Scatter plot graph representing the percentage of cell growth (luminescence signal by CellTiter-Glo assay), normalized to that of Non Targeting oligo (siNT) 100%, 10 days after siRNA transfection in Nthy-ori 3–1 and BCPAP cells; siPSMC3 was used as positive control; one out of three representative experiments is shown. **C.** Representative pictures at 10X magnification of BCPAP cells 6 days after siRNA transfection. **D.** Cell proliferation assay of BCPAP cells 6 days after siRNAs transfection; the growth rate was determined by the trypan blue exclusion assay. Cell count of viable cells was normalized to that of siNT (100%); data represent the mean +/− sd of two independent experiments; the asterisks indicate differences significant by the unpaired Student's *t*-test (**$P < 0.01$, ***$p < 0.001$). **E.** Western blot analysis of MASTL and Cyclin D1 expression performed in the same samples of panel D; actin was used as loading control for cell extracts.

We next performed some experiments to further corroborate the dependency of thyroid cancer cells upon Cyclin D1, MASTL and COPZ1 activity.

We tested thyroid tumor cell lines for susceptibility to palbociclib (PD-0332991), a specific inhibitor of Cyclin D1 associated kinases CDK4/6 [19]. Treatment with increasing doses of palbociclib showed a consistent antiproliferative effect in thyroid cancer cells, with an IC_{50} value ranging from <0.003 μM for BCPAP cells to 0.20 μM for HTC/C3 cells (Figure 7A and 7B). Representative images of thyroid cancer cell lines untreated or treated with 2.2 μM palbociclib for 72 h are reported in Figure 7C.

It has been reported that inhibition of *MASTL* induces multiple mitotic defects [20]. To investigate this issue in MASTL-depleted thyroid tumor cells, we performed the analysis reported in Figure 8. Asynchronous 8505C cells

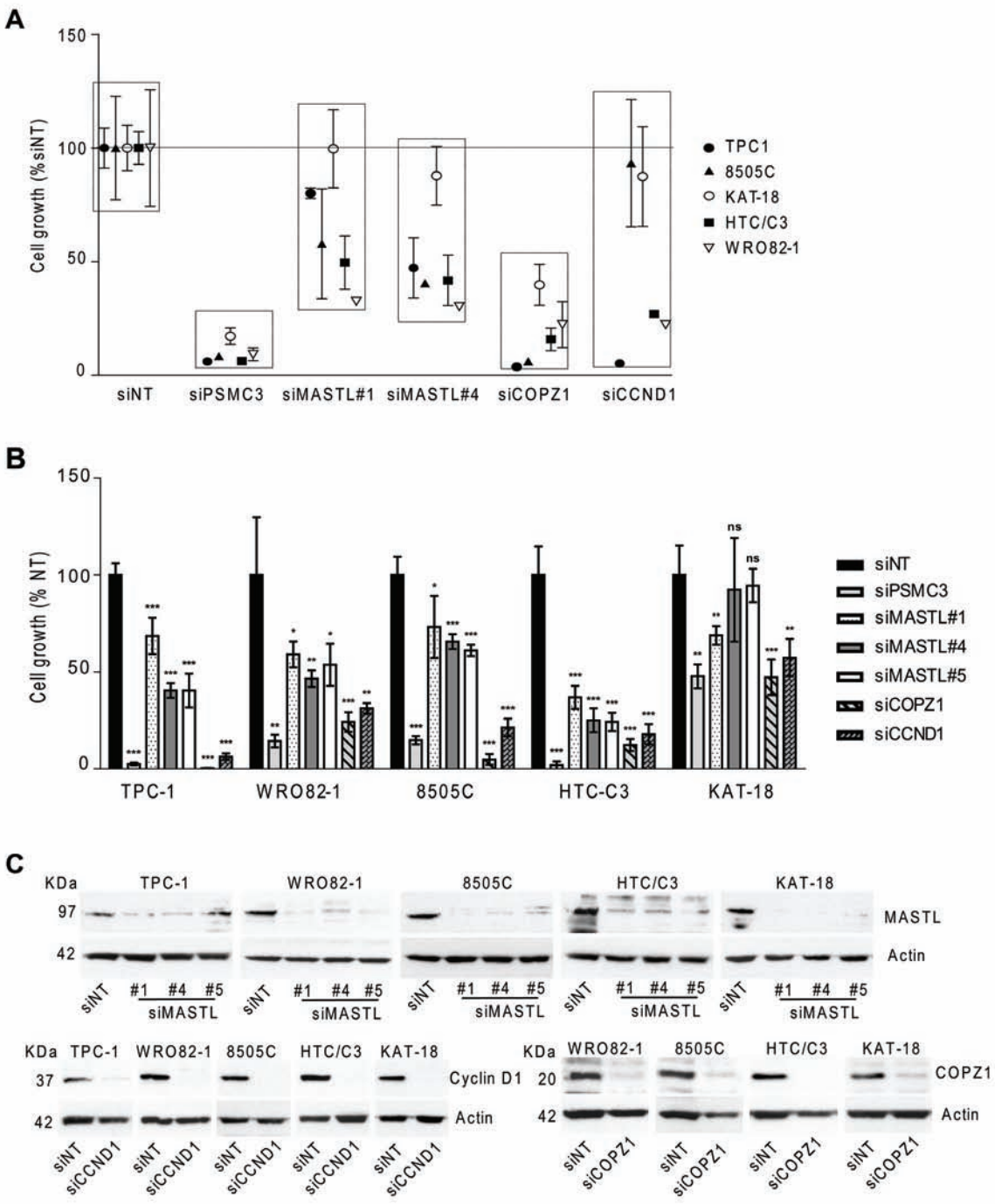

Figure 6: Effect of CCND1, *MASTL* and *COPZ1* silencing on different thyroid tumor cell lines. A. Scatter plot graph representing the percentage of cell growth (luminescence signal by CellTiter-Glo assay), normalized to that of Non Targeting oligo (siNT) 100%, 10 days after siRNA transfection in a panel of thyroid cell lines; siPSMC3 was used as positive control. One out of three representative experiment is shown. **B.** Cell proliferation assay 4 days (for TPC1, 8505C and HTC/C3 cells), 5 days (for KAT-18 cells), 6 days (for BCPAP cells), 7 days (for WRO82–1 cells) after siRNAs transfection; the growth rate was determined by the trypan blue exclusion assay. Cell count of viable cells was normalized to that of siNT (100%); data represent the mean +/− sd of two independent experiments; the asterisks indicate differences significant by the unpaired Student's *t*-test (*$P < 0.05$, **$P < 0.01$, ***$p < 0.001$). **C.** Western blot analysis of MASTL, Cyclin D1 and COPZ1 expression performed in the same samples of panel B; actin was used as loading control for cell extracts.

were transfected with the siMASTL or NT siRNA oligos and, 48 hours later, analyzed by immunofluorescence for β-tubulin, phospho-histone H3, and DNA for the presence of mitosis and nuclei aberrations. Several abnormalities associated with *MASTL* knockdown [20] were observed in MASTL-depleted 8505C cells. These include:

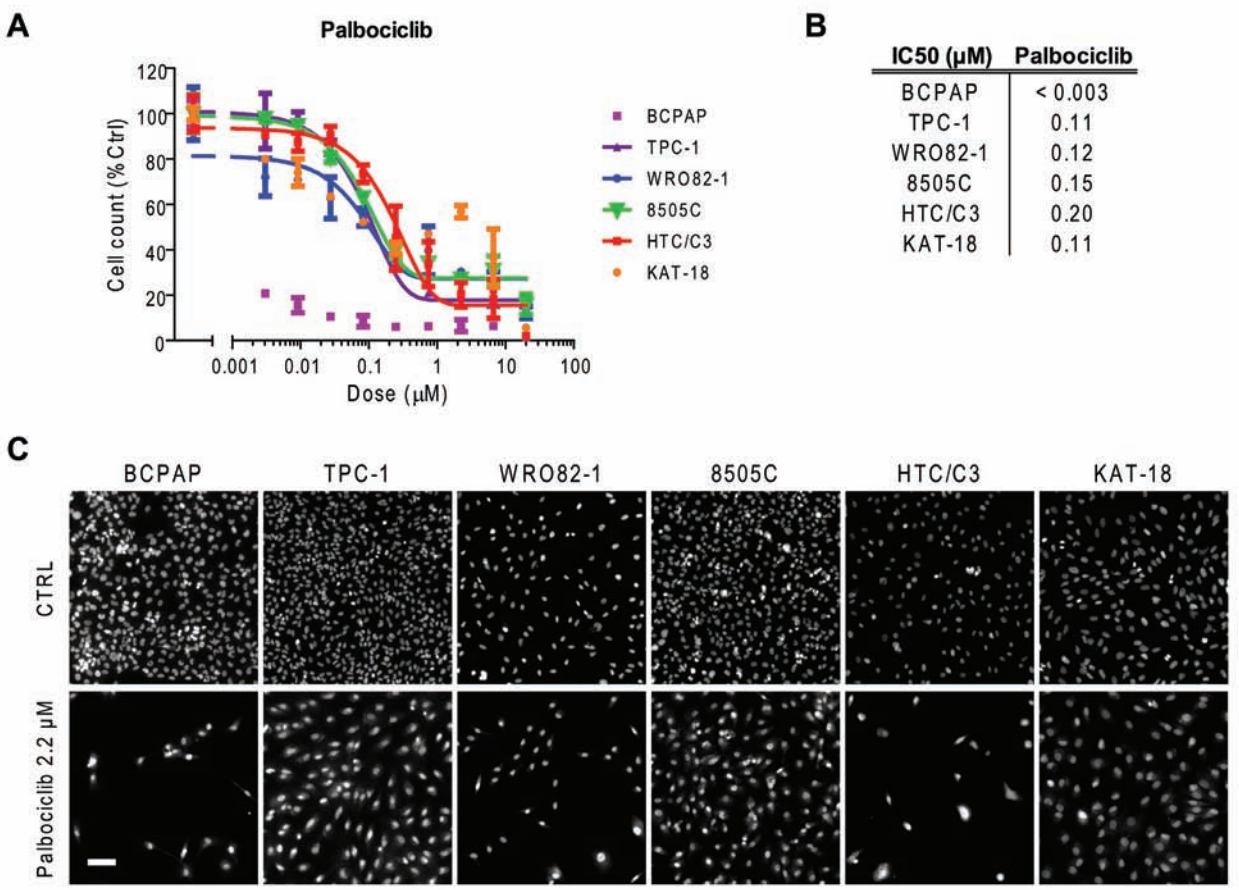

Figure 7: Thyroid cancer cell line sensitivity to palbociclib. A. Proliferation dose response curves of thyroid cancer cell lines treated with palbociclib for 72 hours. Nuclei were stained with Hoechst and counted in each well by means of an ArrayScan high-content screening reader. The cell count per field, derived from nuclear staining, was reported as proliferative parameter and normalized with respect to untreated controls (100%). Each value represents the mean and standard deviation of two replicates. **B.** IC50 values (μM) obtained using a sigmoid function for nonlinear interpolation of experimental points; for KAT-18, the IC50 value was derived from graphical analysis. **C.** Representative ArrayScan fields of the thyroid cancer cell lines untreated (CTRL) or treated with 2.2 μM palbociclib for 72 h and stained with Hoechst (bar = 50 μm).

multinuclear cells (panel B); abnormal mitotic figures, documented by the presence of condensed chromosomes that did not correctly align to metaphase plate (panel C); and chromatin bridges connecting daughter cells during anaphase (panel D). None of these abnormalities was observed in the control siNT cells (panel A). These results suggest that the growth inhibitory effect of *MASTL* silencing in thyroid tumor cells may be the consequence of failure of correct cell division process.

Shtutman et al [21] have recently reported that tumor cell *COPZ1* vulnerability is related to downregulation of the paralogous *COPZ2* gene. To assess whether this occurs also in thyroid tumor cells we investigated the expression of *COPZ2* by Real Time PCR (Figure 9). With respect to control Nthy-ori 3–1 all the tumor cell lines analyzed, but WRO 82–1, showed downregulation of *COPZ2* mRNA. This result indicates that for the majority of thyroid tumor cell lines the *COPZ1* dependence may result from downregulation of *COPZ2*.

Collectively, our study identified Cyclin D1, MASTL and COPZ1 as thyroid cancer cell specific vulnerabilities, suggesting that they could provide a common therapeutic target in thyroid cancer treatment.

DISCUSSION

Despite much progress having been made in the genetic and molecular characterization of thyroid carcinoma, few or no therapeutic options are currently available for patients with aggressive and iodine-refractory thyroid tumors. Kinase inhibitors (KIs) in particular are being intensively studied in clinical trials in thyroid cancer: of note, various BRAF inhibitors for tumors that bear mutation of this gene [22–24], as well as a series of multi-kinase inhibitors, are emerging as potentially effective options in the treatment of advanced TC that are not responsive to traditional therapies [10]. However, the efficacy of KIs in patients with differentiated thyroid

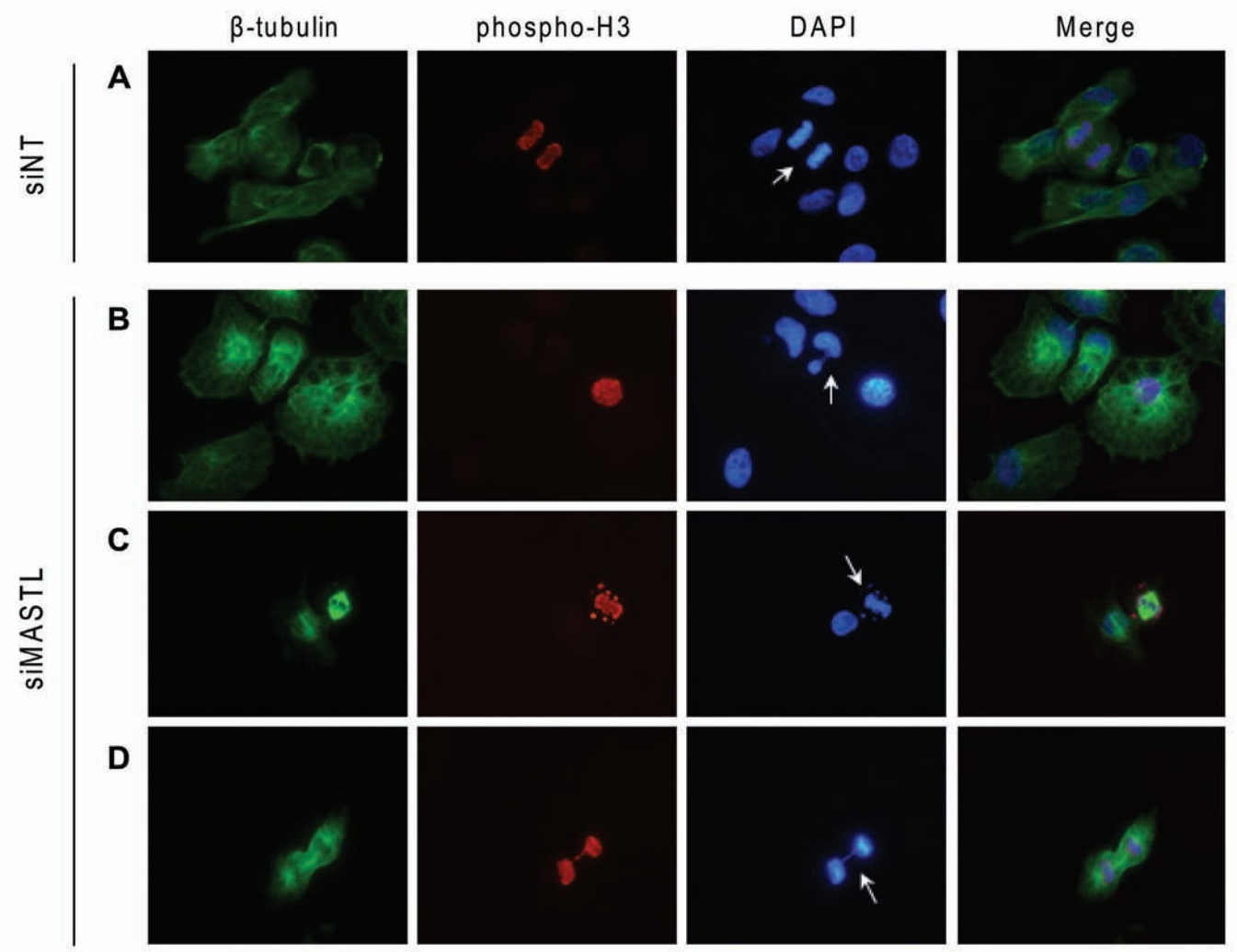

Figure 8: *MASTL* silencing causes abnormal mitotic figures. 8505C cells transfected with the indicated siRNAs were analyzed by immunofluorescence for β-tubulin (green), phospho-histone H3 (red) and DAPI (DNA, blue). Arrows indicate normal mitosis **(A)**, multinuclear cell **(B),** condensed chromosomes not correctly congressed to metaphase plate **(C)**, DNA bridge **(D)** (Magnification 40x).

carcinoma has given contrasting evidence in the clinical trials, probably due to the drug resistance (as in other tumor types). Furthermore, KIs might cause significant side effects. This underlines the need for further efforts aimed at the identification of novel therapeutic approaches for thyroid tumors [10].

Large-scale siRNA-based functional screening on cancer cell lines are nowadays widely used for the identification of tumor cells vulnerabilities to be explored for therapeutic purposes [12]. Interestingly, such approaches allow the discovery of target genes that are required by tumor cells in specific contexts, thus providing the premise for the identification of therapeutic approaches with no or limited effect on normal cells.

In this paper, we described, for the first time, a high-throughput siRNA phenotypic screening campaign for the identification of thyroid tumor cell vulnerabilities. By screening a "druggable genome" siRNA library, we identified 398 siRNA oligos (targeting 386 genes) which preferentially inhibited the growth of the BCPAP papillary thyroid cancer cell line as compared to that of non-transformed thyrocytes (Nthy-ori 3–1). Fifteen out of 28 hit genes were technically confirmed. The relevance of this screening study and its ability to identify bona fide cell vulnerabilities is supported by two lines of evidence. First, *BRAF* was detected among the top BCPAP vulnerability genes. This was expected, as the dependency of BCPAP cells upon *BRAFV600E* oncogene has been previously documented [16]. Second, the screen efficiently detected genes that were indiscriminately lethal for both the Nthy-ori 3–1 and BCPAP cell lines: in many cases, these were found to be genes that encode proteins of essential function and have been identified as survival genes in previous functional screenings [14, 18, 25].

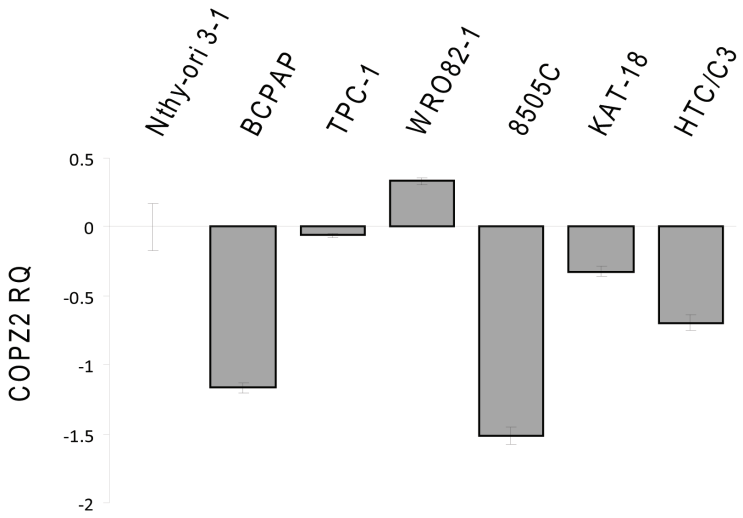

Figure 9: Expression of *COPZ2* in thyroid tumor cell lines. Real-time PCR analysis of COPZ2 gene expression; results are presented as log10-transformed relative quantity (RQ) of COPZ2 mRNA normalized for HPRT1 housekeeping gene expression. Data represent the mean +/− sd of three independent experiments.

Analyzing the thyroid TCGA data set, we found no mutations affecting the confirmed hit genes, besides *BRAF*, suggesting that functional alterations in PTC may be excluded. With respect to gene expression the hit genes were found to be either equally or differentially (both upregulated and downregulated) expressed in PTC in comparison with normal samples.

Three hit genes, namely *Cyclin D1*, *MASTL* and *COPZ1*, were selected for further confirmation. Their vulnerability for BCPAP cells was confirmed by using siRNA oligos different from the screening. Interestingly, we showed that the silencing of *Cyclin D1*, *MASTL* and *COPZ1* reduces the growth and survival of several different TC cell lines, regardless the histotype and the oncogenic lesion.

Cyclin D1 is an important cell cycle regulator that promotes G1/S phase transition by activation of CDK4 and CDK6 kinases [26]. Cyclin D1 is frequently overexpressed in human cancer, and it has been proposed as a therapeutic target. Several approaches aimed at its inhibition are presently ongoing. As for all cyclins, while the lack of enzymatic activity makes direct targeting of Cyclin D1 difficult, a much more amenable approach is to target cyclin functions by inhibition of their associated kinases. Indeed, several CDK4/6 inhibitors have shown promising antitumor activity in experimental systems, and are presently under clinical evaluation for different tumor types [26]. Alternative approaches are also currently under investigation, including the targeting of factors which regulate Cyclin D1 protein turnover, such as the USP2 deubiquitinase [27]. In thyroid carcinoma overexpression of *Cyclin D1* at mRNA and protein level has been documented, and has been suggested to contribute to tumor progression [28–30]. However, no functional data dissecting the role of Cyclin D1 in thyroid tumorigenesis are available. We found that *Cyclin D1* inhibition led to a consistent reduction of cell growth in all the thyroid tumor cell lines analyzed. This was not associated with Cyclin D1 expression level, suggesting that the dependency of thyroid tumor cells upon Cyclin D1 activity may not require aberrant protein expression. We also found that all the thyroid tumor cell lines are sensitive to palbociclib (PD-0332991), a selective CDK4/6 inbititor approved for the treatment of ER+/HER2- breast cancer in combination with letrozole [31]. Whether the antiproliferative effect after *Cyclin D1* silencing or palbociclib treatment in thyroid tumor cells, but not in normal ones, is related to the presence of functional pRB, as reported for other tumor types [19], remains to be investigated. Our studies identified Cyclin D1 as a therapeutic target for thyroid tumors, and provide a rationale for preclinical and clinical studies aimed to assess the efficacy of inhibitors of Cyclin D1 function in thyroid cancer.

MASTL (Microtubule associated serine/threonine kinase-like) regulates mitosis progression by inhibiting PP2A/B55δ, the principal protein phosphatase complex that dephosphorylates CDK1 substrates. MASTL activity is essential for prevention of defects in chromosome condensation and segregation, prometaphase arrest and mitotic collapse during cell division [32]. Furthermore, it modulates DNA damage response by promoting checkpoint recovery and cell cycle progression [33]. Little is known about MASTL in cancer. Nagel et al. [34] reported that the knockdown of *MASTL*, through promoting defects in in cytokinesis and a shortened G2/M phase arrest, is capable of sensitizing lung cancer cells to radiations. Notably, *MASTL* inhibition affects tumor cell but not normal primary fibroblast radiosensitivity, thus suggesting that MASTL could represent a druggable target to combine with radiotherapy. In head and neck carcinoma *MASTL* was found involved in progression and recurrence and proposed as therapeutic target [35]. We

have identified *MASTL* as vulnerability gene for thyroid carcinoma. In fact, *MASTL* silencing interfered with the growth of all thyroid cell lines, although with variable extents. Moreover, evidence of failure of correct cell division process was found in MASTL-depleted cells. Of note, our study identified MASTL as a novel mitotic machinery target in thyroid tumor, in addition to PLK1 and AURKs, both overexpressed and proposed as therapeutic targets in ATC [36, 37]. Remarkably, we found that MASTL vulnerability in thyroid tumor cell lines is not associated with overexpression; on the contrary, *MASTL* is slightly downregulated in PTC samples and in thyroid tumor cells. Overall these findings highlights the need of further investigation in order to assess whether MASTL may represent a useful target in different tumor types, as well as the search/design of strategies to block the activity of MASTL, for which no specific inhibitors have been so far identified.

COPZ1 (coatomer protein complex ζ1) is a subunit of coatomer protein complex I (COPI), a secretory vesicle coat protein complex involved in Golgi apparatus and endoplasmic reticulum traffic, endosome maturation, autophagy [38, 39] and lipid homeostasis [40]. *COPZ1* has been proposed as a tumor-specific gene target. It has been shown that tumor cells become dependent on *COPZ1*, as a result of a tumor-specific downregulation of its isoform *COPZ2* [21]. Interestingly, *COPZ1* knockdown kills both proliferating and non-dividing tumor cells, but does not affect normal cells, thus suggesting that COPZ1-targeting therapies have the potential for eradicating cancer cells, independently of whether they are actively proliferating. Our screening and validation identified *COPZ1* as a thyroid tumor cell specific survival gene. Interestingly, we also found a significant downregulation of *COPZ2* mRNA expression in the majority of thyroid tumor cell lines. An exception is represented by WRO82–1 which, despite expressing *COPZ2* mRNA levels higher than control, is sensitive to *COPZ1* silencing. This raises the possibility that other mechanisms, in addition to *COPZ2* downregulation, may be involved in determining tumor cell *COPZ1* dependency. Whether the thyroid tumor cell dependency upon *COPZ1* is related to downregulation of *COPZ2* isoform, or to deregulation of other COPI components, as well as the modalities through which COPZ1 inhibition leads to growth suppression of thyroid tumor cells, remains to be investigated.

In conclusion, by a siRNA-based functional screening we have identified a signature of vulnerability for thyroid carcinoma cells, thus identifying novel potential therapeutic targets in this setting. Further characterization of three hit genes, namely *Cyclin D1*, *MASTL* and *COPZ1*, demonstrates that their abrogation selectively impairs the growth of several thyroid tumor cell lines, irrespective of the histotype or driving genetic lesion, thus indicating that they represent common examples of "non-oncogene addiction" in thyroid cancer. Variable extents of cell growth inhibition among the cell lines upon silencing of these target genes were observed. Whether these differences are related to genetic background and/or intrinsic sensitivity to cell death remains to be investigated. The dependency upon Cyclin D1, MASTL and COPZ1 activity is restricted to tumor cells and not normal thyroid cells, as previously reported for other tumor types [21, 27, 34, 35]. Thus we envisage that Cyclin D1, MASTL and COPZ1 are attractive targets for new therapeutic approaches for thyroid cancer which spare normal cells and which would thus have limited side effects.

MATERIALS AND METHODS

Cell lines

Nthy-ori 3–1 cell line (SV-40 immortalized normal human thyroid follicular cells) was purchased from European Collection of Cell Cultures (ECACC) (Salisbury, UK); BCPAP, TPC-1, WRO82–1, 8505C, KAT-18 were obtained from Prof. A. Fusco (University Federico II, Naples, IT); HTC/C3 was purchased from Riken Cell Bank (Tsukuba, Japan).

Nthy-ori 3–1 and the PTC-derived BCPAP cell lines were cultured in RPMI 1640 medium (Gibco Life Technologies, Carlsbad, CA, USA) supplemented with 10% (v/v) heat-inactivated fetal bovine serum (FBS) (EuroClone, Pero, Italy), penicillin (100 U/ml) and streptomycin (100 mg/ml). The other cell lines PTC-derived TPC1; FTC-derived WRO82-1; ATC-derived 8505C, KAT18 and HTC/C3 were maintained in DMEM (Gibco, Life Technologies, Carlsbad, CA, USA) medium containing 10% FBS and 2 mM glutamine. All cell lines were cultured as monolayer at 37°C in a 5% CO_2 humidified atmosphere.

Cell lines were genotyped at the Fragment Analysis Facility of Fondazione IRCCS Istituto Nazionale dei Tumori, using Stem Elite ID System (Promega Corporation, Madison, USA) according to the manufacturer's instructions and ATCC guidelines. The profiles obtained matched to their original profiles [41, 42]. WRO82–1 profile matched to that reported by Xu et al. [43] and HTC/C3 to that reported by JCRB Cell Bank (http://cellbank.nibio.go.jp/legacy/celldata/jcrb0164.htm).

Mycoplasma contamination was tested periodically and found negative in all cell lines (PCR Mycoplasma Detection Set, TAKARA Bio Inc).

siRNA transfection optimization

Optimal conditions for reverse siRNA transfection of Nthy-ori 3–1 and BCPAP cells were determined by comparing cell viability after transfecting a positive control siRNA targeting the proteasome subunit PSMC3, and a negative control non-targeting oligo (siNT), in the presence of different cell densities and Lipofectamine

RNAiMAX reagent (Invitrogen Life Technologies Carlsbad, CA, USA) concentrations. The best reagent and transfection conditions were those that produced the least (<10%) cell loss with siNT, and the greatest (>90%) cells decrease with the lethal PMSC3 oligo.

High throughput siRNA screening

The human Silencer Select Druggable Genome siRNA Library V4 (Ambion Life Technologies, Carlsbad, CA, USA) is composed by 309 96-well plates containing 25139 unique lyophilized siRNA oligos targeting 9031 human genes (three oligos per gene, on average). Stock plates were obtained by dissolving oligonucleotides with 100 µl of DEPC-treated water (Ambion Life Technologies, Carlsbad, CA, USA) (final concentration 2.5 µM) and by adding NT and PSMC3 siRNA oligos (2.5 µM) in alternate position in the empty column 12 of each plate (see Figure 1A). Library oligonucleotides were further diluted to 800 nM with DEPC-treated water (mother plates). Daughter plates were prepared by transferring 17 µl/well of mother plate oligonucleotide solution in plates prefilled with 119 µl of Opti-MEM® I medium (Gibco Life Technologies, Carlsbad, CA, USA) containing 4 µl/ml of lipofectamine® RNAiMAX. The solution was gently mixed by pipetting and incubated for 20 minutes room temperature, and then 30 µl/well were split into four transfection plates, to which 120 µl/well of cell suspension (1250 cells /ml) were added. Two plates for each cell line (Nthy-ori 3–1 and BCPAP) were used. Each well contained 150 cells, 20 nM oligo, RNAiMAX 0.1% vol/vol. After transfection, plates were kept at room temperature for 15–20 minutes to minimize uneven distribution of the cells in each well [44], and then incubated at 37°C for 7–8 days by stacking in alternate orientations to limit uneven medium evaporation and to facilitate gas exchange. As a result of this procedure, no edge effects or evidences of asymmetric cell growth emerged from screening data analysis, and visual inspection of plate scans confirmed homogeneous cell distribution in all plates. The following custom-barcoded 96-well microplates purchased from Greiner Bio-One (Frickenhausen, Germany) were used: U-bottom microplate for mother and daughter plates; CELLSTAR®, Black /µClear® plate for transfection plates. All liquid handling and plate tracking were performed with a Freedom EVO® robotic platform (Tecan, Männedorf, Switzerland); disposable MCA384 Tips and reservoirs were purchased from Tecan.

siRNAs

Information on siRNAs used in the transfection setup, as control in the screening, or in confirmation and validation studies is summarized in the Table S4. Oligos produced in house were designed and synthesized with stabilizing modifications (i.e.: phosphorylation in 5′ position of the antisense strand and 2′-*O*-methyl ribosyl substitution at position 2 of the sense strand) known to reduce off-target effect [45].

Colony formation assay (CFA)

Seven-eight days after transfection, cells were fixed with formaldehyde 3.7% v/v solution at room temperature for 30 minutes, washed with PBS and stained for 20 minutes with a PBS solution containing 0.05% v/v Triton® X-100 (Sigma-Aldrich, St. Louis, MO, USA) and TO-PRO®-3 iodide (Invitrogen Life Technologies (Carlsbad, CA, USA) diluted 1:1000. After a second wash, 50 µl PBS were left in each well. Plates were sealed and analyzed with an Odyssey® infrared scanner (LI-COR Biosciences, Lincoln, NE, USA) which provides whole-well fluorescence quantification of cells stained with TO-PRO®-3 dye. The fluorescence intensity (FI) was considered as readout, which is proportional to both colony number and size.

Screening data analysis

FI values were registered in a proprietary Oracle database through Symyx Assay Explorer® and matched with the library information. The FI of each sample was divided by the average FI of the three non-targeting oligos within the same plate (set as 100%) for interplate normalization. TIBCO SpotFire (Boston, MA, USA) and Microsoft Excel (Redmond, WA, USA) were used for statistical analysis and visualization of screening data distributions. The means and standard deviations of FI (% siNT) values and z*-scores [46] were calculated from the two technical replicates for each cell line and reported in Table S1 (Excel file with screening results).

To identify genes whose RNAi-mediated inhibition affects the growth of BCPAP but not Nthy-ori 3–1 cells, a distance factor (*d*) expressed as:

$$d = \sqrt{(100 - \%\,\mathrm{NTO}_{Nthy-ori\,3-1})^2 + (\%\,\mathrm{NTO}_{BCPAP})^2}$$

was introduced. "*d*" represents the distance between the %NT value of any given siRNA oligo and the point of maximal lethality towards BCPAP without effects on Nthy-ori 3–1 (coordinate $\%\mathrm{NT}_{\text{Nthy-ori 3–1}} = 100$, $\%\mathrm{NT}_{\mathrm{BCPAP}} = 0$). Screening hits were selected among siRNA oligos with significantly low *d* values, whereas oligos either equally inactive on both cell lines, or equally lethal on both cell lines, or preferentially lethal on Nthy-ori 3–1, are excluded. Based on the distribution analysis of *d* scores, a -3σ threshold (corresponding to $d = 47.2$) in the primary screening, and a -2σ threshold (corresponding to $d = 49.8$) in the confirmation study, were applied to define hits.

Cell proliferation assay

Cells (500 cells/well) were reverse transfected in 96-well plate with 20 nM specific siRNAs using

the Lipofectamine RNAiMAX reagent, according to manufacturer's instruction. Ten days later, cell viability was assessed by CellTiter-Glo Luminescent Cell Viability Assay (Promega Corporation, Madison, USA), performed as recommended by the supplier. Luminescence signals were acquired using a microplate reader (TecanUltra, Tecan Trading AG, Switzerland).

For the trypan blue exclusion assay, BCPAP and 8505C (1×10^5), TPC-1 (6×10^4), WRO82–1, HTC/C3 and KAT-18 ($8 \times 10^{4)}$ cells were transfected the day later in 6-well plate with 20 nM of specific siRNAs using Lipofectamine RNAiMAX, according to manifacturer's instruction. At different days after transfection (4 days for TPC1, 8505C and HTC/C3 cells; 5 days for KAT-18 cells, 6 days for BCPAP cells, 7 days for WRO82–1 cells) the fraction of viable and dead cells was analyzed. For palbociclib experiments, cells (8000 cells/well) were seeded in black/clear bottom 96-well plates and, the following day, treated with increasing doses of the palbociclib (PD 0332991) inhibitor (Selleck Chemicals, Houston, TX, USA, cat. S2768). After 72 hours, cells were fixed with 3.7% paraformaldehyde solution for 30 minutes at RT, washed and stained with 1 mg/ml Hoechst 33342. The plates were analyzed with an ArrayScan VTI high-content screening reader (Thermo-Fisher Scientific, Pittsburgh, PA): at least 800 cells were acquired in each well with a 10X objective in one fluorescence channel (XF93 optical filter set). Cell nuclei were automatically recognized and counted in ten fields to estimate the cell number per well as proliferation readout. IC50 values were calculated by sigmoid curve fitting of experimental points.

Gene Ontology and gene expression analyses

The functional annotation analysis on the identified gene lists was performed by means of the Database for Annotation, Visualization and Integrated Discovery (DAVID) tool v6.7 (https://david.ncifcrf.gov/). Gene Ontology (GO) Biological Process (BP) and Molecular Function (MF) terms were used as annotation categories and medium classification stringency was set for the functional annotation clustering analysis. The annotation clusters with an Enrichment score (ES) >1.3 were selected and representative GO-terms were indicated for each significant cluster. To assess the interactions between the validated fifteen genes, network analysis was carried out using the Ingenuity Pathway Analysis Tool (Ingenuity® Systems, http://www.ingenuity.com). The Core Analysis function was used to compare genes pooled from literature and other molecules in IPA's database.

The thyroid TCGA data set, containing the molecular data on nearly 500 PTC, is the largest data collection so far available (https://tcgadata.nci.nih.gov/tcga/tcgaCancerDetails.jsp?diseaseType=THCA&diseaseName=Thyroid). Illumina HiSeq Level 3 data were downloaded from TCGA Data Portal and RSEM [47] gene normalized expression values of selected genes were derived for 58 PTC patients, in tumor and adjacent normal samples, respectively. The statistical significance of gene expression difference between PTC and normal groups was assessed using Wilcoxon test.

RNA extraction, RT-PCR and Real time PCR

RNA extraction and RT-PCR were performed as previously described [48], using the following primer: 5′-ATGAGAGGCCTGTGGAGCACT-3′ (forward), 5′-TCATGTGTCGACTTGCAGGAG-3′(reverse) for RGS3 fragment amplification; 5′-GCAGATCCTCAGATCAGTGAA-3′(forward), 5′-TATAATGGGATCTGCAGCGTG-3′ (reverse) for NUDT9; 5′-CGAGGTCTACCAGCTCGACAT-3′ (forward), reverse 5′-CACGTCCACGTTCTCCTTGGT-3′ (reverse) for RASD1; 5′-ATGTGGAGCGTCTGGGATGC-3′ (forward), 5′-GCTCAGGACAAAGGAGGACG-3′ (reverse) for OXTR [49].

For Real Time PCR analysis 20 ng of retrotranscribed RNA were amplified in PCR reactions carried out in triplicate on an ABI PRISM 7900 using TaqMan gene expression assays (Applied Biosystem, Foster City, CA). Hs00212698_m1 was used for COPZ2 expression; human HPRT1 (HPRT-Hs99999909_A1) was used as housekeeping gene for the normalization among samples. Data analysis was performed using the SDS (Sequence Detection System) 2.4 software.

Western blot analysis

Western blot analysis was performed as previously described [48], using the following antibodies: anti-Cyclin D1 (DCS-6: sc-20044, 1:500), anti-COPE, (E-20: sc-12104, 1:500), anti-PLA2G15 (LYPLA3, H-167: sc-135297, 1:500), anti-MAP4K5 (KHS, N-19: sc-6429, 1:1000), anti-COPZ1 (D-20: sc-13349, 1:750), anti-GAPDH (6C5, sc-3223: 1:2000) purchased from Santa Cruz, CA, USA; anti-MASTL (ab86387, 1:7000) from Abcam, Cambridge, UK; anti-β-actin (A2066, 1:5000) and anti-vinculin (V9131, 1:1000) from Sigma-Aldrich, St Louis, Mo, USA.

Immunofluorescence analysis

Cells growing on glass coverslips were transfected with 20 nM NT or MASTL siRNAs and, 48 hours later, fixed for 10 minutes with 4% paraformaldehyde (Sigma Aldrich, St Louis, Mo, USA). After permeabilization for 10 minutes with 1% BSA and 0.1% Triton X-100 in PBS, and incubation for 30 minutes with 1X blocking solution (2% BSA in PBS), cells were incubated with anti-β-tubulin (clone TUB 2.1: T4026, 1:400, Sigma Aldrich, St. Louis, MO, USA) or anti-histone H3 (phospho S10) (E173: ab32107, 1:1000, Abcam, Cambridge, UK) primary antibodies for 1 hour. After washing with PBS, cells were incubated with Alexa Fluor® 546 rabbit

(1:500, Invitrogen/Molecular Probes®) and Alexa Fluor 488® mouse (1:500, Invitrogen/Molecular Probes®) secondary antibodies for 1 hour. Slides were then prepared using ProLong Diamond Antifade mountant with DAPI (P36966, Molecular Probes®) and imaged with immunofluorescence microscopy (Eclipse E1000; Nikon Instruments, Inc. NY, USA).

ACKNOWLEDGMENTS AND FUNDING

This work was supported by Associazione Italiana per la Ricerca sul Cancro (AIRC, Grant number 11347 to A.G.) and by a Fondazione Umberto Veronesi Fellowship to M.C.A.

CONFLICTS OF INTEREST

The authors declare no conflict of interest.

REFERENCES

1. Chen AY, Jemal A, Ward EM. Increasing incidence of differentiated thyroid cancer in the United States, 1988–2005. Cancer. 2009; 115:3801–3807.
2. Sherman SI. Thyroid carcinoma. Lancet. 2003; 361:501–511.
3. Greco A, Borrello MG, Miranda C, Degl'Innocenti D, Pierotti MA. Molecular pathology of differentiated thyroid cancer. Q J Nucl Med Mol Imaging. 2009; 53:440–453.
4. The Cancer Gene Atlas Research Network. Integrated genomic characterization of papillary thyroid carcinoma. Cell. 2014; 159:676–690.
5. Anania MC, Sensi M, Radaelli E, Miranda C, Vizioli MG, Pagliardini S, Favini E, Cleris L, Supino R, Formelli F, Borrello MG, Pierotti MA, Greco A. TIMP3 regulates migration, invasion and *in vivo* tumorigenicity of thyroid tumor cells. Oncogene. 2011; 30:3011–3023.
6. Anania MC, Miranda C, Vizioli MG, Mazzoni M, Cleris L, Pagliardini S, Manenti G, Borrello MG, Pierotti MA, Greco A. S100A11 Overexpression Contributes to the Malignant Phenotype of Papillary Thyroid Carcinoma. J Clin Endocrinol Metab. 2013; 98:E1591–E1600.
7. Minna E, Romeo P, De Cecco L, Dugo M, Cassinelli G, Pilotti S, Degl'Innocenti D, Lanzi C, Casalini P, Pierotti MA, Greco A, Borrello MG. miR-199a-3p displays tumor suppressor functions in papillary thyroid carcinoma. Oncotarget. 2014; 5:2513–2528.
8. Lee JC, Gundara JS, Glover A, Serpell J, Sidhu SB. MicroRNA expression profiles in the management of papillary thyroid cancer. Oncologist. 2014; 19:1141–1147.
9. Licitra L, Locati LD, Greco A, Granata R, Bossi P. Multikinase inhibitors in thyroid cancer. Eur J Cancer. 2010; 46:1012–1018.
10. Haraldsdottir S, Shah MH. An update on clinical trials of targeted therapies in thyroid cancer. Curr Opin Oncol. 2014; 26:36–44.
11. Luo J, Solimini NL, Elledge SJ. Principles of cancer therapy: oncogene and non-oncogene addiction. Cell. 2009; 136:823–837.
12. Cowley GS, Weir BA, Vazquez F, Tamayo P, Scott JA, Rusin S, East-Seletsky A, Ali LD, Gerath WFJ, Pantel SE, Lizotte PH, Guozhi J, Hsiao J, et al. Parallel genome-scale loss of function screens in 216 cancer cell lines for the identification of context-specific genetic dependencies. Sci Data. 2014; 1:140045.
13. Petrocca F, Altschuler G, Tan SM, Mendillo ML, Yan H, Jerry DJ, Kung AL, Hide W, Ince TA, Lieberman J. A genome-wide siRNA screen identifies proteasome addiction as a vulnerability of basal-like triple-negative breast cancer cells. Cancer Cell. 2013; 24:182–196.
14. Tiedemann RE, Zhu YX, Schmidt J, Shi CX, Sereduk C, Yin H, Mousses S, Stewart AK. Identification of molecular vulnerabilities in human multiple myeloma cells by RNA interference lethality screening of the druggable genome. Cancer Res. 2012; 72:757–768.
15. Sethi G, Pathak HB, Zhang H, Zhou Y, Einarson MB, Vathipadiekal V, Gunewardena S, Birrer MJ, Godwin AK. An RNA interference lethality screen of the human druggable genome to identify molecular vulnerabilities in epithelial ovarian cancer. PLoS One. 2012; 7:e47086.
16. Sos ML, Levin RS, Gordan JD, Oses-Prieto JA, Webber JT, Salt M, Hann B, Burlingame AL, McCormick F, Bandyopadhyay S, Shokat KM. Oncogene mimicry as a mechanism of primary resistance to BRAF inhibitors. Cell Rep. 2014; 8:1037–1048.
17. Schlabach MR, Luo J, Solimini NL, Hu G, Xu Q, Li MZ, Zhao Z, Smogorzewska A, Sowa ME, Ang XL, Westbrook TF, Liang AC, Chang K, et al. Cancer proliferation gene discovery through functional genomics. Science. 2008; 319:620–624.
18. Murrow LM, Garimella SV, Jones TL, Caplen NJ, Lipkowitz S. Identification of WEE1 as a potential molecular target in cancer cells by RNAi screening of the human tyrosine kinome. Breast Cancer Res Treat. 2010; 122:347–357.
19. Fry DW, Harvey PJ, Keller PR, Elliott WL, Meade M, Trachet E, Albassam M, Zheng X, Leopold WR, Pryer NK, Toogood PL. Specific inhibition of cyclin-dependent kinase 4/6 by PD 0332991 and associated antitumor activity in human tumor xenografts. Mol Cancer Ther. 2004; 3:1427–1438.
20. Burgess A, Vigneron S, Brioudes E, Labbe JC, Lorca T, Castro A. Loss of human Greatwall results in G2 arrest and multiple mitotic defects due to deregulation of the cyclin B-Cdc2/PP2A balance. Proc Natl Acad Sci U S A. 2010; 107:12564–12569.
21. Shtutman M, Baig M, Levina E, Hurteau G, Lim CU, Broude E, Nikiforov M, Harkins TT, Carmack CS, Ding Y,

Wieland F, Buttyan R, Roninson IB. Tumor-specific silencing of COPZ2 gene encoding coatomer protein complex subunit zeta 2 renders tumor cells dependent on its paralogous gene COPZ1. Proc Natl Acad Sci U S A. 2011; 108:12449–12454.

22. Chakravarty D, Santos E, Ryder M, Knauf JA, Liao XH, West BL, Bollag G, Kolesnick R, Thin TH, Rosen N, Zanzonico P, Larson SM, Refetoff S, et al. Small-molecule MAPK inhibitors restore radioiodine incorporation in mouse thyroid cancers with conditional BRAF activation. J Clin Invest. 2011; 121:4700–4711.
23. Sadow PM, Priolo C, Nanni S, Karreth FA, Duquette M, Martinelli R, Husain A, Clohessy J, Kutzner H, Mentzel T, Carman CV, Farsetti A, Henske EP, et al. Role of BRAFV600E in the first preclinical model of multifocal infiltrating myopericytoma development and microenvironment. J Natl Cancer Inst. 2014; 106.
24. Nehs MA, Nagarkatti S, Nucera C, Hodin RA, Parangi S. Thyroidectomy with neoadjuvant PLX4720 extends survival and decreases tumor burden in an orthotopic mouse model of anaplastic thyroid cancer. Surgery. 2010; 148:1154–1162.
25. Schlabach MR, Luo J, Solimini NL, Hu G, Xu Q, Li MZ, Zhao Z, Smogorzewska A, Sowa ME, Ang XL, Westbrook TF, Liang AC, Chang K, et al. Cancer proliferation gene discovery through functional genomics. Science. 2008; 319:620–624.
26. Musgrove EA, Caldon CE, Barraclough J, Stone A, Sutherland RL. Cyclin D as a therapeutic target in cancer. Nat Rev Cancer. 2011; 11:558–572.
27. Shan J, Zhao W, Gu W. Suppression of cancer cell growth by promoting cyclin D1 degradation. Mol Cell. 2009; 36:469–476.
28. Seybt TP, Ramalingam P, Huang J, Looney SW, Reid MD. Cyclin D1 expression in benign and differentiated malignant tumors of the thyroid gland: diagnostic and biologic implications. Appl Immunohistochem Mol Morphol. 2012; 20:124–130.
29. Lee JJ, Au AY, Foukakis T, Barbaro M, Kiss N, Clifton-Bligh R, Staaf J, Borg A, Delbridge L, Robinson BG, Wallin G, Hoog A, Larsson C. Array-CGH identifies cyclin D1 and UBCH10 amplicons in anaplastic thyroid carcinoma. Endocr Relat Cancer. 2008; 15:801–815.
30. Khoo ML, Ezzat S, Freeman JL, Asa SL. Cyclin D1 protein expression predicts metastatic behavior in thyroid papillary microcarcinomas but is not associated with gene amplification. J Clin Endocrinol Metab. 2002; 87:1810–1813.
31. Cadoo KA, Gucalp A, Traina TA. Palbociclib: an evidence-based review of its potential in the treatment of breast cancer. Breast Cancer. Dove Med Press2014; 6:123–133.
32. Kishimoto T. Entry into mitosis: a solution to the decades-long enigma of MPF. Chromosoma. 2015.
33. Peng A, Yamamoto TM, Goldberg ML, Maller JL. A novel role for greatwall kinase in recovery from DNA damage. Cell Cycle. 2010; 9:4364–4369.
34. Nagel R, Stigter-van Walsum M, Buijze M, van den Berg J, van der Meulen I H, Hodzic J, Piersma SR, Pham TV, Jimenez CR, van B V, Brakenhoff RH. Genome-wide siRNA screen identifies the radiosensitizing effect of downregulation of MASTL and FOXM1 in NSCLC. Mol Cancer Ther. 2015; 14:1434–1444.
35. Wang L, Luong VQ, Giannini PJ, Peng A. Mastl kinase, a promising therapeutic target, promotes cancer recurrence. Oncotarget. 2014; 5:11479–11489.
36. Russo MA, Kang KS, Di Cristofano A. The PLK1 inhibitor GSK461364A is effective in poorly differentiated and anaplastic thyroid carcinoma cells, independent of the nature of their driver mutations. Thyroid. 2013; 23:1284–1293.
37. Baldini E, Tuccilli C, Prinzi N, Sorrenti S, Antonelli A, Gnessi L, Morrone S, Moretti C, Bononi M, Arlot-Bonnemains Y, D'Armiento M, Ulisse S. Effects of selective inhibitors of Aurora kinases on anaplastic thyroid carcinoma cell lines. Endocr Relat Cancer. 2014; 21:797–811.
38. Beck R, Rawet M, Wieland FT, Cassel D. The COPI system: molecular mechanisms and function. FEBS Lett. 2009; 583:2701–2709.
39. Razi M, Chan EY, Tooze SA. Early endosomes and endosomal coatomer are required for autophagy. J Cell Biol. 2009; 185:305–321.
40. Beller M, Sztalryd C, Southall N, Bell M, Jackle H, Auld DS, Oliver B. COPI complex is a regulator of lipid homeostasis. PLoS Biol. 2008; 6:e292.
41. Schweppe RE, Klopper JP, Korch C, Pugazhenthi U, Benezra M, Knauf JA, Fagin JA, Marlow LA, Copland JA, Smallridge RC, Haugen BR. Deoxyribonucleic acid profiling analysis of 40 human thyroid cancer cell lines reveals cross-contamination resulting in cell line redundancy and misidentification. J Clin Endocrinol Metab. 2008; 93:4331–4341.
42. Zhao M, Sano D, Pickering CR, Jasser SA, Henderson YC, Clayman GL, Sturgis EM, Ow TJ, Lotan R, Carey TE, Sacks PG, Grandis JR, Sidransky D, et al. Assembly and initial characterization of a panel of 85 genomically validated cell lines from diverse head and neck tumor sites. Clin Cancer Res. 2011; 17:7248–7264.
43. Xu X, Ding H, Rao G, Arora S, Saclarides CP, Esparaz J, Gattuso P, Solorzano CC, Prinz RA. Activation of the Sonic Hedgehog pathway in thyroid neoplasms and its potential role in tumor cell proliferation. Endocr Relat Cancer. 2012; 19:167–179.
44. Lundholt BK, Scudder KM, Pagliaro L. A simple technique for reducing edge effect in cell-based assays. J Biomol Screen. 2003; 8:566–570.
45. Jackson AL, Burchard J, Leake D, Reynolds A, Schelter J, Guo J, Johnson JM, Lim L, Karpilow J, Nichols K, Marshall W, Khvorova A, Linsley PS. Position-specific chemical modification of siRNAs reduces "off-target" transcript silencing. RNA. 2006; 12:1197–1205.

46. Chung N, Zhang XD, Kreamer A, Locco L, Kuan PF, Bartz S, Linsley PS, Ferrer M, Strulovici B. Median absolute deviation to improve hit selection for genome-scale RNAi screens. J Biomol Screen. 2008; 13:149–158.

47. Li B, Dewey CN. RSEM: accurate transcript quantification from RNA-Seq data with or without a reference genome. BMC Bioinformatics. 2011; 12:323.

48. Vizioli MG, Sensi M, Miranda C, Cleris L, Formelli F, Anania MC, Pierotti MA, Greco A. IGFBP7: an oncosuppressor gene in thyroid carcinogenesis. Oncogene. 2010; 29:3835–3844.

49. Kanamori C, Yasuda K, Sumi G, Kimura Y, Tsuzuki T, Cho H, Okada H, Kanzaki H. Effect of cigarette smoking on mRNA and protein levels of oxytocin receptor and on contractile sensitivity of uterine myometrium to oxytocin in pregnant women. Eur J Obstet Gynecol Reprod Biol. 2014; 178:142–147.

SUPPLEMENTARY FIGURES AND TABLES

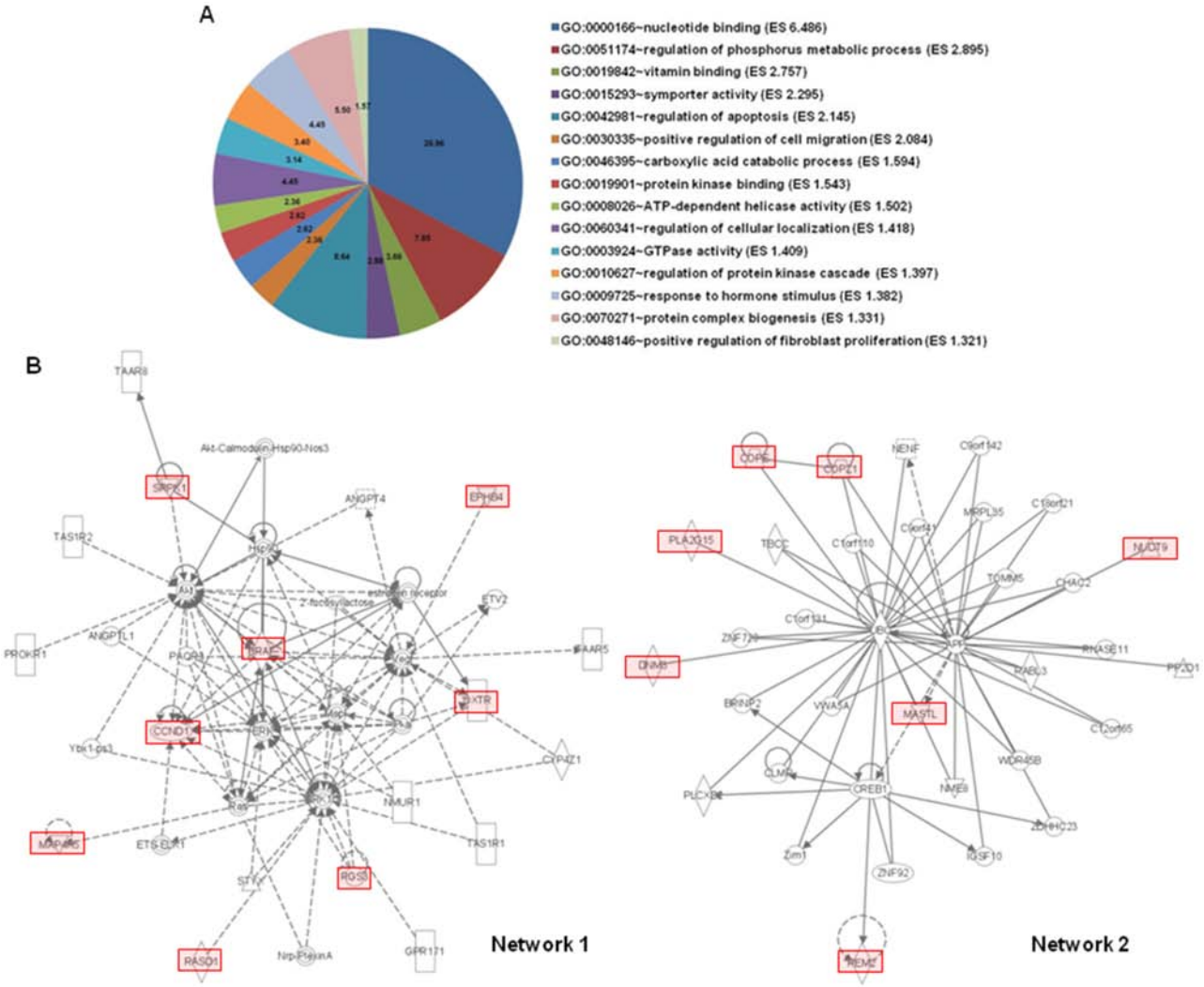

Supplementary Figure S1: A. Pie chart of functional annotation clustering analysis on 386 genes by DAVID 6.7 tool. Only 15 annotation clusters with an Enrichment Score (ES) > 1.3 are reported. A representative Biological Process (BP) or Molecular Function (MF) GO-term and the percentage of the genes on the 382 DAVID IDs globally identified are indicated for each significant annotation cluster; for each selected cluster the ES is also indicated. **B.** Visual representation of the two principal networks generated by Ingenuity Pathway Analysis (IPA) including the fifteen validated hits. Solid lines represent a direct interaction between the two gene products and dotted lines mean an indirect interaction.

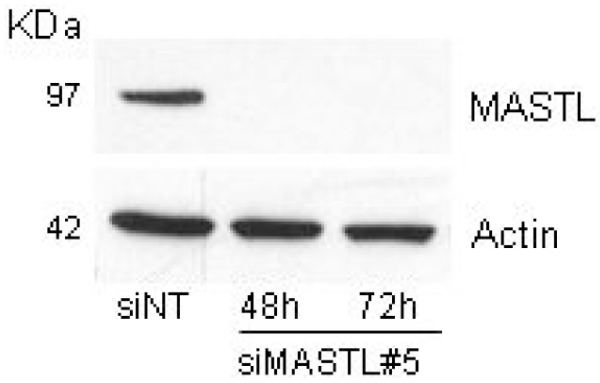

Supplementary Figure S2: western blot analysis of MASTL protein expression in Nthy-ori 3–1 cells, transiently transfected with MASTL#5 siRNA; actin was used as loading control.

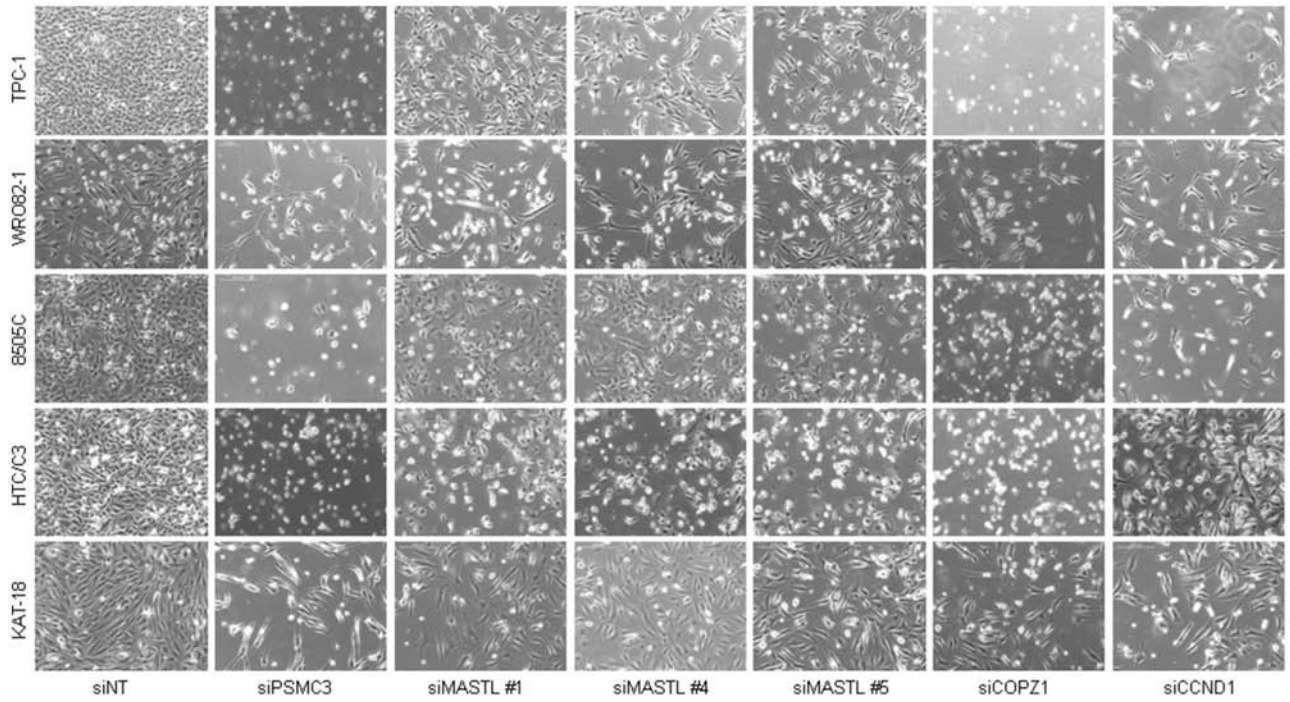

Supplementary Figure S3: representative pictures at 10X magnification of TPC-1, WRO82–1, 8505C, HTC/C3 and KAT-18 cells, taken before the trypan blue exclusion assay

Supplementary Table S1: List of 25139 siRNA oligonucleotides of the human Silencer Select Druggable Genome siRNA Library V4 (Ambion Life Technologies, Carlsbad, CA, USA) and screening results. Average and standard deviation (StDev) of the fluorescence intensity (FI) normalized on siNT (%NT), and average and standard deviation (StDev) of z* scores for BCPAP and Nthy-ori 3–1, distance factor (*d*) and binned *d* (based on σ distribution) are shown. The gene symbols, full gene names, Refseq (http://www.ncbi.nlm.nih.gov/refseq/about/) accession numbers, siRNA batches and their corresponding plate blocks were provided by Ambion.

Supplementary Table S2: List of 398 siRNA oligonucleotides resulted to preferentially inhibit the proliferation of BCPAP cells with respect to Nthy-ori 3–1 ($d < -3\sigma$) and thus defined as "differential hits".

Supplementary Table S3: List of 1695 siRNA oligonucleotides resulted to inhibit the proliferation of both BCPAP and Nthy-ori 3–1 (signal intensity < 20% siNT), therefore defined as "lethal hits".

Supplementary Table S4: siRNA oligos.

siRNA	Sequence/catalog number	Source	Used in
siNT	5′-UGGUUUACAUGUCGACUAAtt-3′	in house	transfection setup, screening, confirmation
siPSMC3	5′-CGGCUGAAGUGCGCAAUAAtt-3′	in house	transfection setup screening, confirmation
siNT	ON-TARGET plus Non-targeting Pool siRNA D-0018–10–05	ThermoScientific, Dharmacon Inc., Chicago, IL, USA	validation
siPSMC3	MISSION esiRNA EHU107331	Sigma-Aldrich, St. Louis, MO, USA	validation
siMASTL #1	ON-TARGET plus set of 4 siRNAs J-004020–12	ThermoScientific, Dharmacon Inc., Chicago, IL, USA	validation
siMASTL #2	ON-TARGET plus set of 4 siRNAs J-004020–11	ThermoScientific, Dharmacon Inc., Chicago, IL, USA	validation
siMASTL #3	ON-TARGET plus set of 4 siRNAs J-004020–10	ThermoScientific, Dharmacon Inc., Chicago, IL, USA	validation
siMASTL #4	ON-TARGET plus set of 4 siRNAs J-004020–09	ThermoScientific, Dharmacon Inc., Chicago, IL, USA	validation
siMASTL#5	5′-UGUGGAUUCUGGUGGGAUAdTdT 3′	in house	validation
siCCND1	MISSION esiRNA EHU153321	Sigma-Aldrich, St. Louis, MO, USA	validation
siCOPZ1	MISSION esiRNA EHU1040461	Sigma-Aldrich, St. Louis, MO, USA	validation

List of siRNA oligos used in the transfection setup, as control in the screening, or in confirmation and validation studies

Appendix B

Accepted Manuscript

Targeting COPZ1 non-oncogene addiction counteracts the viability of thyroid tumor cells

Chiara Anania Maria, Elena Cetti, Daniele Lecis, Katia Todoerti, Alessandro Gulino, Giuseppe Mauro, Tiziana Di Marco, Loredana Cleris, Sonia Pagliardini, Giacomo Manenti, Beatrice Belmonte, Claudio Tripodo, Antonino Neri, Angela Greco

PII: S0304-3835(17)30577-3

DOI: 10.1016/j.canlet.2017.09.024

Reference: CAN 13512

To appear in: *Cancer Letters*

Received Date: 11 July 2017

Revised Date: 15 September 2017

Accepted Date: 16 September 2017

Please cite this article as: C. Anania Maria, E. Cetti, D. Lecis, K. Todoerti, A. Gulino, G. Mauro, T. Di Marco, L. Cleris, S. Pagliardini, G. Manenti, B. Belmonte, C. Tripodo, A. Neri, A. Greco, Targeting COPZ1 non-oncogene addiction counteracts the viability of thyroid tumor cells, *Cancer Letters* (2017), doi: 10.1016/j.canlet.2017.09.024.

Targeting COPZ1 non-oncogene addiction counteracts the viability of thyroid tumor cells

Anania Maria Chiara[a], Cetti Elena[a], Lecis Daniele[a], Todoerti Katia[b], Gulino Alessandro[c], Mauro Giuseppe[a], Di Marco Tiziana[a], Cleris Loredana[a], Pagliardini Sonia[a], Manenti Giacomo[d], Belmonte Beatrice[c], Tripodo Claudio[c], Neri Antonino[e,f] and Greco Angela[a§]

[a]Department of Experimental Oncology and Molecular Medicine, Fondazione IRCCS Istituto Nazionale dei Tumori, Milan, Italy; [b]Laboratory of Pre-Clinical and Translational Research, IRCCS-CROB, Referral Cancer Center of Basilicata, Rionero in Vulture, Italy; [c]Department of Health Science, Human Pathology Section, University of Palermo School of Medicine, Palermo, Italy; [d]Department of Predictive and Preventive Medicine, Fondazione IRCCS Istituto Nazionale dei Tumori, Milan, Italy, [e]Department of Oncology and Hemato-oncology, University of Milan, Milan, Italy; [f]Hematology Unit, Fondazione IRCCS Ca' Granda, Ospedale Maggiore Policlinico, Milan, Italy;

[§]Corresponding author: Angela Greco, Fondazione IRCCS Istituto Nazionale dei Tumori, Via G.A. Amadeo, 42, 20133 Milan, Italy. Tel. 0039 02 2390 3222 Fax 0039 02 23903073 e-mail: angela.greco@istitutotumori.mi.it;

Running title: Targeting COPZ1 in thyroid tumors

Supported by: Associazione Italiana per la Ricerca sul Cancro (AIRC) [Grant IG 11347, 2012; IG 18395, 2017] to A.Greco and by a Fondazione Umberto Veronesi Fellowship to M.C. Anania.

Abstract

Thyroid carcinoma is generally associated with good prognosis, but no effective treatments are currently available for aggressive forms not cured by standard therapy. To find novel therapeutic targets for this tumor type, we had previously performed a siRNA-based functional screening to identify genes essential for sustaining the oncogenic phenotype of thyroid tumor cells, but not required to the same extent for the viability of normal cells (non-oncogene addiction paradigm). Among those, we found the coatomer protein complex ζ1 (COPZ1) gene, which is involved in intracellular traffic, autophagy and lipid homeostasis. In this paper, we investigated the mechanisms through which COPZ1 depletion leads to thyroid tumor cell death. We showed that siRNA-mediated COPZ1 depletion causes abortive autophagy, endoplasmic reticulum stress, unfolded protein response and apoptosis. Interestingly, we observed that mouse tumor xenografts, locally treated with siRNA targeting COPZ1, showed a significant reduction of tumor growth.

On the whole, we demonstrated for the first time the crucial role of COPZ1 in the viability of thyroid tumor cells, suggesting that it may be considered an attractive target for novel therapeutic approaches for thyroid cancer.

Keywords: *thyroid carcinoma, COPZ1, non-oncogene addiction, cell death*

1. Introduction

Cancer cells often depend on non mutated genes and pathways to support their unchecked growth. The activity of these genes is essential for tumor cells, but not required to the same extent by normal cells; this concept is known as "non-oncogene addiction" (NOA) paradigm [1]. NOA genes represent tumor vulnerabilities and their inhibition results in the failure of the oncogenic phenotype. Nowadays, large-scale siRNA-based functional screening of cancer cell lines represent a powerful strategy for the identification of NOA genes that can be investigated as therapeutic targets for many types of tumors [2].We used this approach to unveil nodal points for therapeutic intervention for thyroid carcinoma (TC), which represents the most frequent endocrine cancer, with a rapidly increasing incidence [3].

The majority of TC originates from epithelial cells and includes well-differentiated papillary (PTC) and follicular (FTC) carcinomas, poorly differentiated (PDTC) and undifferentiated anaplastic carcinomas (ATC). Most TC are effectively treated by standard therapy, involving surgery, thyroid stimulating hormone and radioiodine. Nevertheless, a fraction of patients cannot be cured due to local recurrence (in up to 20% of patients), distant metastasis (in approximately 10% at 10 years [4]) and/or radioresistant disease. Furthermore, patients with PDTC and ATC have a very poor prognosis, with survival of few months in the case of ATC [5;6]. Even though recent molecular findings allowed the development of several therapies designed to specifically target thyroid oncoproteins or their downstream pathways, this strategy showed modest results and only partial response [7;8]. Few or no therapeutic options are currently available for patients with aggressive and iodine-refractory thyroid tumors. Thus, there is a need to better understand the mechanisms of thyroid carcinogenesis and to improve the treatment of the most aggressive tumor forms not curable by standard therapy.

We have recently discovered several thyroid tumor cell vulnerabilities. By screening a siRNA library, we identified a set of genes whose silencing inhibited the growth of a panel of thyroid tumor cells, but not of normal immortalized thyrocytes. The COPZ1 gene was found among the top ranked

genes [9]. COPZ1 (coatomer protein complex ζ1) belongs to the coatomer protein complex I (COPI), an heptameric complex which is involved in: assembly of coated vesicles on Golgi membranes, retrograde transport of luminal and membrane proteins in the ER-Golgi secretory pathway, endosome maturation, autophagy [10;11] and lipid homeostasis [12]. It has been demonstrated that COPZ1 knockdown causes cell death in both proliferating and nondividing tumor cells. Unlike tumor cells, normal cells are not sensitive to COPZ1 inhibition [13]. We identified COPZ1 as a thyroid tumor cell specific survival gene, as its inhibition induced cell death in tumor cell lines but not in immortalized thyrocytes. This evidence, together with a not significant variation of expression and absence of mutations in PTC, allowed us to classify COPZ1 as an example of "non-oncogene addiction" for thyroid cancer cells [9].

Here we investigated the mechanisms through which COPZ1 depletion leads to thyroid tumor cell death and explored its potential use as therapeutic target for thyroid carcinoma. We found that cell death induced by COPZ1 depletion is associated with abortive autophagy, ER stress, UPR and apoptosis. Interestingly, local treatment with siCOPZ1 oligos reduced tumor growth in an *in vivo* model of thyroid carcinogenesis.

2. Materials and Methods

2.1 Cell lines

Thyroid tumor cell lines, primary thyrocytes and mammary epithelial h-TERT-HME1 cells were cultured as previously described [9;14;15]. Source and culture conditions are reported in Supplementary. GFP-LC3 stable cell lines were generated by transfecting 2μg of pEGFP-LC3 plasmid (from Tamotsu Yoshimori's laboratory [16], using the Lipofectamine 3000 reagent (Invitrogen Life Technologies, Carlsbad, CA, USA) for TPC-1, and Lipofectamine LTX (Invitrogen Life Technologies) for 8505C cells, according to manufacturer's instruction. Transfected cells were selected and propagated in medium containing G418 (500μg/ml, Invitrogen Life Technologies).

2.2 Detection of LC3 puncta

Cells growing on glass coverslips were transfected as described below and 24h, 48h, 72h later fixed for 20 minutes with 4% paraformaldehyde. After washing with PBS, cells were treated with the ProLong Diamond Antifade mountant with DAPI (P36966, Molecular Probes, Invitrogen Life Technologies) and imaged with immunofluorescence microscopy (Eclipse E1000; Nikon Instruments, Inc. NY, USA). The percentage was calculated as the ratio between cells displaying LC3 puncta and total cells (at least 150), considering six randomly selected 60X fields.

2.3 siRNA reagents and transfection

siRNA transfection was performed using 20 nM of siRNA oligos (see list in Supplementary) and the Lipofectamine RNAiMAX reagent (Invitrogen Life Technologies), according to manufacturer's instruction.

2.4 Colony formation assay

Cells were plated in 100 mm dishes and transfected the following day with 20 nM of siRNAs. One day later, cells were collected and plated as follows: $2x10^4$ cells in 24 well-plates for colony

formation assay; $1.5x10^5$ cells in 60 mm dishes for western blot analysis. For the colony formation assay, cells were fixed five days later with formaldehyde 3.7% v/v solution for 30 minutes, washed with PBS and stained for 20 minutes with 0.1% crystal violet (w/v). Pictures were taken using an Epson image scanner.

2.5 Western blot analysis

WB analysis was performed as previously described [17]. The list of antibodies is provided in Supplementary.

2.6 RNA extraction and Real time PCR

RNA extraction and Real time PCR were performed as previously described [17]. The following TaqMan gene expression assays (Applied Biosystem, Foster City, CA) were used: Hs01023197_m1 for COPZ1 and Hs00358796_g1 for CHOP expression; Hs02800695_m1 for HPRT1, used as housekeeping gene for normalization among samples.

2.7 Apoptosis assay

Cells were transfected with 20 nM of siRNA oligos in the presence of 2 µM of the fluorogenic substrate for activated caspase-3/7 (CellEvent™ Caspase-3/7 Green Detection Reagent, Invitrogen Life Technologies). Live-cell fluorescence images were taken 72h later with microscope (Eclipse TE2000-S; Nikon Instruments).

2.8 In vivo studies

Female CD-1 nu/nu mice (5-weeks old) (Charles River, Calco, Italy) were injected subcutaneously into the left flank with 8505C cells ($10x10^6$). When xenograft tumors reached the mean volume of 0.085 mm^3 (range 0.040-0.144), they were randomly divided into three groups and then locally treated with 20 µg of siCOPZ1 oligos (4457308, Ambion® ID s22427) or non-targeting oligos

(4457289, Ambion® *In Vivo* Negative Control #1 siRNA) mixed in 50 µl of MaxSuppressor™ In Vivo RNA-LANCEr II reagent (Bioo Scientific, Austin, TX, USA), or with MaxSuppressor™ only. Treatments were carried out at day 17, 20, 23, 27, 30 after cell injections. Tumor growth was followed for 34 days and assessed by monitoring tumour weight (TW), as previously described [18]. Animal studies were reviewed and approved by the Ethics Committee for Animal Experimentation of the hosting institution and are in accordance with the guidelines of the UK Coordinating Committee for Cancer Research [19].

2.9 Immunohistochemistry

Serial sections from paraffin-embedded tumor xenografts (2-µm thick) were stained with hematoxylin and eosin and evaluated under a light microscope to assess the pattern of tumor growth. Antigen retrieval was performed using 1 mM citrate buffer (pH 6), then sections were immunostained with a primary rat polyclonal antibody anti-human COPZ1 (1:400 SAB4500896 Sigma-Aldrich St Louis, Mo, USA), anti-human Ki-67 (Mib1) (1:200 M7240 Dako, Agilent Technologies, CA, USA). Immunostains were performed using standard immunoperoxidase protocol followed by diaminobenzidine chromogen reaction (Dako REAL™ EnVision™ Detection System, K5007 Dako). The intensity of staining for COPZ1 was scored as low (1+), medium (2+) or high (3+). The percentage of cells immunostained for Ki67 and necrotic cells was estimated counting one 10X field, randomly selected. One sample of each group of tumor explants was excluded from the IHC analysis due to technical problems.

2.10 Gene/miRNA expression analysis

Gene expression data of *COPZ2* gene (log scale) from 58 normal-thyroid tissue samples compared to 31 ATC, 72 PTC and 17 PDTC samples, were obtained combining GSE3467 [20], GSE6004 [21], GSE33630 [22;23] and GSE76039 [24] publicly available datasets. Raw intensity expression values on U133 Plus 2.0 array (Affymetrix, Santa Clara, CA) were processed by Robust Multi-array

Average procedure [25], with the re-annotated Chip Definition Files from BrainArray libraries version 20.0.0 [26], available at http://brainarray.mbni.med.umich.edu. Batch effects were removed by using sva R/Bioconductor package [27]. The analysis of the thyroid TCGA dataset from 58 paired normal/PTC samples was performed as previously described [9]. Normalized reads per million miRNA mapped (RPM) data were obtained for the same 58 tumor samples from Illumina HiSeq Level 3 isoform quantification files (TCGA Data Portal website), by summing up the reads aligned to each 3p or 5p miRBase v16 mature strands [28;29]. Pearson's correlation method was applied to evaluate the correlation between RNAseq normalized gene and miRNA read counts (log scale) in 58 tumor samples.

3. Results

3.1 COPZ1 depletion affects thyroid tumor cell viability

The issue that COPZ1 represents vulnerability for thyroid tumor cell lines but not for normal thyrocytes [9] is further documented by the colony forming assay in Figure 1A. Upon transfection of siRNA oligos targeting COPZ1 (siCOPZ1), a drastic growth inhibition was observed in thyroid tumor cell lines (PTC-derived: BCPAP and TPC-1; FTC-derived: WRO82-1; ATC-derived: 8505C, KAT-18, and HTC/C3) in comparison to non-targeting (siNT) transfected cells, and to COPZ1-depleted Nthy-ori 3-1 cells, normal immortalized thyrocytes. Western blot (WB) analysis performed in parallel documented the efficient COPZ1 silencing in all the cell lines (bottom panel). SiRNA transfected TPC-1, 8505C, HTC/C3, and Nthy-ori 3-1 cell lines were also analyzed by time-lapse phase-contrast video microscopy (Supplementary Videos). Unlike siNT-transfected cells, COPZ1-depleted tumor cells showed morphological changes, such as shrinking and rounding up 30 hours (h) (for TPC-1 cells) and 48h (for 8505C and HTC/C3 cells) after silencing Then, cells detached from dishes and reached massive cell death at the end of the experiment (68h for TPC-1 cells, 89h for 8505C and HTC/C3 cells). None of these effects was observed in COPZ1-depleted NThy-ori 3-1 cells, which proliferated as the control (siNT) and reached confluence at the end of the experiment (68h). In Figure 1B, representative images of each cell lines at the end of experiment are reported.

Further images documenting cell morphological changes after COPZ1 depletion are shown in Supplementary Figure S1. We also showed the lack of effect of COPZ1 silencing on primary human thyrocytes and human mammary epithelial HME-1 (Figure 1C): COPZ1 depletion leaves unaffected the growth of these non malignant cells, similarly to the negative control siNT; on the contrary, a massive cell death was observed in cells transfected with siRNA oligos targeting Ubiquitin B (siUBB), used as control. WB analysis 72h after siRNA transfection documented the complete abrogation of COPZ1 protein expression.

3.2 COPZ1 depletion affects autophagy

COPI complex members are involved in autophagy [11] and are required for completion of the autophagic process. Moreover, the depletion of COPI members impairs productive autophagy, as demonstrated in prostate, breast and ovarian carcinoma cells [13;30]. TPC-1 and 8505C cell lines, stably expressing the autophagosome marker GFP-LC3 (hereafter referred as TPC1-GL3 and 8505-GL3) were transfected with siCOPZ1 and siNT oligos, and analyzed at different time points by fluorescence microscopy for the presence of the typical autophagy-associated LC3 puncta (Figure 2A). The number of siNT-transfected cells displaying LC3 puncta remained low over the time. On the contrary, the number of COPZ1-depleted cells presenting puncta significantly increased over the time. In TPC1-GL3 cells puncta were detected in 5.7% and 38% at 24h and 48h, respectively; the analysis at 72h was not feasible, as cells detached from glass coverslip due to the lethal effect of COPZ1 silencing. In 8505-GL3 cells, puncta were present in 6%, 14% and 34%, at 24h, 48h and 72h, respectively. In Figure 2B, representative images of COPZ1-depleted cells displaying LC3 puncta and relative controls are shown. Autophagosome formation upon COPZ1 silencing was also demonstrated by assessing the conversion of the endogenous LC3-I to LC3-II by WB. Accumulation of LC3-II protein was observed in COPZ1-depleted naive TPC-1 and 8505C cells. In both cell lines, the endogenous LC3-II was barely detectable at 48 h and progressively increased at the latest time points (Figure 2C). Since an increased steady-state expression of LC3-II could

suggest persistent accumulation of autophagosomes, impaired recycling and consequently block of the autophagic flux, we investigated whether COPZ1 depletion causes abortive autophagy. We monitored by WB whether LC3-II accumulation was associated with increased expression of SQSTM1/p62, an LC3-binding protein mainly degraded through autophagy catabolism and whose increase is a marker of abortive autophagy [31]. We observed an increase of SQSTM1/p62 in both COPZ1-depleted cell lines in comparison to controls (Figure 2D). Such increase was 1.4 and 1.6 fold in TPC-1 cells at 72h and 96h, and 2.9 and 2.5 fold in 8505C cells. The persistent accumulation, rather than turnover/degradation of autophagosomes, and the concomitant increase of SQSTM1/p62 protein expression suggest that COPZ1 depletion is associated with abortive autophagy.

3.3 COPZ1 depletion induces endoplasmic reticulum stress and unfolded protein response

As COPZ1 regulates vesicular transport, its depletion could be associated with protein accumulation in the endoplasmic reticulum (ER) and with a deficit in proteins coming back from the Golgi. Since these effects could be linked to the activation of ER stress and of unfolded protein response (UPR), we investigated the expression of some components of these pathways. COPZ1-depleted TPC-1 and 8505C cells showed an increased expression of the chaperone GRP78/BiP, which, upon ER stress, is the major responsible for the activation of downstream UPR signals [32;33]. In TPC-1 cells, the level of GRP78/BiP increases by 1.5, 2.8 and 11 fold at 48h, 72h and 96h after siRNA transfection, respectively, in comparison to the control; whereas, in 8505C cells the increase was by 1.8, 3.9 and 3.2 fold (Figure 3A). Concomitantly, we observed an increase of another marker of ER stress, the ER lumen chaperone calnexin (1.2 at 48h and 1.6 from 72h fold increase in TPC-1; 1.4 and 2.8 fold increase in 8505C cells) (Figure 3A). CHOP, also known as GADD153, is transcriptionally upregulated during ER stress and UPR [34;35]. We analyzed the expression of CHOP and COPZ1 by Real Time PCR in TPC-1 and 8505C cells at different time points after COPZ1 silencing. As shown in Figure 3B, COPZ1 depletion led to a drastic increase of CHOP expression in comparison

to the control. In conclusion, our data indicate that COPZ1 depletion causes the onset of ER stress and UPR.

3.4 COPZ1 depletion induces apoptotic cell death

Prolonged ER stress or failure of adaptive response can result in cell death [36]. Moreover, CHOP activation triggers apoptotic death [34;35]. TPC-1 and 8505C cells were transfected with siCOPZ1 or siNT oligos in the presence of the fluorescent substrate for activated caspase-3/7. Live-cell fluorescence microscopy performed 72h after transfection showed a significant increase of Caspase-3/7 activity in COPZ1-depleted cells in comparison to the siNT control (Figure 4A). The induction of apoptosis by siCOPZ1 is also documented by the WB analysis in Figure 4B: COPZ1 depletion increases cleaved PARP and cleaved caspase-3 levels, which were detectable at 48h and 72h after siRNA transfection in TPC-1 and 8505C cells, respectively. Overall, these results suggest that the depletion of COPZ1 induces caspase-dependent apoptosis in thyroid tumor cells.

3.5 In vivo effects of COPZ1 depletion

We used 8505C cell mouse xenografts as *in vivo* model of thyroid carcinogenesis and, in a preliminary experiment, we tested the *in vivo* efficacy of siRNA targeting COPZ1. Nude mice were xenografted with 8505C cells and then locally treated with siCOPZ1, explanted and analyzed by WB three days later. As shown in Figure 5A, a consistent reduction (by 40%) of COPZ1 protein in siCOPZ1-treated tumor in comparison to vehicle- or siNT- treated control was observed. The expression of COPZ1 protein in tumor explants was also analyzed by immunohistochemistry (IHC). The intensity of staining for COPZ1 in siCOPZ1 explant was reduced in comparison to siNT explant: score 1+ vs 3+. This was associated with a reduction of the rate of proliferating cells, determined by Ki67 staining: 15% in siCOPZ1 explant vs 50% in siNT explant (Figure 5B). After proving the efficacy of siCOPZ1 in an *in vivo* setting, we evaluated the effect of COPZ1 silencing on *in vivo* tumor growth. Nude mice were xenografted with 8505C cells and, at day 17 after, they

were locally treated twice a week with siCOPZ1, or with siNT, or with the vehicle only. At day 34, tumors were excised and weighted. As shown in Figure 5C, treatment with siCOPZ1 significantly reduced tumor growth compared to siNT or vehicle treatments (controls). Then, tumor explants were analyzed by IHC for the expression of COPZ1 protein. COPZ1 immunostaining was high in two siNT samples and ranged from medium to high in two other samples. Conversely, in COPZ1-depleted explants it was very low (two samples), low with medium areas (two samples) or medium (one sample). In line with this, the mean rate of proliferating cells (Ki67) was 53.7% for siNT and 31% for siCOPZ1 explants. Concomitantly, when we evaluated the neoplastic cellularity, we observed an increase of necrosis (20%) in siCOPZ1 explants in comparison with the controls (11.2%) (Figure 5D). Representative pictures of selected explants are shown in Figure 5E: the siNT-9 sample showed high COPZ1 and Ki67 (50%) expression and low necrotic cells (5%), whereas the siCOPZ1-19 sample displayed an opposite state, being the COPZ1 staining low, Ki67 20% and necrotic cells 25%. Overall, our results demonstrated that the local treatment with siCOPZ1 productively reduced tumor growth in our model of thyroid carcinoma in nude mice.

3.6 COPZ2 is downregulated in thyroid cancers

COPZ1 vulnerability is related to downregulation of the paralogous *COPZ2* gene in tumor cells. While normal cells tolerate COPZ1 inhibition because COPZ2 can replaces its activity in the COPI complex, the absence of COPZ2 in tumor cells confers sensitivity to COPZ1 depletion. Interestingly, *COPZ2* was found downregulated in several primary tumors compared to their normal counterparts [13]. We have previously provided evidence that dependence of thyroid tumor cell lines on COPZ1 may result from downregulation of *COPZ2*, since *COPZ2* mRNA expression is downregulated in the majority of analyzed thyroid tumor cell lines [9]. In order to assess whether also thyroid tumors belonging to different histotypes may be sensitive to COPZ1 targeting, we interrogated several publicly available datasets for the expression status of *COPZ2*. The first analysis combined data from different datasets, including 58 normal thyroid, 72 PTC, 17 PDTC and

31 ATC samples [20-24]: *COPZ2* was found downregulated in all the tumor histotypes (Figure 6A). Furthermore, COPZ2 gene was significantly downregulated in the 58 PTC samples from the thyroid TCGA dataset [28], compared to the paired normal counterpart (Figure 6B, left). Therefore, the frequent downregulation of COPZ2 in thyroid tumors allow predicting their sensitivity to COPZ1 inhibition.

The first intron of the *COPZ2* gene encodes the precursor of miR-152 [37], which exerts a tumor suppressor role and is frequently downregulated in several tumors. miR-152 and its hosting gene *COPZ2* are transcribed from the same promoter and are concurrently silenced in tumor cells [13]. To assess mirR-152 expression in thyroid tumors, data were retrieved from TCGA and correlated with *COPZ2* expression. The analysis shows a notable positive correlation between *COPZ2* and hsa-miR-152 RNAseq expression levels (Figure 6B, right). This result indicates that miR-152, concurrently to *COPZ2*, is downregulated in thyroid cancer, and it may exert an oncosuppressor role also in this tumor type.

4. Discussion

By performing a siRNA-based functional screening, we have recently discovered several thyroid tumor cell vulnerabilities, consisting in a set of genes, defined non-oncogenes, whose silencing inhibited the growth of a panel of thyroid tumor cells, but not that of normal immortalized thyrocytes. The COPZ1 gene was found among the top significant genes, exerting a role in sustaining the phenotype of thyroid tumor cells. In this study, we dissected the mechanisms leading to cell lethality upon COPZ1 depletion, and explored its employability as therapeutic target for thyroid carcinoma.

First, we confirmed that COPZ1 represents vulnerability for several thyroid tumor cell lines since its silencing drastically impairs their viability, and demonstrated the lack of effect also in normal primary thyrocytes, and mammary epithelial cells.

Our study, aimed at better characterizing the mechanisms leading to cell death upon COPZ1 depletion, showed that, similarly to other members of the coatomer complex [11;30], COPZ1 was a

critical player of autophagy. Indeed, COPZ1 silencing initiated autophagy, which became abortive due to an increase rather than a turnover of autophagosomes. Concomitantly, COPZ1-depleted cells displayed the activation of markers of ER stress and UPR. Whether the impairment of autophagy is the cause or the consequence of ER stress remains to be investigated. We then demonstrated that the onset of a prolonged ER stress exacerbates cell death, since COPZ1-depleted cells rapidly underwent caspase-dependent apoptosis.

Interestingly, in support to what observed by functional studies, a preliminary gene expression profiling of COPZ1-depleted 8505C cells indicated that the main upregulated canonical pathways consist of the unfolded protein and ER stress response, lipid metabolism and cell death (apoptosis). In parallel, proteomic profiling of COPZ1-depleted 8505C cells by nano-scale liquid chromatographic tandem mass spectrometry, indicated that the main involved pathways deal with vesicle trafficking, autophagy and caspase cascade in apoptosis (our unpublished results), in keeping with what observed by gene expression analysis.

Our results suggest that thyroid tumor cells dependence upon the activity of COPZ1 may be related to its pivotal involvement on the regulation of autophagy, UPR and ER stress, processes generally known as cytoprotective and adaptive mechanisms for cancer cell survival. Thus, COPZ1 inhibition may represent a strategy to target these processes, and convert their effect into a lethal mechanism. Interestingly, normal cells, which are probably not strictly dependent on these mechanisms, are preserved from cell death. However, apart from the well known role of COPZ1 in vesicle trafficking, the possible direct involvement of COPZ1 in cancer cell survival is still unclear. How COPZ1 depletion modulates the activation of intracellular multiple signalling pathways, executors of the final lethal effect, remains to be better investigated. This will allow identifying other critical nodes in the oncogenic network whose inhibition will result in cell collapse.

In our study, the most striking effect of COPZ1 silencing was observed in mouse tumor 8505C xenografts: in fact, siCOPZ1-treated tumors showed a consistent reduction of tumor growth.

Moreover, IHC analysis of tumor explants showed that COPZ1 silencing was associated with the decrease of the proliferative marker Ki67 and with an increase of necrosis. Further studies are needed to identify the mediators mainly involved in this process. An attractive hypothesis is that COPZ1 depletion could establish an inflammatory microenvironment through the release of cytokines/chemokines; this is supported by gene expression profile of COPZ1-depleted cells, showing upregulation of genes coding for cytokines involved in mediating communication between immune cells. More information on mediators released after cell death will be provided by the characterization of the cellular secretome content after COPZ1 depletion.

Tumor cell sensitivity to COPZ1 depletion is related to downregulation of its paralogous COPZ2 gene. COPZ1 inhibition is tolerated by normal cells because COPZ2 substitutes for it in the COPI complex, whereas tumor cells, characterized by the absence of COPZ2, display sensitivity. This "synthetic lethality" renders COPZ1 depletion an attractive strategy to kill tumor cells. By interrogating publicly available data sets including a large collection of thyroid tumors we found that *COPZ2* was frequently downregulated in PTC, PDTC and ATC samples, thus indicating that the majority of thyroid tumors may be eligible for COPZ1 targeting. As reported in other tumor types [13], we observed a concomitant low expression of miR-152, encoded within the *COPZ2* gene, which exerts a tumor suppressor role and is donwnregulated in different tumors, including thyroid ones [38]. Whether the downregulation of *COPZ2* and miR-152 in thyroid tumors is due to promoter hypermethylation, as reported for other tumor types [39], remains to be investigated. Moreover, we cannot exclude that COPZ1 dependency of thyroid tumors may also rely on other mechanisms or on other components of the COPI complex. Indeed, we had previously observed that the FTC-derived WRO82-1 cell line is sensitive to COPZ1 depletion, even though it expresses high level of COPZ2 mRNA [9].

Recent reports indicate that, as for COPZ1, targeting other COPI complex members may represent a therapeutic approach for cancer. A siRNA-based functional screening proposed COPA gene, encoding the α subunit of COPI complex, as a potential therapeutic target for mesothelioma [40].

Claerhout et al have shown that targeting the COPI complex members is a potent approach to block productive autophagy and stimulate cell death in cancer cells [30]. Recently, ARCN1, the δ-subunit of the COPI complex, has been proposed as a new therapeutic target [41]. COPB2 was found as synthetic lethal partner of mutated KRAS [42]. The co-occurrence of mutations in *KRAS* and *LKB1*, present in a small fraction of lung adenocarcinomas, drives addiction to the COPI complex members [43]. Of note, COPE gene, encoding the ε subunit of COPI complex, emerged from our screening in the list of genes specifically inhibiting thyroid tumor cell growth [9]. All this evidence suggests that targeting the coatomer complex, and consequently causing abortive autophagy and ER stress, may represent an optimal strategy to kill cancer cells, especially those resistant to conventional therapy.

In conclusion, we demonstrated that COPZ1 represents vulnerability for thyroid tumor cells, thus providing the first evidence of non-oncogene addiction for this tumor type. This adds a new element to the list of potential therapeutic targets, which includes, in addition to the driver oncogenic proteins and downstream pathways, several genes and miRNAs differentially expressed in thyroid tumors, some of which identified by our group [17;18;44-47], and whose role in promoting or suppressing the transformation process has been functionally demonstrated. On the whole, our results pave the way for designing novel therapeutic approaches based on COPZ1 inhibition useful for thyroid tumor patients who do not respond to standard therapies and rapidly progress to malignant forms. Notably, being effective on tumor but not on normal cells, these novel therapeutic approaches may have limited side effects.

5. Conflict of interest

None

6. Acknowledgements

We thank Prof. Nica Borgese and Dr.Sara Colombo (CNR Institute of Neuroscience, Milan, Italy), Dr. Italia Bongarzone (Fondazione IRCCS Istituto Nazionale dei Tumori, Milan, Italy) for their unconditional help. We also thank the Immunohistochemistry Facility of Fondazione IRCCS Istituto Nazionale dei Tumori, Milan, Italy.

This work was supported by Associazione Italiana per la Ricerca sul Cancro (AIRC) [Grant IG 11347, 2012; IG 18395, 2017] to A.Greco and by a Fondazione Umberto Veronesi Fellowship to M.C. Anania.

7. Author contribution

AMC conceived the study, designed and performed the experiments, interpreted data and wrote the manuscript; CE, TK, GA, MG, DMT, CL and PS performed the experiments; LD performed the experiments and provided the editing of the manuscript; BB, TC, MG and NA supervisioned the study and revised the manuscript; GA conceived and supervisioned the study, wrote the manuscript.

8. References

[1] J.Luo, N.L.Solimini, and S.J.Elledge, Principles of cancer therapy: oncogene and non-oncogene addiction. Cell. 136 (2009) 823-837.
[2] R.Nagel, E.A.Semenova, and A.Berns, Drugging the addict: non-oncogene addiction as a target for cancer therapy. EMBO Rep. 17 (2016) 1516-1531.
[3] G.Pellegriti, F.Frasca, C.Regalbuto, S.Squatrito, and R.Vigneri, Worldwide increasing incidence of thyroid cancer: update on epidemiology and risk factors. J Cancer Epidemiol. 2013 (2013) 965212.
[4] C.F.Eustatia-Rutten, E.P.Corssmit, N.R.Biermasz, A.M.Pereira, J.A.Romijn, and J.W.Smit, Survival and death causes in differentiated thyroid carcinoma. J Clin Endocrinol.Metab 91 (2006) 313-319.
[5] R.C.Smallridge, L.A.Marlow, and J.A.Copland, Anaplastic thyroid cancer: molecular pathogenesis and emerging therapies. Endocr.Relat Cancer. 16 (2009) 17-44.
[6] M.Ragazzi, A.Ciarrocchi, V.Sancisi, G.Gandolfi, A.Bisagni, and S.Piana, Update on anaplastic thyroid carcinoma: morphological, molecular, and genetic features of the most aggressive thyroid cancer. Int J Endocrinol. 2014 (2014) 790834.
[7] S.I.Sherman, Targeted therapies for thyroid tumors. Mod.Pathol 24 Suppl 2 (2011) S44-S52.
[8] K.C.Bible and M.Ryder, (2016) Evolving molecularly targeted therapies for advanced-stage thyroid cancers, in: 2016
[9] M.C.Anania, F.Gasparri, E.Cetti, I.Fraietta, K.Todoerti, C.Miranda, M.Mazzoni, C.Re, R.Colombo, G.Ukmar, S.Camisasca, S.Pagliardini, M.Pierotti, A.Neri, A.Galvani, and

A.Greco, Identification of thyroid tumor cell vulnerabilities through a siRNA-based functional screening. Oncotarget 6 (2015) 34629-34648.

[10] R.Beck, M.Rawet, F.T.Wieland, and D.Cassel, The COPI system: molecular mechanisms and function. FEBS.Lett. 583 (2009) 2701-2709.

[11] M.Razi, E.Y.Chan, and S.A.Tooze, Early endosomes and endosomal coatomer are required for autophagy. J.Cell Biol 185 (2009) 305-321.

[12] M.Beller, C.Sztalryd, N.Southall, M.Bell, H.Jackle, D.S.Auld, and B.Oliver, COPI complex is a regulator of lipid homeostasis. PLoS.Biol 6 (2008) e292.

[13] M.Shtutman, M.Baig, E.Levina, G.Hurteau, C.U.Lim, E.Broude, M.Nikiforov, T.T.Harkins, C.S.Carmack, Y.Ding, F.Wieland, R.Buttyan, and I.B.Roninson, Tumor-specific silencing of COPZ2 gene encoding coatomer protein complex subunit zeta 2 renders tumor cells dependent on its paralogous gene COPZ1. Proc.Natl.Acad.Sci U.S.A. 108 (2011) 12449-12454.

[14] F.Curcio, F.S.Ambesi-Impiombato, G.Perrella, and H.G.Coon, Long-term culture and functional characterization of follicular cells from adult normal human thyroids. Proc.Natl Acad.Sci U.S.A 91 (1994) 9004-9008.

[15] A.Conti, M.T.Majorini, E.Fontanella, A.Bardelli, M.Giacca, D.Delia, M.Mano, and D.Lecis, Lemur tyrosine kinase 2 (LMTK2) is a determinant of cell sensitivity to apoptosis by regulating the levels of the BCL2 family members. Cancer Letters 389 (2017) 59-69.

[16] Y.Kabeya, N.Mizushima, T.Ueno, A.Yamamoto, T.Kirisako, T.Noda, E.Kominami, Y.Ohsumi, and T.Yoshimori, LC3, a mammalian homologue of yeast Apg8p, is localized in autophagosome membranes after processing. EMBO J 19 (2000) 5720-5728.

[17] M.G.Vizioli, M.Sensi, C.Miranda, L.Cleris, F.Formelli, M.C.Anania, M.A.Pierotti, and A.Greco, IGFBP7: an oncosuppressor gene in thyroid carcinogenesis. Oncogene 29 (2010) 3835-3844.

[18] M.C.Anania, M.Sensi, E.Radaelli, C.Miranda, M.G.Vizioli, S.Pagliardini, E.Favini, L.Cleris, R.Supino, F.Formelli, M.G.Borrello, M.A.Pierotti, and A.Greco, TIMP3 regulates migration, invasion and in vivo tumorigenicity of thyroid tumor cells. Oncogene 30 (2011) 3011-3023.

[19] U.K.Coordinating Committee on Cancer Research, UKCCCR guide lines for the welfare of animals in experimental neoplasia. Br.J.Cancer 58 (1988) 109-113.

[20] H.He, K.Jazdzewski, W.Li, S.Liyanarachchi, R.Nagy, S.Volinia, G.A.Calin, C.G.Liu, K.Franssila, S.Suster, R.T.Kloos, C.M.Croce, and C.A.de la, The role of microRNA genes in papillary thyroid carcinoma. Proc.Natl Acad Sci U.S.A. 102 (2005) 19075-19080.

[21] V.Vasko, A.V.Espinosa, W.Scouten, H.He, H.Auer, S.Liyanarachchi, A.Larin, V.Savchenko, G.L.Francis, C.A.de la, M.Saji, and M.D.Ringel, Gene expression and functional evidence of epithelial-to-mesenchymal transition in papillary thyroid carcinoma invasion. Proc.Natl Acad.Sci U.S.A. 104 (2007) 2803-2808.

[22] G.Dom, M.Tarabichi, K.Unger, G.Thomas, M.Oczko-Wojciechowska, T.Bogdanova, B.Jarzab, J.E.Dumont, V.Detours, and C.Maenhaut, A gene expression signature distinguishes normal tissues of sporadic and radiation-induced papillary thyroid carcinomas. Br.J Cancer 107 (2012) 994-1000.

[23] G.Tomas, M.Tarabichi, D.Gacquer, A.Hebrant, G.Dom, J.E.Dumont, X.Keutgen, T.J.Fahey, III, C.Maenhaut, and V.Detours, A general method to derive robust organ-specific gene expression-based differentiation indices: application to thyroid cancer diagnostic. Oncogene 31 (2012) 4490-4498.

[24] I.Landa, T.Ibrahimpasic, L.Boucai, R.Sinha, J.A.Knauf, R.H.Shah, S.Dogan, J.C.Ricarte-Filho, G.P.Krishnamoorthy, B.Xu, N.Schultz, M.F.Berger, C.Sander, B.S.Taylor, R.Ghossein, I.Ganly, and J.A.Fagin, Genomic and transcriptomic hallmarks of poorly differentiated and anaplastic thyroid cancers. J Clin Invest 126 (2016) 1052-1066.

[25] R.A.Irizarry, B.Hobbs, F.Collin, Y.D.Beazer-Barclay, K.J.Antonellis, U.Scherf, and T.P.Speed, Exploration, normalization, and summaries of high density oligonucleotide array probe level data. Biostatistics 4 (2003) 249-264.
[26] M.Dai, P.Wang, A.D.Boyd, G.Kostov, B.Athey, E.G.Jones, W.E.Bunney, R.M.Myers, T.P.Speed, H.Akil, S.J.Watson, and F.Meng, Evolving gene/transcript definitions significantly alter the interpretation of GeneChip data. Nucleic Acids Res 33 (2005) e175.
[27] J.T.Leek, W.E.Johnson, H.S.Parker, A.E.Jaffe, and J.D.Storey, The sva package for removing batch effects and other unwanted variation in high-throughput experiments. Bioinformatics 28 (2012) 882-883.
[28] The Cancer Gene Atlas Research Network, Integrated genomic characterization of papillary thyroid carcinoma. Cell 159 (2014) 676-690.
[29] C.F.Davis, C.J.Ricketts, M.Wang, L.Yang, A.D.Cherniack, H.Shen, C.Buhay, H.Kang, S.C.Kim, C.C.Fahey, K.E.Hacker, G.Bhanot, D.A.Gordenin, A.Chu, P.H.Gunaratne, M.Biehl, S.Seth, B.A.Kaipparettu, C.A.Bristow, L.A.Donehower, E.M.Wallen, A.B.Smith, S.K.Tickoo, P.Tamboli, V.Reuter, L.S.Schmidt, J.J.Hsieh, T.K.Choueiri, A.A.Hakimi, L.Chin, M.Meyerson, R.Kucherlapati, W.Y.Park, A.G.Robertson, P.W.Laird, E.P.Henske, D.J.Kwiatkowski, P.J.Park, M.Morgan, B.Shuch, D.Muzny, D.A.Wheeler, W.M.Linehan, R.A.Gibbs, W.K.Rathmell, and C.J.Creighton, The somatic genomic landscape of chromophobe renal cell carcinoma. Cancer Cell. 26(3) (2014) 319-330.
[30] S.Claerhout, B.Dutta, W.Bossuyt, F.Zhang, C.Nguyen-Charles, J.B.Dennison, Q.Yu, S.Yu, G.Balazsi, Y.Lu, and G.B.Mills, Abortive autophagy induces endoplasmic reticulum stress and cell death in cancer cells. PLoS.One 7 (2012) e39400.
[31] G.Bjorkoy, T.Lamark, S.Pankiv, A.Overvatn, A.Brech, and T.Johansen, Monitoring autophagic degradation of p62/SQSTM1. Methods Enzymol. 452 (2009) 181-197.
[32] J.Li, M.Ni, B.Lee, E.Barron, D.R.Hinton, and A.S.Lee, The unfolded protein response regulator GRP78/BiP is required for endoplasmic reticulum integrity and stress-induced autophagy in mammalian cells. Cell Death Differ. 15 (2008) 1460-1471.
[33] J.Li and A.S.Lee, Stress induction of GRP78/BiP and its role in cancer. Curr.Mol Med. 6 (2006) 45-54.
[34] E.Szegezdi, S.E.Logue, A.M.Gorman, and A.Samali, Mediators of endoplasmic reticulum stress-induced apoptosis. EMBO Rep. 7 (2006) 880-885.
[35] N.Hiramatsu, W.C.Chiang, T.D.Kurt, C.J.Sigurdson, and J.H.Lin, Multiple Mechanisms of Unfolded Protein Response-Induced Cell Death. Am J Pathol. 185 (2015) 1800-1808.
[36] D.G.Breckenridge, M.Germain, J.P.Mathai, M.Nguyen, and G.C.Shore, Regulation of apoptosis by endoplasmic reticulum pathways. Oncogene 22 (2003) 8608-8618.
[37] A.Rodriguez, S.Griffiths-Jones, J.L.Ashurst, and A.Bradley, Identification of mammalian microRNA host genes and transcription units. Genome.Res. 14 (2004) 1902-1910.
[38] D.Cong, M.He, S.Chen, X.Liu, X.Liu, and H.Sun, Expression profiles of pivotal microRNAs and targets in thyroid papillary carcinoma: an analysis of The Cancer Genome Atlas. Onco.Targets.Ther. 8 (2015) 2271-2277.
[39] T.Tsuruta, K.Kozaki, A.Uesugi, M.Furuta, A.Hirasawa, I.Imoto, N.Susumu, D.Aoki, and J.Inazawa, miR-152 is a tumor suppressor microRNA that is silenced by DNA hypermethylation in endometrial cancer. Cancer Res 71 (2011) 6450-6462.
[40] H.Sudo, A.B.Tsuji, A.Sugyo, M.Kohda, C.Sogawa, C.Yoshida, Y.N.Harada, O.Hino, and T.Saga, Knockdown of COPA, identified by loss-of-function screen, induces apoptosis and suppresses tumor growth in mesothelioma mouse model. Genomics. 95 (2010) 210-216.
[41] D.Oliver, H.Ji, P.Liu, A.Gasparian, E.Gardiner, S.Lee, A.Zenteno, L.O.Perinskaya, M.Chen, P.Buckhaults, E.Broude, M.D.Wyatt, H.Valafar, E.Pena, and M.Shtutman, Identification of novel cancer therapeutic targets using a designed and pooled shRNA library screen. Sci Rep. 7 (2017) 43023.

[42] E.G.Christodoulou, H.Yang, F.Lademann, C.Pilarsky, A.Beyer, and M.Schroeder, Detection of COPB2 as a KRAS synthetic lethal partner through integration of functional genomics screens. Oncotarget 8 (2017) 34283-34297.
[43] H.S.Kim, S.Mendiratta, J.Kim, C.V.Pecot, J.E.Larsen, I.Zubovych, B.Y.Seo, J.Kim, B.Eskiocak, H.Chung, E.McMillan, S.Wu, B.J.De, K.Komurov, J.E.Toombs, S.Wei, M.Peyton, N.Williams, A.F.Gazdar, B.A.Posner, R.A.Brekken, A.K.Sood, R.J.Deberardinis, M.G.Roth, J.D.Minna, and M.A.White, Systematic identification of molecular subtype-selective vulnerabilities in non-small-cell lung cancer. Cell 155 (2013) 552-566.
[44] M.C.Anania, C.Miranda, M.G.Vizioli, M.Mazzoni, L.Cleris, S.Pagliardini, G.Manenti, M.G.Borrello, M.A.Pierotti, and A.Greco, S100A11 Overexpression Contributes to the Malignant Phenotype of Papillary Thyroid Carcinoma. J Clin Endocrinol.Metab 98 (2013) E1591-E1600.
[45] C.Ferrario, P.Lavagni, M.Gariboldi, C.Miranda, M.Losa, L.Cleris, F.Formelli, S.Pilotti, M.A.Pierotti, and A.Greco, Metallothionein 1G acts as an oncosupressor in papillary thyroid carcinoma. Lab Invest. 88 (2008) 474-481.
[46] E.Minna, P.Romeo, L. De Cecco, M.Dugo, G.Cassinelli, S.Pilotti, D.Degl'Innocenti, C.Lanzi, P.Casalini, M.A.Pierotti, A.Greco, and M.G.Borrello, miR-199a-3p displays tumor suppressor functions in papillary thyroid carcinoma. Oncotarget 5 (2014) 2513-2528.
[47] E.Minna, P.Romeo, M.Dugo, L.De Cecco, K.Todoerti, S.Pilotti, F.Perrone, E.Seregni, L.Agnelli, A.Neri, A.Greco, and M.G.Borrello, miR-451a is underexpressed and targets AKT/mTOR pathway in papillary thyroid carcinoma. Oncotarget 7 (2016) 12731-12747.

9. Figure legends

Figure 1. Effect of COPZ1 silencing on cell viability. (A) Colony forming assay of thyroid cell lines, 5 days after siRNA transfection; (B-C) Representative pictures at 10X magnification of Nthy-ori 3-1, TPC-1, 8505C, HTC/C3 cells, primary normal thyrocytes and human mammary epithelial cells (HME-1) at the indicated time points after siRNA transfection. In (A) and (C), cells were assessed by WB for protein levels of COPZ1 72h after siRNA transfection; β-actin was used for normalization of gel loading. siNT: Non-Targeting siRNAs; siCOPZ1: siRNAs targeting COPZ1; siUBB: siRNA targeting Ubiquitin B.

Figure 2. Effect of COPZ1 silencing on autophagy. (A) Percentage of TPC1- and 8505C-GL3 cells displaying LC3 puncta at different time points after siCOPZ1 and siNT oligos transfection; the asterisks indicate differences significant by the unpaired Student's t-test (*P<0.05, **P<0.01). (B) Representative pictures of TPC1- 8505C-GL3 cells, 48h and 72h after siRNA transfection,

respectively; cells were analyzed by fluorescence microscopy for the presence of LC3 puncta (green; arrows); nuclear DNA was stained with DAPI. (C-D) TPC-1 and 8505C cells were analyzed by WB for the expression of LC3-I/II, SQSTM1/p62 and COPZ1 proteins, at the indicated time points after siRNA transfection; β-actin was used for normalization of gel loading. In 8505C cells (D), p62 and COPZ1 expression in the same cell extracts was assessed in two separate gels.

Figure 3. Effect of COPZ1 silencing on ER stress and UPR. (A) WB analysis of calnexin and BiP protein expression in TPC-1 and 8505C cells, at the indicated time points after siRNA transfection; β-actin was used for normalization of gel loading. In TPC-1 cells, calnexin, COPZ1 and BiP expression in the same cell extracts was assessed in two separate gels; in 8505C cells, calnexin and BiP expression was assessed in the same gel of Figure 2D. (B) Real-time PCR analysis of COPZ1 and CHOP gene expression in TPC-1 and 8505C cells at the indicated time points after siRNA transfection; results are presented as log10-transformed relative quantity (RQ) of COPZ1/CHOP mRNA normalized for HPRT1 housekeeping gene expression. Data represent the mean +/- sd of two independent experiments.

Figure 4. Effect of COPZ1 silencing on cell death. (A) TPC-1 and 8505C cells were transfected with siCOPZ1 or siNT oligos in the presence of 2 µM of the fluorogenic substrate for activated caspase-3/7; live-cell fluorescence images (10X magnification) were taken 72h later with microscope. (B) WB analysis of cleaved PARP (arrowhead), cleaved caspase 3 and COPZ1 protein expression, at the indicated time points after siRNA transfection; β-actin was used for normalization of gel loading. Cleaved PARP expression in the same cell extracts was assessed in two separate gels.

Figure 5. Effect of COPZ1 silencing on 8505C *in vivo* tumor growth. (A) WB analysis of COPZ1 expression in tumour xenografts, excised three days after siRNA treatment; actin was used as

loading control for cell extracts. The graph represents the densitometric analysis of the bands; data are reported as ratio of COPZ1 to actin and normalized for the siNT sample value. (B) IHC analysis of COPZ1 and Ki67 expression in siNT and siCOPZ1 tumor explants. (C) *In vivo* tumorigenicity assay: the line within each box represents the median tumor weight (g) value of 10 controls (five vehicle and five siNT) and six siCOPZ1 treated explants at the end of the experiment (34 days); upper and lower edges of each box represent the 75th and 25th percentile, respectively; upper and lower bars indicate the highest and lowest values less than one interquartile range from the extremes of the box. **P*= 0.026, controls vs. siCOPZ1-treated mice, Kruskal-Wallis Test. (D) Mean percentage of Ki67 positive and necrotic cells in tumor explants (four siNT and five siCOPZ1 samples); the asterisk indicates differences significant by the unpaired Student's t-test (*P< 0.05). (E) IHC analysis of COPZ1 and Ki67 expression and H&E staining of two representative tumor explants (siNT-9, siCOPZ1-19); black arrow indicates areas of necrosis.

Figure 6. Expression of *COPZ2* and mir-152 in thyroid carcinomas. (A) Scatter plot distribution of *COPZ2* gene expression levels (log_2 scale) in 58 normal thyroid-tissues, 72 PTC, 17 PDTC and 31 ATC primary tumor samples; in the graph the median is recorded. Nonparametric pairwise multiple comparisons between all analyzed groups were performed by Dunn's test and Benjamini-Hochberg correction, following a significant Kruskal-Wallis test ($p= 5.733\ e^{-11}$). (B) (left) Scatter plot distribution of RNAseq normalized expression values (natural scale) from the thyroid TCGA dataset of *COPZ2* in 58 matched normal (N) and PTC samples. Illumina HiSeq Level 3 data were downloaded from TCGA Data Portal website and RSEM gene normalized expression values were derived for 58 PTC patients, in tumor and adjacent normal samples, respectively; in the graph the median is recorded. Differential gene expression levels between tumor and normal groups were evaluated by Wilcoxon test (p-value= $2.442x10^{-10}$); (right) dispersion plot of *COPZ2* (x-axis) and hsa-miR-152 (y-axis) RNAseq normalized expression levels (log_2 scale) in the 58 PTC samples. Normalized reads per million miRNA mapped (RPM) data were obtained for the same 58 tumor

samples from Illumina HiSeq Level 3 isoform quantification files (TCGA Data Portal website), by summing up the reads aligned to each 3p or 5p miRBase v16 mature strands. Pearson's correlation method was applied to evaluate the correlation between RNAseq normalized gene and miRNA read counts in 58 tumor samples ($r= 0.67$, p-value= $8.41x\ 10^{-9}$).

Figure 1

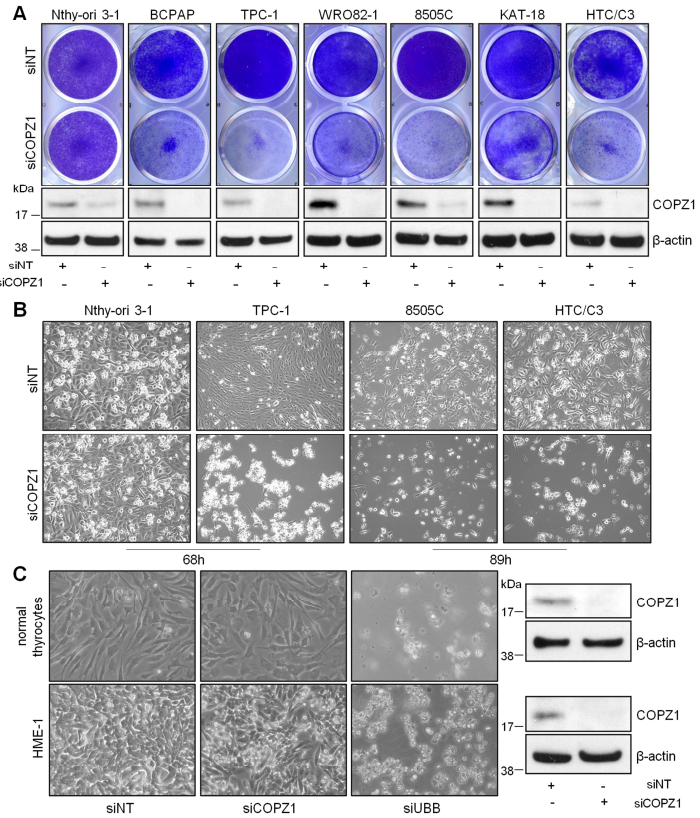

Figure 2

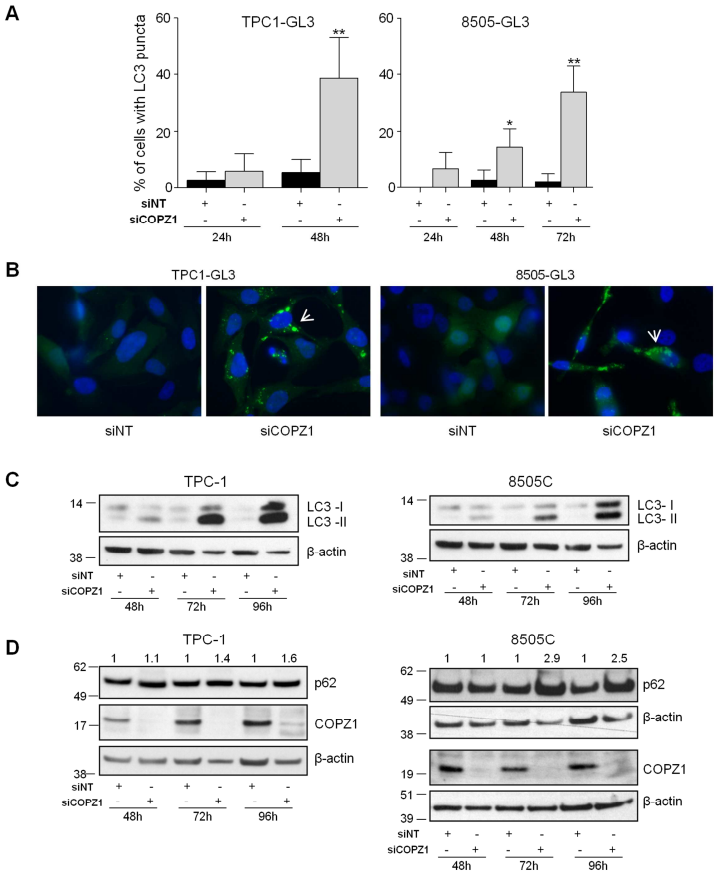

Figure 3

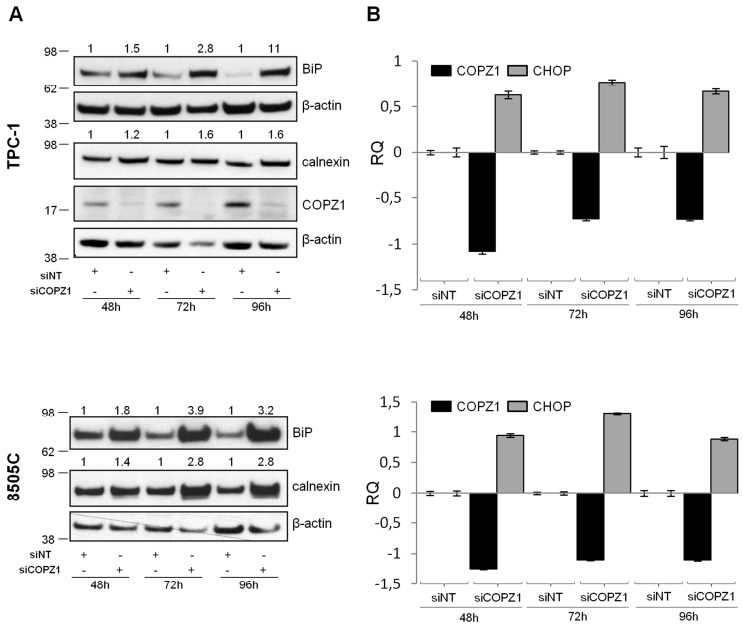

Figure 4

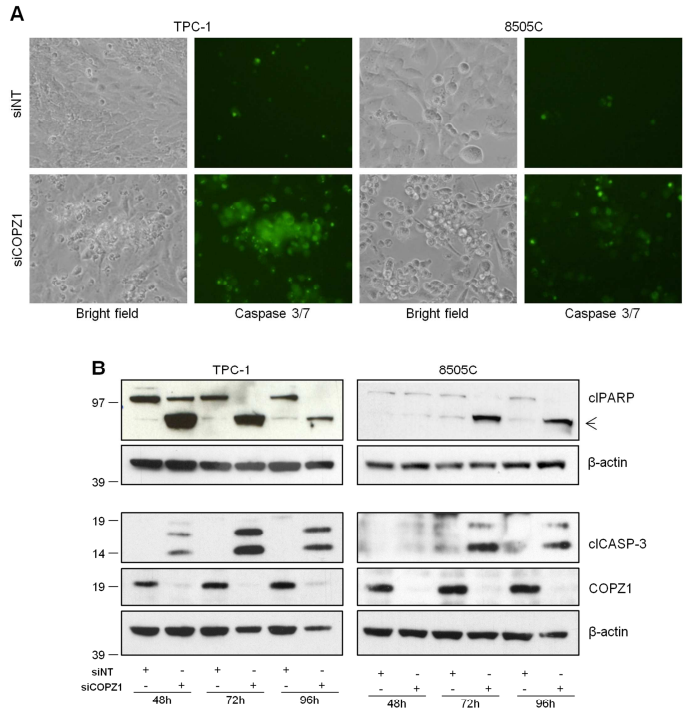

Figure 5

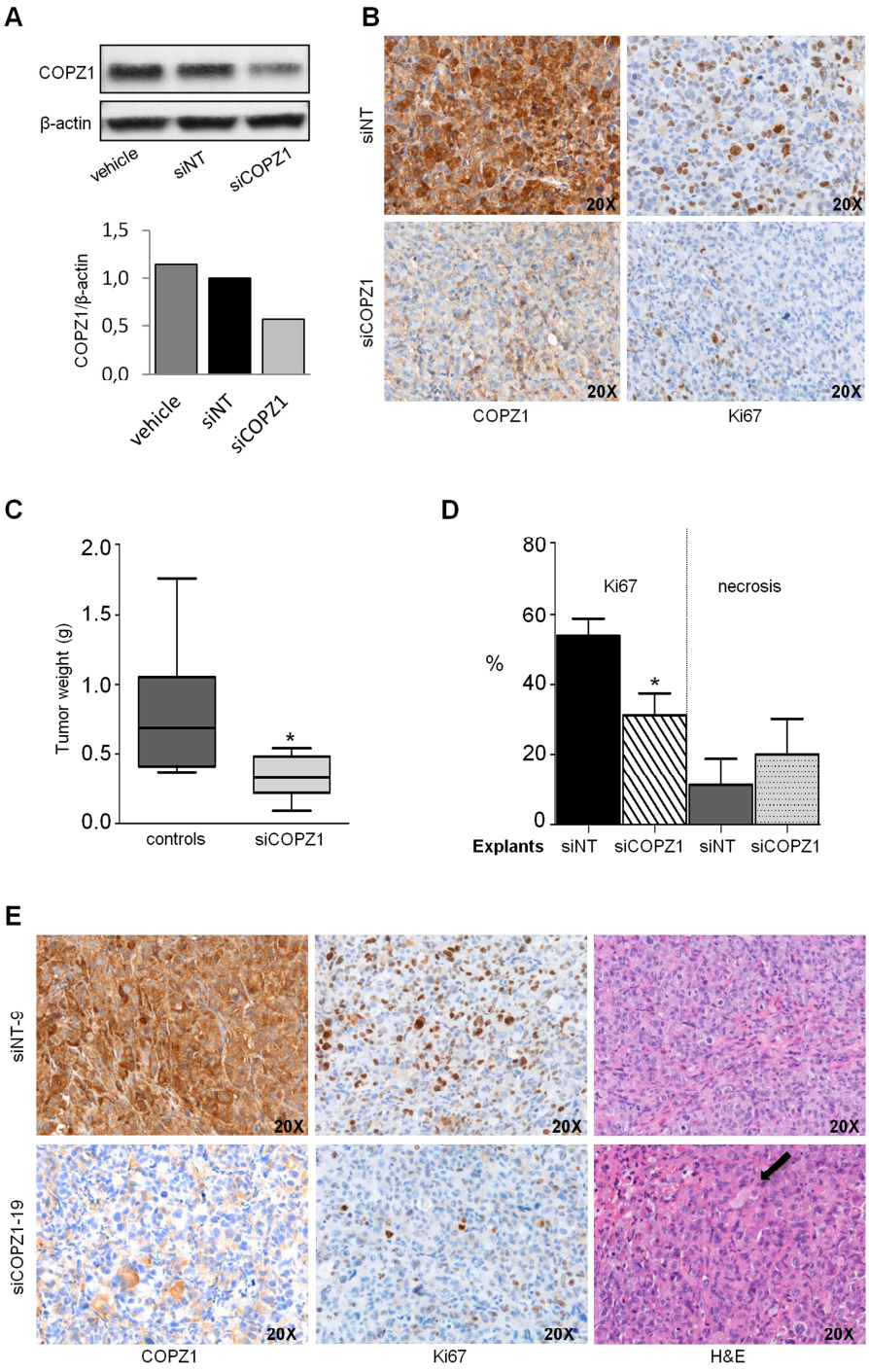
A
COPZ1
β-actin
vehicle
siNT
siCOPZ1
COPZ1/β-actin
1,5
1,0
0,5
0,0
B
siNT
siCOPZ1
20X
COPZ1
Ki67
C
Tumor weight (g)
2.0
1.5
1.0
0.5
0.0
controls
siCOPZ1
D
%
80
60
40
20
0
Ki67
necrosis
Explants
siNT
siCOPZ1
E
siNT-9
siCOPZ1-19
COPZ1
Ki67
H&E

Figure 6

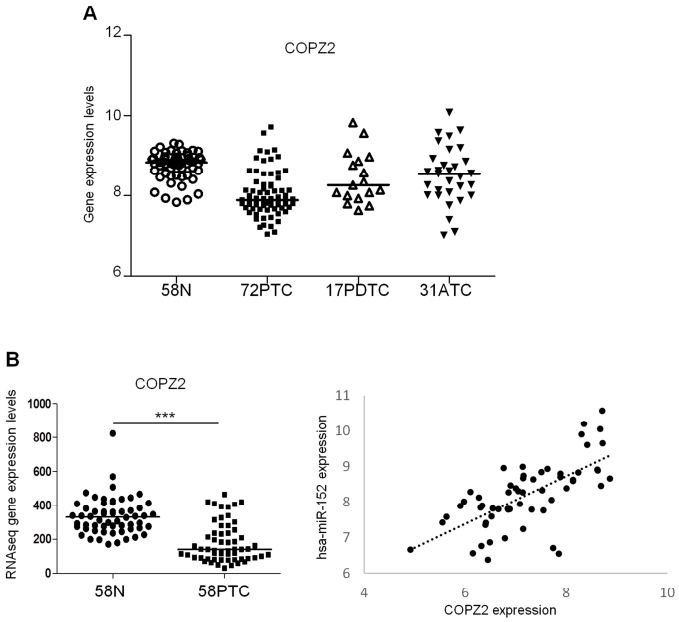

Highlights

- COPZ1 represents an example of non-oncogene addiction in thyroid tumor cells
- COPZ1 depletion affects thyroid tumor cell viability
- Cell death is associated with abortive autophagy, ER stress, UPR and apoptosis
- *In vivo* COPZ1 depletion reduces the growth of thyroid tumor mouse xenografts
- COPZ1 represents an attractive therapeutic target for thyroid cancer